PREDICTION OF FORMATION AND TRACKS OF BAY OF BENGAL CYCLONES

A thesis submitted to
the University of Dhaka
in partial fulfilment of the requirements
for the degree of Doctor of Philosophy
(Faculty of Science)

Md. Mahbub Alam

Theoretical Physics Laboratory
Department of Physics
Dhaka University
Dhaka-1000, Bangladesh

December, 1998

Dedicated to my parents and father-in-law and mother-in-law whose blessing and inspiration have enabled me to complete the thesis

ACKNOWLEDGEMENT

I am grateful to my revered teachers Dr. Sultana Shafee and Dr. Ahmed Shafee, Professors, Department of Physics, Dhaka University, Dhaka, Bangladesh, without whose help it would not have been possible for me to complete this thesis.

I wish to express my gratitude to the members of the Academic Committee of the Physics Department, Dhaka University for giving me the permission for admission as a Ph.D. student.

I am especially indebted to Dr. A. M. Choudhury, C.S.O., Space Research and Remote Sensing Organization (SPARRSO) and also to Mr. S. Karmakar, Head of Synoptic Division, SAARC Meteorological Research Centre (SMRC), for giving many valuable suggestions and helping me at different stages of this work.

I am grateful to Mr. M. H. Khan Chowdhury, Ex- Director, Bangladesh Meteorological Department (BMD) and also to Dr. D. A. Quadir C.S.O., SPARRSO for giving many useful suggestions.

I am also grateful to Mr. Sujit Kumar Debsarma and Mr. Shah Alam, Meteorologist and other staff of the Storm Warning Centre (SWC), BMD for supplying data and helping me in many ways.

I am also grateful to the Director, Bangladesh Institute of Technology (BIT) Khulna for giving me leave on deputation and the University Grants Commission (UGC), Bangladesh for financial support.

My heartiest thanks go to my wife and daughter for their constant encouragement and forbearance.

Declaration

I hereby declare that the research work presented in this thesis entitled ``**Prediction of Formation and Tracks of Bay of Bengal Cyclones**'' has been carried out by me under the supervision of Professor Sultana Shafee, Department of Physics, University of Dhaka, Dhaka-1000, Bangladesh. The work has not been submitted elsewhere for any other degree or diploma.

Professor Sultana Shafee
Supervisor

Md. Mahbub Alam
Ph. D. Research Fellow
Reg. No. 31/1991-92.
Re Reg. No. 36/1998-99
Department of Physics
Dhaka University
Bangladesh

Abstract

Rawindsonde data of 0000 UTC for standard isobaric surfaces at the surface, 850, 700, 500, 400, 300, 200, 150 and 100 hPa levels for the periods of different cyclones in the last decade were considered to study the different meteorological parameters. The vertical wind shear, the vertical variation of zonal wind speed and meridional wind speed and temperature were studied for different cyclones in the surroundings of the Bay of Bengal in relation to the movement of cyclones.

The dry static energy, the latent heat energy, the moist static energy, the total energy, the meridional and zonal fluxes of moist static energy and their vertical distribution were studied in the surroundings of the Bay of Bengal in relation to the movement of cyclones and their ultimate landfall.

A two dimensional model is developed for the prediction of cyclone tracks in the Bay of Bengal. The boundary value problem is then solved by using the complex potentials. The different cyclones are integrated in different time steps to find the relationship between the actual travel time and observed time by the models. The results obtained for cyclone tracks by this model are almost the same as the actual track. The cyclonic track data were collected from the Storm Warning Centre (SWC) of Bangladesh Meteorological Department (BMD).

A simplified system of equations that can simulate the evolution and mature stages of tropical cyclones is presented. The study has been done using a three-dimensional numerical model constructed which produces circularly symmetric feature of the tropical cyclone. It has 5 layers in the vertical with the horizontal extent of 1200 km. The horizontal grid length of the model is 80 km. The model equations have been solved using the Leapfrog scheme. Numerical simulation shows that the model sensitivity to the vertical stability is similar to results obtained from other general models. Latent heat release associated with condensation is calculated from the moisture equation. The sensible heating parameter is added to the heating term. Initially the model atmosphere is

assumed to be at rest and is then excited by a large scale heating to generate an initial vortex.

The evolution of surface pressure drop, tangential wind, radial wind, heat released due to condensation, temperature anomaly, D-value, horizontal structure of vertical p-velocity, vertical structure of vertical p-velocity, vorticity and static stability parameter have been discussed based on the results obtained from the tropical cyclone modelling experiment.

Contents

PUBLICATIONS

1. Analysis of tropospheric energy fluxes in the surroundings of the Bay of Bengal for different tropical cyclones. *Dhaka Univ. J. Sci.* , 44(2): 275-284, 1996 (July). (Parts of chap. 4)
2. Analysis of some meteorological parameters in the surroundings of the Bay of Bengal during different cyclonic periods. *Journal of Bangladesh Academy of Sciences*, 21, 1, 89-98, 1997. (Parts of chap. 3)
3. Analysis of different tropospheric energies in the surroundings of the Bay of Bengal during different cyclonic periods. *Mausam* , 48, 3 (July 1997), 367-374. (Parts of chap. 4)

LIST OF SYMBOLS

C_P	=	Specific heat at constant pressure
C_H	=	Coefficient of sensible heat flux
Cq	=	Surface exchange coefficient of water vapour
C_D	=	Horizontal drag coefficient which is dependent on the wind speed
d	=	(x-) and (y-) component grid separation
E	=	$\frac{1}{2}V^2$ Kinetic energy per unit mass
E_{sl}	=	Surface contribution of moisture flux due to turbulence
E_{ss}	=	Surface contribution of sensible heat
$E_{s(T_d)}$	=	Saturation vapour pressure at dew point temperature
$E_{s(T_T)}$	=	Saturation vapour pressure at dry-bulb temperature
e_s	=	Saturation vapour pressure
f	=	$2\Omega \sin\phi$ = Coriolis parameter
F_H	=	Surface fluxes of sensible heat
F_M	=	Surface fluxes of momentum
F_Q	=	Surface fluxes of water vapour
g	=	Gravity
h	=	Moist static energy
i, j, k	=	Index in x, y and p- co-ordinates
k	=	Vortex strength
L	=	Latent heat of condensation
M	=	Source strength
n	=	Index; time
p	=	Component of Cylindrical co-ordinate
P_B	=	Cloud base
P_T	=	Cloud top
q_B	=	Specific humidity at the boundary layer
q_w	=	Specific humidity over water or Sea surface
q	=	Specific humidity
q_s	=	Saturation specific humidity
Q	=	Mean heating rate per unit mass over the whole column
r	=	Relative humidity; Component of Cylindrical co-ordinate
R	=	Universal gas constant
s	=	Dry static energy

T_a	=	The air temperature over the water at anemometer level
T_d	=	Dew point temperature
T_T	=	Dry bulb temperature
T_w	=	Surface water temperature
u	=	Radial component of wind
v	=	Tangential component of wind
V_a	=	Wind speed at the anemometer level
V_x	=	x – component steering wind
V_y	=	y – component steering wind
V_s	=	Wind speed at the surface
W	=	Complex potential
Z	=	Instantaneous position of the cyclone
Z	=	Position of the sink and the vortex
α_d	=	Horizontal diffusion coefficient
η	=	Mesoscale convergence parameter
φ	=	Geopotential
ϕ	=	Latitude; Velocity potential
ψ	=	Stream function
υ	=	Complex velocity
Ω	=	Angular rotation of the earth
ω	=	$\frac{dp}{dt}$ Vertical velocity in p-system
ρ_s	=	Density of air near the surface
σ	=	The static stability parameter
τ_u	=	Eddy stress in x-direction
τ_v	=	Eddy stress in y-direction
θ	=	Potential temperature; Component of Cylindrical co-ordinate
ξ	=	Absolute vorticity

Chapter 1

Introduction

Bangladesh is devastated from time to time by different natural disasters, e.g. floods, nor'westers, tornado and cyclones. The tropical cyclone indeed is the cause of many of our socio-economic miseries, because though a cyclone lasts only a few days, the havoc it brings about can take a long time to recover from, diverting many valuable resources to reconstruction and renewal of old structures instead of adding to further growth. The loss of life and movable property can also be astronomical.

It is, therefore, of great importance to understand how cyclone form and the nature of their movement, so that accurate predictions can be made about when to expect such a calamity and be able to predict the actual path of its destruction. This may minimise the damage by these phenomena, because the extent of damage is in a large part due to the element of surprise and unpreparedness.

Cyclones are not unique to Bangladesh. Many other tropical countries have to bear the brunt of these marauders. In the east even countries as north as Japan are lashed by cyclones. Philippines, Taiwan, Indonesia, Northern Australia, tropical USA and the Caribbean islands all suffer frequently. There is, therefore, a global awareness of the need for understanding cyclones, not only for the purpose of prediction, but also in the hope that one day such knowledge may enable us to prevent their formation or at least divert them to tracks where damage can be minimised. It is true that intensive research work is going on in some of the best-equipped meteorological and related laboratories and institutions of the world on this subject. However, such studies are usually of a very general nature, or are of regional interest only, making it imperative that studies be carried out independently also for Bangladesh with our limited resources.

The formation of cyclones and the paths they choose depend on many parameters of the atmosphere. The cyclone is an intense atmospheric vortex of mesoscale dimensions, i.e. it involves rotations of huge masses of air at very high speed, the energy for which comes from the interaction of solar radiation with the sea, which causes phase transition of water on a gigantic scale producing a huge heat engine. However though solar radiation on the sea is a predictable periodic variable, the formation of a cyclone is a much more complex phenomenon depending on the totality of the existent state of the atmosphere in the region. This in turn involves the entire past history of the atmosphere, on the topography, or the ever-changing nature of vegetation and man-made structures and processes. As a result, the state of the atmosphere can never be exactly duplicated and the fine differences may be amplified to determine when a cyclone may form, or what path it will take.

In fact it has been shown by Lorenz (1963) that even a simple subset of the dynamical equations governing the atmosphere can give ``chaos", where the initial state can never predict what the final state may be. But it is also known that with reasonable approximations weather forecasting is becoming an increasingly more accurate science. We, therefore, take the optimistic attitude that our knowledge of atmospheric systems may indeed lead to prediction models for cyclones, and that this may involve simply a study of that meteorological variables and their dynamical relations, as given by the laws of physics. There are many factors responsible for the formation of cyclones. According to Gray (1968, 1975, 1979), these factors are sea surface temperature, conditional instability through a deep atmospheric layer, relative humidity, Coriolis parameter, low level relative vorticity and weak vertical wind shear. Observations on cyclones yield interesting features, which identify a cyclonic state.

Tropical cyclones form from initial convective disturbances known as cloud clusters. As they evolve from loosely organised states into mature intense storms, they pass through several characteristic stages. A uniform terminology does not exist to describe these stages over the different regions of the globe. However, general agreement exists that a key stage in the formation process is when the surface wind reaches 17.5 m /s (34 kt.).

The large-scale tropospheric vortex may extend over 1000 - 2000 km from the region of minimum surface pressure at its centre. On this scale, the wind and the mass fields are in approximate gradient balance through the depth of the troposphere. The distinction between core formation and large-scale vortex formation is important because different dynamical processes are involved. The mature tropical cyclone has a characteristic structure on two horizontal scales.

The existence of the two horizontal scales has presented great difficulties. Various authors' use of terms such as "genesis", "formation", and "development" is dependent on the method of analysis, database, and objective of each study. Although the larger scale (i.e., 1000 km) vortex already exists when the core develops, much of the research in tropical cyclone formation has examined the formation of this large-scale vortex.

The large scale circulation contains the inner region, termed as the cyclone "core", the spiral bands of precipitation, the eye wall, and the eye that characterise tropical cyclones in radar and satellite imagery (e.g. Wexler 1947; Dvorak 1975). The horizontal extent of the core is of the order of 100 km. The core region has the same basic thermal structure, but it is characterised by very large horizontal gradients in comparison with the large-scale system. Generally, the existence of a core region can be identified with the time that the system is classified as a tropical cyclone (i.e., wind speed exceeding 17.5 m/s). Further development of the maximum wind speeds beyond 17.5 m/s is referred to as intensification. This stage includes the evolution of the core into a well-defined radar eye. The inner region winds can become intense, and in extreme cases reach 90 m/s just outside the eye.

The winds that swirl about the centre decrease with height, but typically fill the depth of the troposphere (Haurwitz, 1935). From angular momentum considerations, an increase of the rotational wind speed of the core may be accomplished by an import of angular momentum from the surrounding regions. As the radius of the core region is small, large increases in core wind speeds may occur from only small changes in the large-scale vortex.

As the cyclone matures, the tangential wind in the core becomes strongly axisymmetric and it is termed as primary circulation. In addition to the primary circulation, a secondary circulation arises in response to surface friction and condensational heating. The secondary circulation supplies the angular momentum and thermal energy that intensify the primary circulation and maintain it against friction and radiative cooling (Riehl and Malkus, 1961). In the core, the primary circulation is much stronger than the secondary circulation.

A tropical cyclone is a warm-core vortex. The thermal wind considerations require that the strength of the vortex decreases rapidly with height in the upper troposphere, and on the larger scale it turns anticyclonic.

The characteristics of horizontal pressure gradients are of the order of 1 hPa/km (as compared with approximately 0.01 hPa/km for the larger scale envelope). In the core, the wind magnitudes are such that the balance is approximately cyclostrophic rather than gradient.

The intensity of the storm may be sensitive even in a small change in temperature of the ocean or land surface. The physical parameters such as the surface roughness, surface albedo, and soil wetness (in case of land) are locally related to the surface exchange of heat and momentum (Y. Kurihara, *et al.*, 1992). The change in the wind speed of the tropical cyclone moving over land is determined by the surface frictional elements (e.g., grass, trees and buildings) and by hills and mountains.

In most of the tropical oceans in summer, the process of bringing the tropospheric column to thermodynamic equilibrium with the sea would add enough heat to decrease the surface pressure by 5-10% (Miller, 1958). The tropical cyclogenesis is emphatically not a simple mixing process. The reason of existence of tropical cyclone is the balance between wind and mass on a rotating earth towards the low pressure.

The role of energy fluxes is to govern the atmospheric circulation as well as the physical processes responsible for the formation and the movement of tropical cyclones (Palmen

and Newton, 1969). Chowdhury and Karmakar (1995) studied the tropospheric energy fluxes of a cyclone formed in the Bay of Bengal during its movement.

During the development and movement of a tropical cyclone, the changes of tropospheric energy and fluxes in the surrounding are important for its prediction. Therefore, it is essential to study the role of tropospheric energy and fluxes and their vertical distribution in prediction of formation and movement of tropical cyclones in respect of their intensity, track and landfall. Virtually no work has been done on the formation of tropical cyclones near Bangladesh. A preliminary attempt was the work of Khanam (1989) who developed a simple one level barotropic model to predict the track of tropical cyclones in this region.

Though our eventual goal is to devise a model which would be able to indicate the formation of cyclones and be able to predict their tracks, in view of the importance of different meteorological parameters in controlling these events, in this work we have also made a fairly exhaustive analysis of such parameters during cyclonic periods.

Some quantities of special interest vis a vis cyclone formation and movement are vertical wind shear and vertical variation of zonal and meridional wind speed as well as temperature. We have, therefore, analysed these quantities in detail during cyclonic periods in the Bay of Bengal, using rawindsonde data at various pressure levels. Though the spatial and temporal abundance of the data in this region was not as high as could be desired, and consequently any attempt at model making had to face limitations on account of this scarcity, we believe a beginning had to be made with what is currently available.

As energy considerations are of paramount significance in determining when a cyclone would originate and also its dynamical behaviour, in this work we have also made a through study of dry static energy, latent heat energy, moist static energy, total energy and meridional and zonal flux of moist static energy. The vertical distribution of these variables was determined during different cyclonic periods in the Bay of Bengal.

In view of the great number of parameters involved and the difficulty of accurately solving all the set of coupled equations of motion relating them, and in view of the scarcity of

relevant data over a sufficiently fine spatio-temporal grid, one can also take a completely different attitude in model building for cyclone track prediction. This approach would involve replacing all the equations by a simple physical model, which can be treated analytically and numerically with great accuracy. Such a model would also substitute effective parameters for the actual physical ones, and be content with only a few of the most significant ones. While obviously such an approach cannot hope to have the full power of the actual set of dynamical equations, they may serve as a rough guide where nothing better exists.

We have, therefore, in this work tried to formulate such a simple model, which is two-dimensional and uses the complex potential. It is known that in hydrodynamics such 2-D models can be of great utility in enlightening us about fluid motion, where obstacles and reflectors are present. The shape of the subcontinental coastline in and in the vicinity of Bangladesh does seem to offer the possibility of using a simplification in a two-dimensional problem that can be analysed fairly simply.

We have developed this 2-dimensional model with no vertical layer separation. The justification for such simplification is the fact that the cyclone extends to a great height beyond the troposphere and all layers move together. Choudhury (1978) gave a model for tropical cyclones in the Bay of Bengal. In this model the tracks for cyclone could be drawn only for those which crossed the Meghna estuary. Our model can be used for any track of a cyclone in the Bay of Bengal that hits anywhere along the coastline.

However, for the study of formation of cyclones such a two-dimensional model would be irrelevant. In this work we have also tried to use all the dynamical equations connecting the atmospheric parameters to build a model where a cyclone does emerge in the right conditions. We have made a few reasonable assumptions and simplifications, about periodicity and some axial symmetry, but have retained the full set of equations of motion, continuity and energy conservation. Even with limited computing power and data, we have been able to study the variation of parameters during the evolution of a cyclone using our model, and also to verify the emperical beliefs about the preconditions necessary for

cyclone formation, e.g. absence of vertical wind shear, sufficient sea surface temperature, Coriolis acceleration off the Equator etc.

In this model we consider in detail the energy equation. The latent heat release associated with condensation is calculated from the moisture equation. The latent heat of condensation is considered in the model has three components associated with i) moisture convergence above the boundary layer (e.g. cloud base) due to horizontal advection ii) Ekman pumping of moisture from the boundary layer iii) surface evaporation. Also the sensible heat transfer from the surface to the cloud i.e. above the boundary layer.

In chapter 3 the different meteorological parameters such as wind speed and temperature in the surroundings of the Bay of Bengal have been investigated during the life cycle of a few cyclones. We have also investigated the vertical wind shear on the basis of land observational data to observe the relation with the movement of the cyclone.

In chapter 4 we have examined the behaviour of different tropospheric energies and fluxes such as the dry static energy, the latent heat energy, the moist static energy, the total energy, the meridional flux of moist static energy and the zonal flux of moist static energy and their vertical distribution in the surroundings of the Bay of Bengal during the cyclonic periods.

In chapter 5 we have attempted to construct a novel model for cyclone track prediction, which take into account some of the physical characteristics of a cyclone.

In chapter 6 we have developed a three-dimensional numerical model for the formation of tropical cyclones in the Bay of Bengal.

In chapter 7 we summarise our results and present our conclusions.

Chapter 2

Available Information on Tropical Cyclone Formation and its Movement

2.1 Classification

Cyclonic disturbances in the North Indian Ocean are classified according to their intensity. The following nomenclature is in use:

1. Low: Wind Speed < 31 km/hr.
2. Well marked low: Wind Speed equals to 31 km/hr.
3. Depression: Wind Speed ranges from 32 - 48 km/hr.
4. Deep Depression: Wind Speed ranges from 49 - 62 km/hr.
5. Cyclonic Storm: Wind Speed ranges from 63 - 88 km/hr.
6. Severe Cyclonic Storm: Wind Speed ranges from 89 - 117 km/hr.
7. Severe Cyclonic Storm a core of hurricane intensity: Winds≥118km/hr.

2.2 Life Cycle of Tropical Cyclones

The life span of tropical cyclones with full cyclonic intensity averages at about 6 days from the time they form until the time they enter land or recurve into the temperate zone. Some storms last only a few hours; a few as long as two weeks. The evolution of the average storm from birth to death has been divided into four stages (Tarakanov, 1980).

- **Formative Stage:** Tropical storms form only in near pre-existing weather systems. Deepening can be a slow process, requiring days for the organisation of a large area with diffuse winds. It can also produce a well-formed eye within 12 hours. Wind speed usually remains below hurricane force in the formative stage. Unusual fall of pressure

over 24 hours by 2 - 3 hPa or more takes place in the centre of the vorticity concentration.

- **Immature Stage:** A large number of formative cyclones die within 24 hours. Others travel long distances as shallow depressions. Wind of cyclonic force forms a tight band around the centre. The cloud and rain pattern changes from disorganised squalls to narrow organised bands, spiralling inward. Only a small area is as yet involved, though there may be a large outer envelope. The eye is usually visible but ragged and irregular in shape.

- **Mature Stage:** The force of cyclonic winds may blow within a 30 - 50 km radius during immature stage. This radius can increase to over 300 km in mature storms. On the average, the mature stage occupies the longest part of the cycle and most often lasts several days. The eye is prominent and circular and the cloud pattern is almost circular and smooth. The surface pressure at the centre is no longer falling and the maximum wind speeds no longer increasing. At this stage, heating from convective clouds furnishes the largest amount of energy for cyclone maintenance. Pressure gradient is largest at the surface. Wind speed range is between 128 - 322 km/hr.

- **Terminal Stage:** Nearly, all cyclones weaken substantially upon entering land, because they lose the energy source furnished by the underlying ocean surface. The decay is especially rapid where the land is mountainous. Movement of a cyclone over land cuts off the surface energy source and increases the surface friction, especially when the land is mountainous. Some cyclones die out over sea and this event can be related to their moving over a cold ocean current or being invaded by a surface cold airmass behind a cold front or by a cold centre at high levels moving over their top.

2.3 Climatological Conditions for Tropical Cyclone Formation

The first global climatology of tropical cyclone genesis by Gray (1968, 1975, 1979) demonstrated that the genesis may be related to six environmental factors:

- (i). large values of low level relative vorticity;
- (ii). a location at least a few degrees pole ward of the equator, giving a significant value of planetary vorticity;
- (iii) weak vertical shear of the horizontal winds;
- (iv) sea-surface temperatures (SSTs) exceeding 26°C and a deep thermocline;
- (v) conditional instability through a deep atmospheric layer; and
- (vi). large values of relative humidity in the lower and middle troposphere.

The first three factors are functions of the horizontal dynamics, while the last three are thermodynamic parameters. Gray defined the product of (i), (ii,) and (iii) to be the dynamic potential for cyclone development, while the product of (iv), (v,) and (vi) may be considered as the thermodynamic potential. However, the combination of the above six parameters were ``tuned" to agree with the mean seasonal and geographical distributions of tropical cyclone developments. As discussed by Gray (1975) and McBride (1981a), the thermodynamic parameters vary slowly in time and would be expected to remain above any threshold values necessary for tropical cyclone development throughout the cyclone season. On the other hand, the dynamic potential can change dramatically through synoptic activity. Thus, it was hypothesised by Gray that cyclones form only during periods when the dynamic potential is perturbed to a value above its regional climatological mean.

Frank (1987) noted that the above six environmental parameters are not independent. In the tropics, regions of high sea-surface temperatures are invariably correlated with conditional instability due to weak horizontal temperature gradients in the lower troposphere. High humidities in the middle levels also tend to occur in convective clusters over warm waters, and virtually all areas with widespread deep convection are associated with mean ascending motion. Thus, Frank reduced the list to four parameters by combining (i) and (ii) into the absolute vorticity at low levels, deleting (v), and adding mean upward vertical motion to (vi).

2.3.1 North Indian Ocean

Although only about 7 % of the global tropical cyclones occur in the North Indian Ocean, they are the most deadly. The shallow waters of the Bay of Bengal, the low flat coastal terrain, and the funnelling shape of the coastline can lead to devastating losses of life and property due to the surge from a storm of even moderate intensity. The Backerganj cyclone of 1876 and the Bhola cyclone of 1970 each killed more than 200,000 persons in Bangladesh. Recently in 1991 about 1,38,000 people were killed by a storm surge in Bangladesh.

Although the development from a tropical depression into a tropical cyclone usually occurs in about 12 - 24 hr, 15 % require more than 48 hr and others are reported to undergo formation in less than 12 hr (Srinivasan and Ramanamurty, 1973). Most North Indian Ocean cyclones form within the monsoon trough or ITCZ. Formation may occur either as reintensification of westward-propagating disturbances or from in situ disturbances that develop within the trough. The zone of formation shifts meridionally between 5° - 20° N following the annual migration of the monsoon trough.

2.4 Large Scale Conditions associated with Tropical Cyclone Formation

Tropical cyclones form only over tropical oceans where upper air observations are sparse, which has made it difficult to document the structure and evolution of the flow during the formation process. Consequently, much of the early understanding of formation was gained from case studies based on innovative use of the existing data networks (e.g. Riehl, 1948; Hubert, 1955; and Yanai, 1961). Subsequent studies that exploited improved observational systems have led to further refinement and detail in documentation of the tropical cyclone formation process. However, no well-accepted closed theory of formation exists.

The observational studies have isolated a number of synoptic-scale aspects that have an important role in the formation process:

(i) Tropical cyclones form from pre-existing disturbances containing abundant deep convection;

ii) The pre-existing disturbance must acquire a warm core thermal structure throughout the troposphere;

(iii) Formation is prescribed by an increase (spin-up) of lower tropospheric relative vorticity over a horizontal scale of approximately 1000 - 2000 km;

(iv) A necessary condition for cyclone formation is a large-scale environment with small vertical shear of the horizontal wind;

(v) An early indicator that cyclone formation has begun is the appearance of curved banding features of the deep convection in the incipient disturbances;

(vi) The inner core of the cyclone may originate as a mid-level meso-vortex that has formed in association with a pre-existing mesoscale area of altostratus (i.e. a Mesoscale Convective System or MCS); and

(vii) Formation often occurs in conjunction with an interaction between the incipient disturbance and an upper-tropospheric trough.

2.4.1 Pre-existing disturbance

"We observe universally that tropical storms form only within pre-existing disturbances. An initial disturbance, therefore, forms part of the starting mechanism. A weak circulation, low pressure and a deep moist layer are present at the beginning. The forecaster need not look into areas which contain no such circulation's." These statements by Riehl (1954) have stood the test of time. The structure of these tropical "cloud clusters" has been documented by many authors (e.g. Ruprecht and Gray, 1976 a, b; Johnson and Houze, 1987). The cloud clusters have an upper tropospheric warm core and mean (averaged over a 4° latitude-longitude square) upward velocities of about 100 hPa/day (McBride and Gray, 1980; Lee, 1989). Although the diameter of the convective area is typically only a few hundred km, the rotational circulation's associated with the systems usually extend over a diameter of approximately 1000 - 1500 km.

2.4.2 Lower-tropospheric warm core

Although tropical cloud clusters have a warm core in the upper troposphere, they typically have a cold core below approximately 700 hPa, or generally below the level of maximum cyclonic circulation. Thus, a major theme of the early observational studies was the mechanism for transformation from a cold core to a warm core in the lower troposphere (Riehl, 1948; Hubert, 1955; Yanai, 1961). A transformation from cold core to warm core was observed by Davidson et al. (1990) prior to the formation of two tropical cyclones during the Australian Monsoon Experiment (AMEX). These two cyclones were well observed as they formed within an approximately 600-km diameter array of six rawinsonde stations. Approximately 2-3 days prior to cyclone formation, the vorticity maximum migrates downward to approximately the top of the boundary layer (900 hPa), which implies the establishment of a lower-tropospheric warm core. The physical mechanism for this downward migration of the mid-level vortex toward the surface, and thus into contact with the oceanic heat and moisture source, is one of the missing links in our understanding of tropical cyclone formation.

2.4.3 Small vertical wind shear

One of the environmental factors associated with the mean seasonal and geographical distributions of tropical cyclone frequency is small vertical shear of the horizontal wind. For example, Gray (1984a) and Shapiro (1987) have found inverse relationship between frequency of cyclones in the North Atlantic Ocean and seasonal mean vertical wind shear. It is also generally accepted that a small vertical wind shear is a necessary condition for an individual pre-existing disturbance to develop into a tropical cyclone. The physical reasons usually given for the importance of small (or even zero) shear is to accumulate moisture and temperature anomalies in a vertical column above the incipient disturbance. By contrast, the presence of large vertical shear is said to "ventilate" the column by advecting the warm core aloft away low-level circulation centre. Some support for this idea is provided in the numerical simulations of Tuleya and Kurihara (1981), Kurihara and Kawase (1985) and Tuleya (1988). In those studies, the vertical wind shear had to be such that a strong vertical coupling exists via the phase speed of the incipient (low-level) disturbance and the upper level winds. This coupling serves to keep

the warm area above the disturbance and thereby maintains a favorable condition for growth of the disturbance.

2.4.4 Curved cloud features

Although the horizontal scale of the pre-existing convective cloud cluster is usually of the order of 500 km, it may range from as small as 200 km too as large as 1500 km. A persistent cloud cluster consists of many Mesoscale Convective Systems (MCSs) that are continually evolving on time scales of 6-18 hr. This MCSs are associated with a number of cumulonimbus elements that feed moisture to a deep altostratus deck.

Dvorak (1975, 1984) states that the convective elements form into curved cloud lines or bands approximately 36 hr prior to classification as a tropical cyclone. According to Dvorak, "a T1 classification is made when curved cloud lines or bands indicate that a system centre has been near to or within a deep-layer convective cloud system for a period of at least 12 hours. It is the close association of moderately curved cloud lines or bands and a sizeable amount of deep-layer convection that signals cyclogenesis." This configuration can appear in various forms.

2.4.5 Mid-level mesoscale vortex

Mesoscale Convective Complexes (MCC's) were first identified as long-lived convective weather systems in the middle latitudes by Maddox (1980), Fritsch and Maddox (1991) and Bosart and Sanders (1981). Similar systems have been identified in other regions of the world (Houze et *al.* , 1981; Velasco and Fritsch, 1987 and Fritsch, 1991). The MCSs can be identified as the large areas of cloud with temperatures lower than - 70°C, which signifies the presence of long-lived altostratus decks. A pre-cyclone cloud cluster may contain one or more MCSs.

In mid-latitude MCCs with an intensifying Mesoscale Convective Vortex (MCV), the system becomes stronger, persists longer, and induces heavy precipitation (Bosart and

Sanders, 1981; Kuo *et al.*, 1986). In some cases the vortex appears to be responsible for subsequent development of MCCs Menard and Fritsch (1989).

Velasco and Fritsch (1987), Frank and Chen (1991), and Chen and Frank (1993) have hypothesised that ``if an MCC forms or propagates into a large-scale environment favourable for tropical cyclogenesis, the MCC - generated warm-core vortex may play a catalytic and crucial role in initiating tropical storm development" (Velasco and Fritsch, 1987). Such a hypothesis appears to be consistent with the study of Zehr (1992) based on satellite data, operationally analysed wind fields and reconnaissance aircraft data in the Western North Pacific. In the early stages, the vorticity maximum is in the middle troposphere between 700 and 300 hPa and no appreciable vorticity is detected near the surface. In the TEXMEX studies, the surface flow is divergent below the mesovortex. McKinley and Elsberry (1993) and Ritchie (1993) note that the pre-cyclone cloud cluster may contain a number of ``secondary" mesovortices that appear to be directly related to altostratus areas with strong convection.

These preliminary observations suggest that the central core of the cyclone may begin as a small vortex at middle levels that extends downward toward the surface and increases in horizontal scale.

Zehr (1992, 1993) and Emanuel (1993) have divided the formation process into two or more stages with an important transition point being the formation of the persistent mesoscale vortex. In Zehr's stage 1, a mesoscale vortex is embedded within the pre-existing disturbance (cloud cluster) circulation. During stage 2, the central pressure of that vortex decreases and the tangential wind increases to result in a minimal tropical cyclone.

2.4.6 Interaction with upper-level disturbances

Case studies by many authors (Riehl, 1948; Bath *et al.* , 1956; McRae, 1956; Fett, 1966, 1968; Ramage, 1974; Sadler, 1976, 1978; McBride and Keenan, 1982; McBride and Holland, 1989) have demonstrated an apparent initiation of the formation process through interaction with surrounding upper-tropospheric synoptic systems, particularly upper level

troughs. In particular, Sadler (1976, 1978) showed that cyclone formation in the western North Pacific frequently occurs in association with intense cyclonic cells embedded within a large-scale climatological feature known as the Tropical Upper Tropospheric Trough. McBride and Keenan (1982) showed that rapidly developing tropical cyclones in the Australian region were associated with slowly moving troughs in the upper troposphere displaced by approximately 5° longitude on either side of the developing disturbance. On the other hand, slowly developing cyclones were associated with fast moving upper-level troughs, which usually lay over the disturbance at the time of classification as a tropical cyclone.

2.5 Theoretical Models and Physical Concepts

No primary mechanism has been isolated as being responsible for the formation of tropical cyclones. It is generally accepted that the basic source of energy for the formation of a tropical cyclone is the latent heat released in clouds, and that in turn is acquired from the underlying sea through the surface evaporative flux. The mature tropical cyclone is a vertically stacked, warm core vortex occupying the complete depth of the troposphere. The tangential winds are to first order in gradient balance with this warm core. Frank (1987) noted that the average rainfall within the inner 200 km radius of a typhoon averages about 10 cm /day which provides sufficient latent heat release to heat the atmosphere from the surface to 100 hPa at a rate of about 25°C/day. Although rainfall in a cloud cluster is approximately 1/ 4 th of this value, it is still sufficient to heat the troposphere by 6°C/day. In a non-developing cluster, this latent heat release is offset by the expansion cooling in the ascending cores, and the net warming is small (order of tenths of a degree). When a tropical cyclone actually forms, the net response is of the order of 1°C/day warming integrated through the depth of the troposphere.

The approximate balance in the tropics between the diabatic heating and the adiabatic cooling associated with upward vertical motion can be understood in terms of scaling of the large-scale equations (e.g. Charney, 1963; Webster, 1983), or in terms of geostrophic adjustment theory, or of Eliassen balanced vortex theory. In summary, the ambient conditions in the tropics are such that inertial effects dominate over rotational effects.

Consequently, the energy released as heat is distributed in the form of potential energy over very large areas by gravity waves and by slowly varying divergent or secondary circulations. For this reason, theoretical studies of tropical cyclone formation have addressed processes that would allow the cloud cluster to retain the heat release locally.

Another fundamental question to the understanding of tropical cyclone formation is that of scale selection. Theoretical models of convection in a saturated environment have maximum growth at vanishingly small horizontal scales, i.e. the scale of individual cumulus clouds. A conceptual breakthrough occurred in the early 1960's in a series of studies that modelled tropical cyclone formation due to the Conditional Instability of the Second Kind (CISK) mechanism (Charney and Eliassen, 1964; Ooyama, 1964; Ogura, 1964; Kuo, 1965; Syono and Yamasaki, 1966). The CISK mechanism does require that the atmosphere be conditionally unstable (lapse rates between dry and moist adiabatic rates), but does not require large-scale saturation. In the presence of a background rotational field, the effect of the heating on the large-scale flow assumes a different functional form. Specifically, the cloud-scale condensation rate is proportional to vertical motion along a moist adiabat. In contrast, the collective effects of the heating on the large-scale motions are due to a distribution of individual cumulonimbus and mesoscale updrafts, downdrafts, altocumulus anvils, cloud radiative effects, etc.

A third issue in understanding the dynamical reasons for tropical cyclone formation is that it is a multi-stage process. These stages include the large-scale spin-up, the formation of the pre-existing convective disturbance or cloud cluster, the formation of a persistent mesoscale vortex, and the formation of an eye. It is highly likely that different dynamical mechanisms may be responsible for these different stages of formation. Once a particular stage of formation (even the first) has been reached, the other stages may follow automatically given the presence of sufficiently high sea-surface temperatures and given no dramatic changes in the large-scale flow.

2.5.1 Conditional Instability of the Second Kind (CISK)

The basic theoretical framework for many research studies of tropical cyclone formation (e.g. Syono and Yamasaki, 1966; Charney, 1973a, b; Bates, 1973; Koss, 1976; Mak, 1981; Fraedrich and McBride, 1989; Wiin-Nielson, 1993) has been the CISK theory. The basic concept is that the cyclone arises from a hydrodynamic instability produced by gravitation and Coriolis forces that utilises the latent heat energy released through condensation. Although CISK depends on the release of latent heat in a conditionally unstable atmosphere, it is distinctly different from the ordinary conditional instability that is responsible for the growth of the cumulus clouds. Three basic assumptions are made: (i) the initial perturbation is a synoptic-scale wave with quasi-geostrophic or "balanced" dynamics such that boundary layer convergence occurs in regions of low-level cyclonic vorticity; (ii) latent heat release will occur in the free atmosphere above these regions of frictionally-induced upward motion; and (iii) the magnitude of this heat release is proportional to the Ekman pumping. A feedback loop occurs in the regions of low-level cyclonic vorticity where upward motion is forced at the top of the boundary layer due to Ekman-induced frictional convergence. Since this increase in low-level vorticity will be accompanied by an increase in Ekman pumping and an increase in latent heat release, a positive feedback loop exists. According to Yamasaki (1988), the key to understanding CISK is the mechanism(s) by which cumulus convection is organized and convective activity is maintained for a long period of time.

A related instability known as Wave-CISK was developed by Yamasaki (1969), Hayashi (1970), Lindzen (1974), and others. This mechanism also assumes that the latent heat release in the free atmosphere is governed by convergence at low levels. In this case, the ascending motion incorporated in the dynamics of an equatorial wave mode governs the organisation of the convergence. Bolton (1980) demonstrated that the instability is mathematically equivalent to large-scale convective overturning (*i.e.* conditional instability of the first kind). The difference is that the vertical structure of the unstable waves gives a complex form to the heating. Thus, Wave-CISK modes are amplified and also propagated, owing to the phase shift between vertical velocity and heating.

The major application of the Wave-CISK to tropical cyclone formation was by Kurihara and Kawase (1985). Through both linear and non-linear integration of a highly simplified numerical model, they demonstrated that the Wave-CISK mechanism can reproduce the transformation of a synoptic wave in the easterlies into a warm-cored closed vortex (Kurihara and Kawase, 1985, 1986; McBride and Willoughby, 1986).

Criticisms of CISK-type instabilities as a mechanism for understanding tropical cyclone formation have been given. Emanuel (1989) states that the CISK models are based on an incorrect assumption that a reservoir of Convective Available Potential Energy (CAPE) exists to drive the large-scale motions. Since CAPE does not appear explicitly in the basic equation set of most CISK models, it is evidently assumed that surface heating and evaporation will maintain the CAPE at the initial value. A weakness of this class of models is that the major component of the physics is in the formulation of the cumulus parameterization, which necessarily contains coefficients dependent on the large-scale moisture field. As shown by Fraedrich and McBride (1995), the solutions vary significantly depending on how the model moisture budget is constructed. Because these theoretical CISK models do not have an explicit (*i.e.* prognostic) moisture equation, they are incomplete theories.

The original CISK mechanism and the large-scale overturning mechanism are both critically dependent on the Ekman lower boundary condition. Ooyama (1982) and Montgomery and Farrel (1993) noted that the assumed relationship is valid only after an incipient vortex has attained sufficient strength and organisation so that the cloud organizing mesoscale motions are correlated with the large-scale balanced flow.

2.5.2 Cyclone development as a response to heating

When heat is released as rainfall in the tropics there is usually only a very small local response in terms of realised warming or temperature change. The dynamical reason is that the horizontal scale of the heating is small so that gravity wave and other divergent circulation's dominate over rotational effects.

Tropical cyclone formation may be considered as a non-linear process where by local warming by cumulus convection and mesoscale elements is enhanced if the convection is confined to regions of relatively high inertial stability. Under these circumstances, the energy released as latent heat can bring about a localised increase in kinetic energy and vorticity, which further increases the local inertial stability, and therefore the "efficiency" of the heating. This process is fundamentally non-linear in character, which distinguishes it from the CISK models that depend on an instability that is present in the linearized equations.

An alternative method to bring about a localised warming of the tropical atmosphere may be through localised sources of momentum rather than of heat. The redistribution of mass by the secondary circulation exports energy away from the region of heating. Referring to the Eliassen balanced vortex equation, the secondary circulation is forced by the horizontal gradients in heat sources and by vertical gradients of momentum sources. McBride (1991b) and Davidson (1995) have proposed that the initial warming of the atmosphere in cyclone formation may occur in response to the direct modification of the vorticity fields by the cumulonimbus elements.

Another form of direct modification of the momentum fields is through the eddy import of angular momentum through interaction with surrounding upper-level weather systems.

2.5.3 Recent theories of tropical cyclone formation

Emanuel and co-authors (Emanuel, 1989, 1993; Yano and Emanuel, 1991; Emanuel *et al.*, 1994) proposed the tropical cyclones are formed by a mechanism known as WISHE (wind-induced surface heat exchange). The basic idea is that the latent heat release in the free troposphere is governed by the evaporation of moisture (and therefore moist static energy or θ_E) from the sea, which is primarily determined by the magnitude of the surface winds. Whereas the cumulus parameterization in a simplified WISHE model has heat release proportional to the low-level wind speed, in the CISK models it is proportional to the vorticity, which is effectively the gradient of the low-level wind speed. The WISHE mechanism alone will not bring about amplification of a large-scale, warmed-core vortex, because deep convection initiated through Ekman pumping will typically be accompanied

by convective-scale downdrafts that will lower the moist static energy of the subcloud layer air. This cooling and drying will negate any increase in moist static energy due to the increased surface winds, and the vortex will decay.

Based on the observations in the TEXMEX experiment, the additional condition for amplification of an initial vortex is that the troposphere becomes nearly saturated on the mesoscale in the vortex core (Emanuel, 1989). That is, the mid-tropospheric minimum in moist static energy must be reduced so that evaporation of rain does not generate downdrafts that import cool, dry air to the subcloud layer. Thus, the enhanced surface fluxes associated with the strong surface winds near the core can increase the subcloud moist static energy and through convection can increase the temperature of the vortex core. In a moist tropical atmosphere, the WISHE process can thus act as a positive feedback to the warm-core cyclone (Emanuel *et al.*, 1994).

2.6 Physical mechanisms in tropical cyclone motion

Observational studies indicated that tropical cyclone move with some layer average of the lower tropospheric environmental flow. In case of symmetric vortex and a vertically and horizontally uniform basic current, it is show that on a flat earth the translation of the vortex is exactly equal to the speed and direction of the basic current. In terms of the vorticity equation, the vorticity tendency in the non-divergent, $\beta = 0$, and frictionless example will be equal to the horizontal advection of vorticity due to the basic current. Since the vortex is a relative vorticity maximum, the advection by the uniform basic current flow through the vortex leads to a positive (negative) tendency downstream (upstream) of the vortex centre. That is, the vortex is translated toward (away from) the positive (negative) vorticity tendency.

Observational studies have also indicated that the tropical cyclones have tracks that deviate from such a simple steering flow concept. The theoretical studies result in predictions of the asymmetric structures that may be compared with the observed propagation speed and direction. It will be shown that several physical processes lead to

an asymmetric circulation that has a wave number one structure with a flow between the gyres that leads to an additional advective component relative to the steering effect.

In the barotropic models, a rotating, spherical earth, which adds the β term in the vorticity equation, will be considered with a quiescent flow. Thus, any vortex motion in this case must be due to propagation.

When the baroclinic effects are included in the physical mechanism tropical cyclone motion arises. First, allowing the vortex to vary in the vertical will cause differential beta-induced propagation at various levels. Different results occur if the vortex has only cyclonic winds versus the more realistic case with anticyclonic circulation aloft. Second, diabatic and frictional processes increase the vertical coupling and may lead to symmetric heat release and wind structures that may produce track deviations relative to the environmental steering. Third, an environmental vertical wind shear may cause a vertical tilt of the vortex system that may lead to rotational motion or net meridional displacements depending on whether the vortex is purely cyclonic or includes an anticyclonic aloft, respectively.

2.6.1 Tropical cyclone baroclinic structure

Near the centre of a mature tropical cyclone, the vertical wind shear is small in the lower troposphere and the cyclonic circulation extends to great depths. However, an anticyclone is found aloft, especially at outer radii. Thus, a tropical cyclone can be represented as a pyramid-shaped cyclonic vortex penetrating upward into an anticyclone aloft. Because the radial extent of the cyclonic vortex decreases with increasing elevation, the propagation vector associated with the beta effect should diminish aloft based on barotropic model reasoning. Wang and Li (1992) tested this effect with a 10-level baroclinic model of a quiescent environment in which a tropical cyclone vortex had maximum winds at 900 hPa and decreased linearly to zero at 100 hPa. Such a vertical wind shear is consistent with a warm core in the tropical cyclone. The radial variation has a maximum at 200 km and decreases to zero at 750 km. Thus, the specified vortex has only cyclonic winds.

Because the Wang and Li model is adiabatic and frictionless (no heating or convective momentum mixing to maintain the warm core and vertical stacking), it is expected that the differential beta-effect propagation with elevation disperse the vortex. The key result is that this propagation vector is close to that expected from a barotropic model initialized with the vertically integrated vortex wind structure. Specifically, the upper (lower) levels of the vortex in the Wang and Li model propagate faster (slower) than would be expected based on beta plane reasoning for the wind structure at that level. Because the secondary vertical circulation that maintains a vertically coupled models.

Fiorino and Elsberry (1989a) demonstrated that the advection of symmetric vorticity by the wave number one gyres is the primary term in the vorticity equation on a beta plane with a quiescent flow. In particular, positive (negative) vorticity regions will be found to the north-west (south-east) of the centre at each level. This vorticity advection dipole will initially have a maximum value at 900 hPa and decrease upward because of the assumed vortex structure. This differential vorticity advection will lead to an downward (upward) vertical motion ahead of (behind) the propagating storm. The existence of a deep vertical motion couplet with downward motion ahead and upward motion behind has been documented by Chan (1984) and confirm in a five-layer adiabatic model by Wang and Holland (1995). In the Wang and Holland model, the vertical profile of tangential winds was nearly constant up to about 600 hPa, so the maximum vertical motion was near this level.

From mass continuity considerations, the vertical motion differences must be balanced by horizontal convergence/divergence. Horizontal convergence above 900 hPa will create positive vorticity tendencies ahead of the cyclone, and negative vorticity tendencies aloft will be created behind the cyclone due to the divergence. Because the cyclonic vortex will tend to move the positive vorticity tendency region aloft, it will actually be displaced faster than the beta-plane propagation vector expected at upper levels. Conversely, the vortex displacement at 900 hPa will be smaller than expected. In addition, the vertical velocity advections associated with the vertical motion in the secondary circulation contribute to negative (positive) vorticity tendencies at low levels ahead (behind) the vortex. Therefore,

the net translation of the vortex at low levels is slower than the beta-plane propagation expected for the vortex structure.

The combined barotropic-baroclinic reasoning leads to a secondary circulation that is consistent with a propagation vector that is slower (faster) than expected values at lower (upper) levels. As Wang and Li (1992) demonstrate, a completely cyclonic vortex remains vertically coherent. When Wang and Li add an anticyclonic flow aloft to better represent the tropical cyclone structure the anticyclone moves west-south-west while the cyclone below moves north-west. This separation of the centres occurs due to lack of a vertical coupling mechanism as in the secondary circulation associated with the completely cyclonic vortex. Thus an adiabatic model can not sustain the anticyclone aloft over the tropical cyclone against the beta-effect dispersion.

2.6.2 Diabatic contributions to motion

The diabatic processes occur on a range of scales from small convective towers, spiral rain bands, and the secondary circulation (inflow at low levels, ascent in the eye wall, and outflow aloft). Clearly, a fine horizontal resolution is required to address the heating and flow responses on all of these scales. Even given the proper grid resolution, the physical processes in such clouds may not be well presented by latent heat parameterization presently available. The relationships between the frictional and diabatic processes are critical in the tropical cyclone.

Shapiro (1992) includes convective heat release in response to boundary layer friction and the convective momentum transports. Although only three layers are used in the vertical, a multiple-nested grid allows a wide range of horizontal scales to be simulated.

The vertical heating distribution creates negative potential vorticity anomalies in the upper layer of the Shapiro model and the convective momentum flux deposits positive potential vorticity from below.

Flatau *et al.*, (1994) avoid the spatial and temporal variability's of the diabatic frictional processes of real tropical cyclones by imposing a constant heat source, which has the advantage that the diabatic input is presently known. Because the heat source is continually added over the low-pressure centre and minimal frictional damping is included, the vortex continues to develop in the three dimensional model.

In the Wang and Holland (1995) model, the only diabatic process is a CISK-type convective heating proportional to the relative vorticity in the lowest middle layer. Wang and Holland include a frictional boundary layer with a wind speed-dependent drag coefficient, and horizontal and vertical diffusion of momentum and heat on the grid scale. Thus, the Wang and Holland model is more similar to the Shapiro model than the Flatau *et al.* model.

Wang and Holland (1995) also examined the various terms in the vorticity equation for the diabatic model to compare with the adiabatic model. The vertical advection of vorticity is an important term in the middle and upper troposphere in advancing the upper portion of the vortex to maintain a vertical consistency with the lower troposphere vortex. As in the adiabatic model, this vertical advection is a result of vertical motion induced by other physical processes, and thus is a secondary process rather than a first-order effect.

Flatau *et al.*, (1994) superposed their analytical heating function directly over the surface pressure centre, which would tend to maintain the low centre in its present location. That is, the Flatau et *al.* (1994) application of the heat source would tend to retard the vortex motion relative to the vorticity advection that is tending to propagate the vortex forward.

2.6.3 Vertical shear effects

The basic physical mechanism for tropical cyclone motion due to vertical shear in the environmental flow arises from a vertical tilt of the vortex. The tilt of the anticyclone to the east due to a westerly shear should induce (based on the invertibility principle of Hoskins *et al.*, 1985) a northward deflection of the low-level vortex. Conversely, the flow around the low-level vortex should induce a northward deflection of the upper level

vortex. Thus, the cyclone-anticyclone couplet can translate northward together. With an easterly shear, the anticyclone aloft is tilted to the west, and this upper level potential vorticity anomaly induces a southward flow across the low-level cyclone. Conversely, the projection upward of the low-level vortex will induce a southward flow across the upper layer anticyclone. In the easterly shear case, the cyclone-anticyclone couplet can translate southward together. Thus, Northern (Southern) Hemisphere tropical cyclones are expected to translate the left (right) of the vertical wind shear vector as the upper-level anticyclone becomes tilted relative to the centre.

Vortex motion in baroclinic conditions is much more complicated than in barotropic conditions. First, the baroclinic structure of a lower cyclone and an upper anticyclone leads to different propagation directions on a beta plane. Wang and Li (1992) showed that the cyclonic vortex tends to remain vertically coupled even in an adiabatic model. With the diabatic and convective momentum fluxes associated with the deep convection near the centre of tropical cyclone, the tendency for the vortex to remain vertically coupled and upright is even stronger. The baroclinic models of Shapiro (1992), Flatau et al 1994, and Wang and Holland (1995), strongly indicate that the motion of the tropical cyclone is governed by the dynamics of the lower cyclonic circulation. In particular, the cyclone tends to propagate relative to the potential vorticity gradient as though it were a barotropic vortex with a vertically averaged wind profile over the cyclonic layer. Thus, the first order propagation effect in baroclinic conditions is the same as in the barotropic models. However, asymmetries in the heating and friction may also contribute to deflections relative to the environmental steering. For example, stronger heating on one side may lead to greater surface pressure falls, which may deflect the low-pressure centre toward that direction. The evolution of the anticyclonic outflow layer in the multi-layer baroclinic models appears to contribute little to track changes, which is contrary to the simple two-layer model of Wu and Emanuel (1993). Moreover, the multi-level baroclinic model results agree with observations that dramatic changes occur in the outflow layers of tropical cyclone without noticeable changes in the track.

2.7 Tropical cyclone track prediction

2.7.1 Establishing the present location

The first step in tropical cyclone track prediction is to determine the present location of the storm centre. Because of the formation of tropical cyclone over the ocean, there are seldom-conventional meteorological observations near the centre. As the storm intensifies, the ships tend to avoid the cyclone centre, and the number of ship observation decreases.

Aircraft reconnaissance, which is now available on a regular basis only in the Atlantic region, is generally accepted to be the most accurate positioning method (average errors nearly 20 km). Radar provides frequent and relatively accurate locations when the storm is close to land and the eye is well developed. Unfortunately, the cyclone is frequently out of radar range (typically 400 km). Thus, the most important role of radar is for the landfall forecast. There may be inconsistencies in the centre position between the coastal radar's viewing the storm simultaneously, because the attenuation of the radar beams from different angles may vary considerably. Position errors derived by radar vary from 20 to 55 km depending on the degree of organisation of the tropical cyclone.

Satellite imagery has become the most important source of information on the location of tropical cyclones throughout the globe. The Dvorak (1984) technique is widely used in combination with spiral overlays and subjective interpretations. Though polar-orbiting systems provide very detailed views of the convection in the tropical cyclone, geostationary satellite provide more frequent images that may be animated to improve fix accuracy. Satellite-derived centre positions are less accurate when the incipient storm is in the early stages of development. Microwave imagery is particularly valuable when the centre is obscured, but the narrow swaths of these systems on polar orbiting satellites mean that cyclones may not be viewed in each orbit.

2.7.2 Persistence

One of the simple track prediction schemes is to assume persistence of recent motion. The physical basis for this assumption is that the entire tropical cyclone system has

considerable inertia that can not be turned rapidly. If the vortex, large-scale flow and the interaction processes do not change, the future motion should resemble the past motion. Thus, persistence is a reasonable, first order approximation for predicting short-term motion. Uncertainties in warning positions considerably affect the accuracy of persistence forecast. Considerable improvements in short-range predictions could result from improved initial motion vectors.

2.7.3 Climatology

A climatological track prediction assumes that the present storm will move with the average direction and speed of all past storms near that location. To make a track prediction, the climatological vectors at the appropriate locations are multiplied by the time interval and the displacements are added to the present latitude and longitude. This simple application of climatology does not take into account the variability in past tracks through each location.

A statistical combination of CLImatology and PERsistence (CLIPER) developed for the Atlantic region by Neumann (1972) has been extended to other basins (Leftwich and Neumann, 1977; Xu and Neumann, 1985). Predictors such as the present latitude and longitude, the components of recent motion of the storm and the intensity are used. Least-squares fitting of the basic predictors and various polynomial combinations is used in CLIPER to derive regression equations for future latitudinal/longitudinal displacements in 12-hr increments. Thus, this technique makes use of the ``climatology" of past tropical cyclone tracks and the persistence components of the present storm to generate a forecast.

2.7.4 Analogue technique

The basic assumption of the analogue techniques is that a given storm will move with the mean speed and direction of all storms that occurred in that region within some time interval centred on the current day. Automated techniques for selecting such analogous have been developed for the Atlantic by Hope and Neumann (1970), for the western North Pacific by Jarrell and Somervell (1970), for the eastern North Pacific by Jarrell *et al.* (1975), and for the Australian region by Annette (1978).

The utility of these techniques primarily depends on the accuracy of the initial positions and the applicability of the ``climatological-storm" assumption. Only in the analogue technique is the variance about the climatological mean position specified.

2.7.5 Baroclinic model

The objective of earlier dynamical tropical cyclone models (Elsberry 1987) had been to predict the future positions. The new models now include tropical cyclone related precipitation prediction as a secondary objective. In addition, the model developers are somewhat optimistic that trends in the intensity of the tropical cyclone may also be predicted with these higher resolution baroclinic models, even though the resolution is still not adequate to represent the details of the inner core wind distribution.

An important physical process in the tropical cyclone is the release of latent heat in convective and large-scale clouds. Most operational models use some modification of the Kuo (1974) representation of cumulus convection. This technique relates the total latent heat release to the moisture convergence in the column, and partitions of the moisture supply between moistening and heating of the environmental air during a moist adiabat ascent from the boundary layer. Iwasaki *et al.* (1987) found the Kuo technique had excessive cooling in the subcloud layer that damped the tropical cyclone. Chen *et al.* (1995) impose an analytical heating rate (maximum between 100°K/day to 400°K/day depending on typhoon intensity) as a lower bound.

The energy sources for the tropical cyclone is the latent heat and sensible heat gained from the warm tropical oceans. Thus the modern operational models directly predict these surface fluxes over the ocean and over the land. In most cases, the exchange coefficients for moisture, heat and momentum are dependent on wind speed.

Mathur (1991) also uses the observed central surface pressure observation in the QLM, except that values less than 970 hPa are set to equal to 970 hPa. The reported size is used to scale the symmetric vortex, except that the size must be at least 170 km. Mathur uses

an empirical vertical structure function to represent the cyclonic portion of the vortex. The anticyclonic portion aloft is assumed to be represented in the global model background fields, or will be developed during the integration. A gradient wind is calculated, but no secondary circulation or initial vertical motion is imposed as an initial condition. A relative humidity of almost 100% is specified near the centre to trigger convective latent heat release quickly.

Chapter 3

Analysis of Different Meteorological Parameters in the Surroundings of the Bay of Bengal during the Lifetime of Cyclones

3.1 Introduction

The intensity of the storm may be sensitive to even a small change in the temperature of the ocean or land surface. The physical parameters such as the surface roughness, surface albedo, and soil wetness (in case of land) are locally related to the surface exchange of heat and momentum (Y. Kurihara et al., 1992). The change in the wind speed of the tropical cyclone moving over land is determined by the surface frictional elements (e.g. grass, trees and buildings) and by hills and mountains.

It is generally accepted that the track and intensity of tropical cyclone in the tropics depend largely on the steering wind at the anticyclonic level (300 or 200 hPa) and the sea surface temperature (SST) respectively. Once formed, the cyclone is known to move over middle latitude oceans where the ocean is colder (Krishnamurti, 1979). Anjaneyulu et al. (1965) studied some aspects of Bay of Bengal cyclone of October 1963 and observed a noticeable zone of divergence to the northwest of the storm, the direction in which the storm subsequently moved. It is also noted that if there is large vertical wind shear the cyclone would degenerate. The cyclone is usually formed in an area of light wind shear (Steven and Stanly, 1984).

In view of the usually observed and theoretically hypothesised relations between different atmospheric parameters on the formation and movement of cyclones, in the present study, the different meteorological parameters such as wind speed and temperature in the surroundings of the Bay of Bengal have been investigated during different cyclonic periods. Several severe cyclonic storms with a core of hurricane winds and one cyclonic

storm formed in the Bay of Bengal which crossed Bangladesh coast in the last decade have been selected. The severe cyclonic storms with a core of hurricane winds of 1985, 1988, 1991, 1992 and 1994 and the cyclonic storms of 1992 are considered for analysis. Several stations such as Dhaka, Chittagong, Calcutta, Cuttack, Madras, Port Blair and Bangkok in the surroundings of the Bay of Bengal have been chosen to see the possible variation of temperature and wind speed over the area for different cyclones during their movement. The vertical wind shear has also been investigated on the basis of land observational data to study the relation with the movement of the cyclone.

3.2 Method of Analysis

The meridional wind, zonal wind and vertical wind shear during the life cycle of different cyclonic storms have been computed for different meteorological stations in the surrounding of the Bay of Bengal by using the relation (Essenwanger, 1985):

Meridional wind $v = -V\cos\phi$ (3.1)

Zonal wind $u = -V\sin\phi$ (3.2)

Vertical wind shear $V_{w.shear} = U_{200} - U_{850}$ (3.3)

where

ϕ = direction of wind speed

U_{200} = the zonal component of wind at 200 hPa, and

U_{850} = the zonal component of wind at 850 hPa.

For analysis of vertical wind shear, the available data have been plotted on synoptic maps. The maps for vertical wind shear have been analysed manually by using the standard technique.

3.3 Results

We have discussed some meteorological parameters for the severe cyclonic storms with a core of hurricane winds of 1994, 1992, 1991, 1988 and 1985 and the cyclonic storm of 1992. The tracks of the cyclones are shown in Figs. 3.3(a-f).

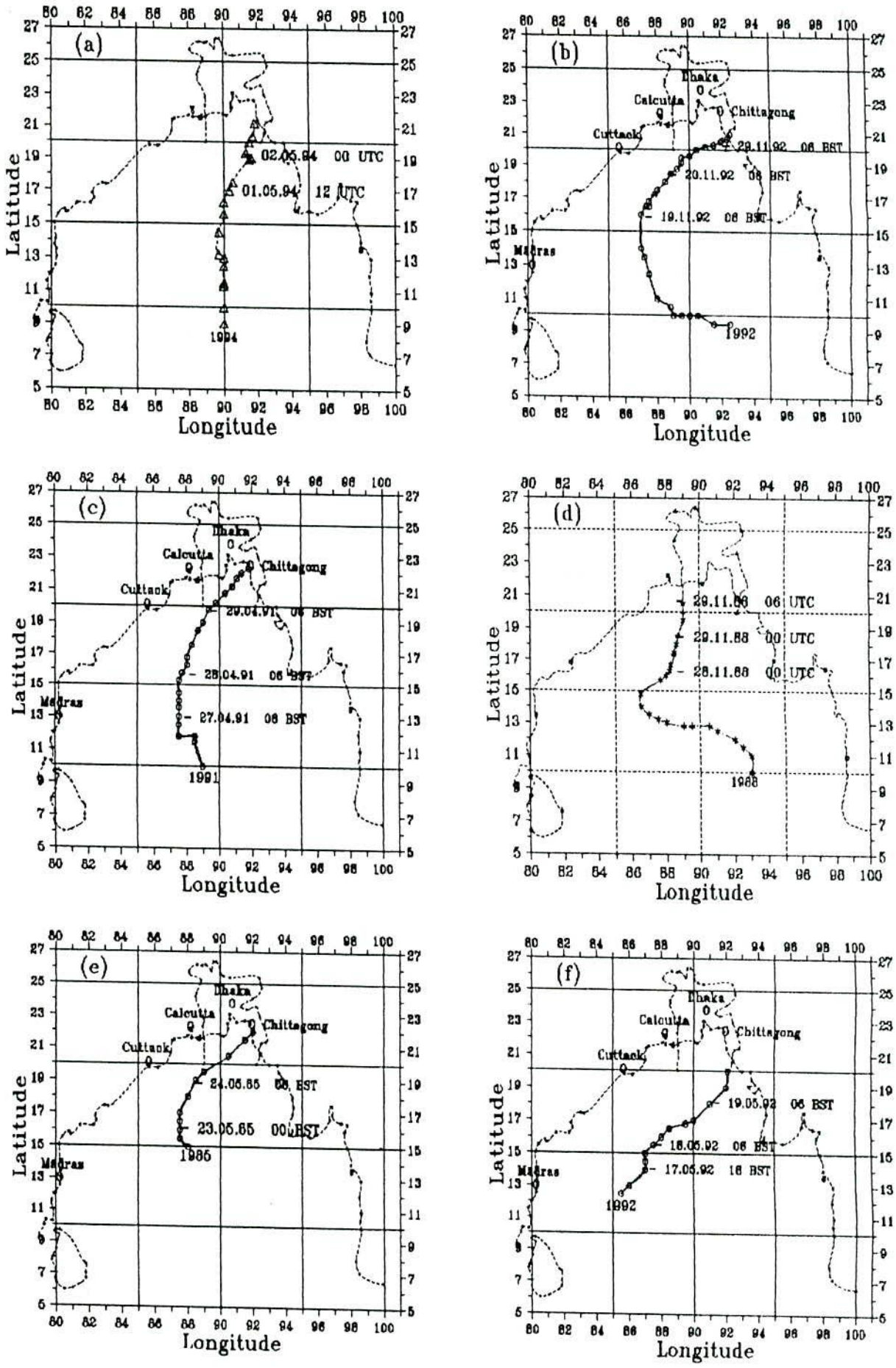

Figs.3.3(a-f) Tracks of severe cyclonic storm with a core of hurricane winds of 1994, 1992, 1991, 1988, 1985 and the cyclonic storm 1992 respectively.

3.3.1 Severe Cyclonic Storm with a core of hurricane winds of 1994

In this section we have analysed in detail the vertical variation of meridional wind speed, zonal wind speed and temperature for the severe cyclonic storm with a core of hurricane winds of May 1994. Day-to-day changes of these parameters have been discussed as the cyclone progress. The vertical wind shear has also discussed in the surroundings area on the day of landfall of the cyclone.

3.3.1.1 Meridional wind speed

The meridional wind speed increases (Fig. 3.3.1(a)) at all levels over Dhaka on 30th April with respect to that of 29th April 1994. The meridional wind speed decreases gradually over the station during 30th April to 2nd May as the cyclone moves towards the coast.

The meridional wind speed increases (Fig. 3.3.1(b)) from the surface to 750 hPa and decreases from 750 to 100 hPa over Chittagong on 30th April with respect to that of 29th April. The figure also shows that the meridional wind speed decreases at all levels on 2nd May with respect to that of 1st May over the station.

The meridional wind speed decreases (Fig. 3.3.1(c)) from surface to 550 hPa and increases significantly from 550 to 100 hPa over Calcutta on 1st May with respect to that of 30th April. It also shows that the meridional wind speed decreases gradually over the station during 1st to 3rd May as the cyclone moves just before and after the landfall.

The irregular pattern of meridional wind speed is observed (Figs. 3.3.1(d-e)) over Cuttack and Bangkok during 29th April to 2nd May.

The meridional wind speed increases (Fig. 3.3.1(f)) from the surface to 350 hPa and decreases from 350 to 150 hPa over Madras on 1st May with respect to that of 30th April. It also shows that the meridional wind speed decreases at all levels on 2nd May i.e. on the day of landfall and increases on 3rd May i.e. after the landfall with respect to that of previous day over the station.

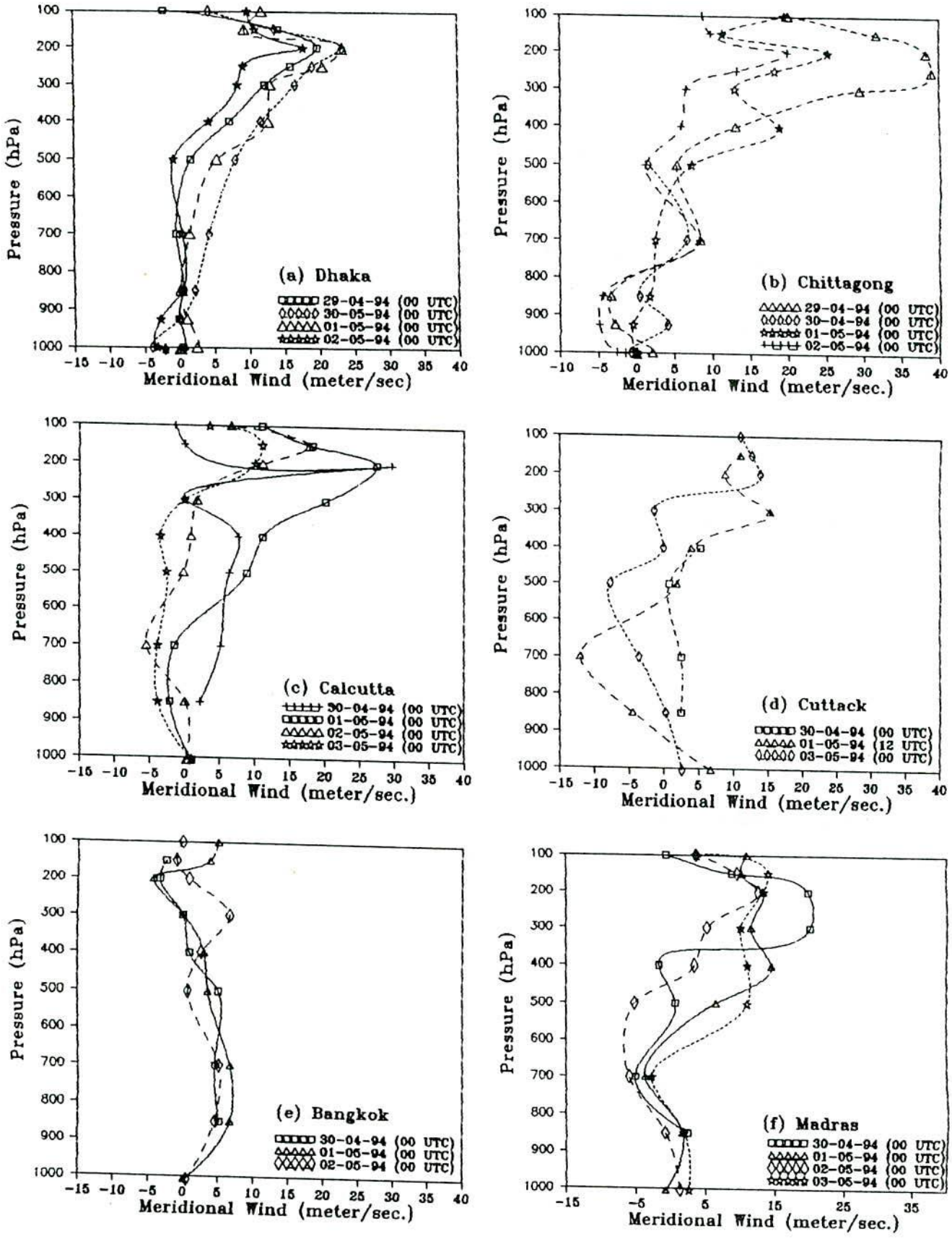

Figs. 3.3.1(a - f) Vertical profile of meridional wind over Dhaka, Chittagong, Calcutta, Cuttack, Bangkok and Madras for the cyclone 29th April to 2nd May 1994.

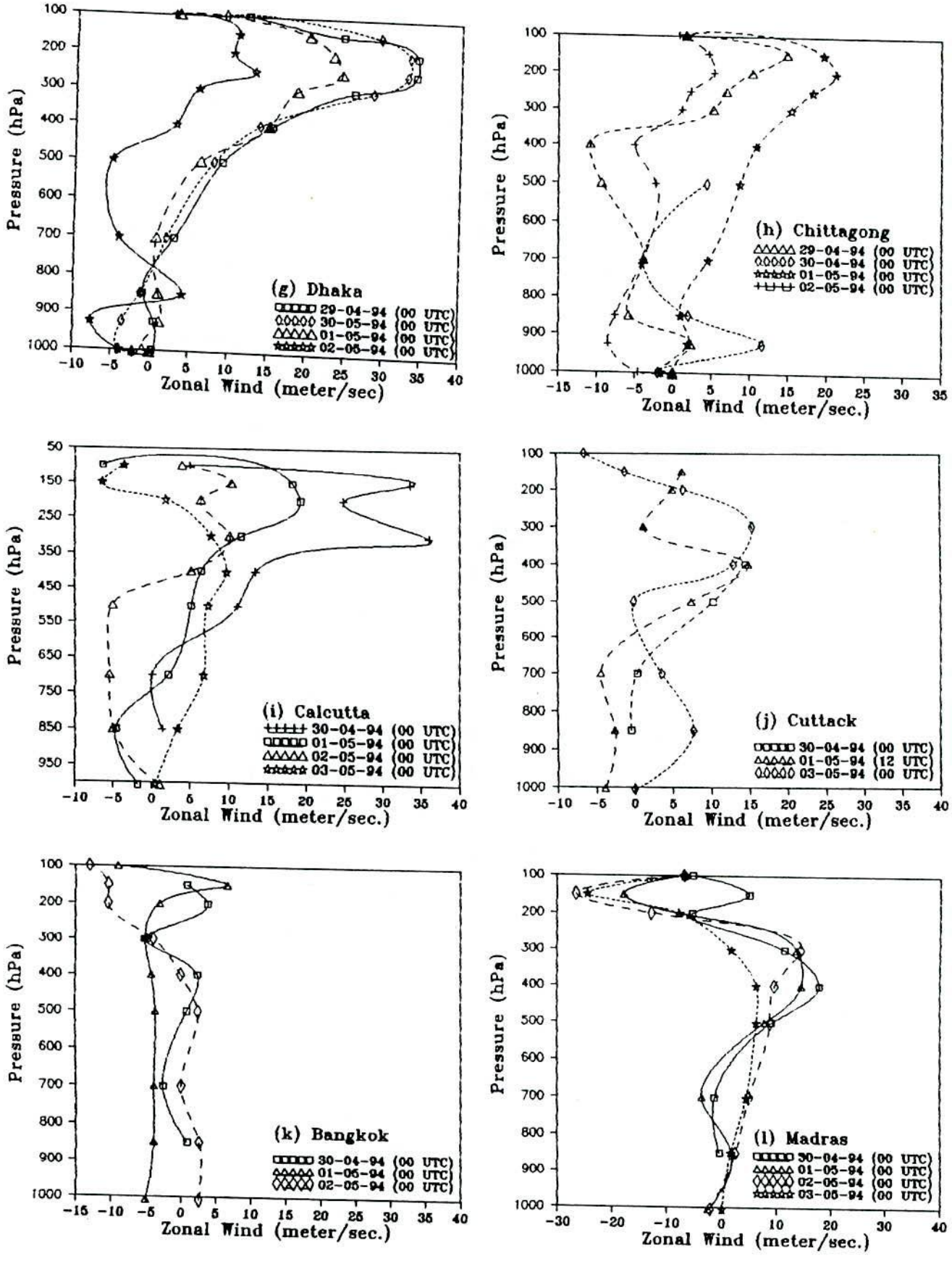

Figs. 3.3.1(g - l) Vertical profile of zonal wind over Dhaka, Chittagong, Calcutta, Cuttack, Bangkok and Madras for the cyclone 29th April to 2nd May 1994.

The result shows that the meridional wind speed decreases gradually in the region in which the cyclone moves. There is not any significant change of meridional wind speed in the region from where the cyclone goes far away. There is an exception that the meridional wind speed decreases on the day of landfall with respect to that of the previous day over Madras.

3.3.1.2 Zonal wind speed

The zonal wind speed decreases gradually (Fig. 3.3.1(g)) from 800 to 100 hPa and irregular pattern is observed below these levels over Dhaka during 29th April to 2nd May.

The Fig. 3.3.1(h) shows that the zonal wind speed increases gradually at all levels except little anomalies over Chittagong during 29th April to 1st May. It also shows that the zonal wind speed decreases at all levels on 2nd May i.e. on the day of landfall with respect to that of 1st May over the station.

In Fig. 3.3.1(i), it is observed that the zonal wind speed decreases gradually at all levels over Calcutta during 30th April to 2nd May. The figure also shows that the zonal wind speed increases from the surface to 350 hPa and decreases from 350 to 100 hPa on 3rd May i.e. after the landfall over the station.

Figure 3.3.1(j) shows that the zonal wind speed decreases at all levels with little anomalies over Cuttack on 1st May with respect to that of 30th April and increases on 3rd May with respect to that of 1st May.

The zonal wind speed decreases (Fig. 3.3.1(k)) over Bangkok on 1st May with respect to that of 30th April. It also shows that the zonal wind speed increases from the surface to 300 hPa and decreases from 300 to 100 hPa on 2nd May with respect to that of 1st May over the station.

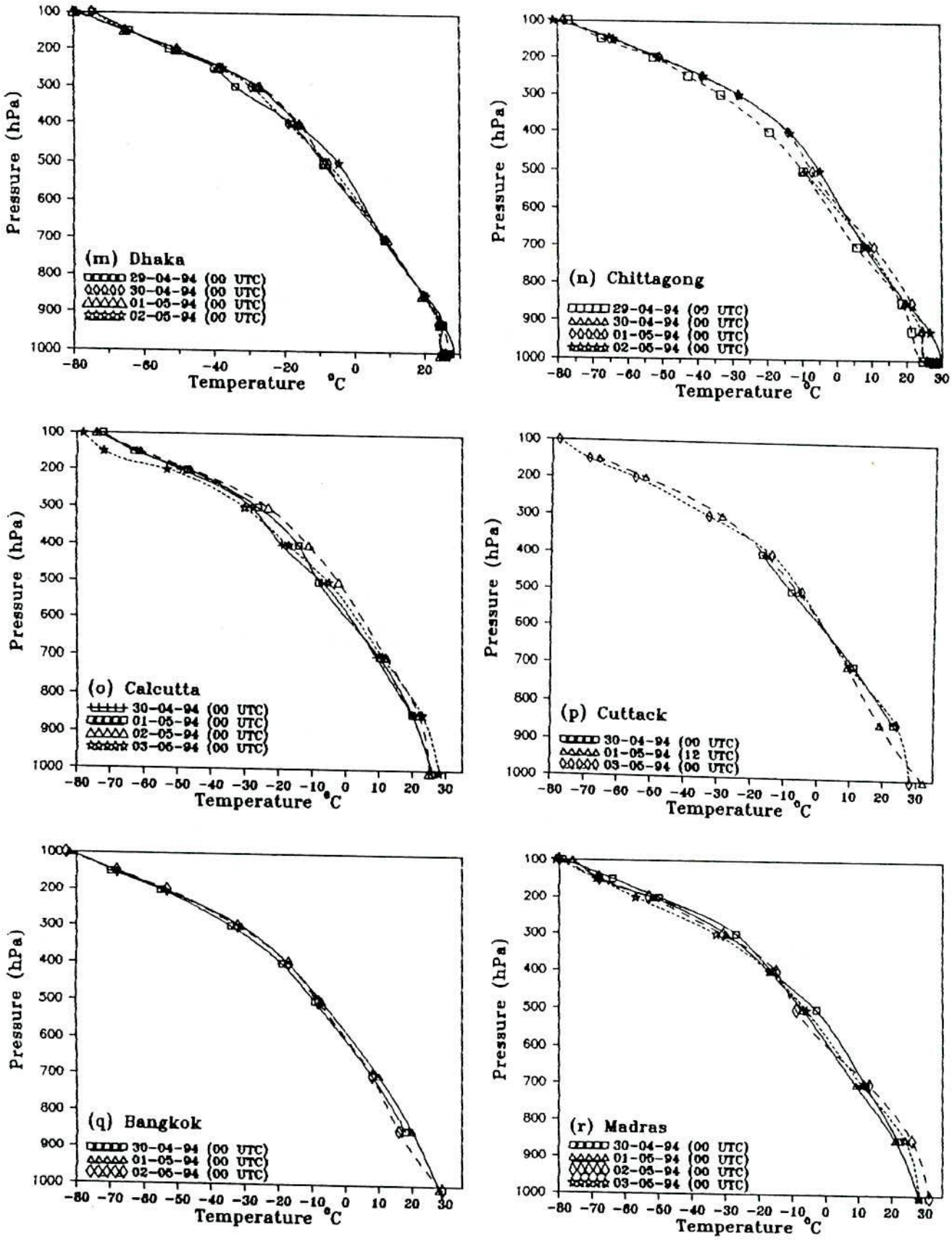

Figs. 3.3.1(m - r) Vertical temperature profile over Dhaka, Chittagong, Calcutta, Cuttack, Bangkok and Madras for the cyclone 29th April to 2nd May 1994.

The zonal wind speed decreases (Fig. 3.3.1(l)) at all levels over Madras on 1st May with respect to that of 30th April. It also shows that the zonal wind speed increases from the surface to 500 hPa and decreases from 500 to 100 hPa on 2nd May with respect to that of 1st May over the station.

The analysis shows that the zonal wind speed decreases gradually in the region in which the cyclone moves. The analysis also shows that the zonal wind speed increases in the region from where the cyclone goes far away.

3.3.1.3 Vertical temperature variation

The temperature is almost constant (Fig. 3.3.1(m)) from the surface to 600 hPa and from 300 to 100 hPa over Dhaka during 30th April to 2nd May. The figure also shows that the temperature increases from 500 to 300 hPa and 600 to 400 hPa on 1st and 2nd May respectively. The temperature increases from the surface to 400 hPa on 3rd May i.e. after the landfall.

The Fig. 3.3.1(n) shows that the temperature decreases from the surface to 600 hPa and almost same from 600 to 100 hPa over Chittagong on 2nd May with respect to that of the 1st May.

Fig. 3.3.1(o) gives the vertical variation of temperature over Calcutta which reveals that the temperature is almost constant from the surface to 500 hPa and increases from 500 to 200 hPa on 1st May with respect to that of 30th April. The figure also shows that the temperature increases from the surface to 200 hPa level over Calcutta on 2nd May with respect to that of 1st May. On 3rd May the temperature again decreases at all levels i.e. after the landfall with respect to that of 2nd May.

The temperature decreases (Fig. 3.3.1(p)) from the surface to 600 hPa level and increases from 600 to 100 hPa over Cuttack at 1200 UTC on 1st May with respect to that at 0000 UTC of 30th April. The figure also shows that the temperature increases from 950 to 350

hPa and decreases from 350 to 100 hPa over Cuttack at 0000 UTC on 3rd May with respect to that at 1200 UTC of 1st May.

The temperature increases (Fig. 3.3.1(q)) from 850 to 200 hPa over Bangkok on 1st May with respect to that of 30th April. The figure also shows that the temperature decreases from the surface to 500 hPa and is almost constant from 500 to 100 hPa levels on 2nd May with respect to that of 1st May over the station.

The temperature decreases (Fig. 3.3.1(r)) from 850 to 100 hPa over Madras on 1st May with respect to that of 30th April. The figure also shows that the temperature increases from the surface to 200 hPa on 2nd May with respect to that of 1st May and is almost constant from surface to 650 hPa and decreases from 650 to 100 hPa on 3rd May with respect to that of 2nd May over the station.

From the above discussion, it is found that the temperature decreases from the surface to 600 or 500 hPa and approximately constant above these levels on 2nd May with respect to that of 1st May over Chittagong and Bangkok respectively. The temperature increases from 600 to 400 hPa over Dhaka and at all levels over Calcutta and Madras on 2nd May with respect to that of the 1st May. It is also found that the temperature increases over Dhaka and decreases over Calcutta at all levels and in the upper troposphere from 700 to 100 hPa level over Madras on 3rd May with respect to that of 2nd May.

3.3.1.4 Vertical wind shear

Fig. 3.3.1(s) also shows little or no vertical wind shear near the centre of the cyclone on 2nd May at 00 UTC. The magnitude of this shear is approximately zero near the centre of the cyclone. Vertical wind shear is large towards the north at a greater distance from the centre of the cyclone. As the distance increases towards the north of the cyclone centre, the horizontal gradient of vertical wind shear increases gradually.

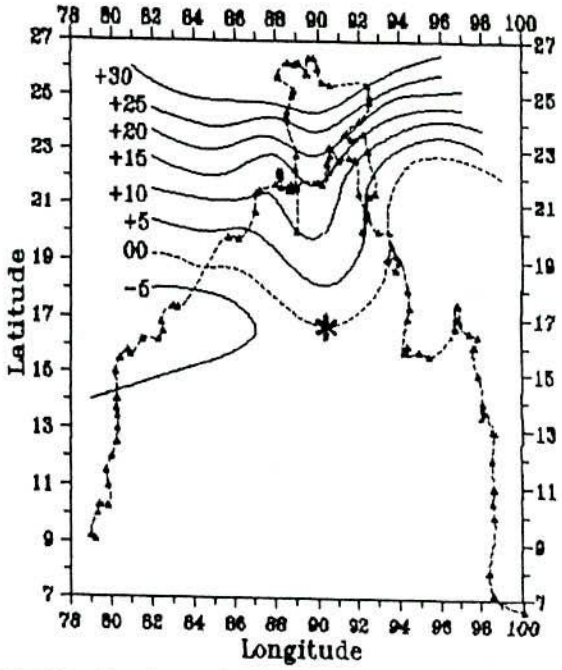

Fig. 3.3.1(s) Distribution of vertical wind shear on 2nd May 1994

3.3.2 Severe Cyclonic Storm with a core of hurricane winds of 1992

We have analysed in detail the vertical variation of meridional wind speed, zonal wind speed and temperature for the severe cyclonic storm with a core of hurricane winds of 1992. Day-to-day changes of these parameters have been discussed as the cyclone progress. The vertical wind shear has also discussed in the surroundings area on the day before the day of landfall of the cyclone.

3.3.2.1 Meridional wind speed

The meridional wind speed decreases (Fig. 3.3.2(a)) at all levels over Dhaka on 18th November with respect to that of 17th November 1992. It also shows that the meridional wind speed increases from surface to 800 hPa and 250 to 100 hPa level, and decreases from 800 to 250 hPa on 20th November with respect to that of 19th November. The figure also shows that the meridional wind speed decreases at all levels over the station on 21st November i.e. on the day of landfall with respect to that of the previous day.

Fig. 3.3.2(b) shows that the meridional wind speed increases from the surface to 800 hPa and 300 to 100 hPa and decreases from 800 to 300 hPa over Chittagong on 19th November with respect to that of 17th November. It also shows that the meridional wind

speed decreases from the surface to 750 hPa and increases from 750 to 100 hPa on 20th November with respect to that of 19th November. Also the meridional wind speed increases significantly from surface to 600 hPa and decreases significantly from 600 to 300 hPa level on 21st November with respect to that of 20th November over the station.

Over Calcutta, the meridional wind speed decreases gradually (Fig. 3.3.2(c)) at all levels during 19th to 21st November as the cyclone moves towards the landfall.

The meridional wind speed increases (Fig. 3.3.2(d)) at all levels on 18th November with respect to that of 17th November and decreases up to 300 hPa over Cuttack on 20th with respect to that of 19th November. It also shows that the meridional wind speed increases gradually from 250 to 100 hPa levels over the station during the period.

There is no regular increasing or decreasing (Fig. 3.3.2(e)) tendency of meridional wind speed over Bangkok during the period. The meridional wind speed decreases gradually (Fig. 3.3.2(f)) from surface to 300 hPa and has no regular trend from 300 to 100 hPa over Port Blair during 18-20th November.

The above analysis show that the meridional wind speed decreases over Dhaka and Calcutta during the life cycle of the cyclone and increases over Chittagong on 20th and 21st November. The result also shows that the irregular pattern of meridional wind speed is observed over Cuttack, Bangkok and Madras during the period. The analysis also shows that the meridional wind speed decreases during 18-20 November over Port-Blair.

3.3.2.2 Zonal wind speed

Fig. 3.3.2(g) shows the vertical variation of zonal wind speed over Dhaka. The figure shows that the zonal wind speed increases at all levels over Dhaka on 18th November with respect to that of 17th November. It can also be seen that the zonal wind speed decreases at all levels on 20th November with respect to that of 18th November and increases at all levels on 21st November with respect to that of 20th November over the station.

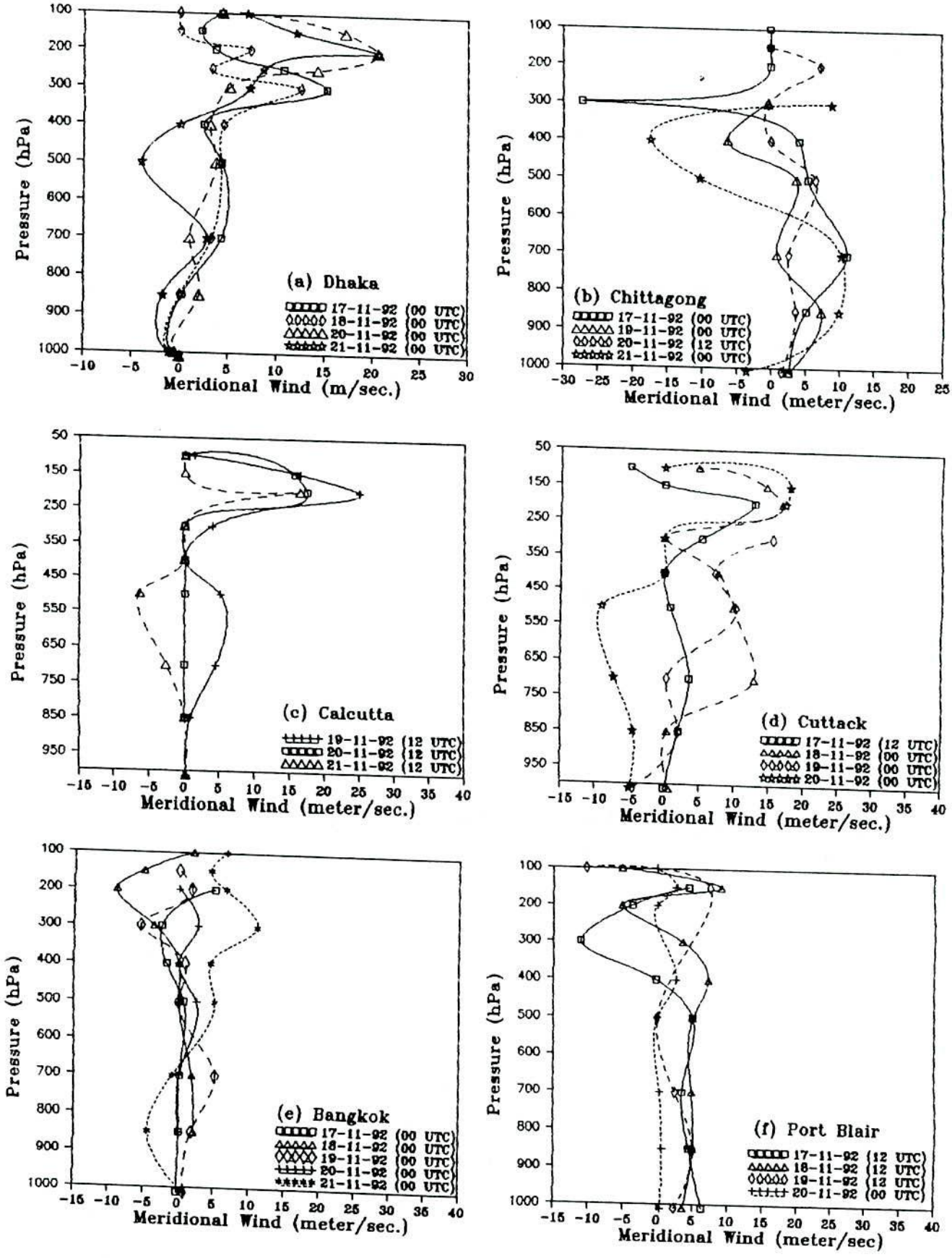

Figs. 3.3.2(a - f) Vertical profile of meridional wind over Dhaka, Chittagong, Calcutta, Cuttack, Bangkok and Port Blair for the cyclone 17 - 21 November 1992.

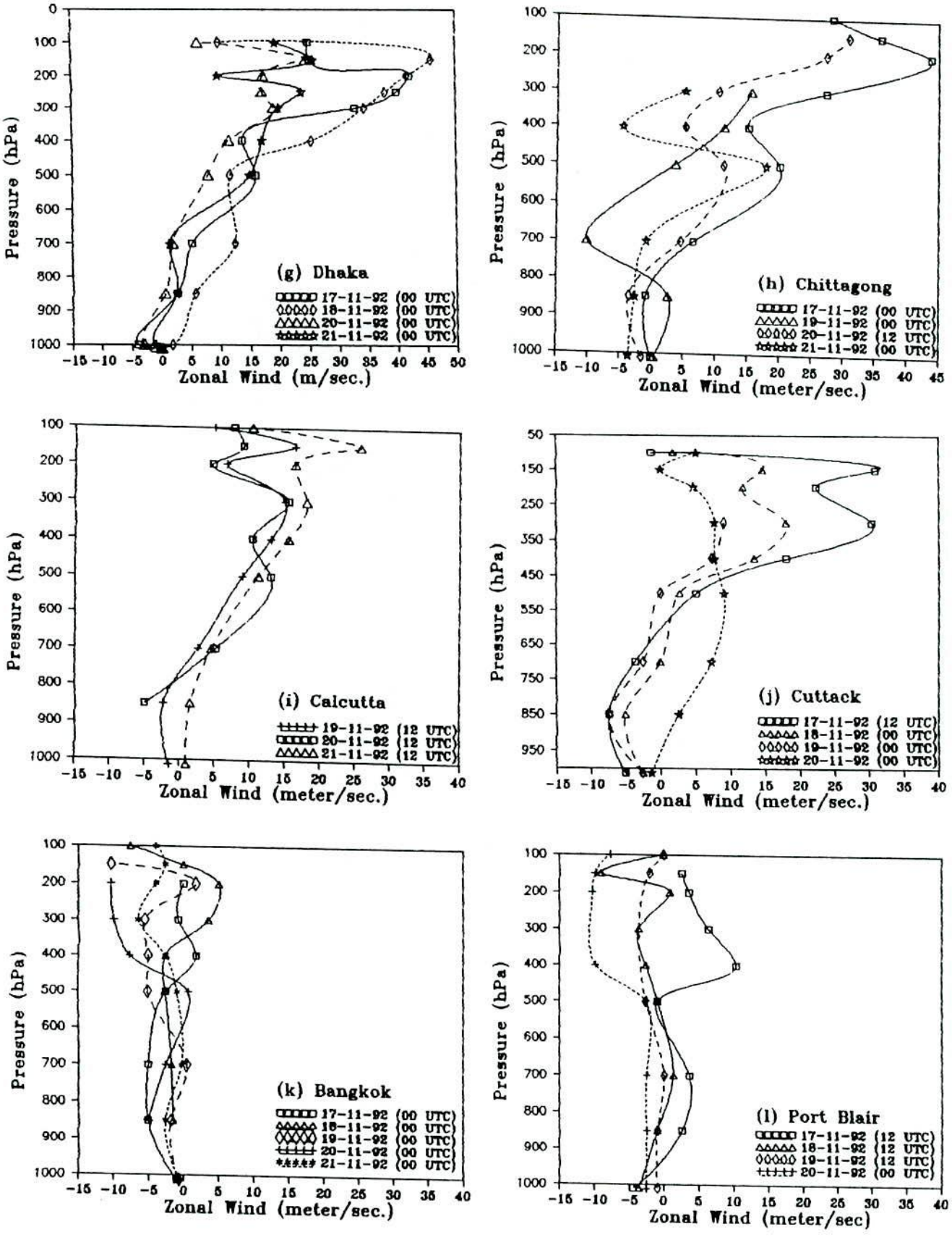

Figs. 3.3.2(g - l) Vertical profile of zonal wind over Dhaka, Chittagong, Calcutta, Cuttack, Bangkok and Port Blair for the cyclone 17 - 21 November 1992.

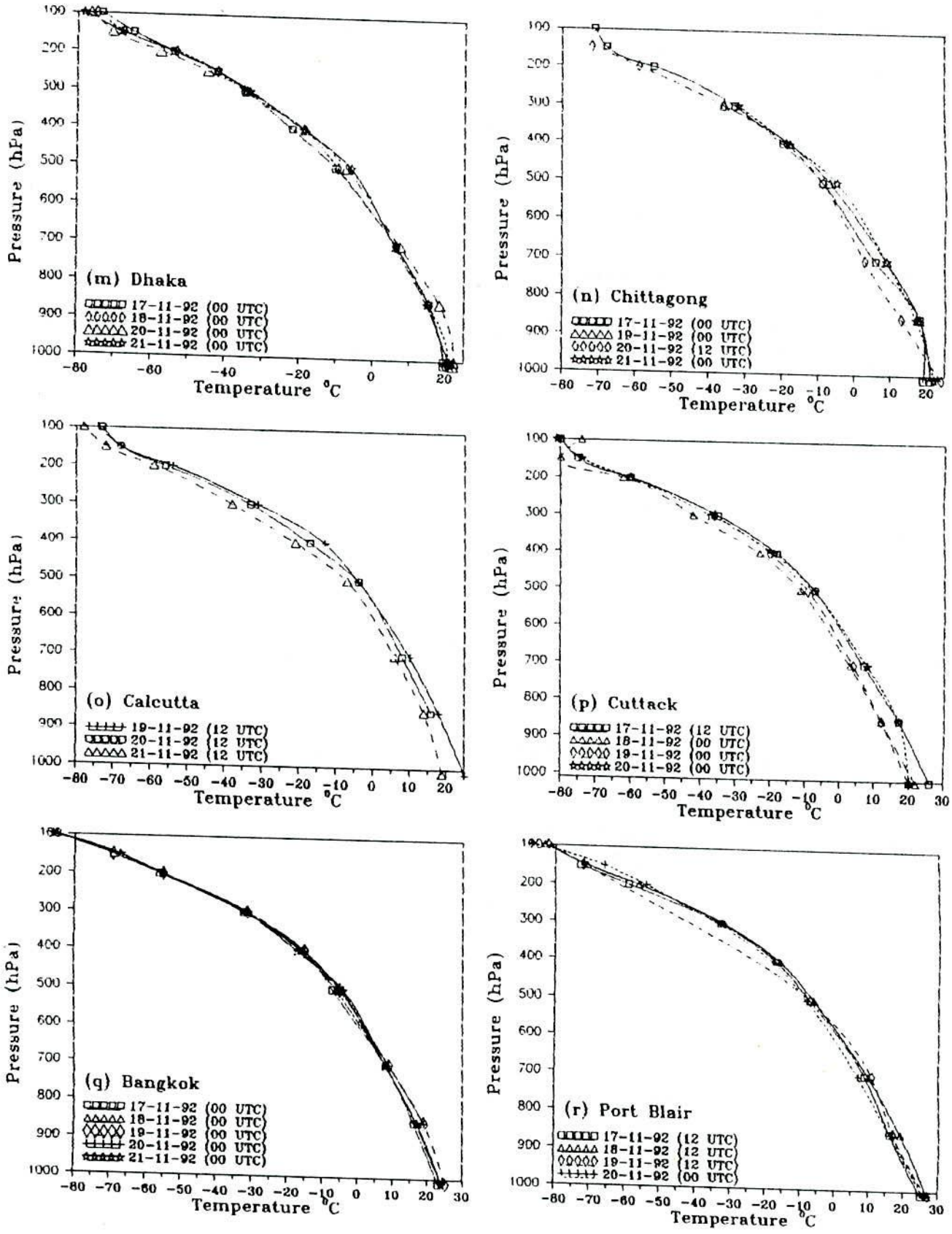

Figs. 3.3.2(m - r) Vertical temperature profile over Dhaka, Chittagong, Calcutta, Cuttack, Bangkok and Port Blair for the cyclone 17 - 21 November 1992.

Over Chittagong the zonal wind speed increases from the surface to 800 hPa and decreases from 800 to 100 hPa on 19th November with respect to that of 17th November as can be seen from Fig. 3.3.2(h). The figure also shows that there is no regular increasing or decreasing pattern of wind speed over the station during 19-21 November.

The Fig. 3.3.2(i) shows that the zonal wind speed increases gradually at all levels having some anomalies over Calcutta during 19th to 21st November as the cyclone moves towards the landfall. The zonal wind speed increases gradually from the surface to 450 hPa and decreases from 450 to 100 hPa with little anomalies over Cuttack during 17-20 November as are evident from Fig. 3.3.2(j).

There is no regular increasing or decreasing pattern (Fig. 3.3.2(k)) of zonal wind speed observed over Bangkok during 17-21 November. The zonal wind speed decreases gradually (Fig. 3.3.2(l)) over Port-Blair during 17-20 November.

The analysis shows that zonal wind speed has no regular trend over Dhaka, Chittagong and Bangkok during the movement of the cyclone. The analysis also shows that the zonal wind speed decreases gradually over Madras and Port-Blair and increases gradually with little anomalies over Calcutta and Cuttack during the movement of the cyclone.

3.3.2.3 Vertical temperature variation

Little or no temperature variation (Fig. 3.3.2(m)) is observed at all levels over Dhaka on 17th and 18th November. It also shows that the temperature increases significantly on 20th November with respect to that of 17th and 18th November and decreases at all levels on 21st November with respect to that of 20th November. The data were not available on 19th November over the station.

Fig. 3.3.2(n) shows that the temperature increases from the surface to 350 hPa over Chittagong on 19th November with respect to that of 17th November. The figure also shows that the temperature decreases from surface to 400 hPa and is constant above these

levels on 20th November with respect to that of 19th November and increases from surface to 300 hPa level on 21st November with respect to that of 20th November over the station.

It is seen from Figs. 3.3.2(o & p) that the temperature decreases gradually at all levels over Calcutta and Cuttack during 19-21 November and 18th November with respect to that of 17th November respectively. There is little or no change of temperature over Bangkok during 17-20 November as seen from Fig. 3.3.2(q). The temperature decreases at all levels on 21st November with respect to that of any other days over Madras.

The temperature increases (Fig. 3.3.2(r)) slightly at all levels over Port Blair on 18th November with respect to that of 17th November. The temperature decreases at all levels having little anomalies on 19th November with respect to that of 18th November and decreases from surface to 500 hPa and increases from 500 to 100 hPa on 20th November with respect to that of 19th November over the station.

From the above discussion, it is found that the temperature increases over Dhaka at all levels and decreases over Chittagong from surface to 400 hPa on 20th November with respect to that of the previous day. Again, the temperature decreases at all levels over Dhaka and increases from surface to 300 hPa over Chittagong on 21st November with respect to that of 20th November. The temperature decreases gradually at all levels over Calcutta during 19-21 November and increases gradually over Cuttack during 18-20 November. The temperature is almost constant over Madras and Bangkok during the period. The temperature decreases from surface to 500 hPa and increases from 500 to 100 hPa over port Blair on 20th November with respect to that of 19th November.

3.3.2.4 Vertical wind shear

The distributions of vertical wind shear over the Bay of Bengal and adjoining area at 0000 UTC and 1200 UTC on 20th November have been studied and are given in Figs. 3.3.2. (s & t) respectively. Fig. 3.3.2 (s) shows small vertical wind shear near the centre of the

cyclone having magnitude ranging between 3 ms^{-1} and 4 ms^{-1} at 0000 UTC. Whereas the Fig. 3.3.2 (t) shows little or almost no vertical wind shear near the centre of the cyclone.

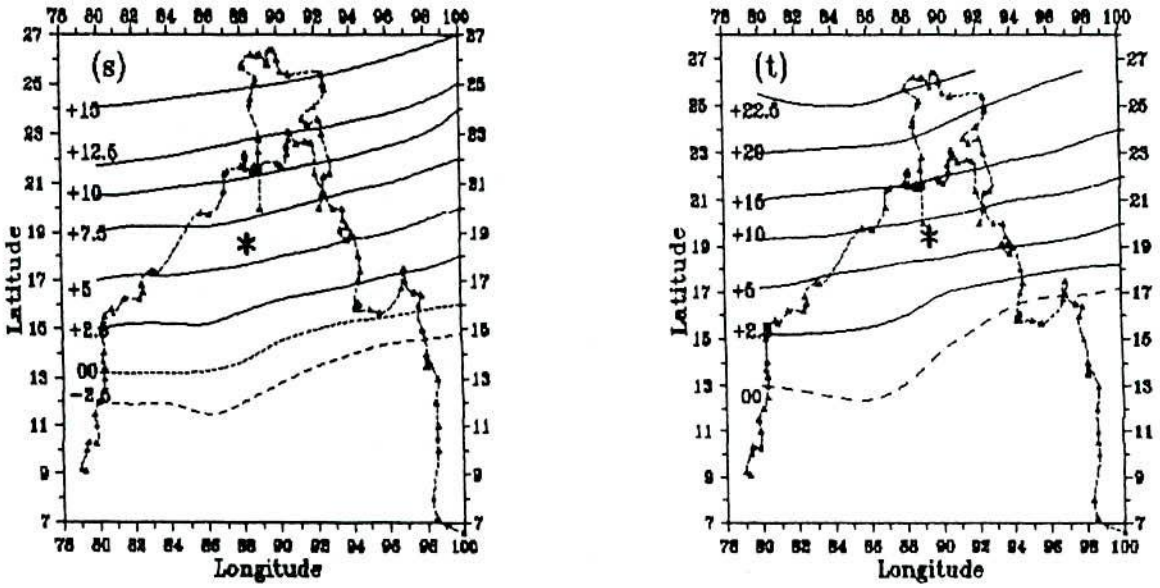

Fig. 3.3.2(s & t) Distribution of vertical wind shear on 20th November at 0000 & 1200 UTC respectively

3.3.3 Severe Cyclonic Storm with a core of hurricane winds of 1991

We have discussed in detail the vertical variation of meridional wind speed, zonal wind speed and temperature for the severe cyclonic storm with a core of hurricane winds of 1991. Day-to-day changes of these parameters have been analysed as the cyclone progress. The vertical wind shear has also discussed in the surroundings area on the day before the day of landfall of the cyclone.

3.3.3.1 Meridional wind speed

The meridional wind speed decreases from the surface to 500 hPa and increases from 500 to 100 hPa over Dhaka on 27th April with respect to that of 26th April 1991 as can be seen from Fig. 3.3.3(a). It also shows that the meridional wind speed increases gradually during 27-29 April as the cyclone moves towards the landfall.

Over Chittagong the meridional wind speed increases gradually from 900 to 300 hPa and decreases gradually from surface to 900 hPa during 26-29 April (Fig. 3.3.3(b)). The figure also shows significantly greater meridional wind on 29th April over the station.

Fig. 3.3.3(c) shows that the meridional wind speed increases over Calcutta on 27th April with respect to that of 26th April. It also shows that the meridional wind speed decreases from the surface to 750 hPa and increases from 750 to 200 hPa over the station on 28th April with respect to that of 27th April. The figure also reveals that the meridional wind speed decreases on 29th April with respect to that of 28th April over the station.

The meridional wind speed decreases gradually at all levels over Cuttack during 26-29 April as can be seen from Fig. 3.3.3(d). The figure also shows that large amount of northerly (-ve) wind was flowing at all levels on 29th April over the station.

The meridional wind speed increases gradually from the surface to 250 hPa over Madras during 27-29 April (Fig. 3.3.3(e)). Although the meridional wind speed increases but still the wind is northerly (-ve) over the station.

The meridional wind speed increases over Port Blair on 26th April with respect to that of 25th April and decreases at all levels on 28th April with respect to that of 26th April as observed from Fig. 3.3.3(f).

From the above discussion, it is found that the southerly (+ve) wind speed increases in the region where the cyclone moves. The meridional wind speed decreases or has no regular trend in the region from where the cyclone goes far away.

3.3.3.2 Zonal wind speed

Fig. 3.3.3(g) shows that the zonal wind speed decreases gradually over Dhaka during 26-29 April at all levels having some anomalies from surface to 750 hPa on 29th April where the zonal wind speed increases.

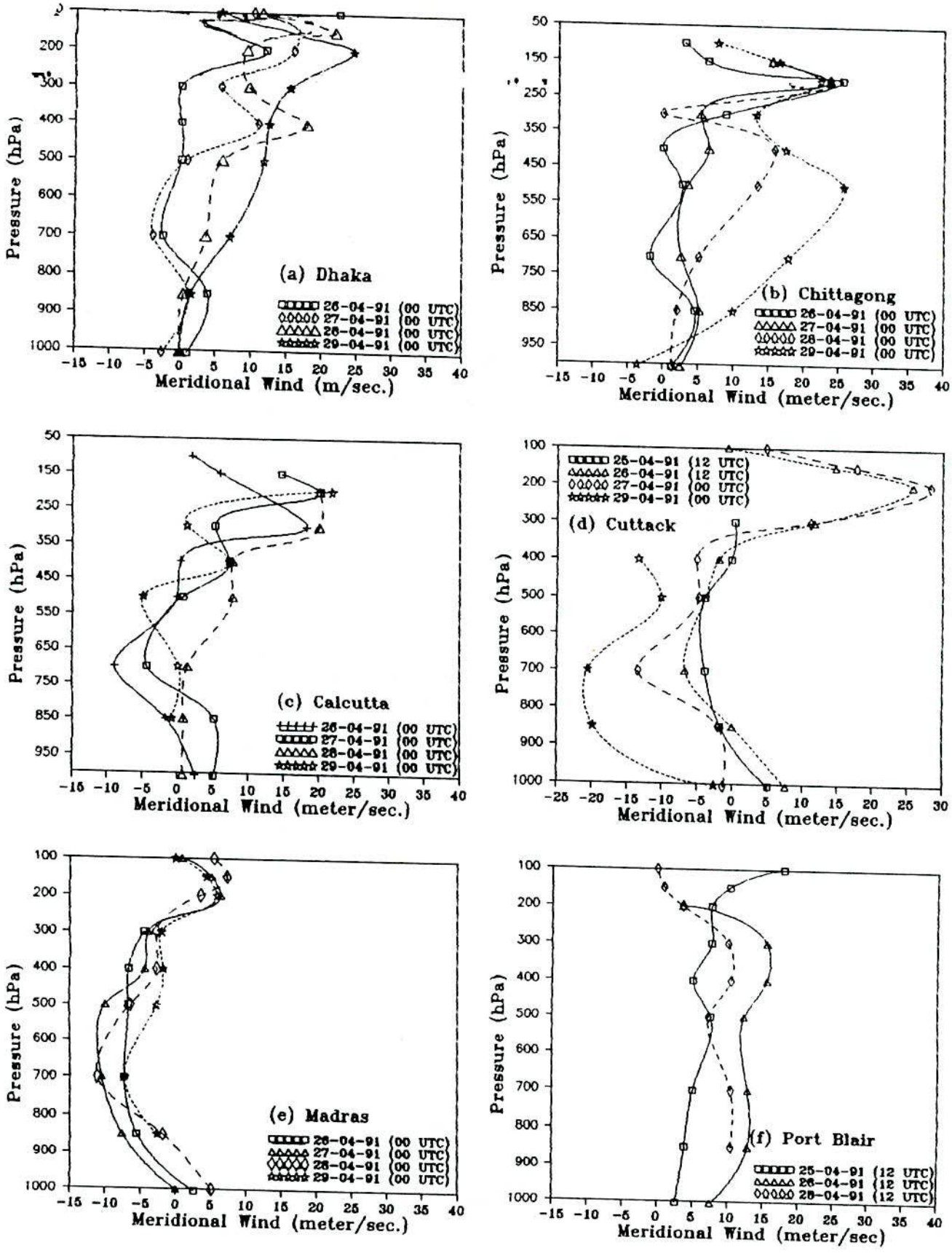

Figs. 3.3.3(a - f) Vertical profile of meridional wind over Dhaka, Chittagong, Calcutta, Cuttack, Madras and Port Blair for the cyclone 27 - 29 April 1991.

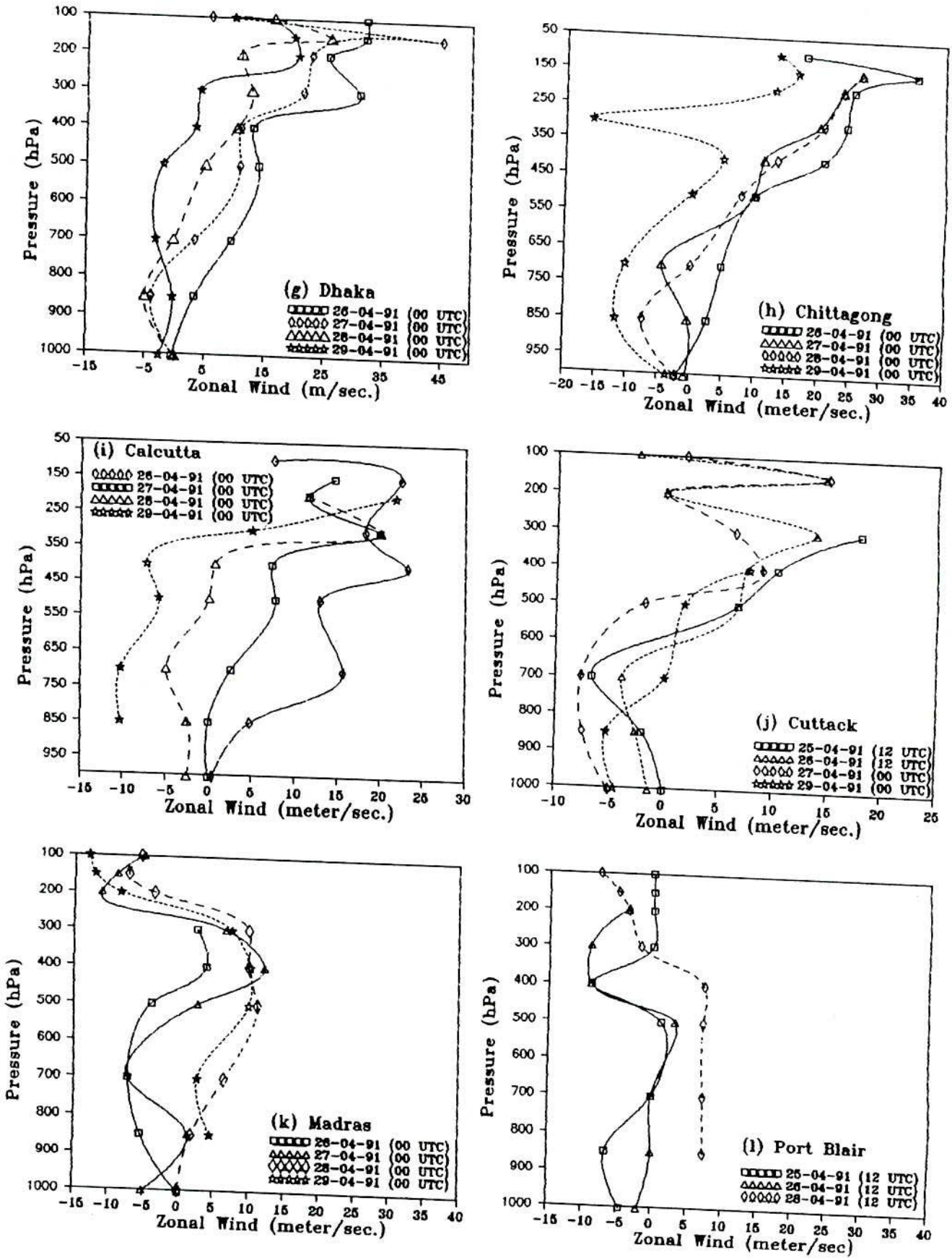

Figs. 3.3.3(g - l) Vertical profile of zonal wind over Dhaka, Chittagong, Calcutta, Cuttack, Madras and Port Blair for the cyclone 27 - 29 April 1991.

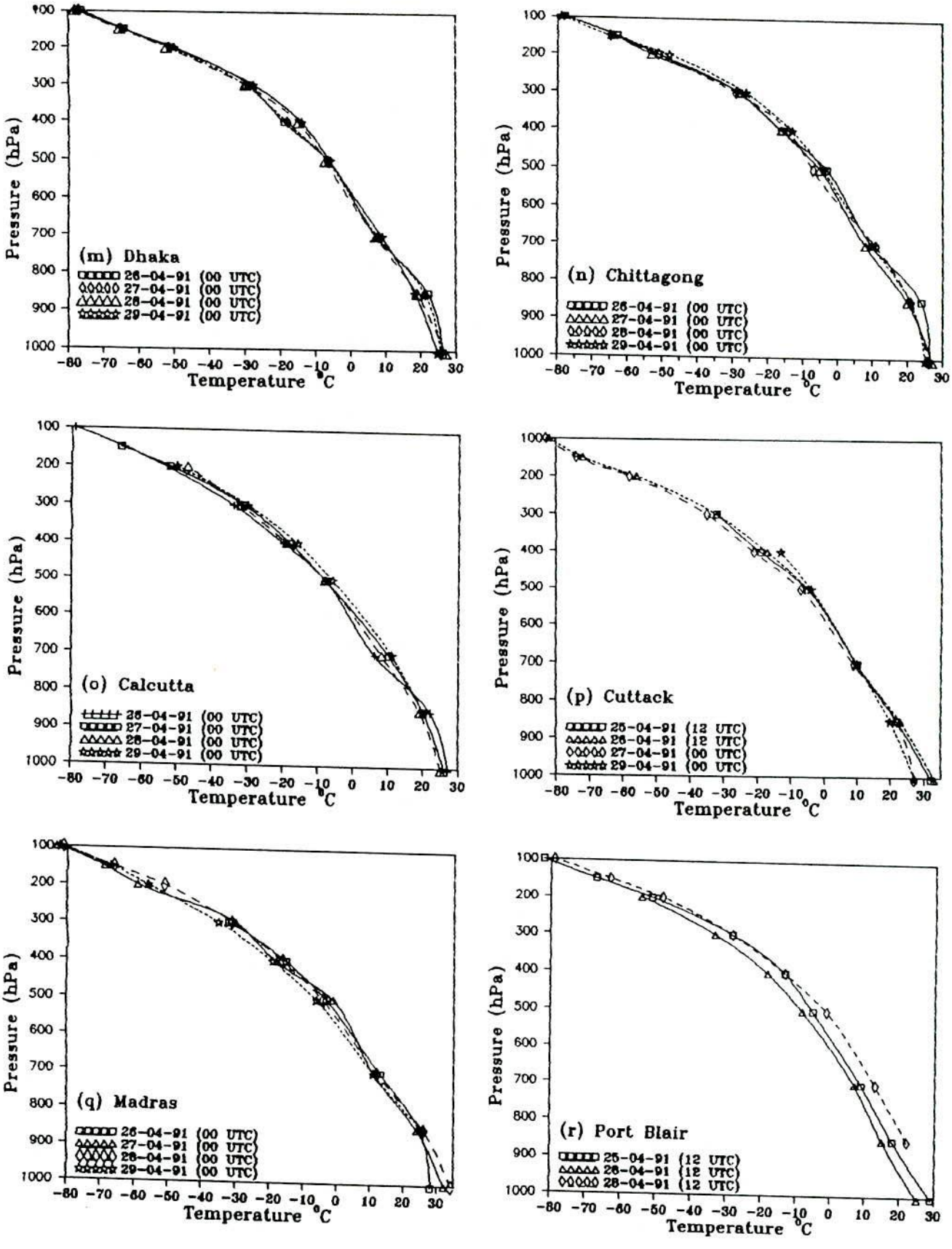

Figs. 3.3.3(m - r) Vertical temperature profile over Dhaka, Chittagong, Calcutta, Cuttack, Madras and Port Blair for the cyclone 27 - 29 April 1991.

Over Chittagong the zonal wind speed decreases gradually during 26-29 April as the cyclone moves towards the landfall as can be seen from figure Fig. 3.3.3(h). The figure also shows that large amount of easterly (-ve) wind is observed around 300 hPa on 29th April over the station.

The zonal wind speed decreases gradually from surface to 250 hPa and irregular pattern is observed above these levels during 26-29 April over Calcutta (Fig. 3.3.3(i)).

Over Cuttack the irregular pattern of zonal wind speed is observed on 25th and 26th April as can be seen from Fig. 3.3.3(j). It also shows that the zonal wind speed decreases at all levels on 27th with respect to 26th April and increases at all levels on 29th April with respect to 27th April over the station.

The zonal wind speed increases gradually (Fig. 3.3.3(k)) at all levels during 26-28 April and decreases from 800 to 100 hPa on 29th April with respect to that of 28th April over Madras.

The zonal wind speed has no regular trend (Fig. 3.3.3(l)) over Port Blair on 25th and 26th April and increases at all levels on 28th with respect to that of 26th April.

From the above discussion, it is found that the zonal wind speed decreases gradually in the region in which the cyclone moves. It is also found that the zonal wind speed increases or has no regular trend in the region from where the cyclone goes far away.

3.3.3.3 Vertical temperature variation

The temperature decreases gradually (Fig. 3.3.3(m)) from the surface to 750 hPa over Dhaka during 26-29 April as the cyclone moves towards the landfall. It also shows that the temperature increases from 750 to 200 hPa on 29th April with respect to that of 28th April and is almost constant from 750 to 200 hPa on 26th and 27th April over the station.

Fig. 3.3.3(n) shows that the temperature decreases from the surface to 400 hPa over Chittagong on 27th April with respect to that of 26th April and is almost constant from 400 to 100 hPa on both the days. The temperature is almost equal from the surface to 650 hPa and increases from 650 to 250 hPa and decreases from 250 to 150 hPa on 29th April with respect to that of 28th April over the station.

It is seen from Fig. 3.3.3(o) that the temperature decreases gradually from the surface to 800 hPa over Calcutta during 26-29 April and increases from 800 to 200 hPa on 27th April with respect to that of 26th April. The figure also shows that the temperature increases from 850 to 300 hPa on 29th April with respect to that of 28th April over the station.

The temperature decreases (Fig. 3.3.3(p)) at all levels over Cuttack on 27th April with respect to that of 26th April. Again, the temperature decreases from surface to 750 hPa and increases from 750 to 400 hPa on 29th April with respect to that of the previous day over the station.

From Fig. 3.3.3(q) it is observed that the temperature is almost constant at all levels over Madras during 26-28 April. The temperature decreases at all levels on 29th April with respect to that of 28th April.

The temperature decreases (Fig. 3.3.3(r)) at all levels over Port-Blair on 26th April with respect to that of 25th April and increases at all levels on 28th April with respect to that of 26th April.

From the analysis, it is found that the temperature decreases from the surface to 400 hPa over Chittagong and at all levels over Cuttack on 27th April with respect to that of 26th April. It is also seen that the temperature decreases from the surface to 800 hPa and constant from 800 to 200 hPa and increases from the same level over Dhaka and Calcutta respectively on 27th April with respect to that of 26th April. The temperature decreases from the surface to 750 hPa and increases from 750 to 300 hPa over Dhaka, Calcutta and Cuttack on 29th April with respect to that of 28th April. The temperature remains almost

constant from the surface to 650 hPa and increases from 650 to 250 hPa over Chittagong on 29th April with respect to that of 28th April. The temperature decreases at all levels on 29th April with respect to that of 28th April over Madras. The temperature decreases on 26th and increases on 28th April at all levels over Port Blair.

3.3.3.4 Vertical wind shear

Fig. 3.3.3.(s) shows the distribution of vertical wind shear over the Bay of Bengal and adjoining area on 28th April. The figure shows little or almost no vertical wind shear near the centre of the cyclone. As the distance increases towards the north of the cyclone centre, the magnitude of the vertical wind shear increases gradually.

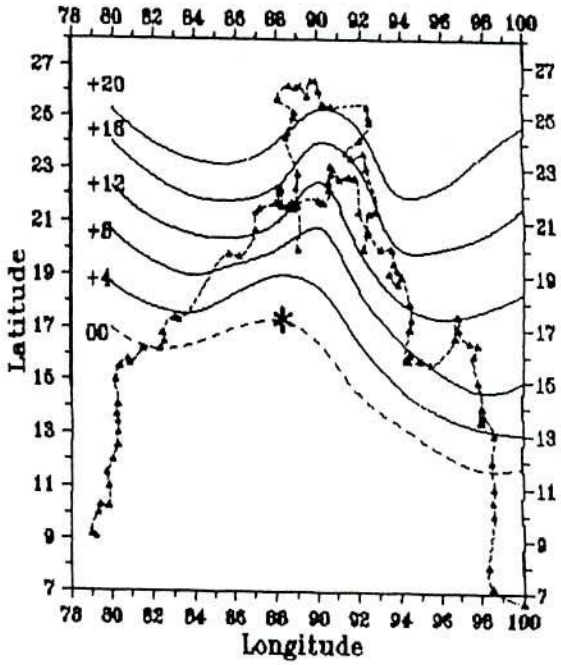

Fig. 3.3.3(s) Distribution of vertical wind shear on 28th April 1991

3.3.4 Severe Cyclonic Storm with a core of hurricane winds of 1988

We have analysed in detail the vertical variation of meridional wind speed, zonal wind speed and temperature for the severe cyclonic storm with a core of hurricane winds of 1988. Day-to-day changes of these parameters have been discussed as the cyclone

progress. The vertical wind shear has also discussed in the surroundings area on the day before the day of landfall of the cyclone.

3.3.4.1 Meridional wind speed

Fig. 3.3.4(a) shows that the meridional wind speed increases gradually from the surface to 350 hPa and irregular pattern is observed above these levels over Dhaka during 27-29 November. The figure also shows that the meridional wind speed decreases at all levels on 30th November with respect to that of 29th November over the station.

Over Chittagong the meridional wind speed increases from surface to 750 hPa and decreases from 750 to 100 hPa on 28th November with respect to that of 27th November as can be seen in Fig. 3.3.4(b). From the figure it is also observed that the meridional wind speed increases from surface to 250 hPa on 29th November with respect to that of 28th November over the station.

The meridional wind speed have irregular tendency over Calcutta on 27th and 28th November and increases from surface to 450 hPa on 29th November with respect to that of 28th November as observed in Fig. 3.3.4(c).

There is no regular increasing or decreasing tendency of meridional wind speed (Fig. 3.3.4(d)) over Madras during 27-30 November.

The meridional wind speed decreases (Fig. 3.3.4(e)) from surface to 600 hPa and increases from 600 to 100 hPa level over Bangkok on 28th November with respect to that of 27th November. The figure also shows that there is no regular pattern of meridional wind speed on 28th and 29th November over the station.

From Fig. 3.3.4(f), it is observed that the meridional wind speed increases at all levels over Port Blair on 28th November with respect to that of 27th November. The figure also shows that the meridional wind speed increases from surface to 800 hPa and decreases

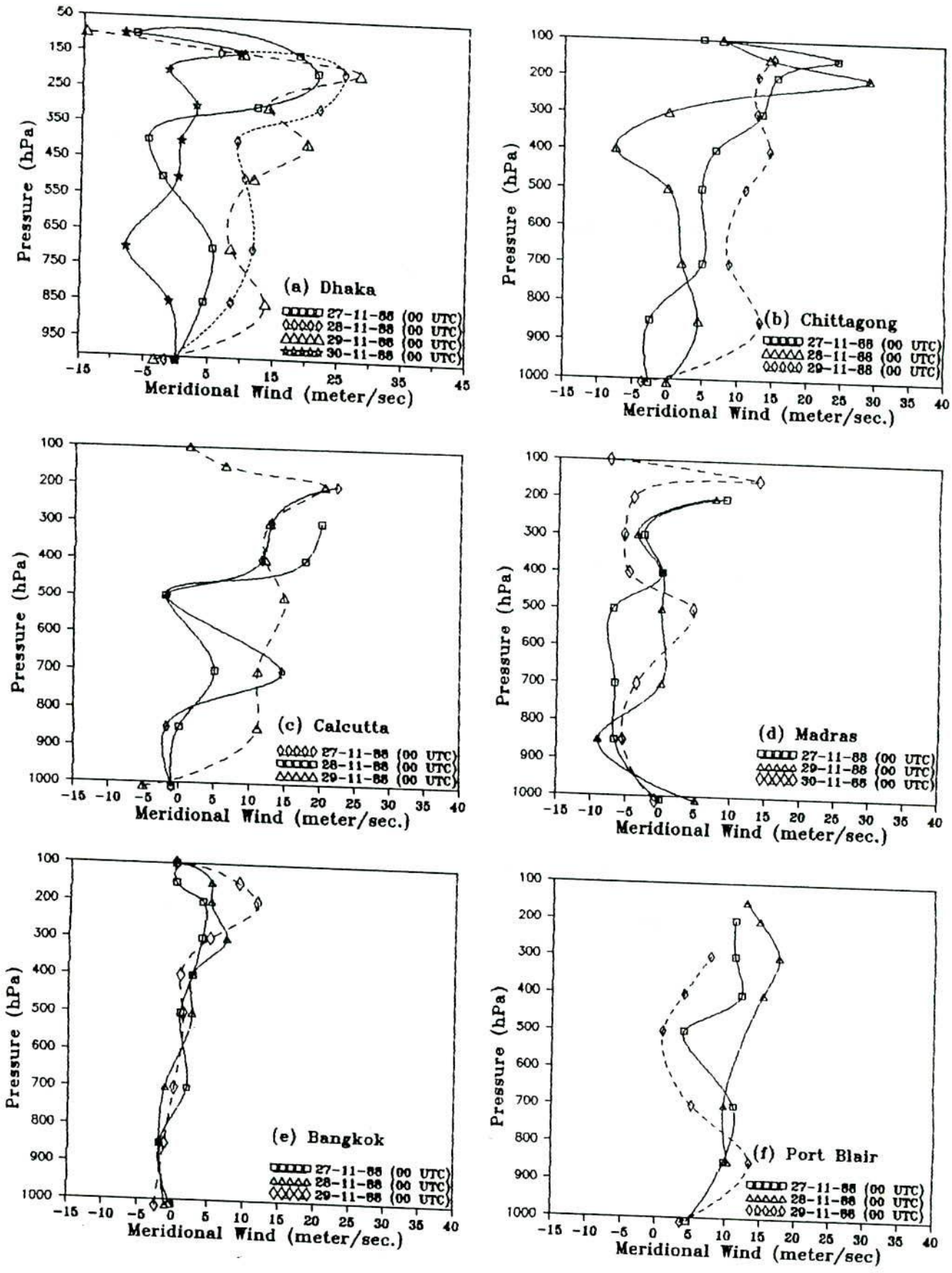

Figs. 3.3.4(a - f) Vertical profile of meridional wind over Dhaka, Chittagong, Calcutta, Madras, Bangkok and Port Blair for the cyclone 27 - 29 November 1988.

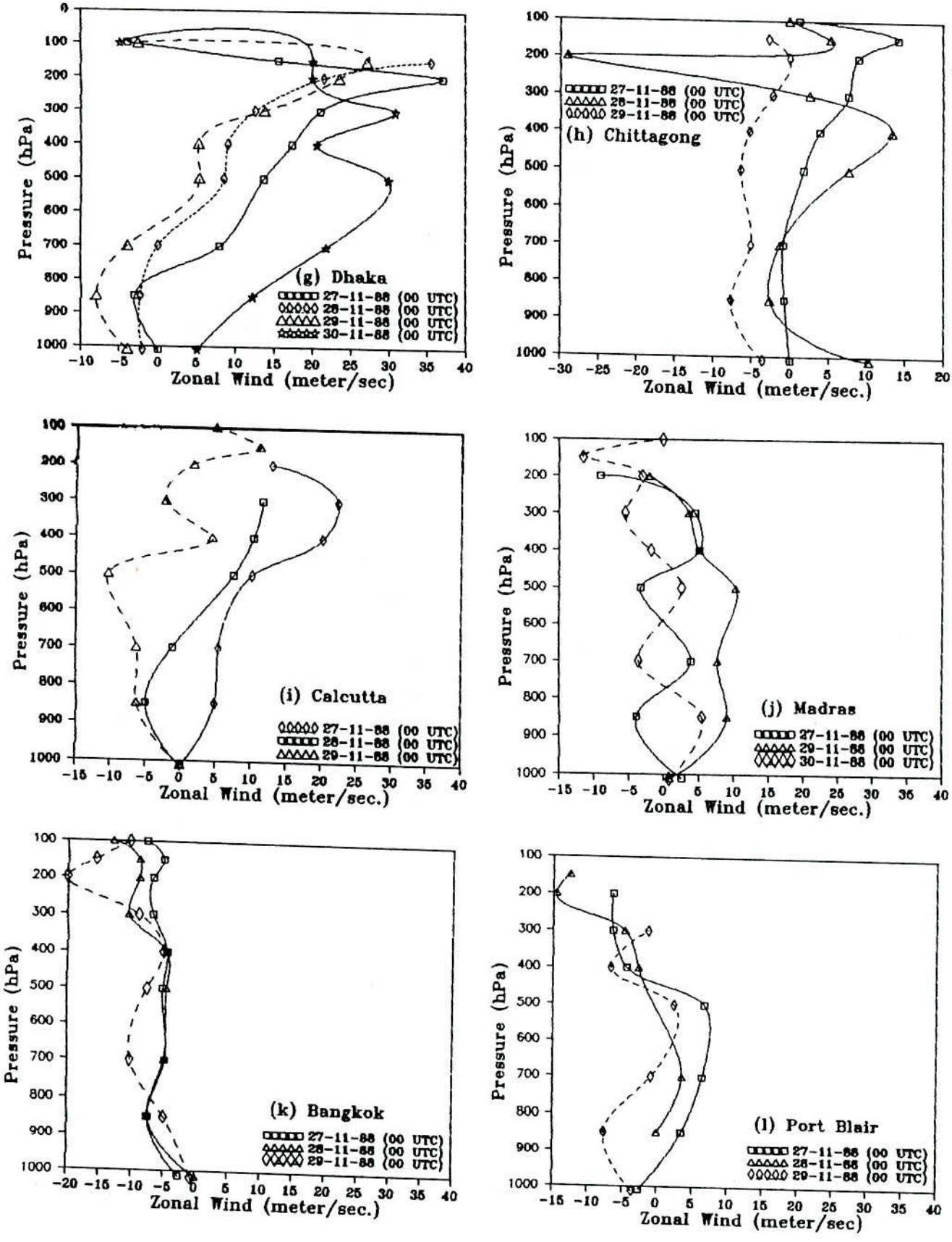

Figs. 3.3.4(g - l) Vertical profile of zonal wind over Dhaka, Chittagong, Calcutta, Madras, Bangkok and Port Blair for the cyclone 27 - 29 November 1988.

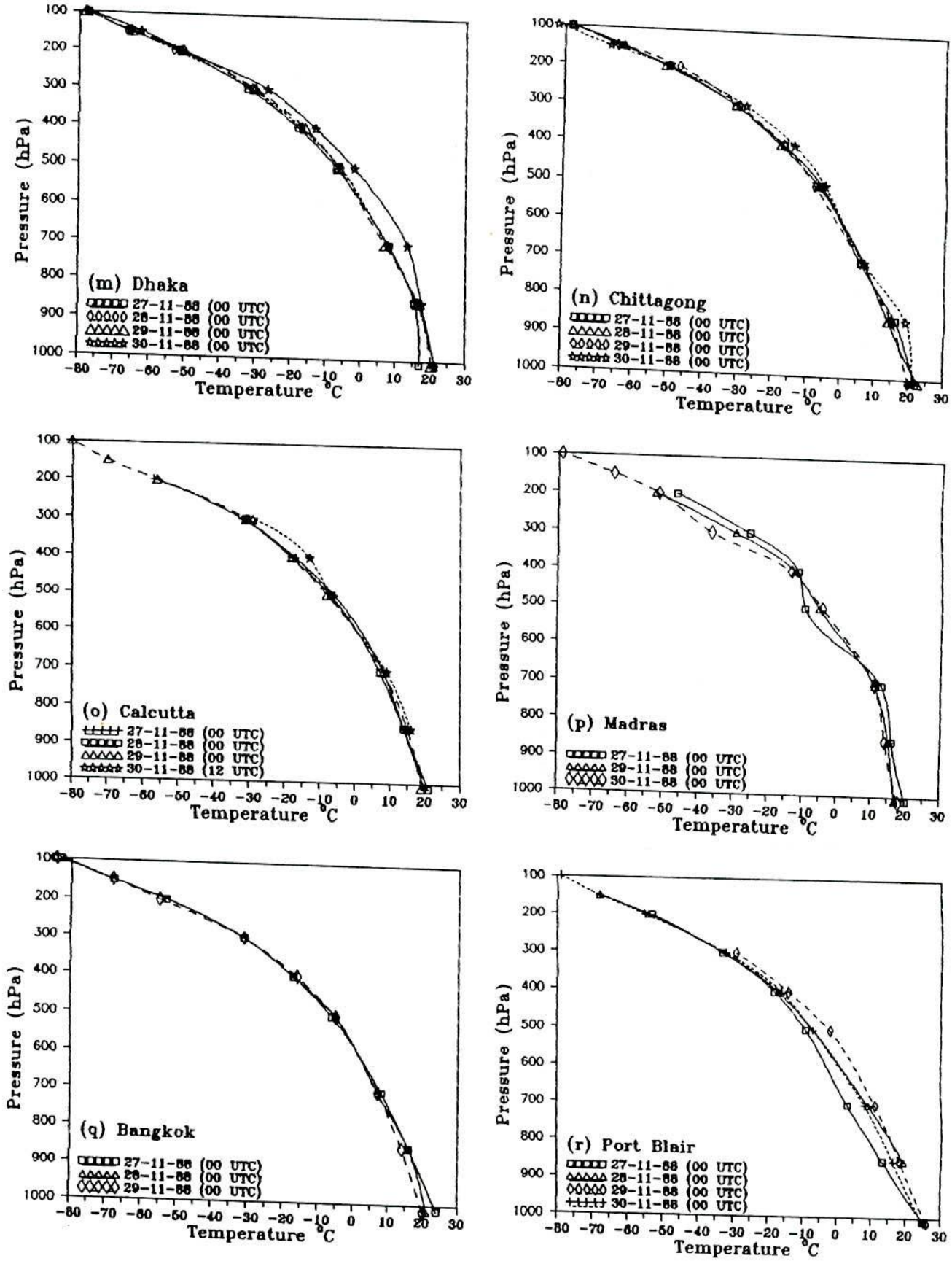

Figs. 3.3.4(m - r) Vertical temperature profile over Dhaka, Chittagong, Calcutta, Madras, Bangkok and Port Blair for the cyclone 27 - 29 November 1988.

from 800 to 100 hPa on 29th November with respect to that of 28th November over the station.

From the above discussion, it is found that the meridional wind speed increases sharply over Calcutta and gradually over Chittagong and Dhaka with little anomalies on the day of landfall with respect to that of the previous day. It is also observed that the meridional wind speed decreases or irregular over the stations which is far away from where the cyclone crosses.

3.3.4.2 Zonal wind speed

The Fig. 3.3.4(g) shows that the zonal wind speed decreases gradually from the surface to 150 hPa over Dhaka during 27-29 November. It also shows that the zonal wind speed increases from the surface to 250 hPa on 30th November with respect to that of 29th November over the station.

Over Chittagong the zonal wind speed increases from the surface to 300 hPa and decreases from 300 to 100 hPa on 28th November with respect to that of 27th November as can be seen in Fig. 3.3.4(h). It also shows that the zonal wind speed decreases from surface to 300 hPa on 29th November with respect to that of 28th November over the station.

It is observed that the zonal wind speed decreases gradually (Fig. 3.3.4(i)) at all levels except little anomalies over Calcutta during 27-29 November as the cyclone moves towards the landfall.

The zonal wind speed increases at all levels over Madras on 29th November with respect to that of 27th November and decreases at all levels on 30th November with respect to that of 29th November as observed in Fig. 3.3.4(j).

Fig. 3.3.4(k) shows that the zonal wind speed increases gradually from the surface to 800 hPa and decreases gradually from 300 to 100 hPa over Bangkok during 27-29 November.

Although the zonal wind speed increases in the lower troposphere and decreases in the upper troposphere but still easterly (-ve) wind was flowing at all levels during the period over the station.

The zonal wind speed decreases at all levels over Port Blair on 28th November with respect to that of 27th November as can be seen in Fig. 3.3.4(l). The figure also shows that the zonal wind speed decreases from the surface to 550 hPa and irregular pattern is observed above these levels on 29th November with respect to that of 28th November over the station.

From the above discussion, it is found that the zonal wind speed decreases significantly at all levels in the region where the cyclone moves. There was an irregular pattern of zonal wind speed or the zonal wind speed increases in the region from where the cyclone goes far away.

3.3.4.3 Vertical temperature variation

Figs. 3.3.4 (m - o) show that there is little or no variation of temperature observed during 27-29 November over Dhaka, Chittagong and Calcutta respectively. The figures also show that the significant increase of temperature is observed from 850 to 250 hPa on 30th November over Dhaka and Chittagong i.e. after the landfall of the cyclone.

The temperature decreases gradually (Fig. 3.3.4(p)) from 850 to 700 and 400 to 200 hPa and increases gradually from 650 to 400 hPa over Madras during 27-30 November.

There is no variation of temperature observed (Fig. 3.3.4(q)) over Bangkok during 26-29 November as the cyclone goes far away from the station.

The temperature increases gradually (Fig. 3.3.4(r)) from 850 - 300 hPa over Port-Blair during 27-29 November. The temperature decreases at all levels on 30th November with respect to that of 29th November over the station.

From the above discussion, it is found that the temperature is almost constant at all levels over Dhaka, Chittagong, Calcutta and Bangkok during 27-29 November. The temperature increases gradually over Port Blair and decreases gradually with little anomalies in the middle troposphere over Madras during the period. It is also seen that the temperature increases over Dhaka and Chittagong and decreases over Port Blair on 30th November with respect to that of the previous day.

3.3.4.4 Vertical wind shear

The distribution of vertical wind shear have been studied on 28th November over the Bay of Bengal and adjoining area (Fig. 3.3.4. (s)). Little or no vertical wind shear is observed near the centre of the cyclone. As the distance increases towards the north of the cyclone centre the magnitude of the vertical wind shear increases gradually.

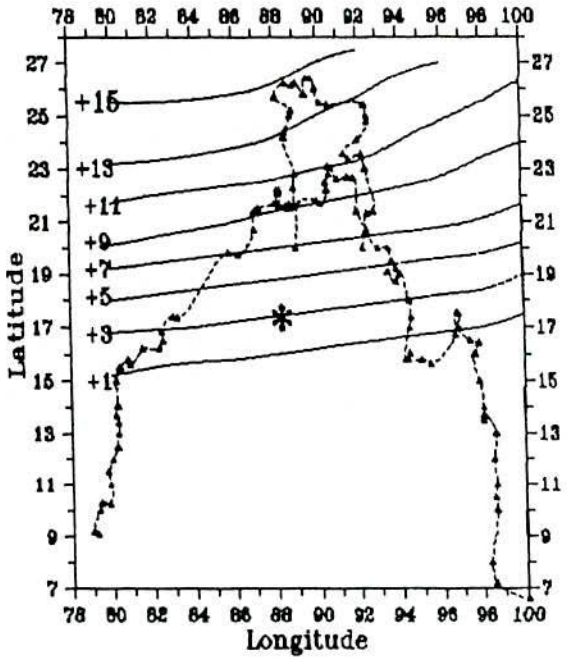

Fig. 3.3.4(s) Distribution of vertical wind shear on 28th November 1988

3.3.5 Severe Cyclonic Storm with a core of hurricane winds of 1985

We have analysed in detail the vertical variation of meridional wind speed, zonal wind speed and temperature for the severe cyclonic storm with a core of hurricane winds of

1985. The variation of these parameters has been discussed as the cyclone progress. The vertical wind shear has also discussed in the surroundings area on the day before the day of landfall of the cyclone.

3.3.5.1 Meridional wind speed

Figs. 3.3.5(a - b) shows that the meridional wind speed decreases gradually at all levels having little anomalies and irregular pattern is observed over Dhaka and Calcutta during 23-25 May respectively.

Over Cuttack the meridional wind speed decreases from the surface to 400 hPa and irregular pattern is observed above these levels on 23rd May with respect to that of 22nd May as can be seen from Fig. 3.3.5(c). It also shows that the meridional wind speed has irregular pattern on 23rd and 24th May over the station.

There is no regular increasing or decreasing tendency of meridional wind speed over Bangkok during 22-24 May (Fig. 3.3.5(d)).

The meridional wind speed decreases from the surface to 600 hPa over Madras on 23rd May with respect to that of 22nd May and increases on 24th May with respect to that of 23rd May and decreases again on 25th May with respect to that of 24th May and irregular pattern is observed above these levels (Fig. 3.3.5(e)).

From the above discussion, it is also found that the meridional wind speed has shown irregular pattern in the region that is far away from the cyclone.

3.3.5.2 Zonal wind speed

Figs. 3.3.5(f-g) show that the zonal wind speed decrease gradually at all levels except little anomalies over Dhaka and Calcutta during 23-25 May and 23rd May with respect to that of 22nd May respectively.

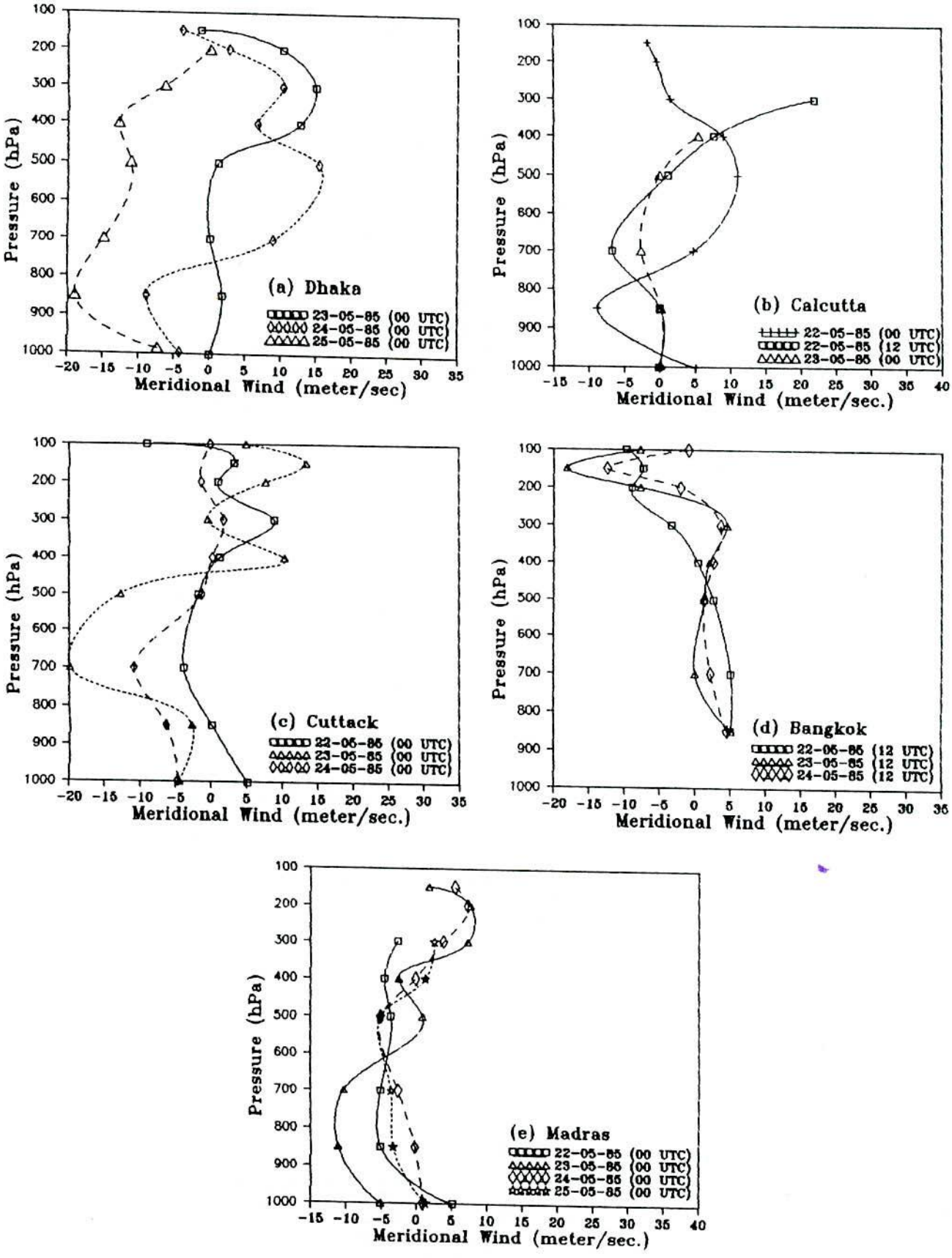

Figs. 3.3.5(a - e) Vertical profile of meridional wind over Dhaka, Calcutta, Cuttack, Bangkok and Madras for the cyclone 23 - 25 May 1985.

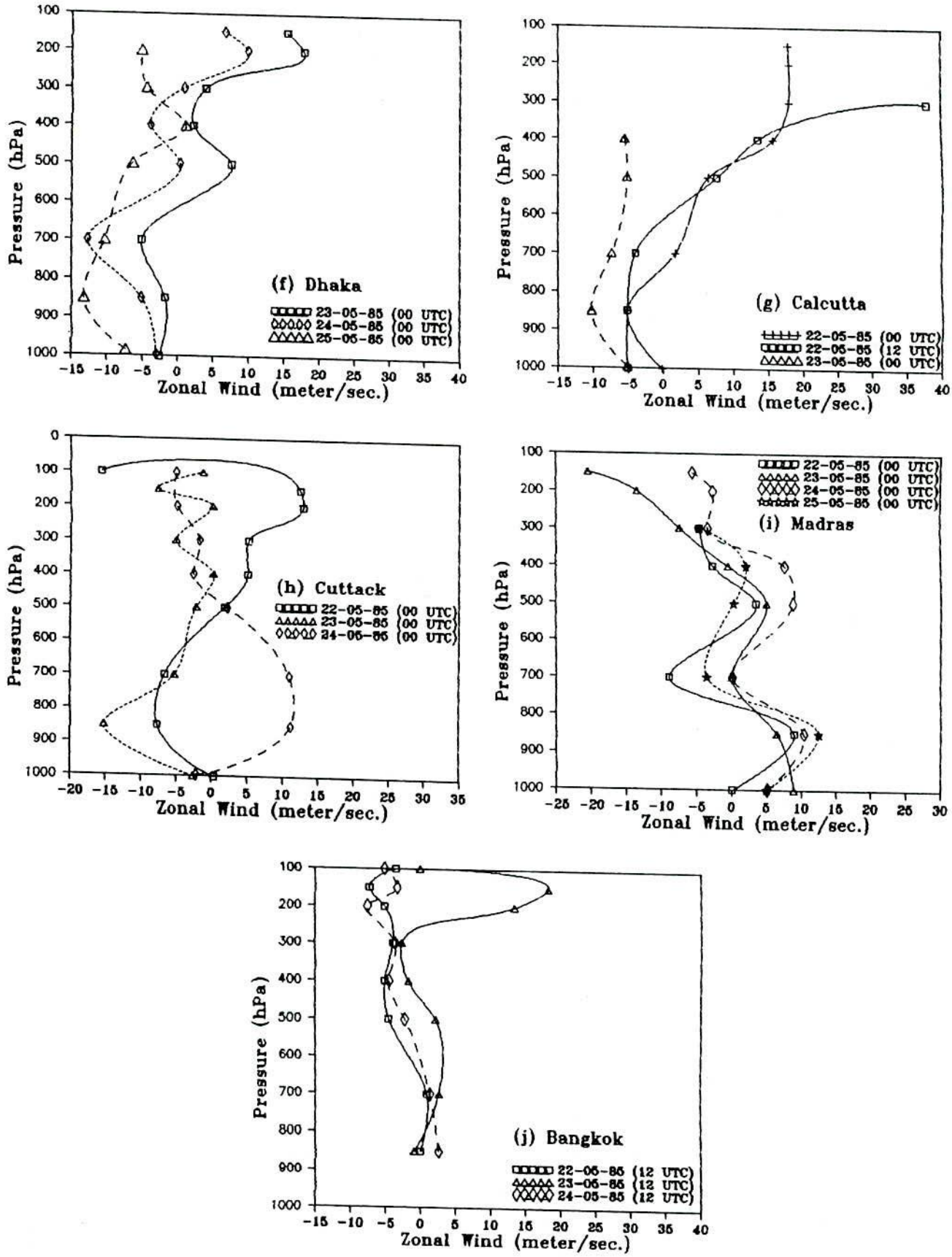

Figs. 3.3.5(f - j) Vertical profile of zonal wind over Dhaka, Calcutta, Cuttack, Madras and Bangkok for the cyclone 23 - 25 May 1985.

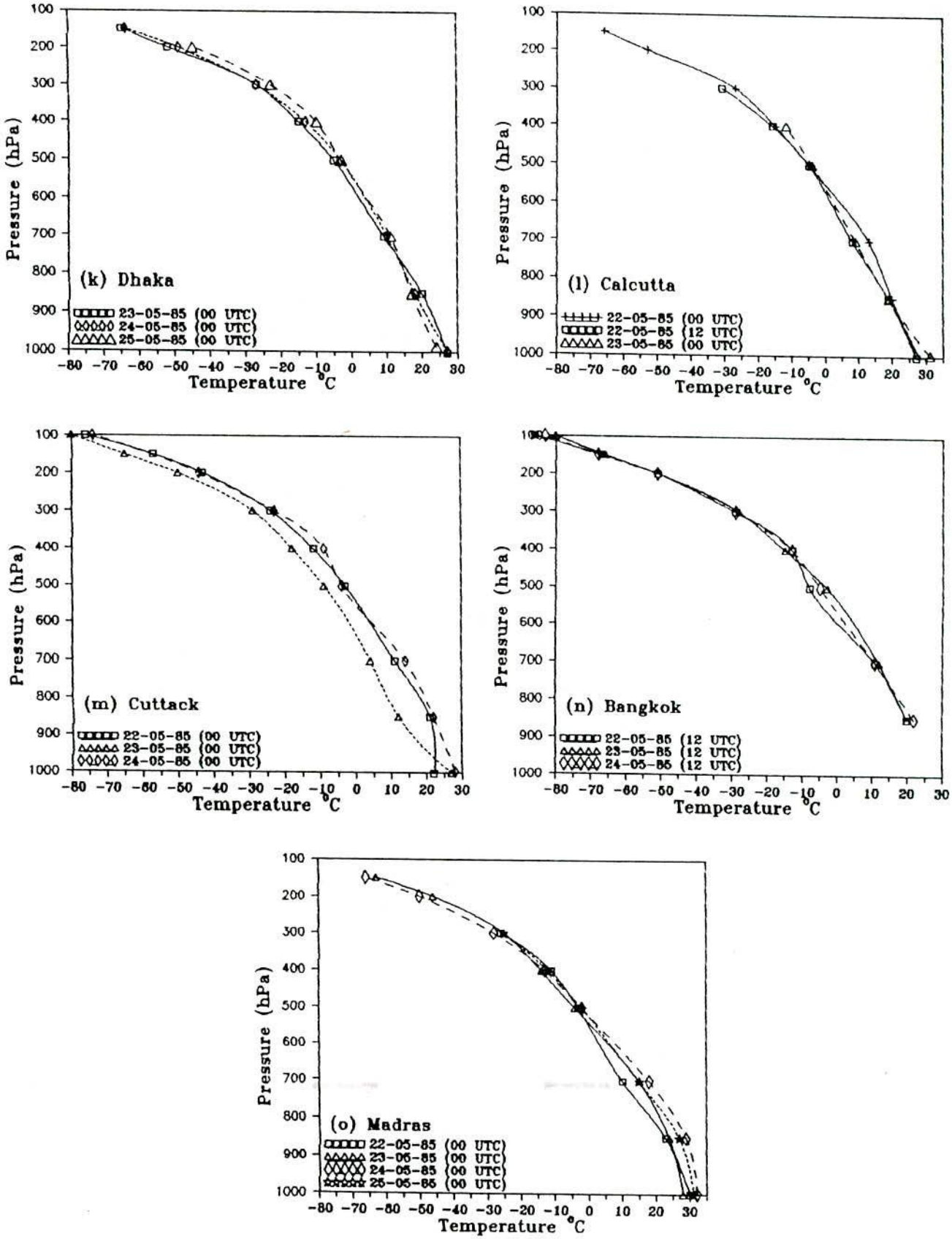

Figs. 3.3.5(k - o) Vertical temperature profile over Dhaka, Calcutta, Cuttack, Bangkok and Madras for the cyclone 23 - 25 May 1985.

The zonal wind speed decreases at all levels over Cuttack on 23rd May with respect to that of 22nd May as is evident from Fig. 3.3.5(h). It also shows that the zonal wind speed increases from the surface to 450 hPa on 24th May with respect to that of 23rd May over the station.

Fig. 3.3.5(i) shows that the zonal wind speed increases gradually at all levels over Madras during 22-24 May. The figure also shows that the zonal wind speed increases from the surface to 800 hPa level and decreases from 800 to 300 hPa on 25th May with respect to that of 24th May over the station.

Over Bangkok the zonal wind speed increases (Fig. 3.3.5(j)) at all levels on 23rd May with respect to that of 22nd May and decreases from 800 to 100 hPa on 24th May with respect to that of 23rd May.

From the above discussion, it is found that the zonal wind speed decreases over the area where the cyclone moves. It is also found that the zonal wind speed increases in the region such as Cuttack and Madras from where the cyclone goes far away.

3.3.5.3 Vertical temperature variation

Fig. 3.3.5(k) shows that the temperature decreases gradually from the surface to 750 hPa and increases gradually from 750 to 150 hPa over Dhaka during 23rd to 25th May as the cyclone moves towards the landfall.

Over Calcutta the temperature increases from the surface to 900 and 500 to 400 hPa and decreases from 850 to 500 hPa level on 23rd May with respect to that of 22nd May (Fig. 3.3.5(l)). It is seen from Fig. 3.3.5(m) that the temperature decreases significantly at all levels over Cuttack on 23rd May with respect to that of 22nd May and increases at all levels on 24th May with respect to that of 23rd May.

The temperature is almost constant (Fig. 3.3.5(n)) having little anomalies in the middle of the troposphere over Bangkok during 22-24 May. A little variation of temperature is observed from 700 to 500 hPa during the same period.

The Fig. 3.3.5(o) shows that the temperature decreases from the surface to 900 hPa and increases from 900 to 550 hPa and is constant above these levels over Madras on 23rd May with respect to that of 22nd May. The temperature increases from surface to 350 hPa and decreases from 350 to 150 hPa on 24th May with respect to that of 23rd May. The temperature decreases from surface to 500 hPa and constant above these levels on 25th May with respect to that of 24th May over the station.

From the above analysis, it is found that the temperature increases from 750 to 200 hPa over Dhaka, from the surface to 100 hPa and 400 hPa over Cuttack and Madras respectively on 24th May with respect to that of 23rd May. The temperature decreases from the surface to 750 and 350 to 150 hPa level over Dhaka and Madras respectively on 24th May with respect to that of 23rd May. The temperature decreases from the surface to 800 hPa and increases from 750 to 200 hPa over Dhaka and decreases from the surface to 500 hPa over Madras on 25th May with respect to that of 24th May. Also the temperature decreases from the surface to 100 hPa over Cuttack on 23rd May with respect to that of 22nd May. The temperature increases from the surface to 900 and 500 to 400 hPa and decreases from 850 to 500 hPa over Calcutta on 23rd May with respect to that of 22nd May.

3.3.5.4 Vertical wind shear

From Fig. 3.3.5(p), it is observed that no vertical wind shear exists near the centre of the cyclone on 24th May at 0000 UTC. As the distance increases towards the north-east and north-west of the cyclone centre, the magnitude of the vertical wind shear increases gradually.

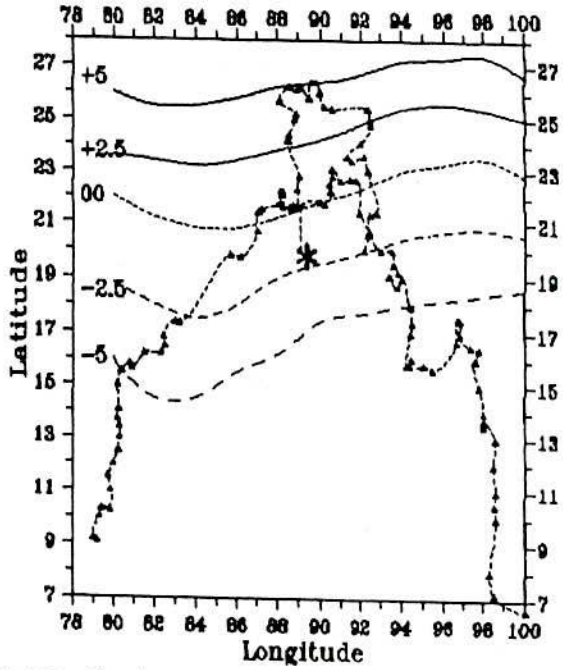

Fig. 3.3.5(s) Distribution of vertical wind shear on 24th May 1985

3.3.6 Cyclonic Storm of 1992

We have analysed in detail the vertical variation of meridional wind speed, zonal wind speed and temperature for the cyclonic storm of May 1992. The variation of these parameters has been discussed as the cyclone progress. The vertical wind shear has also discussed in the surroundings area on the day of landfall of the cyclone.

3.3.6.1 Meridional wind speed

Figs. 3.3.6(a-c) shows that the meridional wind speed has irregular pattern over Dhaka, Chittagong and Cuttack during 17-19 May respectively.

The Fig. 3.3.6(d) shows that the meridional wind speed decreases gradually from the surface to 500 hPa and increases gradually from 500 to 100 hPa over Calcutta during 17-19 May. The meridional wind speed decreases gradually at all levels over Madras during the same period as can be seen from Fig. 3.3.6(e).

From Fig. 3.3.6(f), it is observed that the meridional wind speed increases from the surface to 400 hPa over Bangkok on 18th May with respect to that of 17th May. The figure also shows that the meridional wind speed decreases from surface to 400 hPa level and

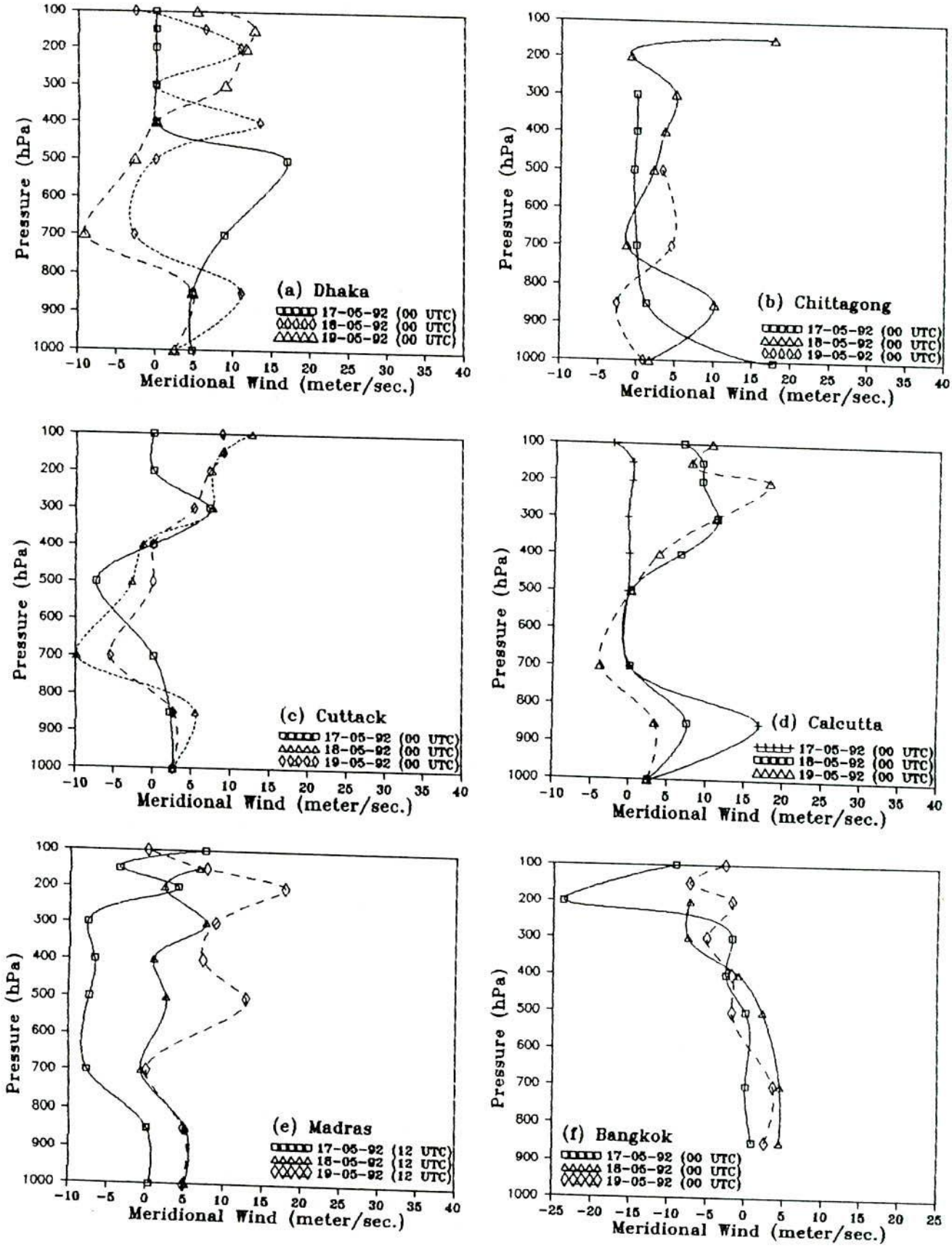

Figs. 3.3.6(a - f) Vertical profile of meridional wind over Dhaka, Chittagong, Cuttack, Calcutta, Madras and Bangkok for the cyclone 17 - 19 May 1992.

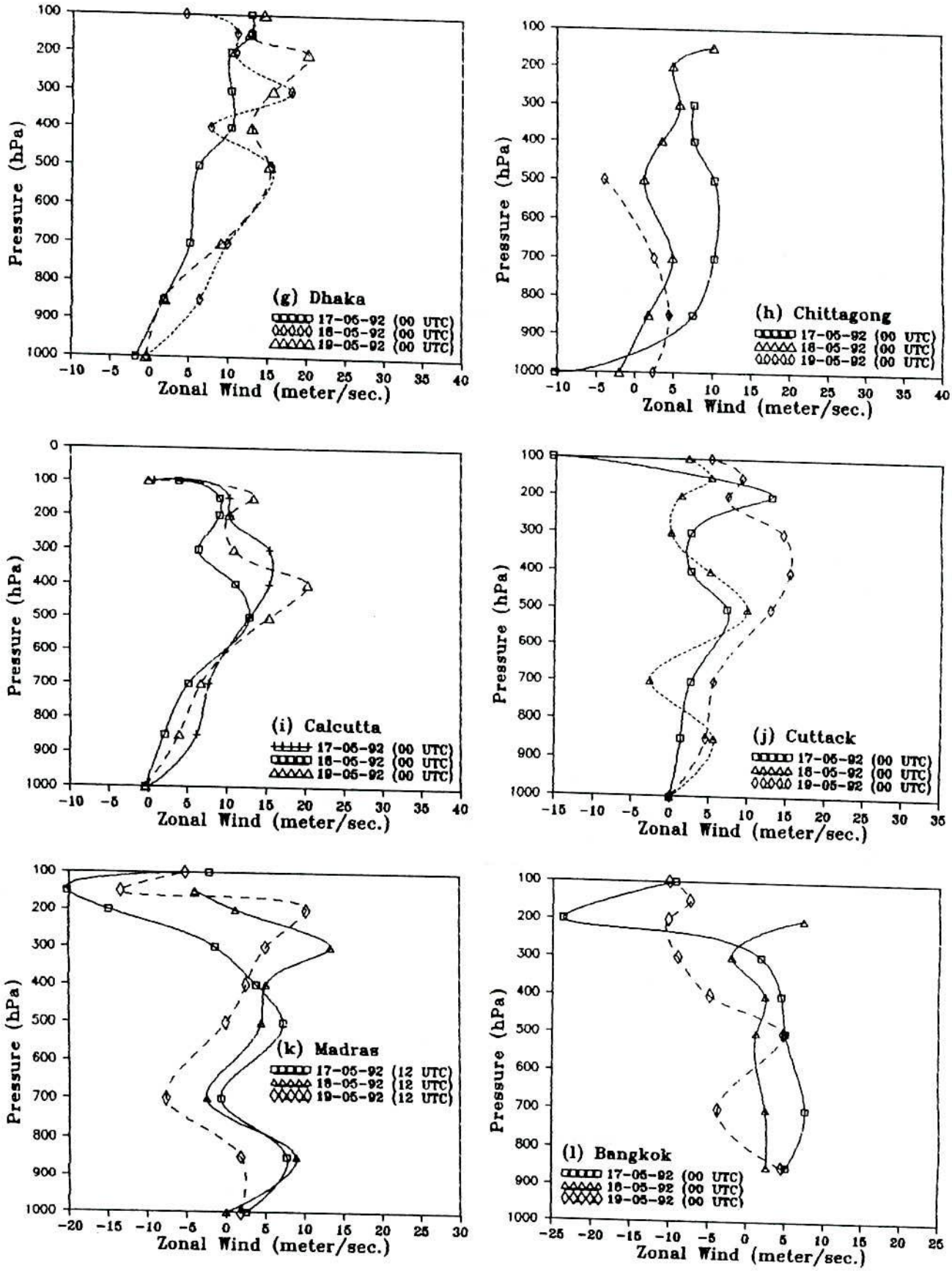

Figs. 3.3.6(g - l) Vertical profile of zonal wind over Dhaka, Chittagong, Calcutta, Cuttack, Madras and Bangkok for the cyclone 17 - 19 May 1992.

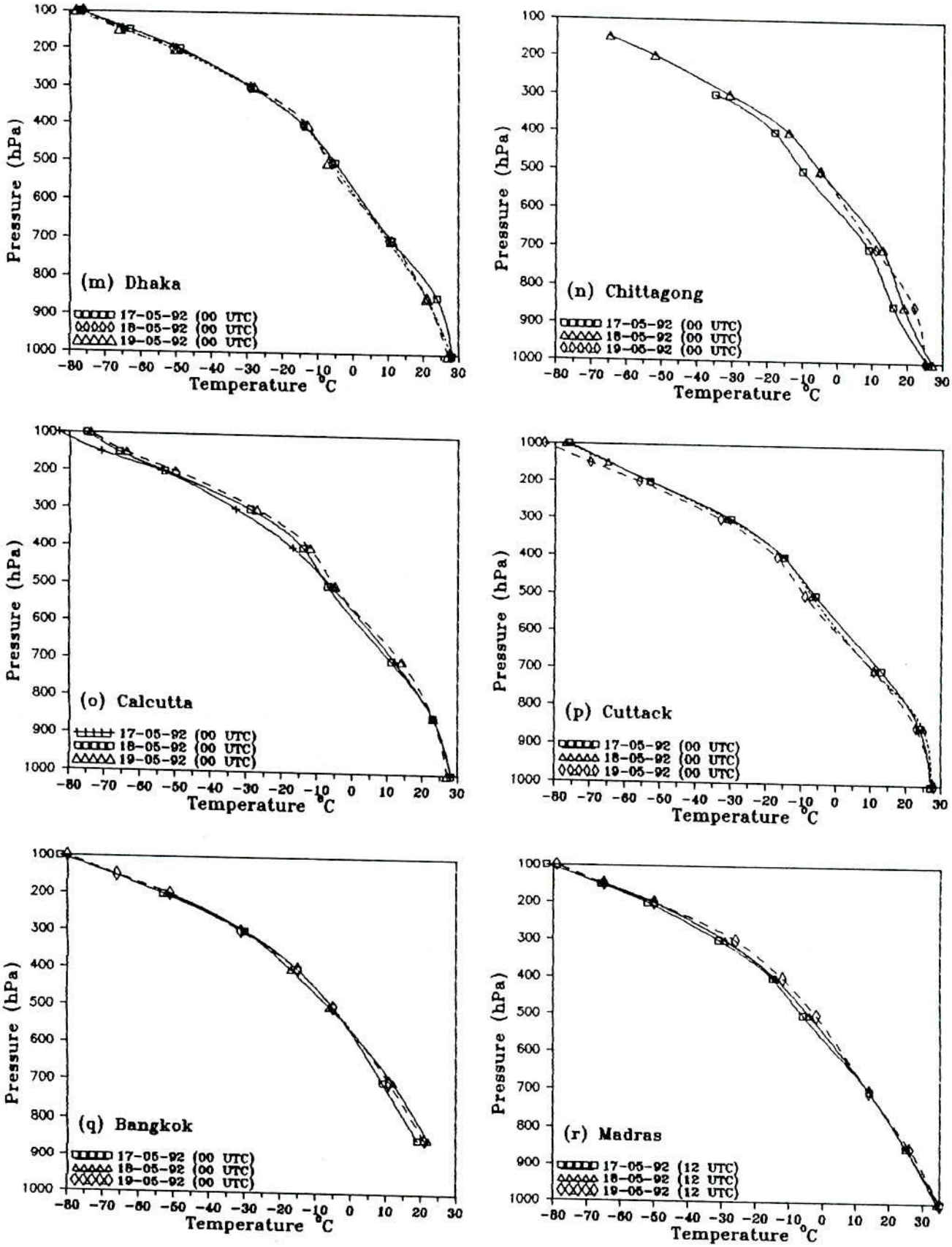

Figs. 3.3.6(m - r) Vertical temperature profile over Dhaka, Chittagong, Calcutta, Cuttack, Bangkok and Madras for the cyclone 17 - 19 May 1992.

increases from 400 to 100 hPa on 19th May with respect to that of 18th May over the station.

From the above discussion, it is found that the cyclonic storm moves in the region from where there is no regular pattern of meridional wind.

3.3.6.2 Zonal wind speed

Over Dhaka the zonal wind speed increases from the surface to 200 hPa and decreases from 200 to 100 hPa level on 18th May with respect to that of 17th May as can be seen from Fig. 3.3.6(g).

The figure also shows that the zonal wind speed decreases from the surface to 700 hPa and increases from 700 to 100 hPa on 19th May with respect to that of 18th May over the station.

From Fig. 3.3.6(h), it is observed that the zonal wind speed decreases at all levels over Chittagong on 18th May with respect to that of 17th May. It also shows that the zonal wind speed increases from the surface to 750 hPa and decreases from 750 to 500 hPa on 19th May with respect to that of 18th May over the station.

The zonal wind speed decreases at all levels over Calcutta on 18th May with respect to that of 17th May and increases at all levels on 19th May with respect to that of 18th May (Fig. 3.3.6(i)).

The Figs. 3.3.6(j-k) show that the irregular pattern of zonal wind speed is observed on 17th and 18th May and the zonal wind speed increases at all levels on 19th May with respect to that of 18th May over Cuttack and Madras respectively. The zonal wind speed decreases gradually from 850 to 250 hPa over Bangkok during 17-19 May (Fig. 3.3.6(l)).

From the above analysis, it is found that the zonal wind speed increases over the stations Calcutta and Cuttack and decreases at all levels over Madras and Bangkok on the day of

landfall with respect to that of the previous day. The analysis also indicates that the zonal wind speed increases from surface to 750 hPa over Chittagong and decreases from surface to 700 hPa over Dhaka on the day of landfall with respect to that of the previous day.

3.3.6.3 Vertical temperature variation

It is found that the temperature decreases from surface to 450 hPa over Dhaka on 18th May with respect to that of 17th May and is almost constant above this level (Fig. 3.3.6(m)). No variation of temperature is observed on 18th and 19th May over the station.

Fig. 3.3.6(n) shows that the temperature increases sharply at all levels over Chittagong on 18th May with respect to that of 17th May. The temperature increases from 950 to 750 hPa and decreases from 750 to 500 hPa on 19th May with respect to that of 18th May.

The temperature decreases from 750 to 475 hPa and increases from 475 to 100 hPa over Calcutta on 18th May with respect to that of 17th May (Fig. 3.3.6(o)). The temperature decreases from surface to 900 hPa and increases from 900 to 100 hPa on 19th May with respect to that of 18th May.

The temperature decreases at all levels over Cuttack on 19th May with respect to that of 17th and 18th May (Fig. 3.3.6(p)). The temperature increases from 850 to 550 hPa over Bangkok on 18th May with respect to that of 17th May and is almost constant at all levels on 18th and 19th May (Fig. 3.3.6(q)).

The temperature is almost constant from the surface to 650 hPa and increases gradually from 650 to 200 hPa over Madras during 17-19 May (Fig. 3.3.6(r)).

From the above discussion, it is found that the temperature decreases from surface to 500 hPa over Dhaka and Calcutta on 18th May with respect to that of 17th May and is constant over Dhaka and increases over Calcutta above these levels. The temperature increases significantly at all levels over Chittagong on 18th May with respect to that of 17th May. The temperature is constant at all levels over Cuttack, from surface to 650 hPa

over Madras and 550 to 100 hPa over Bangkok and increases at all other levels over Madras and Bangkok on this day. The temperature is almost constant at all levels over Dhaka and Bangkok and from surface to 650 hPa over Madras on 18th and 19th May. The temperature increases from 950 to 750 hPa levels over Chittagong and 800 to 100 hPa over Calcutta and decreases at all other levels over both the stations on 19th May with respect to that of 18th May. The temperature is found to decrease at all levels over Cuttack on 19th May with respect to that of 18th May.

3.3.6.4 Vertical wind shear

The distribution of vertical wind shear have been studied on 19th May over the Bay of Bengal and adjoining area (Fig. 3.3.6. (s)). The magnitude of this shear lies between (0-2) ms^{-1} near the centre. As the distance increases towards the north of the cyclone centre, the vertical wind shear increases gradually.

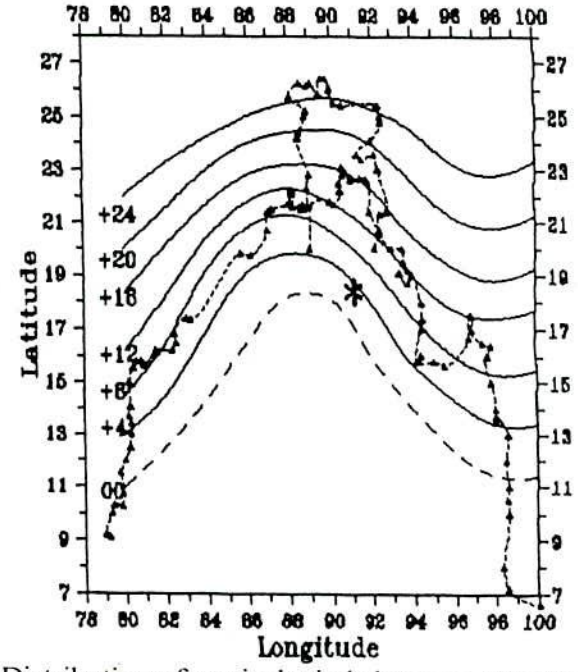

Fig. 3.3.6(s) Distribution of vertical wind shear on 19th May 1992

3.4 Discussion & Conclusions

On the basis of the present study, some specific conclusions have been drawn for the vertical variation of meridional wind, zonal wind and temperature over different stations during cyclonic periods. The spatial distribution of vertical wind shear has also been analysed and studied during different cyclonic periods in the surroundings of the Bay of Bengal.

3.4.1 Vertical variation of meridional wind speed

The distribution shows that the southerly wind speed over Dhaka increases gradually at all levels for the cyclones of 1988 and 1991. The southerly wind decreases gradually at all levels with little anomaly over Dhaka during the period of movement of the cyclones of 1985 and 1994. The southerly wind decreases gradually from 800 to 300 hPa during 18-21 November and irregular pattern is observed below and above these levels over Dhaka for the cyclone of 1992. The southerly wind speed decreases from 800 to 450 hPa and increases from 350 to 100 hPa during the period of movement of the cyclonic storm of 1992.

The southerly wind decreases gradually from 400 to 100 hPa and irregular pattern is observed below these levels over Chittagong during the movement of the cyclone of 1994 and it increases at all levels with little anomalies during the movement of cyclones of 1988 and 1991. The southerly wind increases from surface to 600 hPa and decreases from 600 to 300 hPa over Chittagong on the day of landfall with respect to that of the previous day for the cyclone of 1992. The analysis also shows that large amount of northerly wind is observed on 21st November of 1992 over the station. The southerly wind decreases from surface to 900 hPa and increases from 650 to 200 hPa over Chittagong during the period of movement of the cyclonic storm of 1992.

The southerly wind decreases at all levels with little anomalies over Calcutta on the day of landfall with respect to that of the previous day for the cyclones of 1991, 1992, 1994 and increases for the cyclone of 1988. The increase in southerly wind over Calcutta in 1988 is

due to the movement of the cyclone towards north-east across Sundarban coast. The wind decreases from surface to 500 hPa and increases from 300 to 100 hPa over Calcutta during the period of movement of the cyclonic storm of 1992. This increase from 300 to 100 hPa may be due to the intensification of the upper air westerly trough, which is far away from the cyclone centre.

The southerly wind increases from surface to 400 hPa for the cyclones of 1988, 1985 and the cyclonic storm of 1992 and at all levels for the cyclone of 1994 and decreases from 400 to 100 hPa for the same over Cuttack during the period of movement. The southerly wind decreases from surface to 400 hPa for the cyclones of 1991 and 1992, and increases from 250 to 100 hPa for the cyclone of 1992 during the period of movement over Cuttack. The decrease in southerly wind from surface to 400 hPa over Cuttack is for obvious reason that the station is in the western or northwestern side of the cyclone track.

During the movement of the cyclones of 1988, 1991, 1994 and the cyclonic storm of 1992, the southerly wind over Madras increases at all levels having a gradual decrease for the 1992 cyclone from surface to 600 hPa during 17-20 November and increase on 21st November with respect to that of 20th November 1992 over Madras. The southerly wind decreases at all levels on the day of landfall with respect to that of the previous day over Madras for the cyclone of 1985. The meridional wind is almost constant at all levels for all the cyclones with little variation observed around 200 hPa over Port Blair and Bangkok.

The above discussion clearly indicates that the southerly wind has a tendency to increase significantly at all levels over the area towards which the cyclones move for ultimate landfall and this increase in southerly wind speed depends on the tracks of the cyclones.

3.4.2 Vertical variation of zonal wind speed

The distribution shows that the westerly wind decreases and the easterly wind increases gradually at all levels with little anomaly over Dhaka, Chittagong and Calcutta during the period of movement of cyclones of 1985, 1988, 1991 and 1994. The westerly wind decreases gradually at all levels with little anomalies over Cuttack during the period of

movement of the cyclone and increases at all levels on the day of landfall with respect to that of the previous day for the cyclones of 1985, 1988, 1991 and 1994 and for the cyclonic storm of 1992. The wind speed is almost constant from surface to 400 hPa and little variation is observed around 300 to 200 hPa during the period of movement of all the above mentioned cyclones over Port Blair and Bangkok. The westerly wind increases gradually during the period of movement of the cyclone and decreases on the day of landfall of the cyclones of 1985 and 1991 over Madras whereas the same increases at all levels for the cyclone of 1988 and decreases from 500 to 100 hPa for the cyclone of 1994 over Madras having an anomalous behaviour in the lower troposphere.

The westerly wind decreases gradually over Dhaka during 18-20 November and increases at all levels on 21st November for 1992 cyclone and it increases gradually over Chittagong from 800 to 450 hPa and decreases gradually from 450 to 200 hPa during the period of movement of 1992 cyclone. The magnitude of the westerly wind increases gradually at all levels with little anomalies over Calcutta and from surface to 450 hPa over Cuttack and decreases gradually from 450 to 100 hPa with little anomalies over Cuttack during the movement of 1992 cyclone. The westerly wind decreases gradually during the period of movement of the severe cyclonic storm with a core of hurricane wind of 1992 and the cyclonic storm of 1992 over Madras.

The result shows that the westerly wind increases gradually from surface to 950 hPa and decreases gradually from 800 to 200 hPa level over the stations during 17-19 May 1992. It increases at all levels over Dhaka on 18th May with respect to that of 17th May and decreases from surface to 700 hPa and increases from 500 to 100 hPa on 19th May with respect to that of 18th May for the cyclonic storm of 1992. The westerly wind speed decreases at all levels on 18th May with respect to that of 17th May and increases at all levels on 19th May with respect to that of 18th May over Calcutta during the movement of the cyclonic storm of 1992.

The above discussion indicates clearly that the westerly wind decreases significantly at all levels over the area towards which the cyclones move for ultimate landfall.

3.4.3 Vertical temperature variation

The temperature decreases gradually from surface to 750 hPa and increases gradually from 750 to 200 hPa over Dhaka during the movement of the cyclones of 1985 and 1991. The temperature at the respective levels remains almost constant over Dhaka during the northward advancement of the cyclones of 1988 and 1994. The temperature increases on 20th November with respect to that of 19th November and decreases on 21st November with respect to that of 20th November over Dhaka for the cyclone of 1992. The temperature decreases from surface to 450 hPa on 18th May with respect to that of 17th May and at the respective levels remains almost constant on 18th and 19th May for the cyclonic storm of 1992.

The temperature decreases gradually over Chittagong from surface to 600 hPa during the period of movement of the cyclone of 1994 and at the respective levels remains almost constant during the period of movement of the cyclone of 1988. The temperature decreases gradually over Chittagong from surface to 600 hPa on 27th April and from surface to 900 hPa on 28th and 29th April for the cyclone of 1991. The temperature increases from surface to 300 hPa on 19th, decreases from surface to 400 hPa on 20th and increases again on 21st November from surface to 300 hPa for the cyclone of 1992. The temperature increases over Chittagong during the period of movement of the cyclonic storm of 1992.

During the movement of the cyclone of 1992, the temperature decreases gradually at all levels whereas it decreases gradually from surface to 800 hPa and increases gradually from 800 to 200 hPa over Calcutta with little anomalies during the period of movement of the cyclone of 1991 and the cyclonic storm of 1992. The temperature increases at all levels for the cyclone of 1994 and remains almost constant for the cyclone of 1988 whereas it increases from surface to 900 hPa and decreases from 850 to 500 hPa over Calcutta for the cyclone of 1985.

The temperature decreases at all levels over Cuttack during the formative stages of all the mentioned cyclones and increases gradually at all levels with little anomalies before two to

three days to the landfall of the cyclone. The temperature decreases at all levels over Cuttack on the day of landfall of the cyclonic storm of 1992.

The temperature at the respective levels remains almost constant during the period of movement but decreases at all levels on the day of landfall of the cyclones of 1991 and 1992 over Madras. The temperature increases at all levels during the period of movement of the cyclone of 1994 and increases on 24th May 1985 and decreases on 25th May 1985 for the cyclone of 1985 over Madras. The temperature decreases gradually from surface to 700 hPa and increases gradually from 650 to 400 hPa during the period of movement of the cyclone of 1988. The temperature is almost constant from surface to 650 hPa and increases gradually from 650 to 200 hPa over Madras for the cyclonic storm of 1992.

There is no variation of temperature observed during the period of movement of the cyclones of 1985, 1988, 1991, 1992 and the cyclonic storm of 1992 over Bangkok. The temperature increases from 850 to 200 hPa on 1st May with respect to that of 30th April and decreases from surface to 500 hPa and remains almost constant above these levels on 2nd May with respect to that of 1st May for the cyclone of 1994 over Bangkok.

The temperature increases gradually from surface to 300 hPa during the period of movement of the cyclone of 1988 over Port Blair. The temperature decreases when cyclone reaches nearer the station Port Blair and increases when it goes far away from the station for the cyclone of 1991. Irregular pattern is observed over the station during the period of movement of the cyclone of 1992.

The above discussion substantiates that there is a tendency for the temperature to decrease in the lower troposphere below 600 hPa mainly and increase in the upper troposphere over the areas towards which the cyclones move. The temperature of the troposphere remains almost constant in other areas surrounding the Bay of Bengal.

3.4.4 Vertical wind shear

The spatial distributions of vertical wind shear of all the above mentioned cyclones have been analysed and the conclusions have been drawn on the basis of the results. The pattern of vertical wind shear is the same for all the cyclones. It may be noted that wind observations over the Bay of Bengal in and around the cyclone are not available and the isolines have been drawn by using the land observations around the Bay of Bengal as per standard meteorological practice. The following conclusions can be drawn:

- Little or no vertical wind shear is observed near the centre of the cyclone.
- With the increase of the distance towards the north of the cyclone centre, the magnitude of vertical wind shear increases.
- Large horizontal gradient of vertical wind shear is observed to the north of the cyclone centre.
- Large negative shear is observed to the south of the cyclone centre.
- Maximum horizontal gradient of vertical wind shear is observed near the land-sea interface.

These features are similar to those observed by Mandal et al. (1981) for a cyclone in the Arabian Sea.

Chapter 4

Analysis of Different Tropospheric Energies and their Fluxes in the Surroundings of the Bay of Bengal during the Life Cycle of Different Cyclones.

4.1 Introduction

It is generally accepted that the track and the intensity of the cyclone in the tropics depend mostly on the sea surface temperature (SST). Once formed, the cyclone is found to move over middle latitude oceans where the ocean is colder (Krishnamurti, 1979). The role of energy fluxes is to govern the atmospheric circulation as well as the physical processes responsible for the formation and the movement of tropical cyclones (Palmen and Newton, 1969). Therefore, it is essential to study the tropospheric energy fluxes and their vertical distribution for the prediction of formation and movement of tropical cyclones. Chowdhury and Karmakar (1995) studied the tropospheric energy fluxes of a cyclone formed in the Bay of Bengal during its movement.

In the present study, the behavior of different tropospheric energies such as the dry static energy, the latent heat energy, the moist static energy, the total energy, the meridional flux of moist static energy and the zonal flux of moist static energy and their vertical distribution have been examined in the surroundings of the Bay of Bengal during the life cycle of cyclones. Several severe cyclonic storms with a core of hurricane winds and one cyclonic storm formed in the Bay of Bengal, which crossed the Bangladesh coast in the last decade, have been considered for the present study. The severe cyclonic storms with a core of hurricane winds occurring in 1985, 1988, 1991, 1992 and 1994 and the cyclonic storm of 1992 have been considered for the study.

4.2 Method of Analysis

We computed the different tropospheric energies such as the dry static energy, the latent heat energy, the moist static energy, the total energy, meridional flux of moist static energy and zonal flux of moist static energy by using the following relations (Holton, 1979):

Dry static energy: $s = C_p T + g Z$ (4.1)

Moist static energy: $h = C_p T + g Z + L q$ (4.2)

Total energy: $E = C_p T + g Z + L q + \frac{1}{2}V^2$ (4.3)

Meridional flux of noist static energy: $=(C_p T + g Z + L q) \times (-V \cos \phi)$ (4.4)

Zonal flux of noist static energy: $= (C_p T + g Z + L q) \times (-V \sin \phi)$ (4.5)

where,

C_p = the specific heat of air at constant pressure

T = the basic state absolute temperature

g = the acceleration due to gravity

Z = the geopotential height in meter

L = the latent heat of evaporation of water

V = the wind speed

$C_p T$ = the specific enthalpy

$g Z$ = the potential energy per unit mass

$L q$ = the latent heat energy per unit mass and

$\frac{1}{2}V^2$ = the kinetic energy per unit mass

q = the specific humidity.

The empirical formula (Byers, 1974) for specific humidity is given by:

$$q = \frac{r q_s}{100} = \frac{0.622 \times E_s(T_d)}{P - 0.38 \times E_s(T_T)} \quad (4.6)$$

q_s = the specific humidity at saturation

P = the basic state of pressure

T_d = the dew point temperature

T_T = the dry bulb temperature

$E_s(T_d)$ = the saturation vapour pressure at dew point temperature

$E_s(T_T)$ = the saturation vapour pressure at dry bulb temperature and

r = the relative humidity (Roger and Richard, 1982).

$$r = \frac{sat.\ vapour\ \ pressure\ at\ dew\ \ po\,\text{int} \times 100}{sat.\ vapour\ \ pressure\ at\ air\ temperature} \qquad (4.5)$$

The value of specific heat at constant pressure (C_p) is taken as 1004 J kg^{-1} K^{-1} (Fleagle and Businger, 1980). The latent heat of evaporation and saturation vapour pressure over water at different temperatures was used from Byers (1974). The latent heat of evaporation L over water was extrapolated at 1°C intervals from Byers and q requires separate computation.

4.3 Results

We have discussed different energies and their fluxes for the severe cyclonic storms with a core of hurricane winds of 1994, 1992, 1991, 1988 and 1985 and the cyclonic storm of 1992. The tracks of these cyclones are presented in chapter - 3 (Figs. 3.3(a-f)).

4.3.1 Severe Cyclonic Storm with a core of hurricane intensity of 1994

We have analysed the vertical variation of dry static energy, latent heat energy, moist static energy, total energy and the meridional and zonal fluxes of moist static energy for the severe cyclonic storm with a core of hurricane winds of 1994. Day-to-day variation of these energies has been discussed as the cyclone moves towards the land.

4.3.1.1 Dry static energy

The vertical distributions of the dry static energy per unit mass in the atmosphere are represented in the Figs. 4.3.1(a), 4.3.1(b) and 4.3.1(c).

Fig. 4.3.1(a) shows that the dry static energy decreases from surface to 475 hPa and increases from 475 to 200 hPa over Dhaka on 1st May with respect to that of 30th April and increases at all levels on 2nd May with respect to that of 1st May. The figure also shows that the dry static energy increases at all levels on 3rd May i.e. after the landfall with respect to that of 1st and 2nd May.

The dry static energy decreases (Fig. 4.3.1(b)) from 950 to 575 hPa and increases from 575 to 200 hPa over Chittagong on 2nd May with respect to that of 1st May.

It can also be seen from Fig. 4.3.1(c) that the dry static energy decreases from 600 to 475 hPa and increases from 850 to 600 hPa and 475 to 200 hPa over Calcutta on 1st May with respect to that of 30th April. The dry static energy increases at all levels on 2nd May with respect to that of 1st May. The figure also indicates that the dry static energy decreases from 750 to 200 hPa on 3rd May (i.e. after the landfall) than that of 2nd May over the station.

It is clear from the above discussion that the dry static energy of the troposphere increases at all levels in the far away stations such as Dhaka and Calcutta whereas there exist a decrease and an increase of dry static energy in the lower and upper troposphere respectively at the nearby station such as Chittagong on the day of landfall with respect to that of the previous day.

4.3.1.2 Latent heat energy

Fig. 4.3.1(d) shows that the latent heat energy decreases from 850 to 600 hPa and increases from 600 to 400 hPa over Dhaka on 1st May with respect to that of 30th April. The latent heat energy decreases from surface to 800 hPa on 2nd May with respect to that

of 1st May and has no regular trend above these levels over the station. The figure also shows that the latent heat energy increases from surface to 500 hPa on 3rd May i.e. after the landfall.

From the Fig. 4.3.1(e), it is found that the latent heat energy decreases from surface to 700 hPa and increases from 700 to 300 hPa over Chittagong on 2nd May with respect to that of 1 st May.

The latent heat energy decreases from 850 to 400 hPa having little anomalies over Calcutta on 1st May with respect to that of 30th April (Fig. 4.3.1(f)). The latent heat energy decreases from surface to 850 hPa and increases from 850 to 400 hPa on 2nd May with respect to that of 1st May over the station. The figure also shows that the latent heat energy has no definite trend on 3rd May i.e. after the landfall of the cyclone.

It is found that the latent heat energy decreases from surface to 700, 800 and 850 hPa over Chittagong, Dhaka and Calcutta respectively. The analysis also indicates that the latent heat energy increases from 700 to 300 hPa and 850 to 400 hPa over Chittagong and Calcutta respectively. The latent heat energy increases on 3rd May i.e. after the landfall over Dhaka and has no regular trend of variation over Calcutta.

4.3.1.3 Moist static energy

Figs. 4.3.1(g), 4.3.1(h) and 4.3.1(i) show the vertical variation of the moist static energy per unit mass in the atmosphere over Dhaka, Chittagong and Calcutta respectively.

It has been found that the moist static energy decreases from surface to 525 hPa and increases from 525 to 200 hPa over Dhaka on 1st May with respect to that of 30th April (Fig. 4.3.1(g)). The moist static energy decreases from surface to 775 hPa and increases from 775 to 200 hPa over Dhaka on 2nd May with respect to that of 1st May. This indicates that the moist static energy increases in the upper troposphere from 750 to 200 hPa and decreases in the lower troposphere from surface to 750 hPa as the cyclone moves towards the landfall area. Again the moist static energy increases from surface to 350 hPa and decreases from 350 to 200 hPa on 3rd May as compared to that of 2nd May.

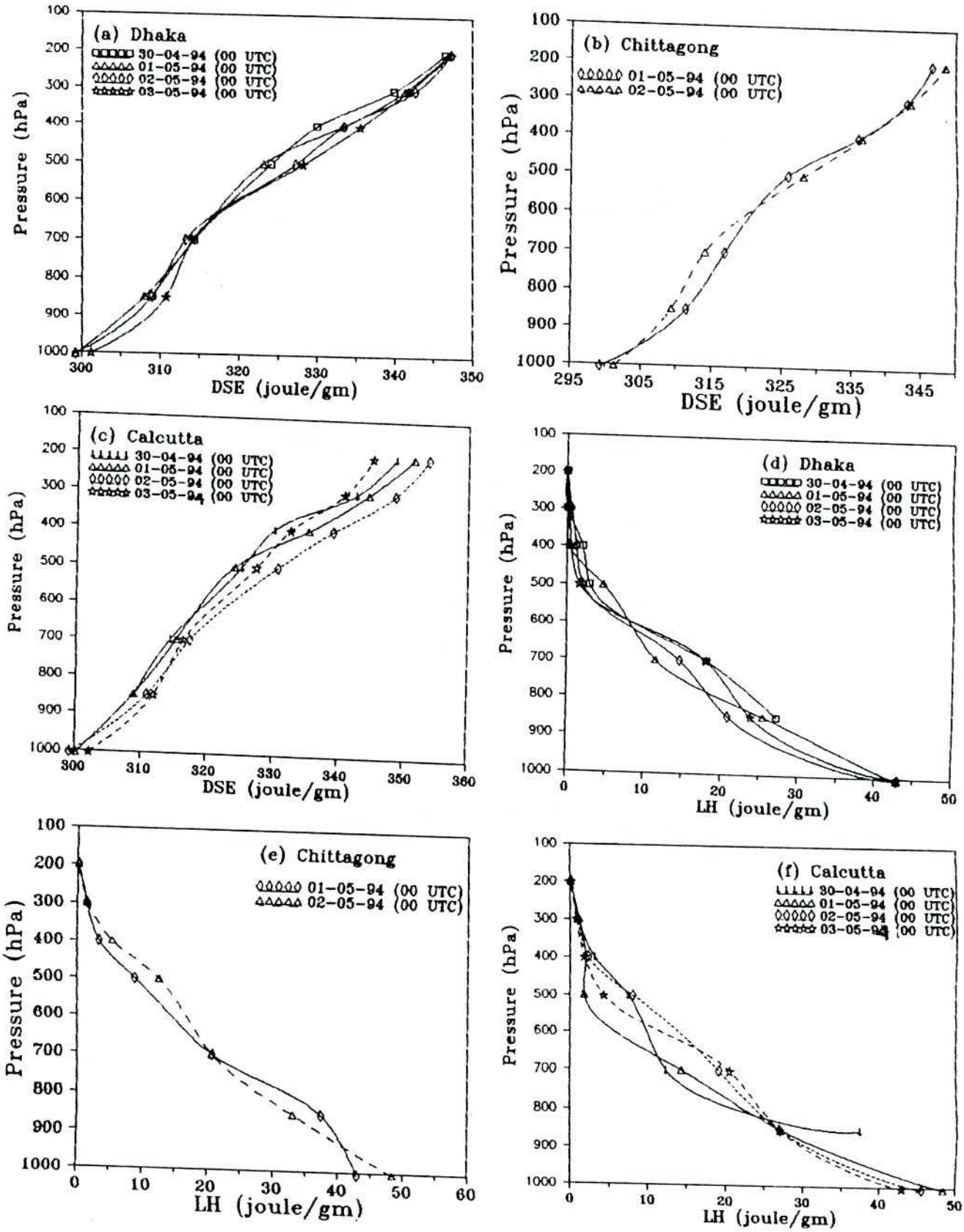

Figs. 4.3.1(a - c) Dry static energy over Dhaka, Chittagong and Calcutta for the cyclone 29th April to 2nd May 1994. Figs. 4.3.1(d - f) Latent heat energy over Dhaka, Chittagong and Calcutta for the cyclone 29th April to 2nd May 1994.

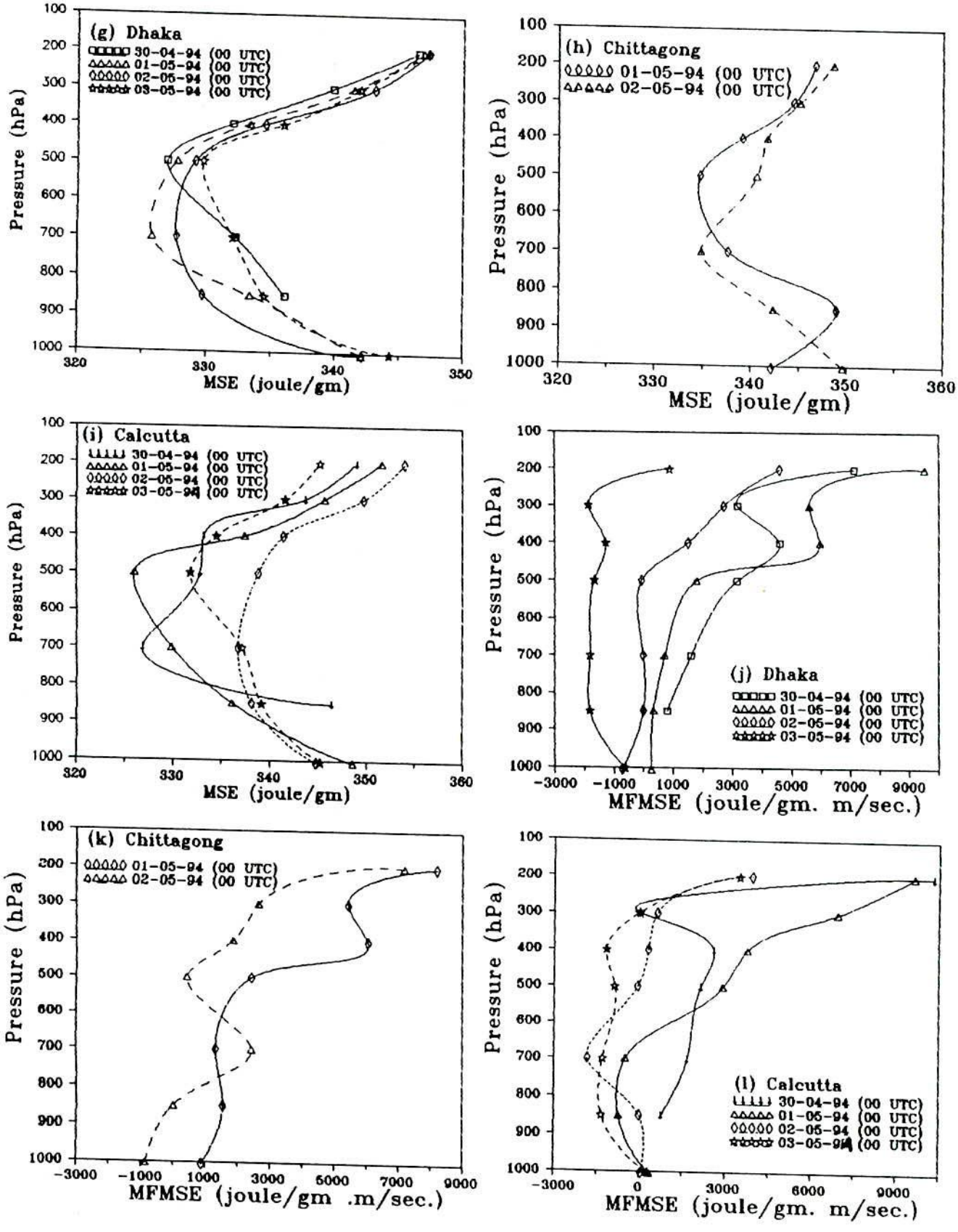

Figs. 4.3.1(g - i) Moist static energy over Dhaka, Chittagong and Calcutta for the cyclone 29th April to 2nd May 1994. Figs. 4.3.1(j - l) Meridional flux of moist static energy over Dhaka, Chittagong and Calcutta for the cyclone 29th April to 2nd May 1994.

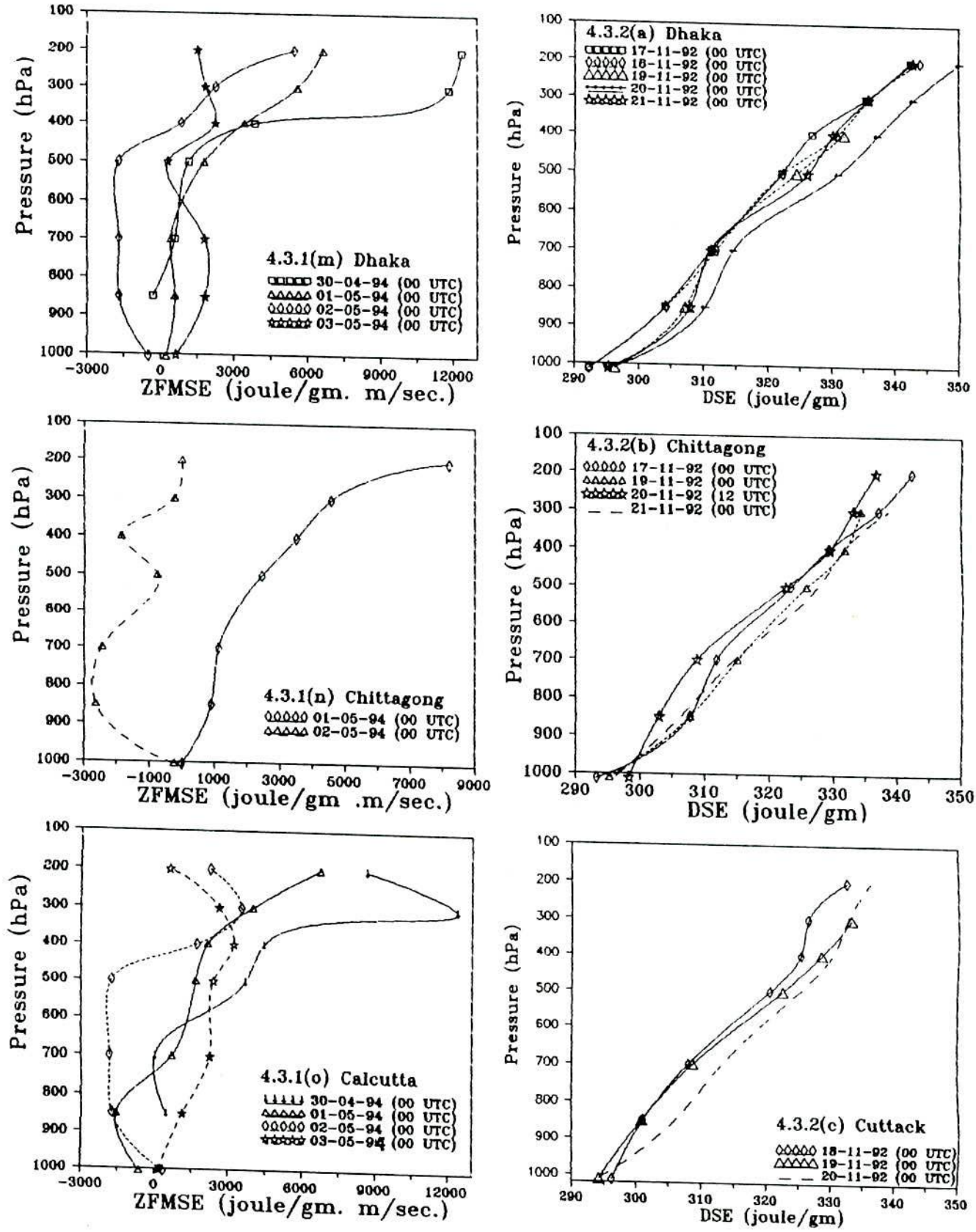

Figs. 4.3.1(m - o) Zonal flux of moist static energy over Dhaka, Chittagong and Calcutta for the cyclone 29th April to 2nd May 1994. Figs. 4.3.2(a - c) Dry static energy over Dhaka, Chittagong and Cuttack for the cyclone 17 - 21 November 1992.

The moist static energy decreases from 950 to 625 hPa and increases from surface to 950 hPa and 625 to 200 hPa over Chittagong on 2nd May as compared to that of 1st May (Fig. 4.3.1 (h)). This indicates that the magnitude of moist static energy increases in the upper troposphere from 650 to 200 hPa and decreases in the lower troposphere from 950 to 650 hPa as the cyclone moves towards the landfall over Chittagong.

Over Calcutta the moist static energy decreases from surface to 425 hPa and increases from 425 to 200 hPa with little anomalies on 1st May with respect to that of 30th April (Fig. 4.3.1(i)). The moist static energy increases from 900 to 200 hPa and little decrease is observed from surface to 900 hPa over Calcutta on 2nd May than that of 1st May. Again the moist static energy decreases at all levels with little anomalies around 700 hPa on 3rd May with respect to that of 2nd May over the station.

It is also found that the moist static energy decreases with height from surface to 700 or 500 hPa and increases from these levels to 200 hPa during the period. The minima are observed at 700 hPa over all stations on the day of landfall and 500 or 600 hPa before and after the landfall. This is due to the conditional instability of the troposphere in the tropics (Krishnamurti, 1979).

The decrease of moist static energy in the lower troposphere is significant in the nearer station such as Chittagong and increase in moist static energy is also significant in the far away station such as Calcutta. The significant decrease of moist static energy in the lower troposphere from surface to 650 hPa level over Chittagong is due to the significant decrease of dry static energy and the latent heat energy, and the increase in the upper troposphere is due to the increase of dry static energy and latent heat energy.

4.3.1.4 Total energy

The changing pattern of variation of total energy is the same as mentioned in case of moist static energy. Due to the contribution of kinetic energy to the moist static energy, there is only fractional variation of the magnitude of total energy.

4.3.1.5 Meridional flux of moist static energy

The Fig. 4.3.1(j) shows that the southerly (+ve) flux decreases from 850 to 450 hPa and increases from 450 to 200 hPa over Dhaka on 1st May with respect to that of 30th April and decreases at all levels on 2nd May than that of 1st May. Tremendous amount of southerly (+ve) flux exists at 200 hPa during the period. The meridional flux of moist static energy is small from surface to 500 hPa and there is southerly (+ve) flux from 500 to 200 hPa on 2nd May. This indicates that the northerly (-ve) flux is flowing in the lower troposphere and the southerly (+ve) flux is flowing in the upper troposphere. After the landfall of the cyclone, the northerly (-ve) flux is significant at all levels on 3rd May over the station.

Fig. 4.3.1(k) shows the presence of southerly (+ve) flux of moist static energy at all levels over Chittagong on 1st and 2nd May with little anomalies near the surface on 2nd May. The southerly (+ve) flux decreases from surface to 200 hPa having little anomalies around 700 hPa on 2nd May with respect to that of 1st May.

In Fig. 4.3.1(l), a decrease of southerly flux is seen from 850 to 550 hPa and increase from 550 to 200 hPa over Calcutta on 1st May with respect to that of 30th April. The magnitude of southerly (+ve) flux decreases and the northerly (-ve) flux increases gradually during 1st to 3rd May from 800 to 200 hPa except little anomalies over the station. The figure also shows that the northerly flux exists and decreases from surface to 800 hPa on 2nd May with respect to that of 1st May and increases after the landfall. The northerly (-ve) flux is flowing from surface to 300 hPa on 2nd and 3rd May and the southerly (+ve) flux is flowing from 300 to 200 hPa on 3rd May over the station.

4.3.1.6 Zonal flux of moist static energy

The westerly flux of moist static energy is almost constant from 850 to 400 hPa and decreases from 400 to 200 hPa over Dhaka on 1st May with respect to that of 30th April (Fig. 4.3.1(m)). The fluxes are westerly (+ve) from surface to 200 hPa on 1st May and from 420 to 200 hPa on 2nd May. The westerly (+ve) flux is found to decrease

significantly whereas the easterly (-ve) flux increases from surface to 400 hPa on 2nd May with respect to that of the 1st May over the station. Again after the landfall on 3rd May, the flux becomes westerly (+ve) at all levels over the station.

The westerly (+ve) flux is significant at all levels with increasing magnitude gradually over Chittagong on 1st May whereas the easterly (-ve) flux is significant at all levels on 2nd May over the station (Fig. 4.3.1(n)).

The westerly flux decreases at all levels with little anomalies over Calcutta on 1st May with respect to that of 30th April (Fig. 4.3.1(o)). The easterly (-ve) flux is observed from surface to 750 and 450 hPa and the westerly (+ve) flux is seen from 750 to 200 hPa and 450 to 200 hPa over the station on 1st and 2nd May, respectively. Again on 3rd May the flux is westerly (+ve) at all levels over the station.

4.3.1.7 Combination of zonal and meridional fluxes

When the zonal and meridional fluxes are combined, it is seen that the flux is south-westerly at all levels with increasing magnitude gradually from surface to 200 hPa and sharp maxima is observed at 200 hPa over Dhaka on 30th April and 1st May. The slight amount of north-easterly flux is flowing from surface to 450 hPa and the south-westerly flux exists from 450 to 200 hPa on 2nd May. On 1st and 2nd May, the flux is significantly south-westerly in the upper troposphere having sharp maxima at 200 hPa whereas the flux is slightly north-easterly in the lower troposphere. Again on 3rd May i.e. after the landfall of the cyclone, the flux is north-westerly at all levels over the station.

The south-westerly flux is found to exist at all levels with tremendous amplitude at 200 hPa over Chittagong on 1st May. On 2nd May, the flux is south-easterly at all levels having a greater southerly component over the station.

Over Calcutta, the south-westerly flux exists at all levels on 30th April and there is north-easterly flux from surface to 700 hPa and south-westerly flux from 700 to 200 hPa with tremendous amplitude at 200 hPa on 1st May. The north-easterly flux is found to extend

from surface to 450 hPa and the south-westerly flux from 450 to 200 hPa on 2nd May over the station. Again on 3rd May i.e. after the landfall of the severe cyclonic storm, the flux changes to north-westerly throughout the troposphere with little anomalies over the station.

4.3.2 Severe Cyclonic Storm with a core of hurricane intensity of 1992

We have analysed the vertical variation of dry static energy, latent heat energy, moist static energy, total energy and the meridional and zonal fluxes of moist static energy for the severe cyclonic storm with a core of hurricane winds of 1992. Day-to-day variation of these energies has been discussed as the cyclone progress.

4.3.2.1 Dry static energy

Fig. 4.3.2(a) shows that the dry static energy is almost constant from the surface to 500 hPa and it increases from 500 to 200 hPa over Dhaka on 18th November with respect to that of 17th November. The dry static energy increases gradually from surface to 400 hPa over Dhaka during 18-20 November as the cyclone moves towards the landfall. This increase is more significant on 20th November than those of any other days over the station. The figure also shows that the dry static energy decreases at all levels on 21st November with respect to that of 20th November over the station.

Over Chittagong the dry static energy decreases gradually from surface to 850 hPa and increases gradually from 700 to 300 hPa on 17th, 19th and 21st November as can be seen from Fig. 4.3.2(b). The figure also shows that the dry static energy decreases at all levels on 20 November at1200 UTC with respect to that of any other days at 0000 UTC.

The dry static energy over Cuttack increases gradually at all levels during 18-20 November with little anomalies around surface on 19th November (Fig. 4.3.2(c)).

In Fig. 4.3.2(d), it is observed that the dry static energy increases at all levels over Port Blair on 18th November with respect to that of 17th November. The figure also shows

that the dry static energy decreases gradually at all levels with little anomalies during 18-20 November as the cyclone moves far away from the station.

From the analysis it is found that the dry static energy increases gradually with little anomaly over all stations except Port Blair as the cyclone moves towards the landfall. Again the dry static energy decreases on 20th at1200 UTC over Chittagong and 21st over Dhaka with respect to that of the previous day.

4.3.2.2 Latent heat energy

The latent heat energy over Dhaka decreases from surface to 450 hPa on 18th November with respect to that of 17th November (Fig. 4.3.2(e)). Again the latent heat energy increases gradually during 18-21 November from surface to 600 hPa with little anomalies observed on 18th November over the station.

The latent heat energy decreases from surface to 725 hPa and increases from 725 to 350 hPa over Chittagong on 19th November with respect to that of 17th November (Fig. 4.3.2(f)). The latent heat energy increases from surface to 775 hPa and decreases from 775 to 300 hPa on 20th November with respect to that of 19th November. The figure also shows that the latent heat energy increases from surface to 600 hPa and decreases from 600 to 300 hPa on 21st November with respect to that of 20th November.

Fig. 4.3.2(g) shows that the latent heat energy decreases from surface to 300 hPa over Cuttack on 19th November with respect to that of 18th November. The figure also shows that the latent heat energy increases from surface to 750 hPa and decreases from 750 to 300 hPa on 20th November with respect to that of 19th November.

From Fig. 4.3.2(h), it is observed that the latent heat energy increases from surface to 500 hPa and decreases from 500 to 200 hPa over Port Blair on 18 November with respect to that of 17 November. It is found that the latent heat energy decreases gradually from surface to 300 hPa during 18-20 November having little anomalies observed around the surface on 19 November.

From the above analysis, it is found that the latent heat energy increases from surface to 700 hPa and decreases from 700 to 300 hPa gradually on 18th, 19th, 20th and 21st November over Dhaka and Chittagong. It has also seen that the latent heat energy decreases gradually from surface to 300 hPa on 18th, 19th and 20th November over Cuttack and Port Blair with little anomalies in the lower levels on 20th November over Cuttack and on 19th November over Port Blair.

4.3.2.3 Moist static energy

The moist static energy over Dhaka decreases significantly from the surface to 450 hPa and has no regular trend from 450 to 200 hPa on 18th November with respect to that of 17th November as seen from the Fig. 4.3.2(i). The figure also shows the significant increase of moist static energy at all levels on 20th November with respect to that of 18th November. Again the moist static energy increases from surface to 600 hPa and decreases from 600 to 200 hPa on 21st November with respect to that on 20th November over the station. The increase of moist static energy on 20th November with respect to that of 18th November at all levels implies that more moisture is coming from the Bay of Bengal towards the land area. This moist static energy increases continuously in the lower troposphere on 21st November and decrease in the upper troposphere. The moist static increases gradually in the lower troposphere due to the increase in latent heat energy and decreases in the upper troposphere on 21st November due to the decrease in dry static energy over the station.

Fig. 4.3.2(j) shows that the moist static energy decreases from the surface to 750 hPa and increases from 750 to 350 hPa over Chittagong on 19th November with respect to that of 17th November. It is found that there is increase in moist static energy from surface to 850 hPa and significant decrease of moist static energy from 850 to 200 hPa on 20th November with respect to that of 19th November. Again the moist static energy increases at all levels with little anomalies around 500 hPa on 21st November with respect to that of 20th November. The significant decrease of moist static energy observed from 850 to 200 hPa on 20th November is due to the significant decrease of dry static energy and little decrease of latent heat energy. The significant increase of moist static energy from surface

to 600 hPa on 21st November with respect to that of 20th November is due to the increase of latent heat energy and dry static energy over the station.

There exist significant decrease of moist static energy from surface to 500 hPa and significant increase in moist static energy from 500 to 200 hPa over Cuttack on 19th November with respect to that of 18th November (Fig. 4.3.2(k)). Again the significant increase of moist static energy is observed from surface to 650 hPa having a slight decrease from 650 to 200 hPa on 20th November with respect to that of 19th November. The decrease in moist static energy on 19th November with respect to that of 18th November in the lower troposphere is due to the decrease of latent heat energy, and increase in the upper troposphere is due to the increase in dry static energy over the region. Again the moist static energy increases in the lower troposphere, which is due to the increase in latent heat energy and dry static energy, and the decrease in the upper troposphere is due to the decrease of latent heat energy.

Fig. 4.3.2(l) shows that the moist static energy increases significantly at all levels over Port Blair on 18th November with respect to that of 17th November. The figure also shows that the moist static energy decreases gradually at all levels over the station during 18-20 November. The moist static energy decreases gradually due to the decrease of latent heat energy and dry static energy over the region.

It is also found that the moist static energy decreases with height with few exceptions from surface to 850 hPa or 700 hPa and increase from these levels to 200 hPa during the period over all stations. The exception is found over Chittagong station where the moist static energy increases from surface to 850 hPa on 17th November and surface to 700 hPa on 21st November.

4.3.2.4 Total energy

The changing pattern of the vertical variation of total energy is the same as mentioned in the case of moist static energy. Due to the addition of the kinetic energy with the moist static energy there is only fractional variation of the magnitude of total energy.

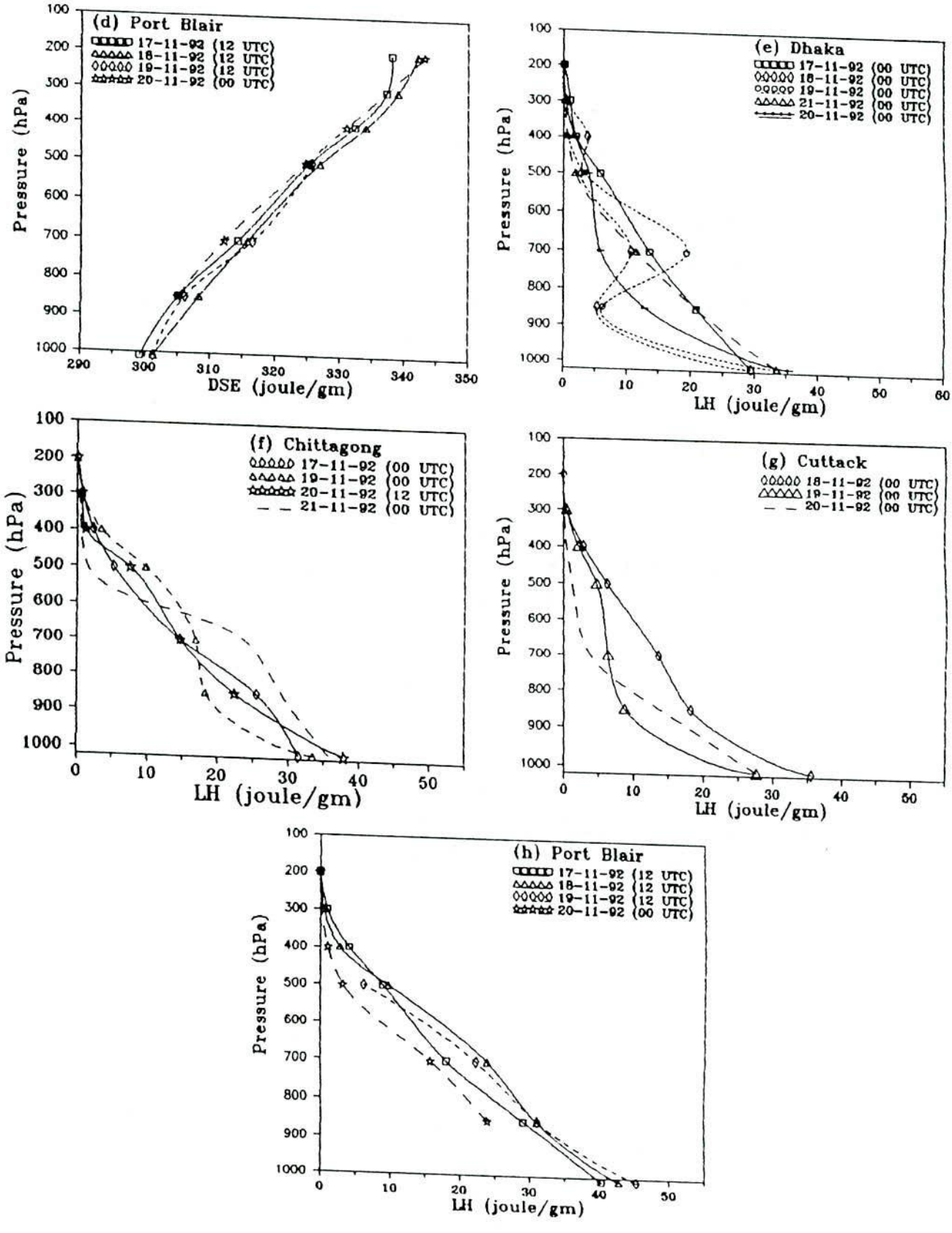

Fig. 4.3.2(d) Dry static energy over Port Blair for the cyclone 17 - 21 November 1992.
Figs. 4.3.2(e - h) Latent heat energy over Dhaka, Chittagong, Cuttack and Port Blair for the cyclone 17 - 21 November 1992.

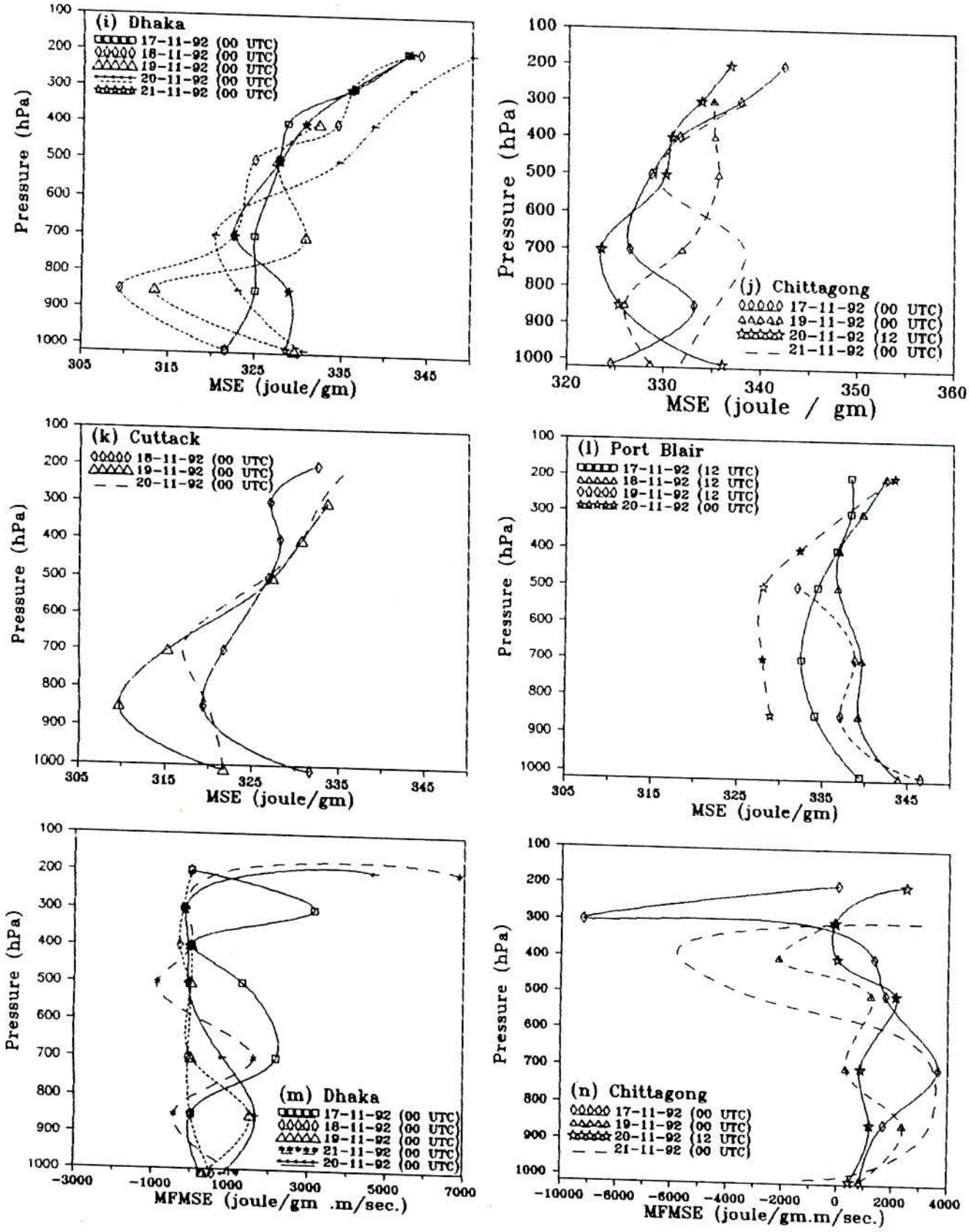

Figs. 4.3.2(i - l) Moist static energy over Dhaka, Chittagong Cuttack and Port Blair for the cyclone 17 - 21 November 1992. Figs. 4.3.2(m - n) Meridional flux of moist static energy over Dhaka and Chittagong for the cyclone 17 - 21 November 1992.

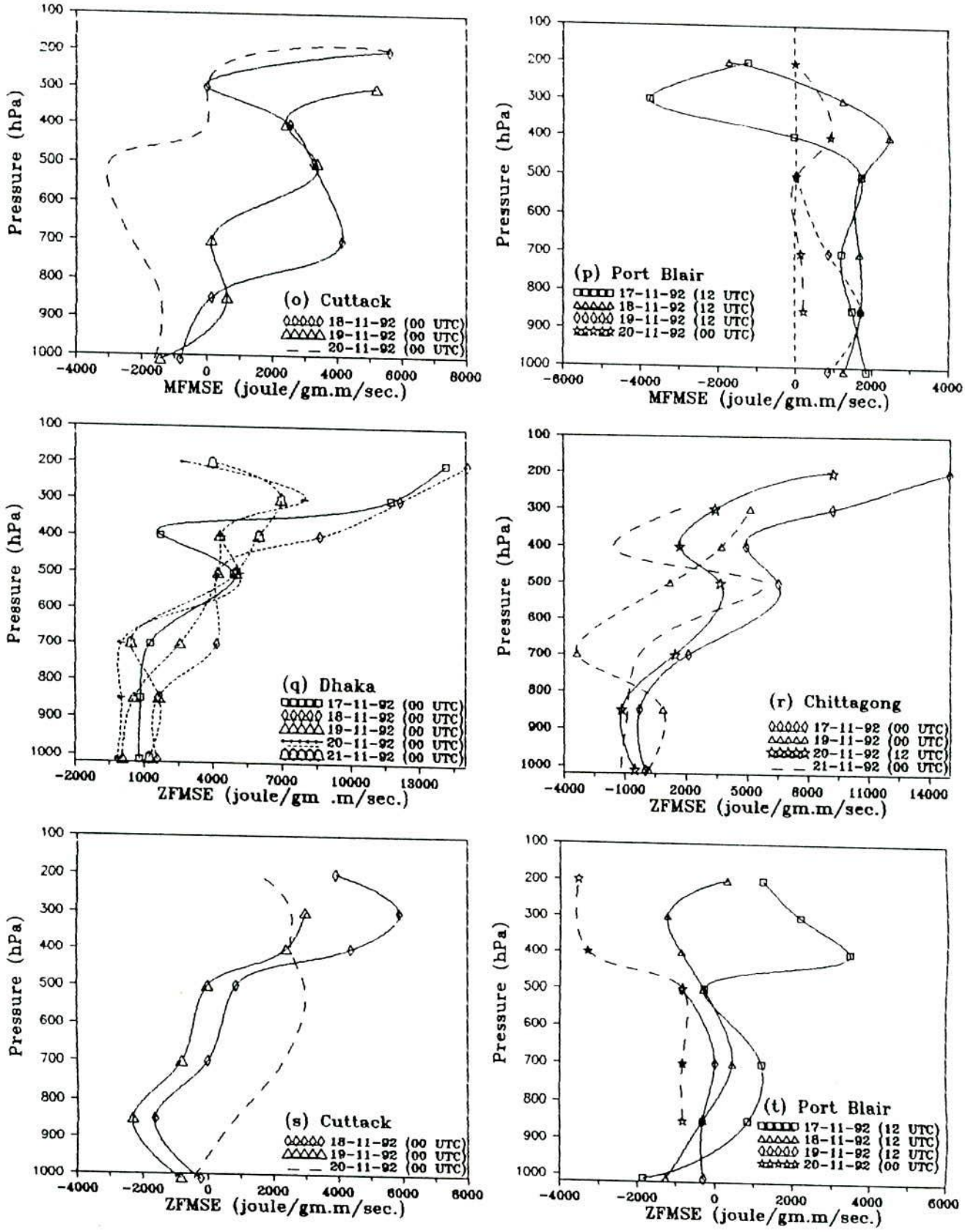

Figs. 4.3.2(o - p) Meridional flux of moist static energy over Cuttack and Port Blair for the cyclone 17 - 21 November 1992. Figs. 4.3.2(q - t) Zonal flux of moist static energy over Dhaka, Chittagong, Cuttack and Port Blair for the cyclone 17 - 21 November 1992.

4.3.2.5 Meridional flux of moist static energy

The Fig. 4.3.2(m) shows that a significant amount of southerly flux exists throughout the troposphere over Dhaka on 17th November. It also shows that a small amount of meridional flux exists during 18th to 21st November from surface to 250 hPa and a large amount of southerly flux exists around 200 hPa on 20th and 21st November respectively over the station.

From Fig. 4.3.2(n), it is observed that there is a large amount of southerly flux from surface to 320 hPa and significant amount of northerly flux is found to exist from 320 to 200 hPa over Chittagong on 17th November. Again on 19th and 20th November slight southerly flux exists at all levels over the station. The large amount of southerly flux exists from surface to 600 hPa and the flux is significantly northerly from 600 to 325 hPa having sharp maxima at 400 hPa on 21st November over the station.

The flux is southerly at all levels over Cuttack on 18th and 19th November and little amount of northerly flux exists near the surface on 19th November over the station (Fig. 4.3.2(o)). On 20th November the flux is northerly from surface to 300 hPa and southerly from 300 to 200 hPa.

Fig. 4.3.2(p) shows the presence of southerly flux from surface to 400 hPa and the northerly flux from 400 to 200 hPa over Port Blair on 17th November. The flux is southerly at all levels and decreases gradually during 18-20 November over the station.

4.3.2.6 Zonal flux of moist static energy

The westerly (+ve) flux of moist static energy increases gradually at all levels except little anomalies over Dhaka on 17th and 18th November (Fig. 4.3.2(q)). Little amount of easterly (-ve) flux exists from surface to 700 hPa and the flux is westerly (+ve) from 700 to 200 hPa and from surface to 200 hPa on 20th and 21st November respectively. The figure also indicates that the westerly (+ve) flux in the upper troposphere decreases as the cyclone moves towards the coast. The magnitude of westerly flux on 18th November is

greater with respect to that of 17th November and 21st November with respect to that of 20th November.

The zonal flux over Chittagong decreases from 800 to 200 hPa having little anomalies during 17th to 21st November except on 19th November (Fig. 4.3.2(r)). The easterly flux is significantly large from 825 to 200 hPa and sharp maxima are observed at 700 hPa on 19th November. The large westerly flux exists from 800 to 200 hPa and small amount of easterly flux exists in the lower troposphere from surface to 800 hPa on 20th November over the station. The maximum amount of westerly (+ve) flux exists at 500 hPa and maximum amount of easterly (-ve) flux at 400 hPa on 21st November. The data were not available on 18th November over the station.

Fig. 4.3.2(s) shows that the flux is easterly from surface to 600 hPa or 500 hPa and westerly from 600 to 200 hPa and 500 to 200 hPa over Cuttack on 18th and 19th November respectively. The magnitude of easterly (-ve) flux increases from surface to 600 hPa and the westerly (+ve) flux decreases from 600 to 200 hPa gradually on 18th and 19th November. There exists westerly flux from 950 to 200 hPa and little amount of easterly flux exists around surface on 20th November over the station.

The Fig. 4.3.2(t) shows that there is westerly flux from 950 to 200 hPa, and little amount of easterly flux of moist static energy exists around surface over Port Blair on 17th November. The easterly flux increases gradually at all levels during 18-20 November over the station.

4.3.2.7 Combination of zonal and meridional fluxes

When the zonal and meridional flux of moist static energy are combined, it is seen that the flux is mainly south-westerly from surface to 300 hPa over Dhaka on 17th, 20th and 21st November. The flux is slightly north-easterly from surface to 300 hPa on 18th November over the station.

There exists south-westerly flux from 800 to 350 hPa and tremendous amount of north-westerly flux exists from 350 to 200 hPa over Chittagong on 17th November. The flux is south-easterly from surface to 550 hPa and north-westerly from 500 to 300 hPa on 19th November. The south-easterly flux is observed from surface to 750 hPa and significant amount of south-westerly flux is also seen from 750 to 200 hPa on 20th November over the station. On 21st November the maximum amount of north-westerly flux exists around 500 hPa and maximum amount of north-easterly flux exists at 400 hPa which are due to the movement of the cyclone away from Chittagong station.

Over Cuttack, there are south-easterly flux from surface to 500 hPa and south-westerly flux from 500 to 200 hPa on 18th and 19th November respectively. Again north-westerly flux is observed from surface to 400 hPa and south-westerly flux from 400 to 200 hPa on 20th November. The south-easterly flux is seen to dominate at all levels over Port Blair during 18-20 November.

4.3.3 Severe Cyclonic Storm with a core of hurricane intensity of 1991

We have analysed the vertical variation of dry static energy, latent heat energy, moist static energy, total energy and the meridional and zonal fluxes of moist static energy for the severe cyclonic storm with a core of hurricane winds of 1991. Day-to-day variation of these energies has been discussed in the surroundings of the Bay of Bengal.

4.3.3.1 Dry static energy

In Fig. 4.3.3(a), the dry static energy decreases gradually from surface to 800 hPa over Dhaka during 27-29 April. The figure also shows that the dry static energy increases from 800 to 200 hPa on 29th April with respect to that of 28th April.

The Fig. 4.3.3(b) shows that the dry static energy has no regular trend on 27th and 28th April but increases from 600 to 220 hPa over Chittagong on 29th April with respect to that of 27th and 28th April.

Fig. 4.3.3(c) shows that the dry static energy decreases from surface to 275 hPa over Calcutta on 28th April with respect to that of 27th April. The figure also shows that the dry static energy increases at all levels on 29th April with respect to that of 28th April.

The dry static energy decreases at all levels over Cuttack on 27 April with respect to that of 26 April (Fig. 4.3.3(d)). Again the dry static energy decreases from surface to 700 hPa and increases from 700 to 400 hPa on 29th April with respect to that of 27th April.

From Fig. 4.3.3(e), it is observed that the dry static energy decreases at all levels over Port Blair on 26th April with respect to that of 25th April. The figure also shows that the dry static energy increases significantly at all levels on 28th April with respect to that of 25th and 26th April.

From the above discussion, it is found that the dry static energy decreases in the farther stations such as Calcutta from surface to 250 hPa, over Dhaka from surface to 500 hPa and increases over Chittagong from 900 to 550 hPa on 28th April with respect to that of 27th April. Again the dry static energy increases in the upper troposphere over all stations on 29th April with respect to that of 28th April.

4.3.3.2 Latent heat energy

The latent heat energy over Dhaka increases significantly from the surface to 300 hPa during 27-29 April except at the surface on 29th April where the latent heat energy decreases slightly (Fig. 4.3.3(f)).

The latent heat energy over Chittagong decreases significantly from the surface to 750 hPa on 28th and 29th April with respect to that of 27th April and increases gradually from 750 to 600 hPa during the period (Fig. 4.3.3(g)). Again the latent heat energy is almost constant from surface to 800 hPa and increases from 800 to 600 hPa on 29th April with respect to that of 28th April over the station.

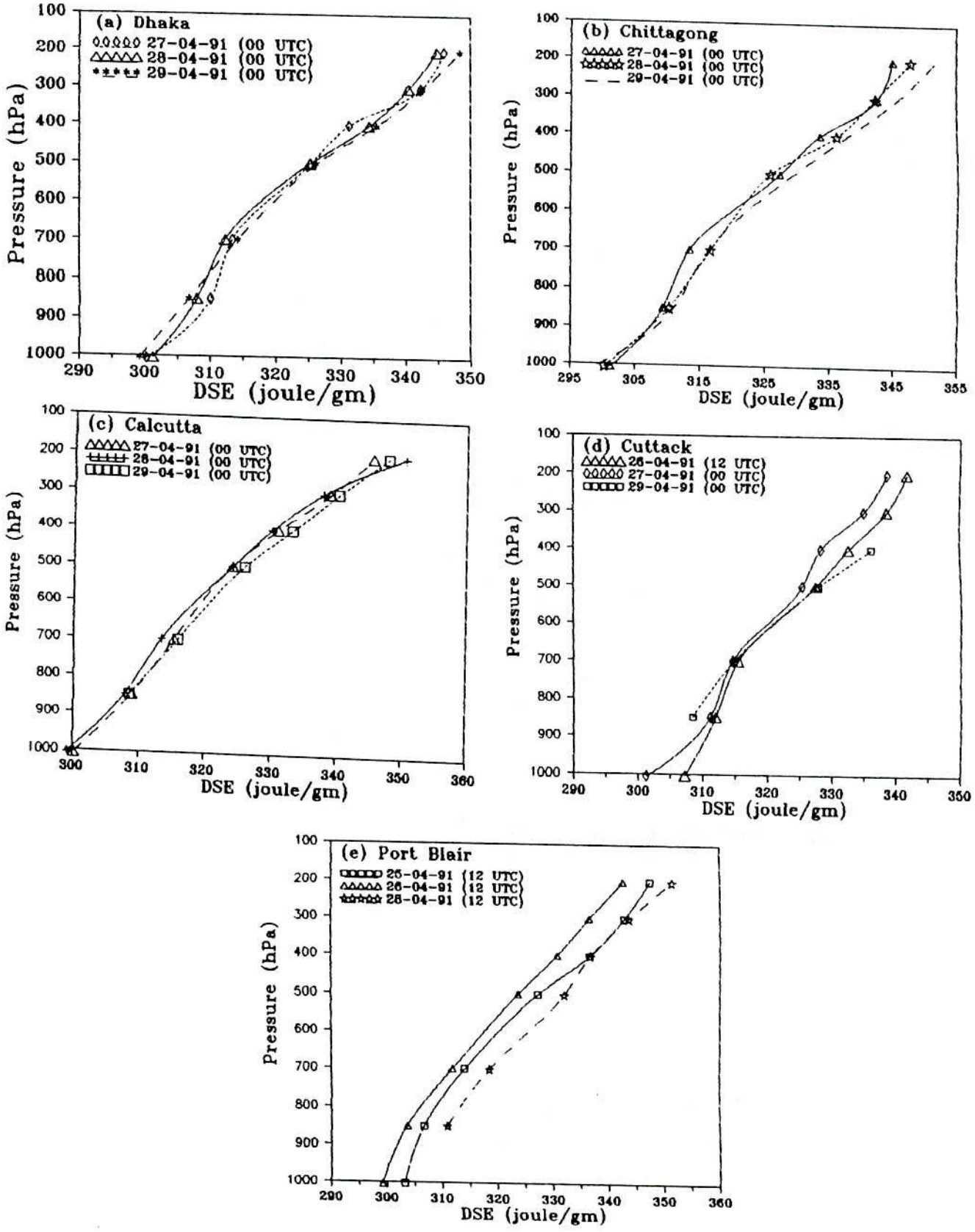

Figs. 4.3.3(a - e) Dry static energy over Dhaka, Chittagong, Calcutta, Cuttack and Port Blair for the cyclone 27 - 29 April 1991.

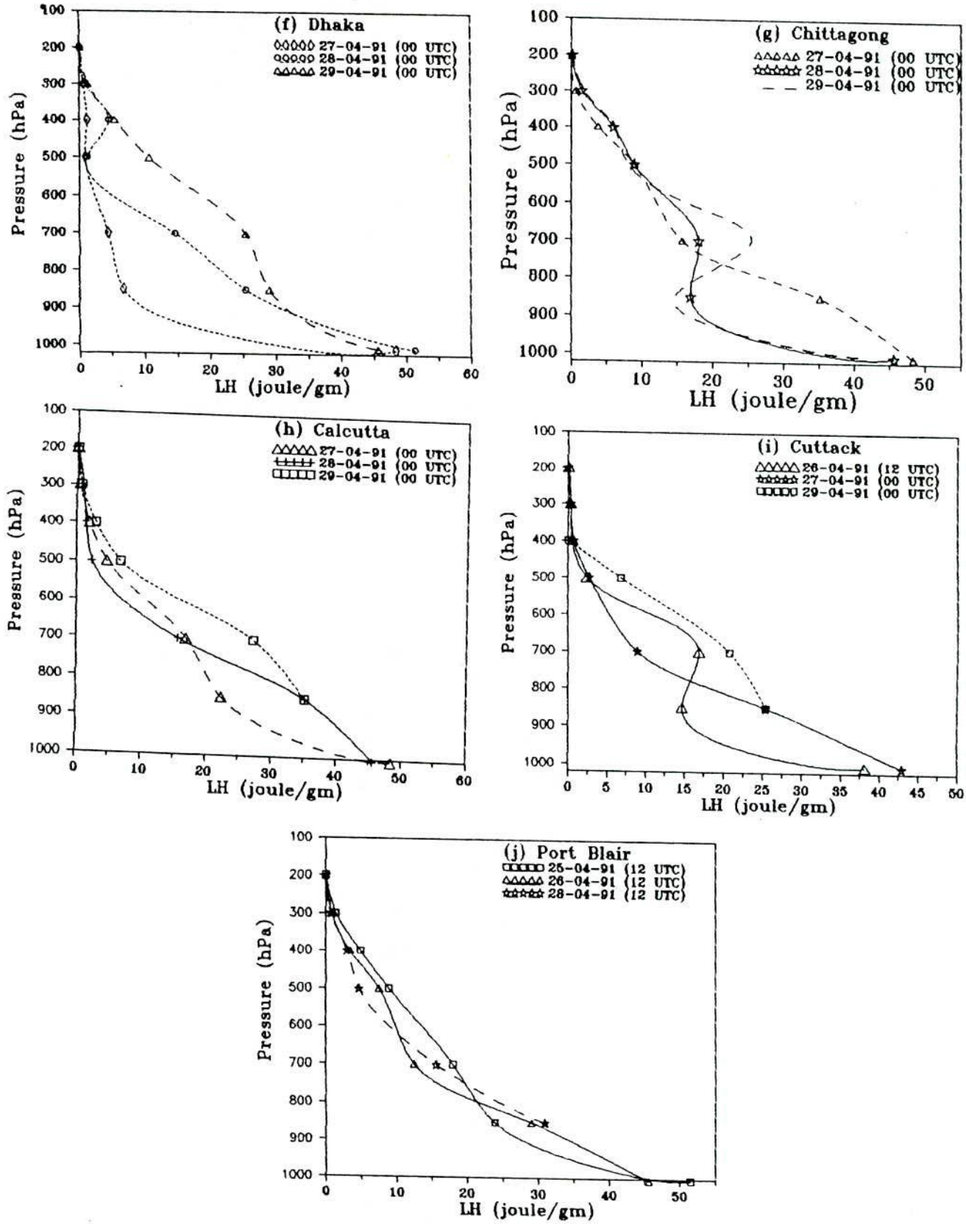

Figs. 4.3.3(f - j) Latent heat energy over Dhaka, Chittagong, Calcutta, Cuttack and Port Blair for the cyclone 27 - 29 April 1991.

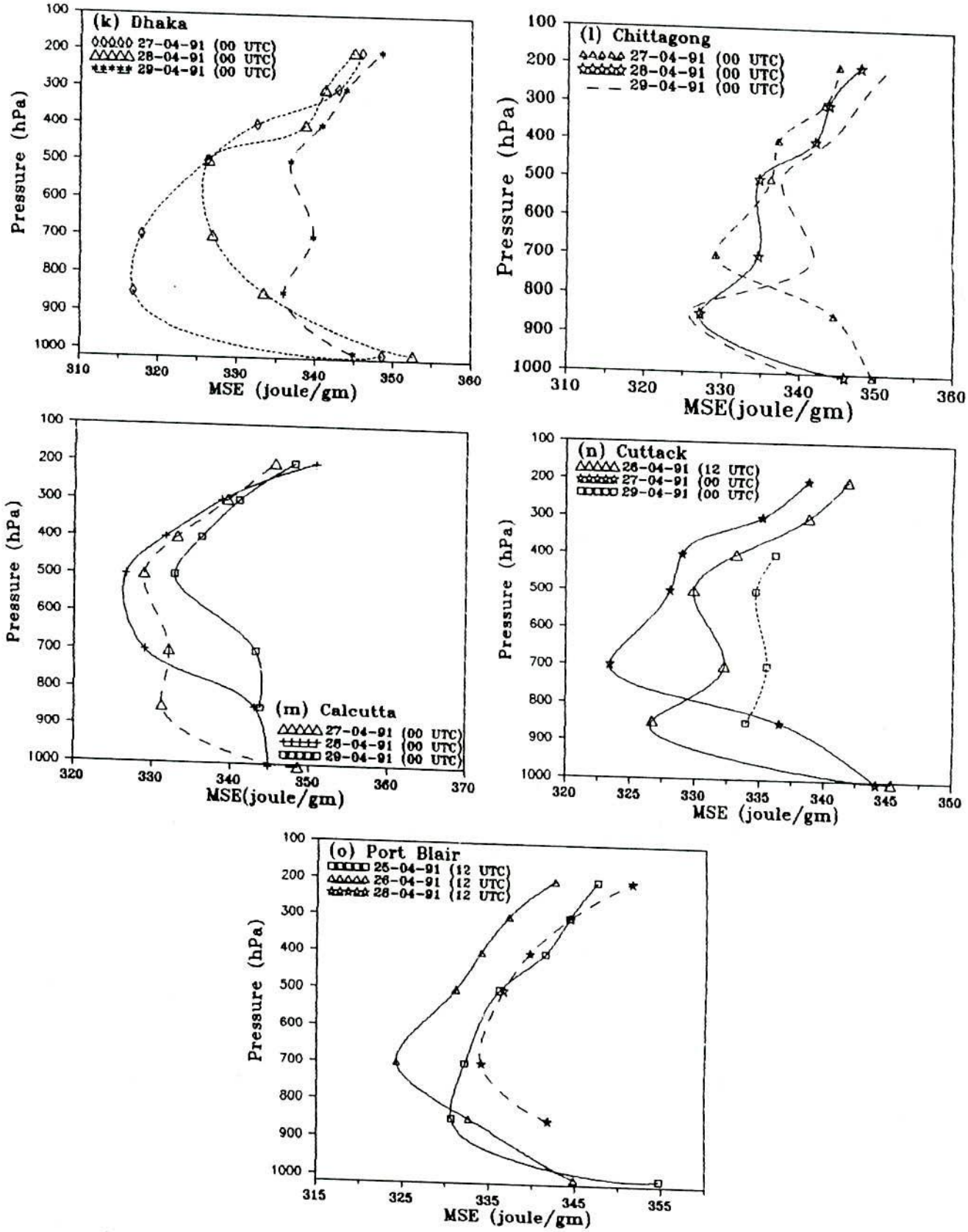

Figs. 4.3.3(k - o) Moist static energy over Dhaka, Chittagong, Calcutta, Cuttack and Port Blair for the cyclone 27 - 29 April 1991.

The latent heat energy over Calcutta increases from the surface to 700 hPa and decreases from 700 to 400 hPa on 28th April with respect to that of 27th April (Fig. 4.3.3(h)). Again the latent heat energy increases from 850 to 350 hPa on 29th April with respect to that of 28th April. The data were not available for the surface on 29th April over the station.

In Fig. 4.3.3(i), it is found that the latent heat energy increases from the surface to 800 hPa and decreases from 800 to 500 hPa over Cuttack on 27th April with respect to that of 26th April. The latent heat energy decreases from surface to 850 hPa and increases significantly from 850 to 400 hPa on 29th April with respect to that of 27th April over the station.

Fig. 4.3.3(j) shows that the latent heat energy increases from surface to 800 hPa and decreases from 800 to 300 hPa over Port Blair on 26th April with respect to that of 25th April. The figure also shows that the latent heat energy increases from 850 to 650 hPa and decreases from 650 to 400 hPa on 28th April with respect to that of 26th April.

From the analysis, it is found that the latent heat energy increases significantly over Dhaka, Calcutta, Cuttack and Port Blair as the cyclone moves towards the landfall and the latent heat energy decreases slightly on 29th April around surface over Dhaka and Cuttack. It is also seen that the latent heat energy decreases significantly from surface to 750 hPa and increases from 725 to 600 hPa on 28th and 29th April over Chittagong.

4.3.3.3 Moist static energy

The moist static energy over Dhaka increases significantly during 27-29 April except little anomalies as the cyclone moves towards the ultimate landfall (Fig. 4.3.3(k)). The anomalous behaviour is observed from surface to 900 hPa on 29th April where the moist static energy slightly decreases. This significant increase of moist static energy during the period is due to the significant increase of latent heat energy and the moist static energy decreases in the lower troposphere on 29th April which is due to the decrease in dry static energy and latent heat energy.

From Fig. 4.3.3(l), it is found that the moist static energy decreases significantly from the surface to 750 hPa over Chittagong on 28th April with respect to that of 27th April and has no regular trend from 750 to 200 hPa. Again the moist static energy decreases from surface to 800 hPa and increases from 800 to 200 hPa on 29th April in comparison to that of 28th April. The significant decrease of moist static energy from surface to 800 hPa on 28th and 29th April is due to the decrease of latent heat energy and increase in moist static energy on 29th April in comparison to that of 28th April is due to the increase in dry static energy over the station.

The moist static energy over Calcutta increases significantly from the surface to 750 hPa and decreases from 750 to 300 hPa on 28th April in comparison to that of 27th April (Fig. 4.3.3(m)). Again the moist static energy increases significantly from 850 to 250 hPa on 29th April in comparison to that of 28th April. This significant increase in moist static energy in the lower troposphere from surface to 750 hPa on 28th April is due to the increase of latent heat energy only. But decrease in moist static energy from 750 to 300 hPa on 28th April and significant increase of moist static energy from 850 to 250 hPa on 29th April are due to the contribution of dry static energy and latent heat energy.

The moist static energy over Cuttack increases significantly from the surface to 800 hPa and decreases significantly from 800 to 200 hPa on 27th April with respect to that of 26th April (Fig. 4.3.3(n)). Again the moist static energy decreases from surface to 825 hPa and increases significantly from 825 to 400 hPa on 29th April in comparison to that of 27th April. The moist static energy increases in the lower troposphere from surface to 800 hPa on 27th April which is due to the increase of latent heat energy and decrease of moist static energy in the upper troposphere from 800 to 200 hPa is due to the decrease of latent heat energy and dry static energy. Again the moist static energy decreases in the lower troposphere and increases significantly in the upper troposphere on 29th April which is due to the variation of latent heat energy and dry static energy.

Fig. 4.3.3(o) shows that the moist static energy increases from surface to 825 hPa and decreases significantly from 825 to 200 hPa over Port Blair on 26th April with respect to

that of 25th April. Again the moist static energy increases significantly on 28th April in comparison to that of 26th April. The moist static energy increases in the lower troposphere on 26th April and at all levels on 28th April which is due to the contribution of latent heat energy and dry static energy respectively. Again the moist static energy decreases in the upper troposphere from 825 to 200 hPa which is due to the decrease of latent heat energy and dry static energy.

It is also found that the moist static energy decreases with height from surface to 850 hPa or 700 hPa or 500 hPa and increases from these levels to 200 hPa during the period. This is due to the conditional instability of the troposphere in the tropics.

From the above discussion, it is found that the moist static energy increases at all levels over all stations except Chittagong during the period. The moist static energy decreases significantly from surface to 750 hPa over Chittagong on 28th and 29th April, and decreases slightly in the lower troposphere over Dhaka and Cuttack on 29th April.

4.3.3.4 Total energy

The changing pattern of the vertical variation of total energy is the same as mentioned in case of moist static energy. Due to the addition of the kinetic energy with the moist static energy there is only fractional variation of the magnitude of total energy.

4.3.3.5 Meridional flux of moist static energy

The Fig. 4.3.3(p) shows that the magnitude of northerly (-ve) flux decreases and the southerly (+ve) flux increases at all levels over Dhaka gradually with little anomalies around surface as the cyclone moves towards the landfall. The significant amount of southerly (+ve) flux is flowing from 850 to 200 hPa on 28th April and surface to 200 hPa on 29th April. This southerly (+ve) flux on 28th and 29th April is due to the northward movement of the cyclone.

Fig. 4.3.3(q) shows the southerly (+ve) flux at all levels, which increases gradually during 27-29 April except at the surface on 29th April over Chittagong. This large amount of southerly (+ve) flux on 28th and 29th April is due to the movement of the cyclone towards the Chittagong coast.

The meridional flux of moist static energy over Calcutta increases from 800 to 200 hPa and decreases from surface to 800 hPa on 28th April with respect to that of 27th April and at all levels on 29th April with respect to that of 28th April (Fig. 4.3.3(r)). The figure also shows the southerly flux (+ve) at all levels on 28th April and 450 to 200 hPa on 29th April. The northerly flux also exists from 850 to 450 hPa on 29th April over the station.

The meridional flux of moist static energy decreases over Cuttack gradually and the northerly flux increases gradually with little anomalies during 26-29 April as the cyclone moves towards the coast of Chittagong (Fig. 4.3.3(s)).

The southerly flux over Port Blair increases at all levels on 26th April with respect to that of 25th April and again decreases at all levels on 28th April with respect to that of 26th April (Fig. 4.3.3(t)).

4.3.3.6 Zonal flux of moist static energy

The Fig. 4.3.3(u) shows that the zonal flux decreases gradually with little anomalies around surface over Dhaka during 27 - 29 April as the cyclone moves towards the landfall. The easterly flux exists from surface to 750 hPa and the westerly flux exists from 750 to 200 hPa on 27th and 28th April over the station.

From Fig. 4.3.3(v), it is observed that the easterly flux increases from surface to 750 hPa over Chittagong on 28th April with respect to that of 27th April and has no regular trend of westerly flux above these levels. The easterly (-ve) flux is flowing from surface to 500 hPa having a slight westerly (+ve) flux above these levels with sharp maxima of easterly observed at 700 hPa on 29th April over the station. This significant amount of low level easterly flux is due to cyclonic circulation of the advancing cyclone.

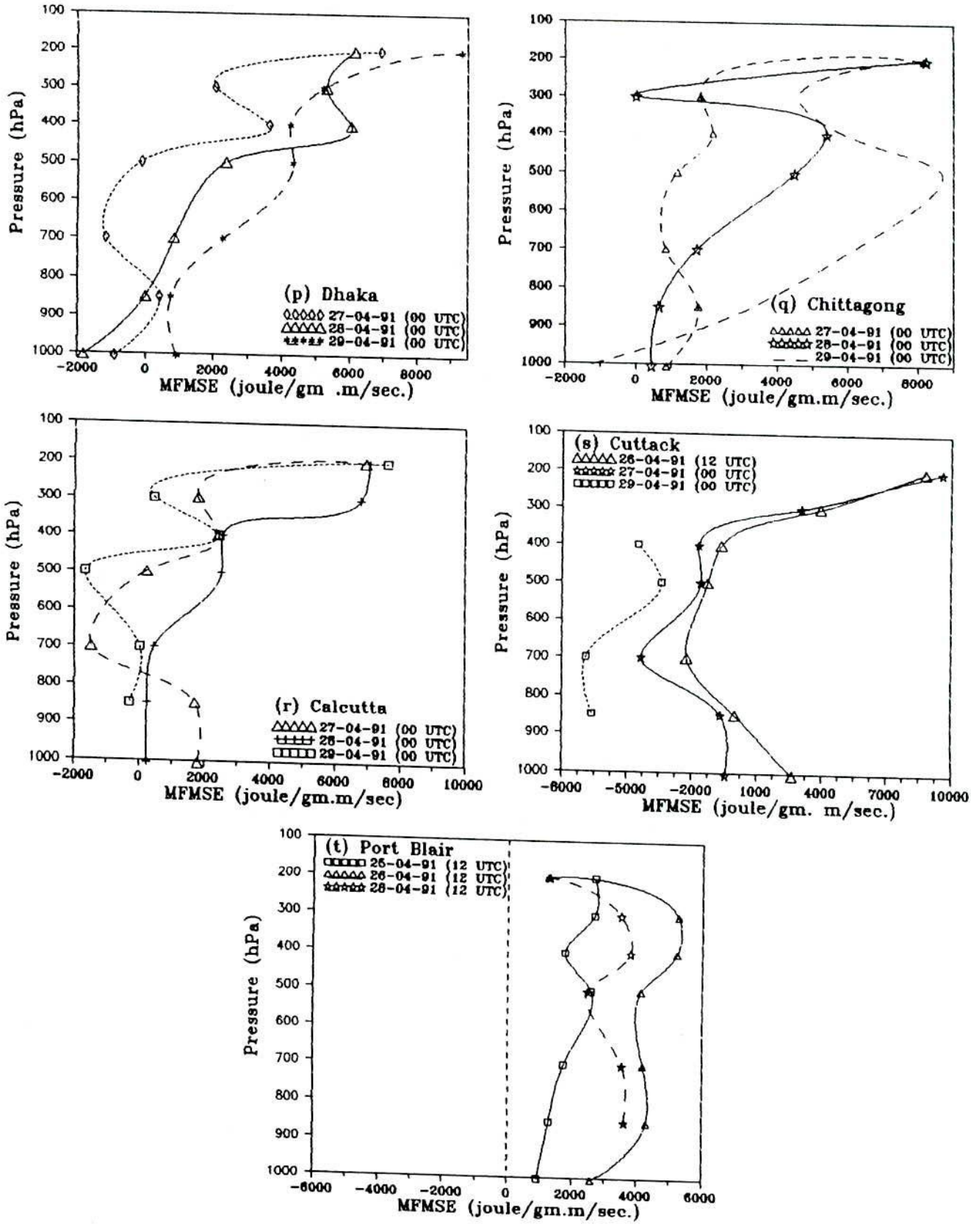

Figs. 4.3.3(p - t) Meridional flux of moist static energy over Dhaka, Chittagong, Calcutta, Cuttack and Port Blair for the cyclone 27 - 29 April 1991.

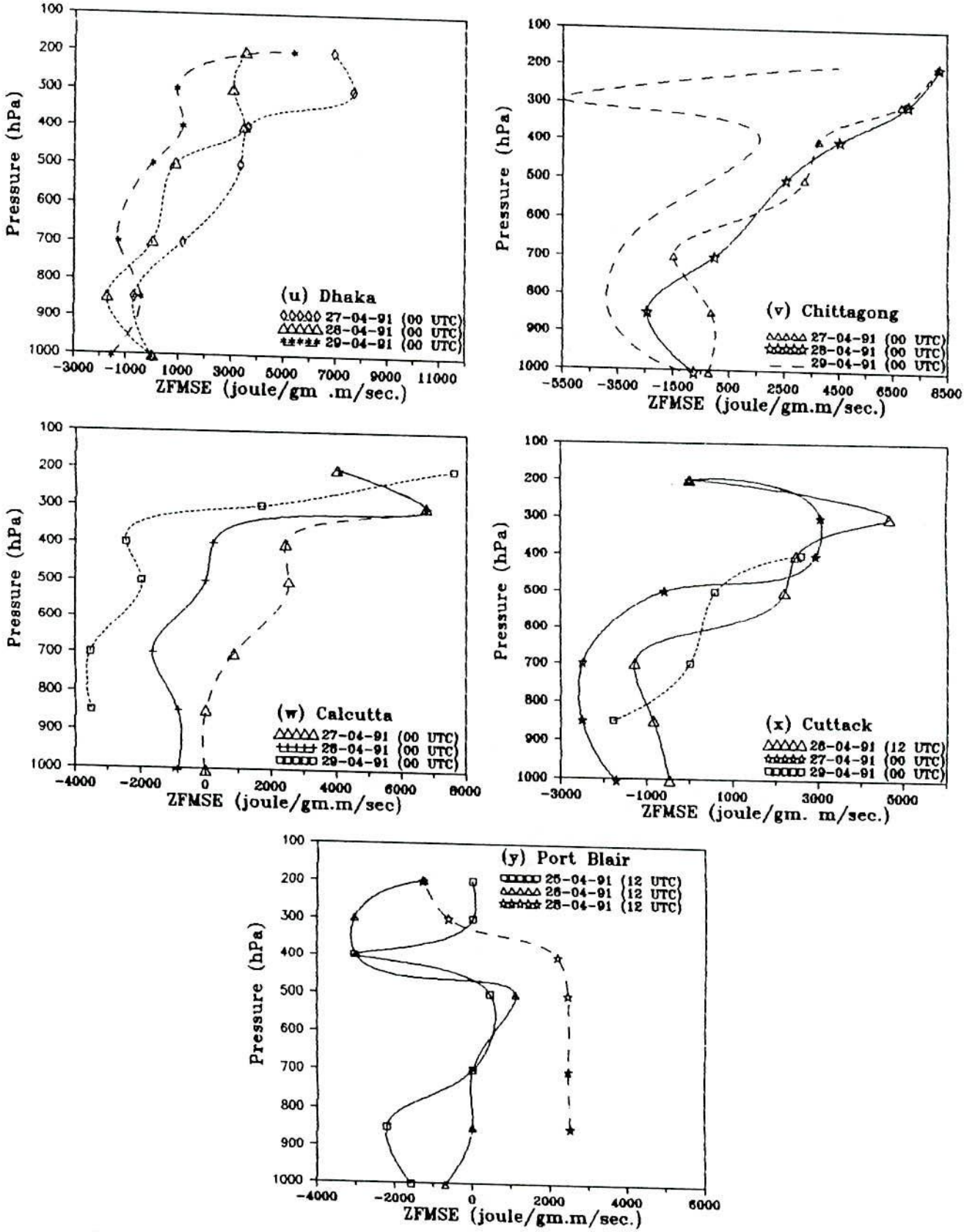

Figs. 4.3.3(u - y) Zonal flux of moist static energy over Dhaka, Chittagong, Calcutta, Cuttack and Port Blair for the cyclone 27 - 29 April 1991.

Fig. 4.3.3(w) shows that the magnitude of westerly (+ve) flux decreases gradually and the easterly flux increases gradually at all levels over Calcutta during 27-29 April as the cyclone moves towards the landfall. The easterly (-ve) flux is flowing from surface to 350 hPa and 300 hPa on 28th and 29th April respectively over the station.

The zonal flux over Cuttack decreases at all levels on 27th April in comparison to that of 26th April (Fig. 4.3.3(x)). Again the flux increases from surface to 500 hPa on 29th April with respect to that of 27th April. The easterly flux exists from surface to 700 hPa and the westerly flux exists from 700 hPa to 400 hPa on 29th April over the station.

From Fig. 4.3.3(y), it is observed that the magnitude of easterly (-ve) flux decreases and the westerly flux increases gradually at all levels with little anomalies during 25-28 April as the cyclone moves far away from the coast of Port Blair.

4.3.3.7 Combination of zonal and meridional fluxes

The north-westerly flux of moist static energy decreases and the south-easterly flux of moist static energy increases over Dhaka during 27-29 April as the cyclone moves towards the landfall. The north-easterly flux exists around surface, the flux is north-westerly from 800 hPa to 500 hPa and south-westerly flux from 500 hPa to 300 hPa with maxima of south-westerly observed from 400 hPa to 200 hPa on 27th April over Dhaka. There exists north-easterly flux around surface and the south-westerly flux from 700 hPa to 200 hPa with sharp maxima observed at 400 hPa on 28th April over the station. Again the south-easterly flux is observed from surface to 500 hPa with the south-westerly flux from 500 hPa to 200 hPa on 29th April over the station.

The south-easterly flux exists from surface to 600 hPa and the flux is south-westerly from 600 hPa to 200 hPa with sharp maxima observed at 200 hPa on 27th April over Chittagong. There exists south-easterly flux from surface to 700 hPa and south-westerly flux from 700 hPa to 200 hPa with sharp maxima of south-easterly observed at the surface and the flux is significantly south-westerly from 500 hPa to 200 hPa on 28th April over the station. There are north-easterly flux around surface and tremendous amount of south-

easterly flux from 900 hPa to 500 hPa and the significant amount of south-westerly flux exists from 500 hPa to 200 hPa on 29th April of which the southerly component is dominant.

The magnitude of north-westerly flux decreases and the south-easterly flux increases on 27th and 28th April over Calcutta as the cyclone moves towards the landfall. Again large amount of north-easterly flux is observed from 850 hPa to 450 hPa and the flux is south-westerly from 350 hPa to 200 hPa on 29th April over the station.

The north-easterly flux increases in the lower troposphere and the south-westerly flux decreases in the upper troposphere on 27th April with respect to that of 26th April over Cuttack. There are large amount of north-easterly flux from surface to 700 hPa and north-westerly flux from 700 to 400 hPa on 29th April over the station. The magnitude of south-easterly flux decreases and the south-westerly flux increases as the cyclone moves far away from the Port Blair.

4.3.4 Severe Cyclonic Storm with a core of hurricane intensity of 1988

We have discussed the vertical variation of dry static energy, latent heat energy, moist static energy, total energy and the meridional and zonal fluxes of moist static energy for the severe cyclonic storm with a core of hurricane winds of 1988. Day-to-day variation of these energies has been analysed as the cyclone progress.

4.3.4.1 Dry static energy

The dry static energy over Dhaka increases at all levels on 28th November with respect to that of 27th November (Fig. 4.3.4(a)). The dry static energy decreases from 850 to 450 hPa and slightly increases from 450 to 200 hPa on 29th November with respect to that of 28th November. Again it increases significantly at all levels on 30th November (i.e. after the landfall) with respect to that of the previous days over the station.

From Fig. 4.3.4(b), it is observed that the dry static energy is almost constant from 850 to 600 hPa over Chittagong during the period. It decreases from 600 to 200 hPa on 28th November with respect to that of 27th November and increases from 500 to 200 hPa on 29th November with respect to that of 28th November over the station. Again the dry static energy increases at all levels on 30th November that is after the landfall with respect to that of the previous days.

The dry static energy over Calcutta decreases at all levels on 28th November with respect to that of 27th November (Fig. 4.3.4(c)). It increases slightly at all levels except little anomalies on 29th November with respect to that of 28th November over the station.

From the analysis, it is found that the dry static energy decreases in the coastal region such as Chittagong and Calcutta and increases over Dhaka on 28th November. Again on the day of landfall the dry static energy decreases over Dhaka and increases slightly over Calcutta and in the upper troposphere over Chittagong. The dry static energy increases at all levels over Dhaka and Chittagong after the landfall.

4.3.4.2 Latent heat energy

The Fig. 4.3.4(d) shows that the latent heat energy increases significantly from surface to 200 hPa over Dhaka on 28th and 29th November with respect to that of 27th November. The figure also shows that the latent heat energy is almost constant on 28th and 29th November whereas it increases from 800 to 500 hPa and decreases from 500 to 300 hPa on 30th November over the station.

From Fig. 4.3.4(e), it is observed that the latent heat increases over Chittagong on 28th and 29th November with respect to that of 27th November. The latent heat energy increases from 800 to 600 hPa on 29th November with respect to that of 28th November and almost equal from 500 to 200 hPa. Again the latent heat energy increases from 850 to 700 hPa and decreases from 700 to 300 hPa on 30th November in comparison to that of 28th and 29th November.

The latent heat energy over Calcutta increases significantly from surface to 300 hPa on 28th November with respect to that of 27th November (Fig. 4.3.4(f)). Again it decreases significantly from 850 to 400 hPa and increases from 400 to 200 hPa and surface to 850 hPa on 29th November with respect to that of 28th November over the station.

From the above analysis, it is found that the latent heat energy increases significantly over all stations on 28th November with respect to that of 27th November. The latent heat energy decreases over Calcutta on 29th November with respect to that of 28th November and almost constant over Dhaka and Chittagong.

4.3.4.3 Moist static energy

The magnitude of moist static energy over Dhaka increases gradually during 27-30 November with little anomalous behaviour observed on 29th November (Fig. 4.3.4(g)). The moist static energy decreases from 850 to 450 hPa and increases from 450 to 200 hPa on 29th November with respect to that of 28th November. The moist static energy increases on 28th November with respect to that of 27th November over the station, which is due to the contribution of latent heat energy. The moist static energy decreases from 850 to 450 hPa and increases from 450 to 200 hPa on 29th November and increases at all levels on 30th November which is due to the contribution of dry static energy.

Fig. 4.3.4(h) shows that the moist static energy increases from surface to 400 hPa and decreases from 400 to 200 hPa over Chittagong on 28th November with respect to that of 27th November. It has no regular trend from 850 to 475 hPa and increases from 475 to 200 hPa and surface to 800 on 29th November and at all levels on 30th November with respect to that of the previous day. The increase of moist static energy from surface to 400 hPa is due to the increase of latent heat energy and the decrease from 400 to 200 hPa is due to the decrease of dry static energy. The increase of moist static energy from 500 to 200 hPa on 29th November and 700 to 200 hPa on 30th November is due to the increase of dry static energy.

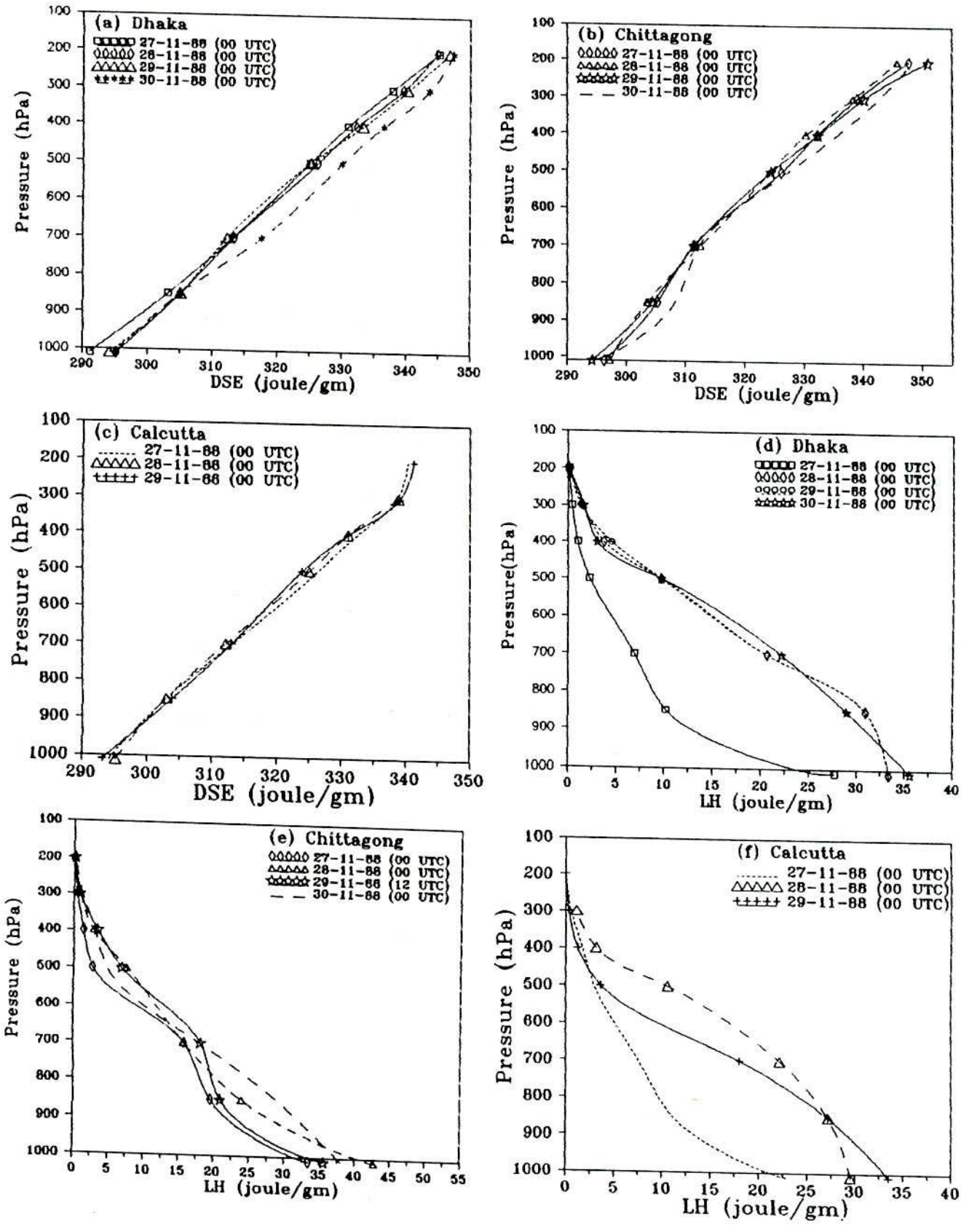

Figs. 4.3.4(a - c) Dry static energy over Dhaka, Chittagong and Calcutta for the cyclone 27 - 29 November 1988. Figs. 4.3.4(d - f) Latent heat energy over Dhaka, Chittagong and Calcutta for the cyclone 27 - 29 November 1988.

From Fig. 4.3.4(i), it is found that the moist static energy increases significantly from surface to 400 hPa over Calcutta on 28th November with respect to that of 27th November. Again it decreases significantly from 850 to 400 hPa and increases significantly from 400 to 200 hPa and surface to 800 hPa on 29th November with respect to that of 28th November. The increase of moist static energy on 28th November and the decrease on 29th November is due to the contribution of latent heat energy.

It is found that the moist static energy increases gradually with height over all stations during the period with few exceptions. The moist static energy decreases with height and the minima are observed at 500 hPa over Calcutta on 29th November and at 700 hPa over Dhaka on 28th and 29th November. The moist static energy increases up to 600 hPa over Dhaka on 30th November and Calcutta on 28th November and the minima are observed at 400 hPa. The changing pattern of moist static energy of this cyclone is not consistent with others that we have analysed.

From the above discussion, it is found that the moist static energy increases significantly over all stations on 28th November with respect to that of 27th November except little anomalies in the upper troposphere. Again the moist static energy decreases from 850 to 400 hPa over Dhaka and Calcutta and increases above and below these levels over Calcutta and decreases from surface to 800 hPa and increases from 500 to 200 hPa level on 29th November over Chittagong.

4.3.4.4 Total energy

The changing pattern of moist static energy and the total energy is the same. Due to the addition of kinetic energy, the pattern of the figure has little or no changes but only little variation of magnitude is observed.

4.3.4.5 Meridional flux of moist static energy

The magnitude of southerly (+ve) flux over Dhaka increases gradually at all levels except little anomalies during 27-29 November as the cyclone moves towards the coast (Fig. 4.3.4(j)). The increase of southerly (+ve) flux is due to the movement of the cyclone towards Dhaka. After the landfall of the cyclone at Khulna coast the flux becomes

northerly (-ve) over Dhaka with larger amplitude at 700 hPa on 30th November. The significant amount of southerly (+ve) flux is observed at all levels on 29th November which is due to the movement of the cyclone towards Dhaka from the south-west.

From Fig. 4.3.4(k), it is observed that the flux is southerly (+ve) with increasing magnitude over Chittagong during 27-30 November as the cyclone moves towards the coast. There is an exception on 28th November when the northerly (-ve) component of flux with sharp maxima is observed at 400 hPa. The large amount of southerly flux on 29th November is due to the movement of the cyclone to the northward direction. On 30th November, there are significant southerly (+ve) flux at 400 hPa and 200 hPa and significant northerly flux around 300 hPa over the station i.e. after landfall of the cyclone at Khulna-West Bengal coast.

The meridional flux over Calcutta has no regular trend on 27th and 28th November (Fig. 4.3.4(l)). The flux increases from surface to 450 hPa and decreases from 450 to 200 hPa over Calcutta on 29th November with respect to that of 28th November. Again large amount of southerly flux is observed at all levels on 29th November. This southerly flux on 29th November is due to the movement of the cyclone to the northward direction.

4.3.4.6 Zonal flux of moist static energy

The Fig. 4.3.4(m) shows that the magnitude of zonal flux decreases gradually during 27-29 November with little anomalies on 28th November over Dhaka as the cyclone moves towards the north. After landfall at Khulna coast the flux becomes significantly westerly (+ve) on 30th November with two sharp maxima observed one at 500 hPa and another at 300 hPa over the station.

The westerly flux over Chittagong increases from surface to 350 hPa and the easterly (-ve) flux increases from 350 to 200 hPa with little anomaly on 28th November than that of 27th November (Fig. 4.3.4(n)). There are maximum easterly flux at 200 hPa and the maximum westerly (+ve) flux at 400 hPa over Chittagong on 28th November. Again the

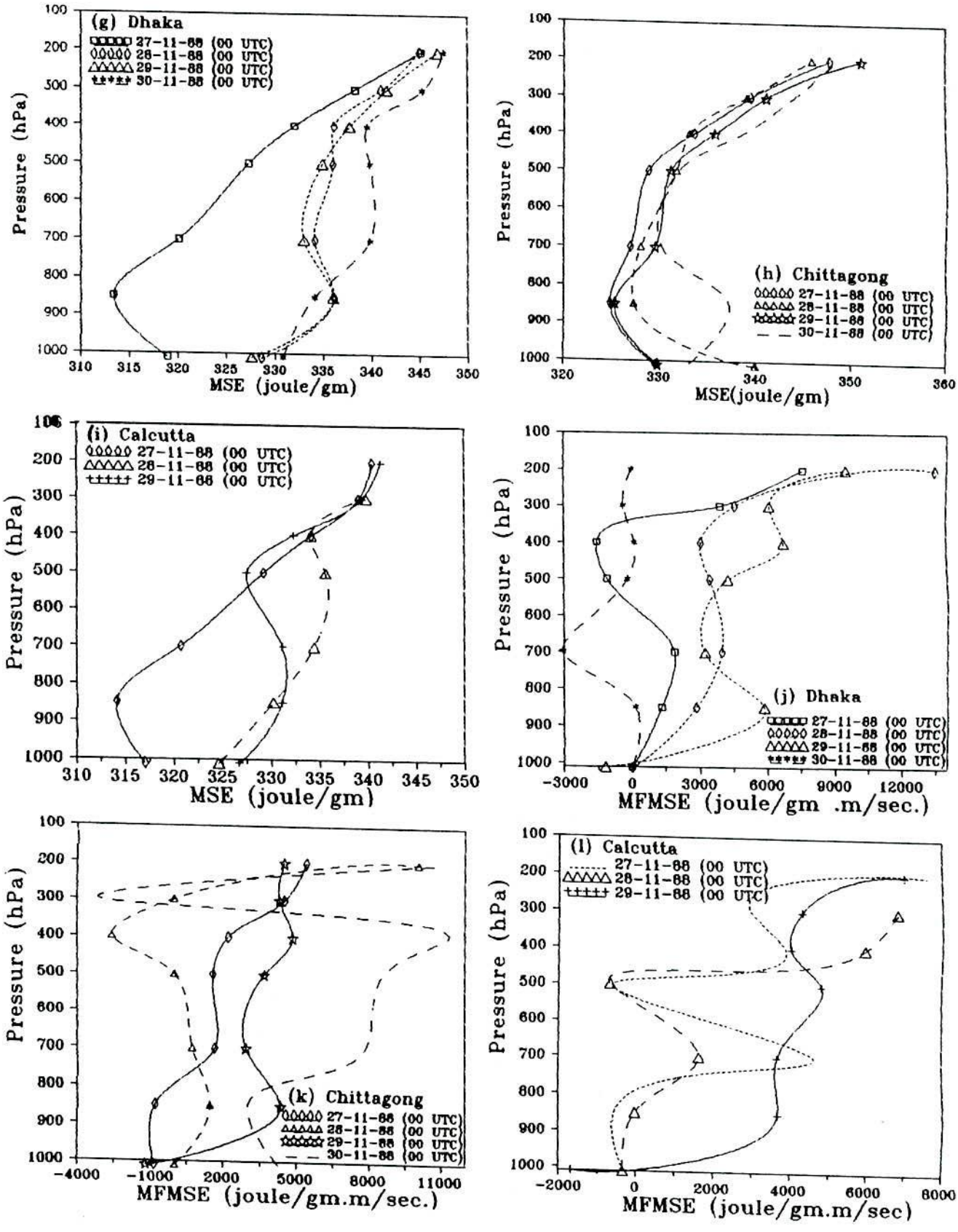

Figs. 4.3.4(g - i) Moist static energy over Dhaka, Chittagong and Calcutta for the cyclone 27 - 29 November 1988. Figs. 4.3.4(j - l) Meridional flux of moist static energy over Dhaka, Chittagong and Calcutta for the cyclone 27 - 29 November 1988.

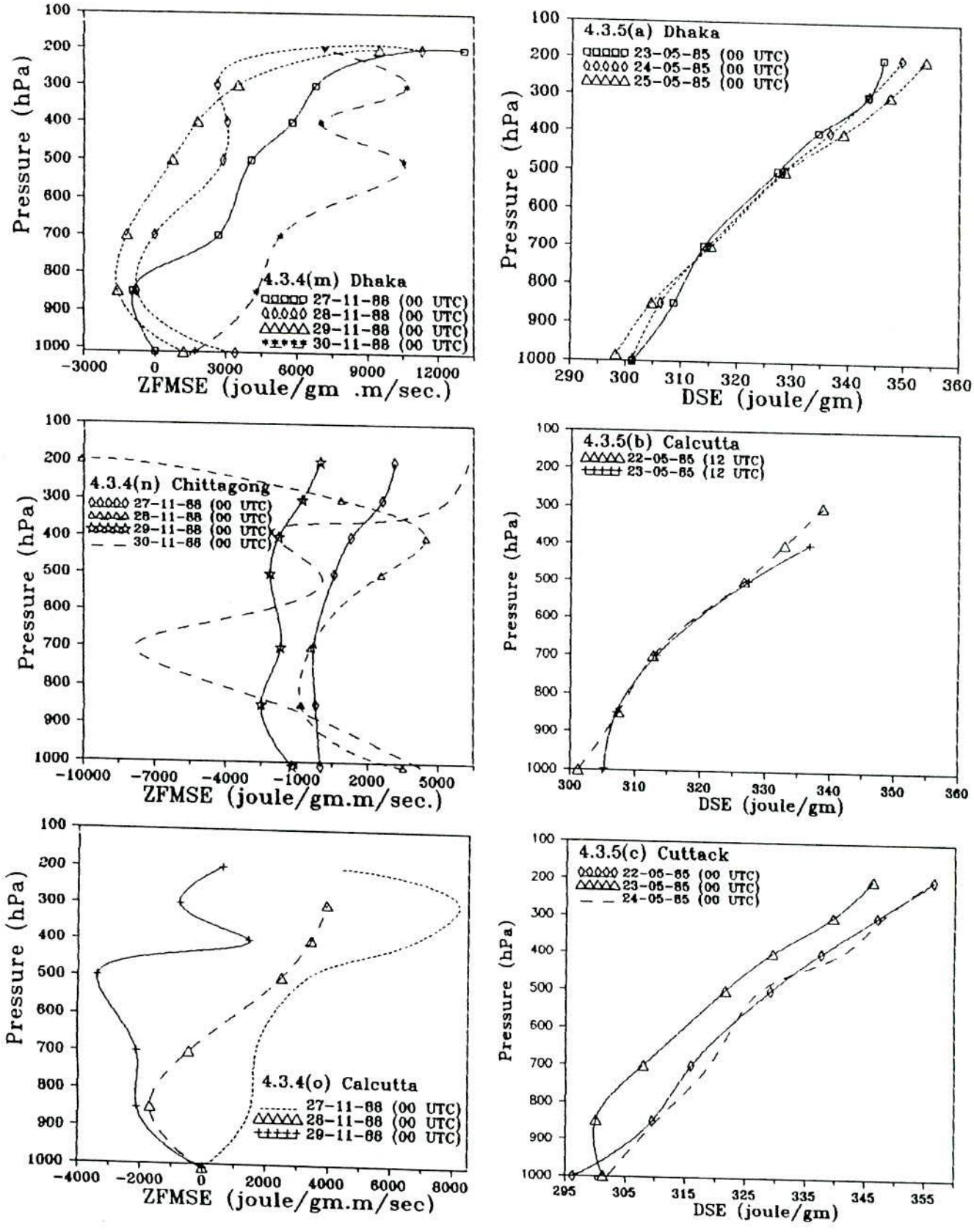

Figs. 4.3.4(m - o) Zonal flux of moist static energy over Dhaka, Chittagong and Calcutta for the cyclone 27 - 29 November 1988. Figs. 4.3.5(a - c) Dry static energy over Dhaka, Calcutta and Cuttack for the cyclone 23 - 25 May 1985.

flux becomes significantly easterly (-ve) at all levels on 29th November over the station. This easterly (-ve) flux increases significantly on 30 th November i.e. after the landfall of the cyclone at Khulna coast.

From Fig. 4.3.4(o), it is observed that the zonal flux decreases gradually at all levels over Calcutta during 27-29 November as the cyclone moves towards the landfall. The large amount of westerly flux exists on 27th November and the flux is easterly (-ve) at all levels on 29th November over the station. The easterly flux exists from surface to 700 hPa and the westerly flux exists from 700 to 300 hPa on 28th November.

4.3.4.7 Combination of zonal and meridional fluxes

There are south-easterly flux from surface to 800 hPa, the south-westerly flux from 800 to 600 hPa and 375 to 200 hPa with sharp maxima observed at 200 hPa, and the north-westerly flux from 600 to 375 hPa over Dhaka on 27th November. The flux is south-easterly from 950 to 600 hPa and south-westerly from 600 to 200 hPa on 29th November and south-westerly at all levels on 28th November over the station. The effect of southerly is the greatest at all levels on 29th November over the station. Again the effect of westerly decreases and the effect of southerly increases gradually during 27-29 November over the station.

Over Chittagong, there are north-easterly flux from surface to 800 hPa and the south-westerly flux from 800 to 200 hPa over Chittagong on 27th November. The flux becomes south-easterly from 900 to 650 hPa and the significant amount of south-easterly flux exists from 300 to 200 hPa having tremendous amount of north-westerly flux in the layer from 600 to 325 hPa on 28th November over the station. Again the flux becomes tremendously south-easterly at all levels on 29th November over the station.

The significant amount of south-westerly flux is observed at all levels over Calcutta on 27th November. There are south-easterly flux from surface to 650 hPa and south-westerly flux from 650 to 200 hPa on 28th November. The flux becomes south-easterly with greater magnitudes at all levels on 29th November over the station.

There are tremendous amount of south-easterly and north-easterly flux over Chittagong and Dhaka respectively on 30th November after the landfall of the cyclone at Khulna coast.

4.3.5 Severe Cyclonic Storm with a core of hurricane intensity of 1985

We have discussed the vertical variation of dry static energy, latent heat energy, moist static energy, total energy and the meridional and zonal fluxes of moist static energy for the severe cyclonic storm with a core of hurricane winds of 1985. Day-to-day variation of these energies has been analysed as the cyclone progress.

4.3.5.1 Dry static energy

Fig. 4.3.5(a) shows that the dry static energy decreases gradually from surface to 725 hPa and increases gradually from 725 to 200 hPa over Dhaka during 23rd to 25th May as the cyclone moves northward.

The dry static energy over Calcutta increases slightly at all levels on 23rd May with respect to that of 22nd May (Fig. 4.3.5(b)).

From Fig. 4.3.5(c), it is observed that the dry static energy decreases significantly at all levels with little anomalies around surface over Cuttack on 23rd May with respect to that of 22nd May and increases significantly at all levels on 24th May with respect to that of 23rd May.

From the analysis it is found that the dry static energy increases significantly in the far away station such as Cuttack and decreases gradually from surface to 725 hPa and increases gradually from 725 to 200 hPa in nearer station such as Dhaka.

4.3.5.2 Latent heat energy

The latent heat energy over Dhaka decreases from surface to 950 hPa and increases from 950 to 300 hPa on 24th May with respect to that of 23rd May (Fig. 4.3.5(d)). The figure also shows that the latent heat energy decreases from surface to 850 hPa and increases from 850 to 300 hPa on 25th May with respect to that of 24th May.

The Fig. 4.3.5(e) shows that the latent heat energy decreases from the surface to 775 hPa and increases from 775 to 300 hPa over Calcutta on 23rd May with respect to that of 22nd May.

The latent heat energy over Cuttack increases from the surface to 950 hPa and decreases from 950 to 200 hPa on 23rd May with respect to that of 22nd May (Fig. 4.3.5(f)). It also increases significantly at all levels on 24th May with respect to that of 23rd May.

From the above discussion, it is found that the latent heat energy decreases on 23rd May with respect to that of 22nd May and increases significantly on 24th May with respect to that of 23rd May. It is also found that the latent heat energy increases gradually over Dhaka during the period but decreases in the lower troposphere on 25th May.

4.3.5.3 Moist static energy

The magnitude of moist static energy over Dhaka decreases gradually from surface to 900 hPa and increases gradually from 800 to 200 hPa during 23rd to 25th May as the cyclone moves towards the landfall (Fig. 4.3.5(g)). The decrease of moist static energy in the lower troposphere and increase from 800 to 200 hPa are due to the decrease and increase of latent heat energy and the dry static energy in that region.

From Fig. 4.3.5(h), it is observed that the magnitude of moist static energy decreases from surface to 775 hPa and increases from 775 to 300 hPa over Calcutta on 23rd May with respect to that of 22nd May. The decrease of moist static energy in the lower troposphere is due to the decrease of latent heat energy and increase in moist static energy in the upper

troposphere is due to the increase of latent heat energy and the dry static energy over the station.

The magnitude of moist static energy over Cuttack decreases significantly at all levels on 23rd May and increases significantly at all levels on 24th May with respect to that of the previous day (Fig. 4.3.5(i)). The decrease of moist static energy on 23rd May with respect to that of 22nd May and the increase on 24th May with respect to that of 23rd May are due to the variations of dry static energy and latent heat energy.

It is found that the moist static energy decreases with height from surface to 850 or 700 hPa and increases from these levels to 200 hPa with few exceptions over all stations during the period. The exception is that the moist static energy increases from surface to 700 hPa on 24th May over Cuttack. It is also seen that the minima are observed at 850 hPa on the day of landfall and at 700 hPa of all stations at all other days over Dhaka.

From the analysis it is found that the moist static energy increases significantly at all levels over Cuttack during the period. The moist static energy increases in the upper troposphere and decreases in the lower troposphere gradually over Dhaka during the period. The data were not available during the period over Chittagong and on 24th and 25th May over Calcutta.

4.3.5.4 Total energy

The changing pattern of moist static energy and the total energy is the same. Due to the addition of kinetic energy with the moist static energy, only fractional variation of magnitude of total energy is observed.

4.3.5.5 Meridional flux of moist static energy

The magnitude of southerly (+ve) flux over Dhaka decreases and the northerly (-ve) flux increases gradually at all levels during 23-25 May with little anomalies on 24th May as the cyclone moves towards the coast (Fig. 4.3.5(j)). A significant amount of northerly (-ve)

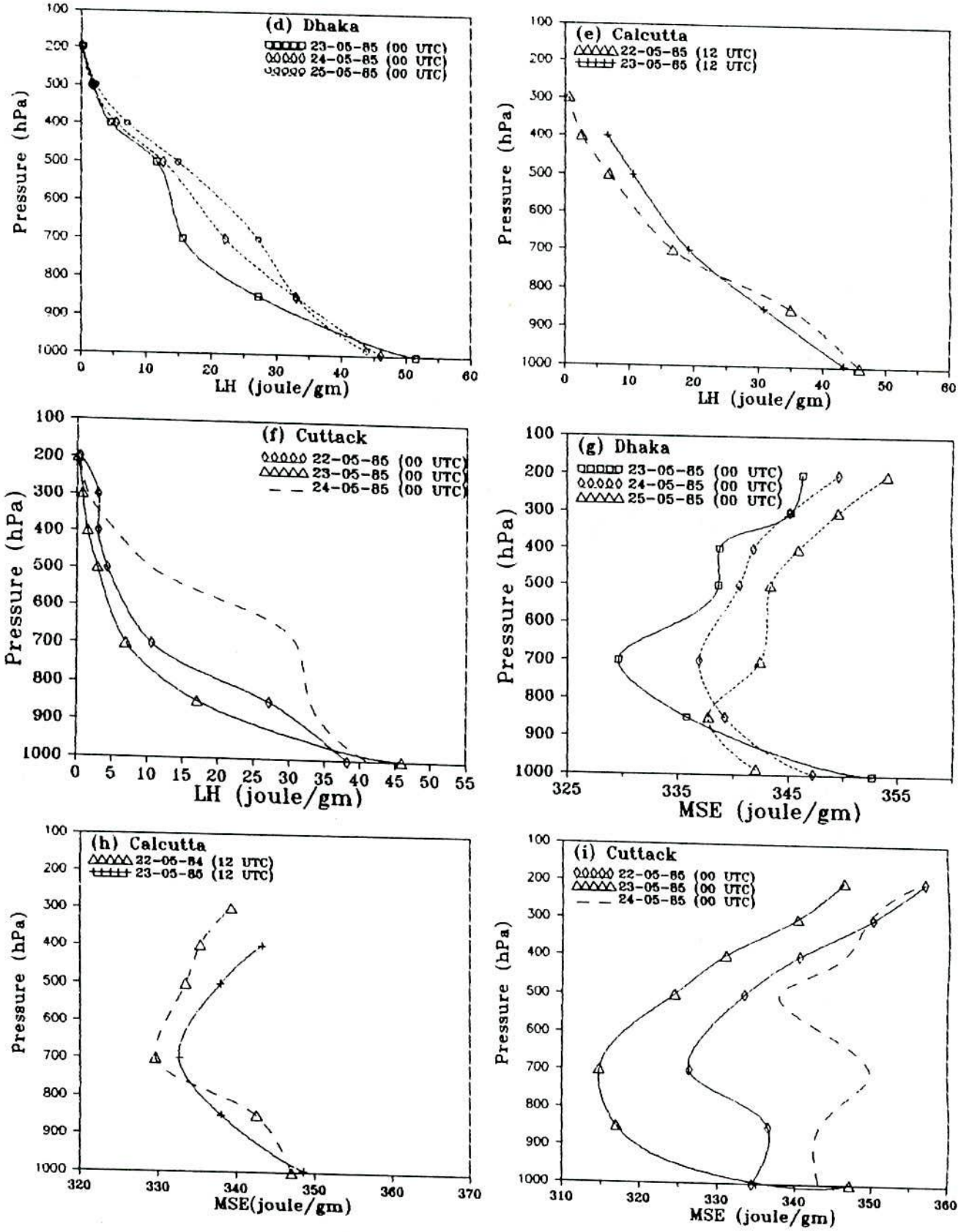

Figs. 4.3.5(d - f) Latent heat energy over Dhaka, Calcutta and Cuttack for the cyclone 23 - 25 May 1985. Figs. 4.3.5(g - i) Moist static energy over Dhaka, Calcutta and Cuttack for the cyclone 23 - 25 May 1985.

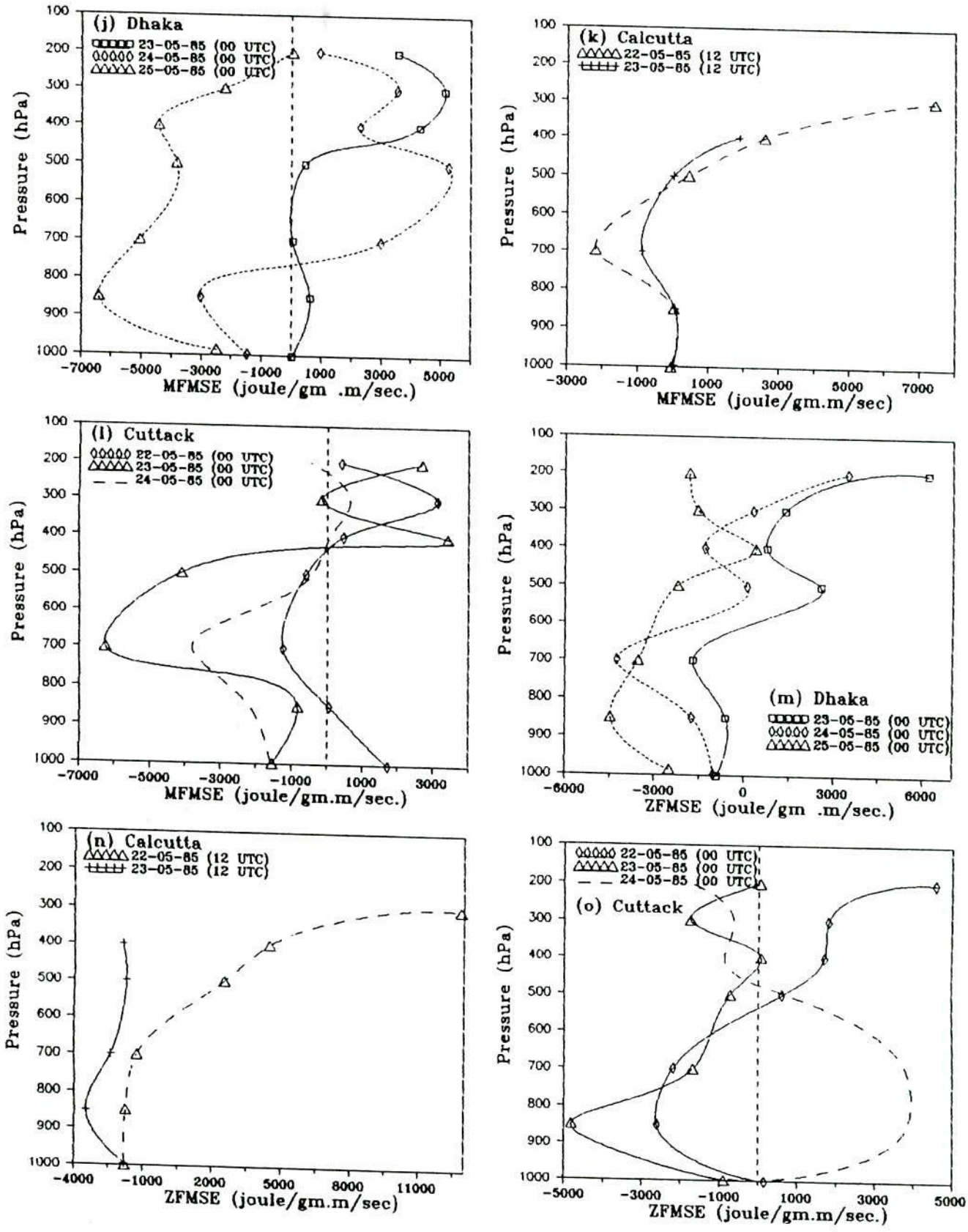

Figs. 4.3.5(j - l) Meridional flux of moist static energy over Dhaka, Calcutta and Cuttack for the cyclone 23 - 25 May 1985. Figs. 4.3.5(m - o) Zonal flux of moist static energy over Dhaka, Calcutta and Cuttack for the cyclone 23 - 25 May 1985.

flux exists at all levels on 25th May and sharp maxima are observed at 850 hPa and 400 hPa.

Fig. 4.3.5(k) shows that the meridional flux increases from 850 to 550 hPa and decreases from 550 to 300 hPa over Calcutta on 23rd May with respect to that of 22nd May. The data were not available on 24th and 25th May over the station.

From Fig. 4.3.5(l), it is found that the meridional flux decreases from surface to 425 hPa and has no regular trend from 425 to 200 hPa over Cuttack on 23rd May with respect to that of 22nd May. A large amount of northerly flux is observed from surface to 400 hPa and the southerly flux exists from 400 to 200 hPa on 24th May over the station.

4.3.5.6 Zonal flux of moist static energy

The zonal flux over Dhaka decreases at all levels with little anomalies during 23-25 May as the cyclone moves towards the coast (Fig. 4.3.5(m)). The flux is easterly from surface to 600 hPa and westerly from 600 to 200 hPa on 23rd May. The figure also shows that the easterly flux extends throughout the troposphere with little anomalies on 24th and 25th May over the station.

Over Calcutta, the zonal flux decreases at all levels on 23rd May with respect to that of 22nd May (Fig. 4.3.5(n)). The data were not available on 24th and 25th May over the station.

Fig. 4.3.5(o) shows that the zonal flux decreases at all levels with little anomalies over Cuttack on 23rd May with respect to that of 22nd May. The easterly flux is large at all levels on 23rd May over the station. It also shows that a significant amount of westerly flux from surface to 475 hPa and little amount of easterly flux exist from 470 to 200 hPa over the station.

4.3.5.7 Combination of zonal and meridional fluxes

The magnitude of south-westerly flux decreases and the north-easterly flux increases over Dhaka on 23rd and 24th May. There is south-westerly flux from 500 to 200 hPa with sharp maxima of south-westerly observed at 200 hPa on 23rd May over the station. On 24th May, there exists south-easterly flux in the layer 300 to 200 hPa having maximum southerly flux at 500 hPa and westerly flux at 200 hPa over the station. A tremendous amount of north-easterly flux exists at all levels on 25th May. The maximum south-westerly flux is observed at 200 hPa on 23rd and 24th May over the station.

Over Calcutta, there is north-westerly flux from surface to 600 hPa and south-westerly flux from 600 to 200 hPa on 22nd May. Again a little amount of north-easterly flux is found to appear from surface to 550 hPa with south-easterly flux in the upper troposphere on 23rd May. The data were not available on 24th and 25th May. So we could not make any conclusion due to lack of data over the station.

The north-easterly flux is found to exist from surface to 500 hPa with south-westerly flux from 500 to 200 hPa over Cuttack on 22nd May. The flux is north-easterly from surface to 425 hPa and south-easterly from 425 to 200 hPa on 23rd May. A significant north-westerly flux is observed from surface to 450 hPa on 24th May over the station.

4.3.6 Cyclonic Storm of 1992

We have discussed the vertical variation of dry static energy, latent heat energy, moist static energy, total energy and the meridional and zonal fluxes of moist static energy for the cyclonic storm of 1992. Day-to-day variation of these energies has been analysed as the cyclone progress.

4.3.6.1 Dry static energy

Over Dhaka, the dry static energy decreases from the surface to 700 hPa and at all other levels is almost constant on 18th and 19th May with respect to that of 17th May (Fig. 4.3.6(a)).

The dry static energy over Chittagong increases significantly at all levels on 18th May with respect to that of 17th May (Fig. 4.3.6(b)). Again the dry static energy has no regular trend on 18th and 19th May over the station.

From Fig. 4.3.6(c), it is observed that the dry static energy decreases from 850 to 475 hPa and increases from 475 to 200 hPa over Calcutta on 18th May with respect to that of 17th May. The figure also indicates that the dry static energy increases from 850 to 200 hPa on 19th May with respect to that of 18th May and below these levels it is almost constant.

The dry static energy over Cuttack decreases gradually at all levels with little anomalies at the surface during 17-19 May as the cyclone moves towards the north (Fig. 4.3.6(d)).

From the analysis it is found that the dry static energy decreases over Cuttack and increases over Calcutta on 19th May with respect to that of 18th May. It is also found that the dry static energy is almost constant and has no regular trend over Dhaka and Chittagong on 18th and 19th May respectively.

4.3.6.2 Latent heat energy

It is observed that the latent heat energy over Dhaka increases significantly from surface to 700 hPa and decreases slightly from 700 to 500 hPa on 18th May with respect to that of 17th May (Fig. 4.3.6(e)). The latent heat energy also decreases significantly from surface to 500 hPa and increases slightly from 500 to 300 hPa on 19th May with respect to that of 18th May over the station.

From Fig. 4.3.6(f), it is observed that the latent heat energy decreases significantly from surface to 700 hPa and increases from 700 to 400 hPa over Chittagong on 18th May with respect to that of 17th May. The figure also shows that the latent heat energy increases significantly from surface to 775 hPa on 19th May with respect to that of 18th May and has no definite trend above these levels over the station.

The latent heat energy over Calcutta increases from surface to 650 hPa and decreases from 650 to 400 hPa on 18th May with respect to that of 17th May (Fig. 4.3.6(g)). The figure also shows that the latent heat energy decreases from surface to 450 hPa on 19th May with respect to that of 18th May as the cyclone moves towards the landfall.

In Fig. 4.3.6(h), the latent heat energy decreases from surface to 300 hPa over Cuttack during 17-19 May as the cyclone moves towards the landfall.

From the analysis it is found that the latent heat energy decreases over Dhaka, Calcutta and Cuttack on 19th May with respect to that of 18th May. It is also seen that the latent heat energy increases significantly from surface to 775 hPa over Chittagong on 19th May with respect to that of 18th May.

4.3.6.3 Moist static energy

In Fig. 4.3.6(i), the moist static energy increases significantly from the surface to 700 hPa and decreases from 700 to 500 hPa over Dhaka on 18th May with respect to that of 17th May. Again the moist static energy decreases significantly from surface to 500 hPa and increases from 500 to 200 hPa on 19th May with respect to that of 18th May. The significant increase in moist static energy on 18th May is due to the increase of latent heat energy and decrease on 19th May is due to the decrease of latent heat energy over the station.

From Fig. 4.3.6(j), it is observed that the moist static energy increases at all levels with little anomalies around 850 hPa over Chittagong on 18th May with respect to that of 17th May. Again the moist static energy increases significantly from surface to 725 hPa and

decreases from 725 to 550 hPa on 19th May with respect to that of 18th May. The increase of moist static energy on 18th May is due to the increase in dry static energy and significant increase on 19th May is due to the significant increase in latent heat energy over the station.

The moist static energy over Calcutta increases at all levels with little anomalies around 500 hPa on 18th May with respect to that of 17th May (Fig. 4.3.6(k)). The figure also shows that the moist static energy decreases from surface to 800 hPa and increases from 800 to 200 hPa on 19th May with respect to that of 18th May. The decrease of moist static energy in the lower troposphere is due to the decrease of latent heat energy and increase in the upper troposphere is due to the increase of dry static energy over the station.

Fig. 4.3.6(l) shows that the moist static energy decreases gradually at all levels over Cuttack during 17-19 May as the cyclone moves towards the landfall. The gradual decrease of moist static energy at all levels is due to the decrease of latent heat energy and dry static energy over the station.

It is found that the moist static energy decreases with height from surface to 850 or 700 or 500 hPa and increases from these levels to 200 hPa over all stations during the period with few exceptions. The exception is observed over Dhaka and Chittagong on 17th and 19th May respectively. The moist static energy increases from surface to 825 hPa and minimum value is observed at 700 hPa over Chittagong on 19th May. Again two minima are observed over Dhaka on 17th May one at 850 hPa and the other at 500 hPa.

From the above discussion, it is found that the moist static energy decreases gradually over Cuttack and increases gradually over Chittagong during the period with few exceptions. The moist static energy decreases in the lower troposphere and increases in the upper troposphere over Dhaka and Calcutta. The moist static energy decreases from surface to 500 hPa and 800 hPa and increases from these levels to 200 hPa over Dhaka and Calcutta respectively. In this cyclonic storm the moist static energy increases near the

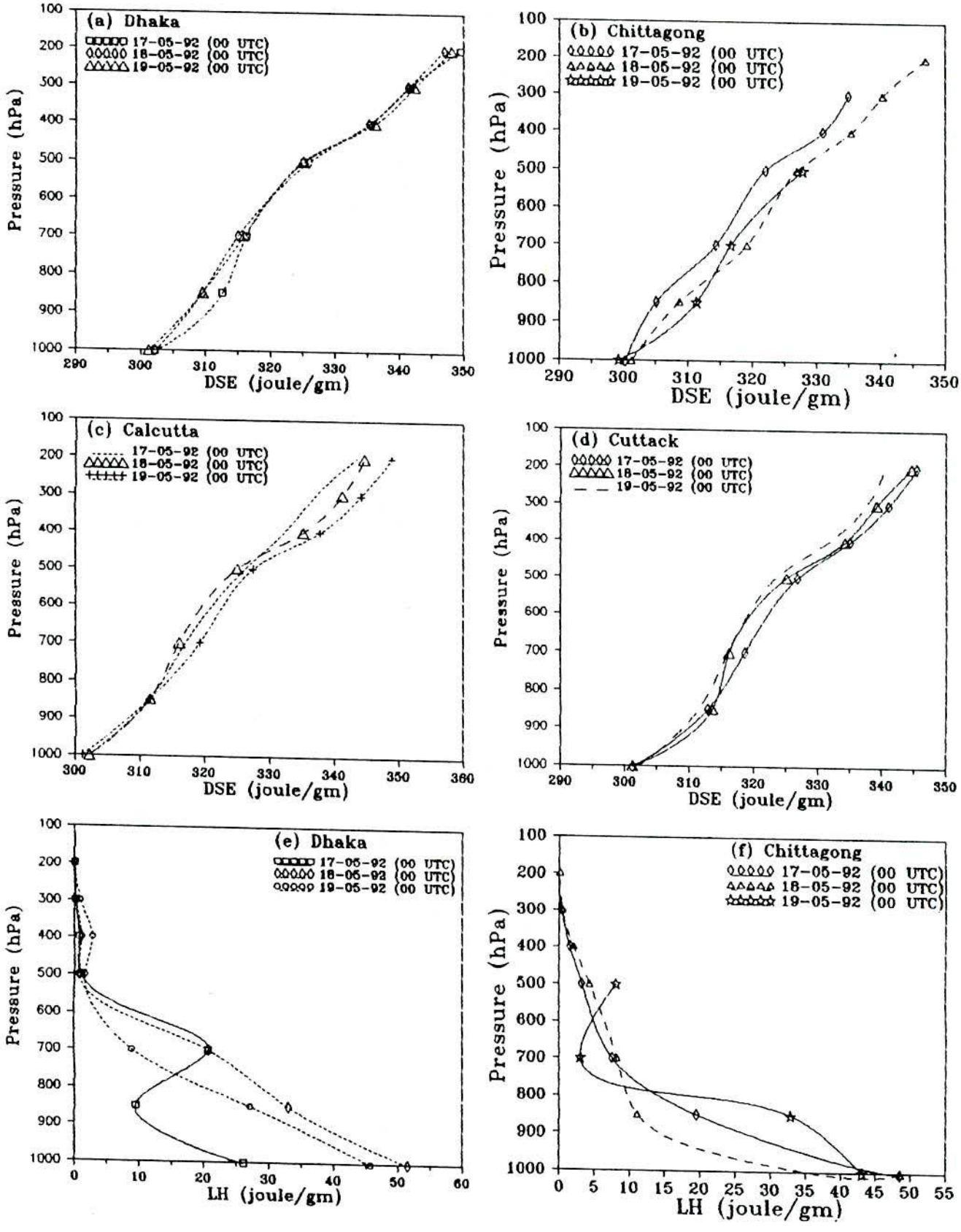

Figs. 4.3.6(a - d) Dry static energy over Dhaka, Chittagong, Calcutta and Cuttack for the cyclone 17 - 19 May 92. Figs. 4.3.6(e - f) Latent heat energy over Dhaka and Chittagong for the cyclone 17 - 19 May 92.

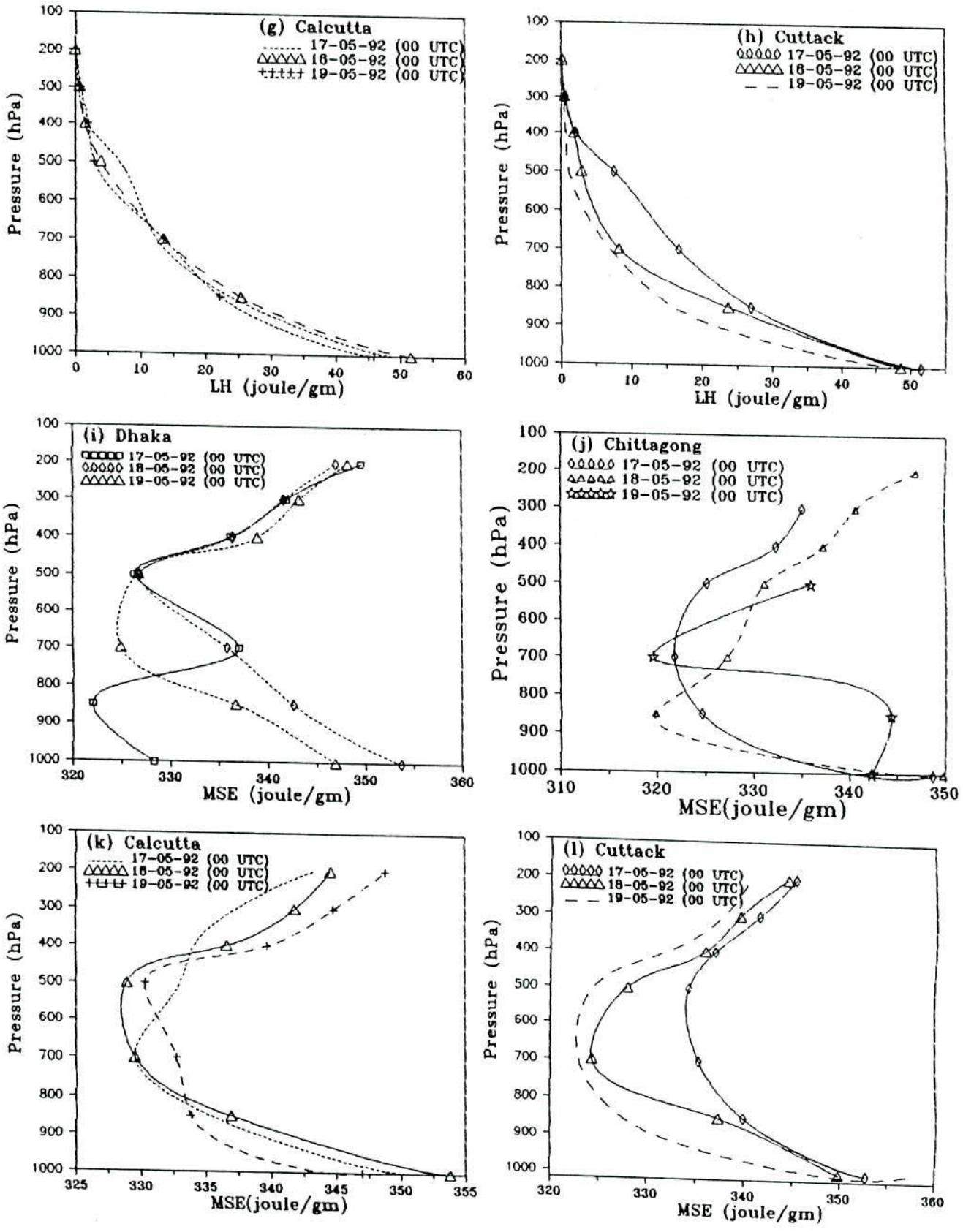

Figs. 4.3.6(g - h) Latent heat energy over Calcutta and Cuttack for the cyclone 17 - 19 May 92. Figs. 4.3.6(i - l) Moist static energy over Dhaka, Chittagong, Calcutta and Cuttack for the cyclone 17 - 19 May 92.

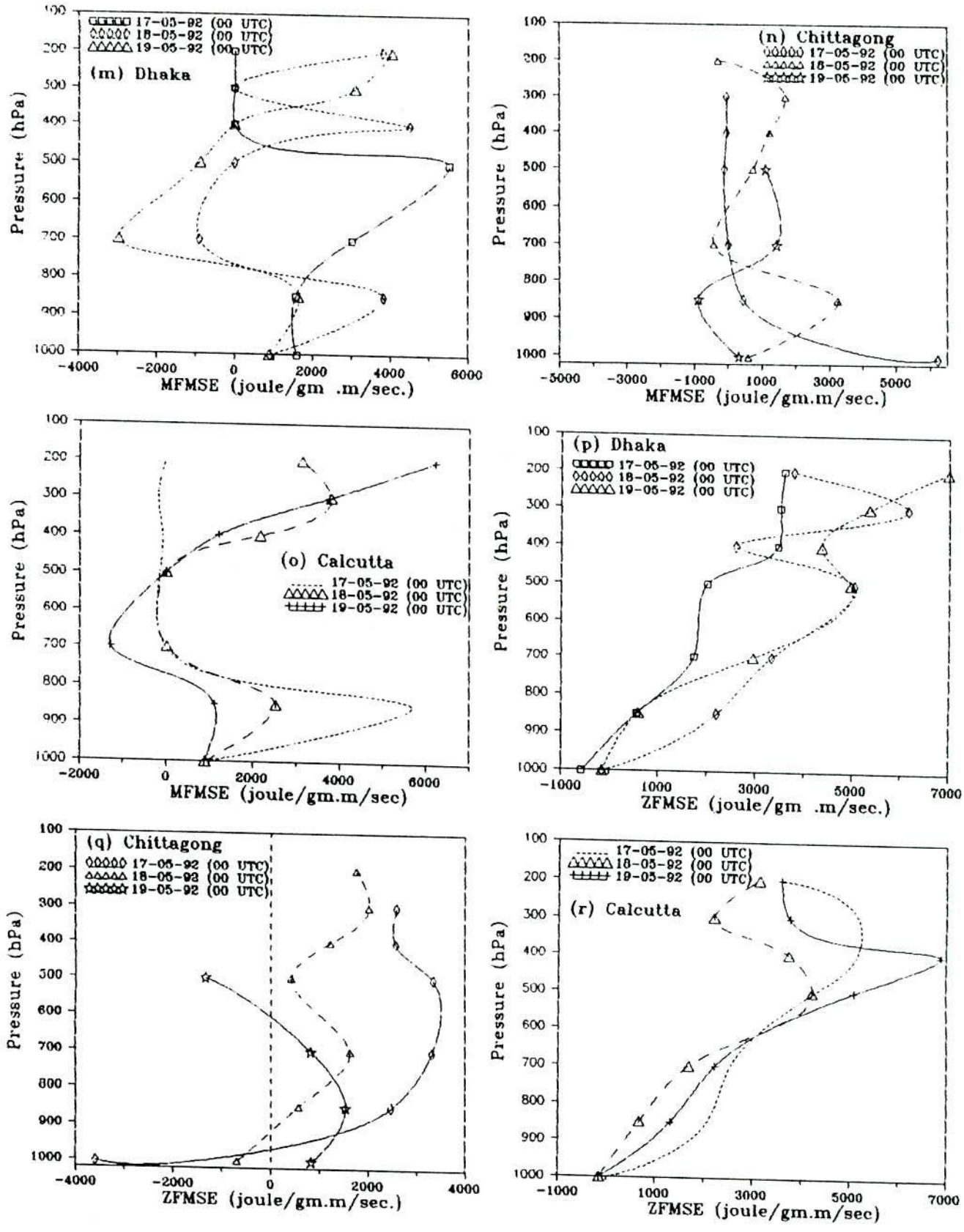

Figs. 4.3.6(m - o) Meridional flux of moist static energy over Dhaka, Chittagong and Calcutta for the cyclone 17 - 19 May 92. Figs. 4.3.6(q - r) Zonal flux of moist static energy over Dhaka, Chittagong and Calcutta for the cyclone 17 - 19 May 92.

landfall station such as Chittagong and decreases far away stations such as Dhaka, Calcutta and Cuttack.

4.3.6.4 Total energy

The changing pattern of moist static energy and the total energy is the same. Due to addition of kinetic energy with the moist static energy only fractional variation of magnitude of total energy is observed.

4.3.6.5 Meridional flux of moist static energy

The magnitude of southerly (+ve) flux over Dhaka decreases and the northerly (-ve) flux increases gradually from 800 to 450 hPa and increases gradually from 350 to 200 hPa during 17-19 May (Fig. 4.3.6(m)).

Fig. 4.3.6(n) shows that the magnitude of southerly (+ve) flux decreases from surface to 900 hPa and increases from 600 to 200 hPa gradually over Chittagong during 17-19 May. Also there is no regular trend of the meridional flux of moist static energy from 900 to 600 hPa during the period. The gradual increase of southerly (+ve) flux from 600 to 200 hPa is due to the dominance of the easterly wind component of the cyclonic circulation of the advancing cyclone.

In Fig. 4.3.6(o), it is observed that the meridional flux decreases from surface to 800 hPa and increases from 500 to 200 hPa over Calcutta on 18th May with respect to that of 17th May. Again the flux decreases at all levels with little anomalies at 200 hPa on 19th May with respect to that of 18th May. The significant amount of southerly flux in the upper troposphere is due to the movement of the cyclone to the northward direction.

4.3.6.6 Zonal flux of moist static energy

The magnitude of westerly (+ve) flux over Dhaka increases significantly at all levels on 18th May with respect to that of 17th May (Fig. 4.3.6(p)). Again the westerly flux

decreases from surface to 500 hPa and increases from 500 to 200 hPa on 19th May than that of 18th May. Only little amount of easterly flux exists around surface during the period.

From Fig. 4.3.6(q), it is observed that a little amount of easterly flux exists at around surface and above the surface level the westerly flux decreases at all levels over Chittagong on 18th May with respect to that of 17th May. Again the zonal flux increases from surface to 750 hPa and decreases from 750 to 550 hPa on 19th May with respect to that of 18th May. The flux is westerly in the layer from 900 to 200 hPa on 18th May and from surface to 600 hPa on 19th May.

The westerly flux over Calcutta decreases at all levels on 18th May than that of 17th May (Fig. 4.3.6(r)). Again the magnitude of westerly flux increases at all levels on 19th May with respect to that of 18th May.

4.3.6.7 Combination of zonal and meridional fluxes

There exists south-westerly flux at all levels with little anomalies over Dhaka on 17th and 18th May. The south-westerly flux is maximum at 500 hPa on 17th May. The flux is south-westerly from surface to 800 hPa and 400 to 200 hPa and north-westerly from 800 to 400 hPa on 19th May. The south-westerly flux decreases and the north-westerly flux increases gradually with little anomalies during the period as the cyclone moves towards the landfall over the station.

There are tremendous amount of south-easterly flux around surface and westerly flux above these levels over Chittagong on 17th May. The flux becomes south-westerly at all levels with little anomalies on 18th and 19th May over the station.

The south-westerly flux exists in the layer from surface to 600 hPa and tremendous amount of westerly flux exists from 600 to 200 hPa over Calcutta on 17th May. The large amount of south-westerly flux exists at all levels on 18th May. The south-westerly flux

exists in the lower troposphere and upper troposphere and the north-westerly flux is found in the middle troposphere on 19th May.

The south-westerly flux is observed in the layer from the surface to 700 hPa and 400 to 300 hPa with north-westerly flux in the layer 700 to 400 hPa over Cuttack during the period.

4.4 Discussion & Conclusions

Efforts have been made to study the five severe cyclonic storms with a core of hurricane winds and one cyclonic storm that formed in the Bay of Bengal and crossed Bangladesh coast during the last decade. One of the severe cyclonic storms recurved and weakened in the Bay of Bengal. The severe cyclonic storms are of the years 1985 (crossed Urir Char coast of Bangladesh), 1988 (crossed Khulna West Bengal coast), 1991 (crossed Chittagong coast), 1992 (weakened in the Bay of Bengal) and 1994 (crossed Cox's Bazar coast) and the cyclonic storm of 1992 (crossed Cox's Bazar coast).

4.4.1 Dry Static Energy

The dry static energy increases in the upper troposphere from approximately 700 to 200 hPa and decreases in the lower troposphere from surface to 700 hPa in the far away stations on the day of landfall with respect to that of the previous day in case of all the severe cyclonic storms with a core of hurricane winds. It is also seen that the dry static energy is almost constant in the lower troposphere and increases in the upper troposphere in the nearby stations on the day of landfall with respect to that of the previous day in case of all the severe cyclonic storms with a core of hurricane winds. However, the dry static energy increases at all levels in the far away stations such as Dhaka and Calcutta and decreases from surface to 550 hPa and increases from 550 to 200 hPa in the nearby station such as Chittagong on the day of landfall with respect to that of the previous day in case of the severe cyclonic storm with a core of hurricane wind of 1994.

The dry static energy decreases in the far away station such as Cuttack and has no definite trend in the nearby station such as Chittagong on the day of landfall with respect to that of the previous day in case of the cyclonic storm of 1992. It is also seen that the dry static energy increases over Calcutta and almost constant over Dhaka.

The dry static energy increases at all levels on the day of landfall with respect to that of the previous day in case of the severe cyclonic storm with a core of hurricane winds of 1992 over Cuttack. The dry static energy decreases at all levels on the day of landfall with respect to that of the previous day in case of the severe cyclonic storm with a core of hurricane winds of 1992 over Dhaka. The dry static energy decreases from surface to 700 hPa and increases from 700 to 200 hPa on 21st with respect to that of 19th November over Chittagong. Again the dry static energy increases at all levels on 21st with respect to that of 20th November at 1200 UTC over Chittagong.

4.4.2 Latent Heat Energy

The latent heat energy decreases significantly in the lower troposphere and increases in the upper troposphere of the nearby stations on the day of landfall with respect to that of the previous day in case of all the severe cyclonic storms with a core of hurricane wind. The latent heat energy decreases slightly in the lower troposphere from surface to 900 hPa and increases significantly in the upper troposphere from 900 to 400 or 300 hPa of the intermediate stations and increases significantly at all other levels in the far away stations on the day of landfall with respect to that of the previous day. It is also seen that the latent heat energy decreases significantly from 850 to 400 hPa in the nearby station such as Calcutta and has little or no change in the far away stations such as Dhaka and Chittagong on the day of landfall with respect to that of the previous day in case of the severe cyclonic storm with a core of hurricane wind of 1988.

The latent heat energy decreases in the far away stations such as Dhaka, Calcutta and Cuttack on the day of landfall with respect to that of the previous day in case of the cyclonic storm of 1992. It is also seen that the latent heat energy increases significantly in

the nearby station such as Chittagong from surface to 775 hPa on the day of landfall with respect to that of the previous day.

The latent heat energy increases from surface to 600 hPa over Dhaka and Chittagong on 21st November with respect to that of 20th November in case of the severe cyclonic storm with a core of hurricane wind of 1992. It is also seen that the latent heat energy increases from surface to 750 hPa and decreases from 750 to 300 hPa and at all levels on 20th November with respect to that of 19th November over Cuttack and Port Blair respectively.

4.4.3 Moist Static Energy

The moist static energy decreases significantly in the lower troposphere from surface to approximately 700 hPa and increases in the upper troposphere from these levels to 200 hPa at the nearby stations on the day of landfall with respect to that of the previous day in case of the severe cyclonic storms with a core of hurricane winds of 1985, 1991 and 1994. It is also seen that the moist static energy increases at all levels with little anomalies in the far away stations. The moist static energy decreases significantly from 850 to 450 hPa over Calcutta and decreases slightly over Dhaka at the same level and increases from 450 to 200 hPa on 29th November with respect to that of 28th November 1988.

The moist static energy increases in the nearby station such as Chittagong and decreases in the far away stations such as Cuttack, Calcutta and Dhaka on the day of landfall with respect to that of the previous day in case of the cyclonic storm of 1992.

The moist static energy increases at all levels over Chittagong and in the lower troposphere over Dhaka on 21st November with respect to that of 20th November 1992. It is also seen that the moist static energy decreases gradually over Port Blair during the period. Since the severe cyclonic storm with a core of hurricane winds weakened in the Bay of Bengal hence the moist static energy increases significantly over Chittagong and lower troposphere over Dhaka.

4.4.4 Total Energy

The changing pattern of total energy and the moist static energy is the same. Only little variation of magnitude is observed between moist static energy and the total energy.

4.4.5 Meridional Flux of Moist Static Energy

There is southerly (+ve) flux at all levels with little anomalies around surface over Dhaka on the day before the day of landfall of all the severe cyclonic storms with a core of hurricane winds and the cyclonic storm of 1992. The northerly (-ve) flux exists from surface to 825 hPa and 750 hPa of the severe cyclonic storm with a core of hurricane winds of 1991 and 1985 respectively and from 800 to 500 hPa of the cyclonic storm of 1992. The flux is southerly (+ve) at all levels with few exceptions over Dhaka on the day of landfall of the severe cyclonic storm with a core of hurricane winds and the cyclonic storm of 1992. The flux is northerly (-ve) at all levels on the day of landfall of the severe cyclonic storm with a core of hurricane winds of 1985 and from 800 to 400 hPa of the cyclonic storm of 1992.

The southerly (+ve) flux is observed at all levels with little anomalies over Chittagong on the day before the day of landfall of all the severe cyclonic storms with a core of hurricane winds and the cyclonic storm of 1992. There is southerly (+ve) flux at all levels with few exceptions in the upper troposphere over Chittagong on the day of landfall of the severe cyclonic storms with a core of hurricane winds and the cyclonic storm of 1992. The northerly (-ve) flux exists from 600 to 300 hPa in case of the severe cyclonic storm with a core of hurricane winds of 1992 (weakened) and from surface to 800 hPa in case of the cyclonic storm of 1992.

The southerly (+ve) flux is observed throughout the troposphere with few exceptions on the day before the day of landfall over Calcutta in case of all the severe cyclonic storms with a core of hurricane winds and the cyclonic storm of 1992. The flux is northerly (-ve) from surface to 675 hPa and southerly (+ve) from 675 to 200 hPa on the day before the day of landfall of the severe cyclonic storm with a core of hurricane winds of 1994. The southerly (+ve) flux dominates at all levels on the day of landfall of the severe cyclonic

storm with a core of hurricane winds of 1988. The flux is northerly (-ve) from surface to 500 or 400 hPa in case of the severe cyclonic storms with a core of hurricane winds of 1985, 1991 and 1994 and from 800 to 500 hPa of the cyclonic storm of 1992 and southerly (+ve) flux above these levels up to 200 hPa in case of all of these cyclones over Calcutta on the day of landfall.

There are northerly (-ve) flux from surface to 300 or 400 hPa and southerly (+ve) flux above these levels to 200 hPa over Cuttack on the day and before the day of landfall of all the severe cyclonic storms with a core of hurricane winds. The flux is northerly (-ve) from 800 to 500 hPa and southerly (+ve) flux from surface to 800 hPa and 400 to 200 hPa over Cuttack on the day and before the day of landfall of the cyclonic storm of 1992.

There is southerly (+ve) flux in the troposphere over Port Blair during the severe cyclonic storms with a core of hurricane winds of 1991 and 1992.

4.5.6 Zonal Flux of Moist Static Energy

The westerly (+ve) flux is observed to dominate at all levels over Dhaka on the day before the day of landfall of the severe cyclonic storms with a core of hurricane winds of 1988, 1992, 1994 and the cyclonic storm of 1992. The flux is easterly (-ve) from surface to 700 and 300 hPa and westerly (+ve) above these levels up to 200 hPa in case the severe cyclonic storms with a core of hurricane winds of 1985 and 1991. The easterly (-ve) flux exists from surface to 450 hPa having the westerly (+ve) from 450 to 200 hPa with little anomalies in case of the severe cyclonic storms with a core of hurricane winds of 1985, 1988, 1991 and 1994 on the day of landfall. The flux is westerly (+ve) at all levels in case of the severe cyclonic storms with a core of hurricane winds of 1992 and the cyclonic storm of 1992 on the day of landfall.

There is easterly (-ve) flux from surface to 700 hPa and westerly (+ve) flux from 700 to 200 hPa over Chittagong on the day before the day of landfall of the severe cyclonic storms with a core of hurricane winds of 1988, 1991 and 1992. The westerly (+ve) flux dominates at all levels in case of the severe cyclonic storm with a core of hurricane winds

of 1994 and the cyclonic storm of 1992 on the day before the day of landfall. The flux is easterly (-ve) at all levels on the day of landfall of the severe cyclonic storms with a core of hurricane winds of 1988 and 1994. Easterly (-ve) flux exists from surface to 500 hPa or 600 hPa having the westerly (+ve) flux above these levels to 200 hPa on the day of landfall of the severe cyclonic storms with a core of hurricane winds of 1991 and 1992. There are westerly (+ve) flux from surface to 600 hPa and easterly (-ve) flux is flowing from 600 to 500 hPa on the day of landfall of the cyclonic storm of 1992.

The easterly (-ve) flux exists in the layer from surface to 750, at 350 and 600 hPa having the westerly (+ve) flux from these levels to 200 hPa on the day before the day of landfall of the severe cyclonic storms with a core of hurricane winds of 1988, 1991 and 1994 respectively. The flux is easterly (-ve) at all levels with little anomalies in the upper troposphere where the westerly (+ve) flux is observed on the day of landfall of the above mentioned cyclones. The westerly (+ve) flux dominates at all levels on the day and before the day of landfall of the cyclonic storm of 1992.

The westerly (+ve) flux exists at all levels with little anomaly over Cuttack on the day before the day of landfall of the severe cyclonic storms with a core of hurricane winds of 1985, 1991 and 1992. The flux is easterly (-ve) from surface to 500 and 450 to 200 hPa in case of the severe cyclonic storms with a core of hurricane winds of 1991 and 1985 respectively. There are easterly (-ve) flux from surface to 700 hPa and westerly (+ve) flux from 700 to 400 hPa on the day of landfall of the severe cyclonic storm with a core of hurricane winds of 1991. The westerly (+ve) flux extends throughout the troposphere on the day and before the day of landfall of the cyclonic storm of 1992 .

The easterly (-ve) flux is observed to dominate at all levels in case of the severe cyclonic storm with a core of hurricane winds of 1992 (weakened) and the flux is westerly (+ve) at all levels with little anomalies in the upper troposphere over Port Blair on the day before the day of landfall of the severe cyclonic storm with core of hurricane winds of 1991.

Chapter 5

A Simple Two Dimensional Cyclone Track Prediction Model

5.1 Introduction

The Bay of Bengal is one of the most important basins in respect of occurrence of tropical cyclones. Although the frequency of occurrence of tropical cyclones is less than those in some of the other basins, Bay cyclones are among the deadliest. In recent years, however, radar and satellite observations of cyclones have become available in this area for the movement of cyclones, but no effective method for the track predictions are yet available.

It may be useful to construct effective methods of track prediction that may not be so rigorous from the point of view of the first principle of Atmospheric Physics, but which can serve as phenomenological guides. In this work an attempt has been made to construct a useful model for cyclone track prediction, which take into account some of the physical characteristics of a cyclone.

A two-dimensional model has been developed with no vertical layer separation. The justification for such a simplification is the fact that the cyclone extends to a great height beyond the troposphere and all layers move together. In this case it can be simply represented by a vortex line, which would be well parameterized by a complex potential. Choudhury (1978) gave a model for tropical cyclones in the Bay of Bengal. In this model the tracks for cyclones could be drawn only for those which crossed the Meghna estuary. The model developed in this study can be used to fit any track of a cyclone in the Bay of Bengal that hits anywhere along the coastline.

In this model a sink and a vortex have been considered to attract the cyclone towards land. To this added the northward, westward and eastward steering wind.

5.2 Theoretical Description

5.2.1 Complex potential

A vector with zero curl must be the gradient of a scalar function. If

$$\nabla \times \vec{V} = \vec{0}$$

then

$$\vec{V} = \nabla \ \phi$$

where $\phi(x,, y, z, t)$ is the velocity potential function.

The components u and v of a vector **v** in two dimensions, which is irrational, can be written as

$$u = \frac{\partial \ \phi}{\partial \ x}, \tag{5.1}$$

$$v = \frac{\partial \ \phi}{\partial \ y} \tag{5.2}$$

The components of a solenoidal vector $\vec{V}$ in two dimensions can be expressed in terms of a stream function ψ can be written as

$$u = \frac{\partial \ \psi}{\partial \ y}, \tag{5.3}$$

$$v = -\frac{\partial \ \psi}{\partial \ x} \tag{5.4}$$

These two scalar functions $\phi(x, y)$ and $\psi(x, y)$ are related by

$$\frac{\partial \ \phi}{\partial \ x} = \frac{\partial \ \psi}{\delta \ y} \tag{5.5}$$

and

$$\frac{\partial \ \phi}{\partial \ y} = -\frac{\partial \ \psi}{\partial \ x} \tag{5.6}$$`

The complex potential for the flow described by ϕ and ψ (Batchelor, 1980) can be written as

$$W = \phi + i\psi \tag{5.7}$$

5.2.2 The Complex velocity

From the complex potential $W = \phi + i\psi$ we have

$$\frac{\partial W}{\partial x} = \frac{\partial \phi}{\partial x} + i\frac{\partial \psi}{\partial x}$$

$$\frac{\partial W}{\partial x} = \frac{dW}{dz} \times \frac{\partial z}{\partial x} = \frac{dW}{dz}$$

where z = x,+ i y. Therefore

$$\frac{dW}{dz} = \frac{\partial \phi}{\partial x} + i\frac{\partial \psi}{\partial x}$$

As $u = \frac{\partial \phi}{\partial x}, v = -\frac{\partial \psi}{\partial x}$ and therefore,

$$\nu = u - iv = \frac{dW}{dz}$$

ν (upsilon) which is the combination of u- i v, is called the complex velocity (Milne-Thompson, 1972). We see that the complex velocity is obtained directly from the complex potential. Graphically, the vector representing the complex velocity is the reflection in the line through the point considered parallel to the x-axis, of the vector of the actual velocity.

5.2.3 The complex potential and the velocity

The velocity components u , v are given by

$$u = \frac{\partial \phi}{\partial x} = \frac{\partial \psi}{\partial y} \tag{5.8}$$

$$v = \frac{\partial \phi}{\partial y} = -\frac{\partial \psi}{\partial x} \tag{5.9}$$

When ϕ and ψ are taken as the real and imaginary parts of a complex function W(z) , these are called the Cauchy - Riemann equations, and they follow from the differentiability of W(z). So for any differentiable function W(z), generally the real part

$\phi(x, y)$ is taken as a velocity potential for fluid motion (of a restricted type) and the imaginary part is taken as the stream function for the same motion.

The derivative $\frac{dW}{dz}$ is related to the derivatives of ϕ and ψ, and hence the velocity components u, v. For differentiable function W(z),

$$\frac{dW}{dz} = \frac{\partial \phi}{\partial x} + i\frac{\partial \psi}{\partial x} \tag{5.10}$$

and consequently

$$\frac{dW}{dz} = u - i\,v \tag{5.11}$$

Hence

$$u = \mathrm{Re}\frac{dW}{dz} = \mathrm{Re}\,W'(z) \tag{5.12}$$

$$v = -\mathrm{Im}\frac{dW}{dz} = -\mathrm{Im}\,W'(z) \tag{5.13}$$

This may also be expressed as

$$u + iv = \overline{W}'(z) \tag{5.14}$$

Where an overbar denotes a complex conjugate. Moreover, if we put this in terms of the speed q of the flow and the angle θ that the streamlines make locally, then

$$u + i\,v = q\,e^{i\theta} = \overline{W'}(z)$$

So that

$$q = \left|\overline{W'}(z)\right| = \left|W'(z)\right| \tag{5.15}$$

$$\theta = \arg\overline{W'}(z) = -\arg\,W'(z) \tag{5.16}$$

5.2.4 The complex potential for a simple source

If the source of strength m is at the origin, the velocity at (r, θ) is $\frac{m}{r}$ radially. Therefore

$$-\frac{dW}{dz} = u - i\ v = \frac{m}{r}(\cos\ \theta - i\ \sin\ \theta) = \frac{m}{z},$$

where $z = r\ e^{i\theta}$. Therefore

$$w = -m\log z = -m\log(r\,e^{i\theta})$$

or

$$w = -m\log r - m\log e^{i\theta}$$

Thus

$$w = \phi + i\psi = -m\ \log r - im\theta \qquad (5.17)$$

Therefore the stream function is ψ= -m θ. If the source is at the point z_0 , we have, by a change of origin,

$$w = -m\ \log(z-z_0) \qquad (5.18)$$

It will be observed that as r increases, the wind speed diminishes, so that at a great distance from the source the fluid is almost quiescent.

5.3 Formulation of the model for Bay of Bengal Cyclones

In this model we have considered a fixed point (arbitrary) where a sink and a vortex is situated on the land of Bangladesh (Fig.5.3.1). The impact of the westward, eastward and the northward steering wind were also taken into consideration. In the first case the effect of Coriolis force was neglected for simplicity and in the second case the Coriolis force was taken into consideration for the track prediction.

Let us consider that the strength of the sink is m and that of the vortex is k. So the complex velocity potentials due to them at the position of the cyclone are given by

$$w_1(z) = m\ \ln(z-z_0) \qquad (5.19)$$

$$w_2(z) = i\ k\ \ln(z-z_0) \qquad (5.20)$$

where $z = x + i\,y$, is the instantaneous position of the cyclone and $z_0 = x_0 + i\,y_0$, is the position of the sink and the vortex.

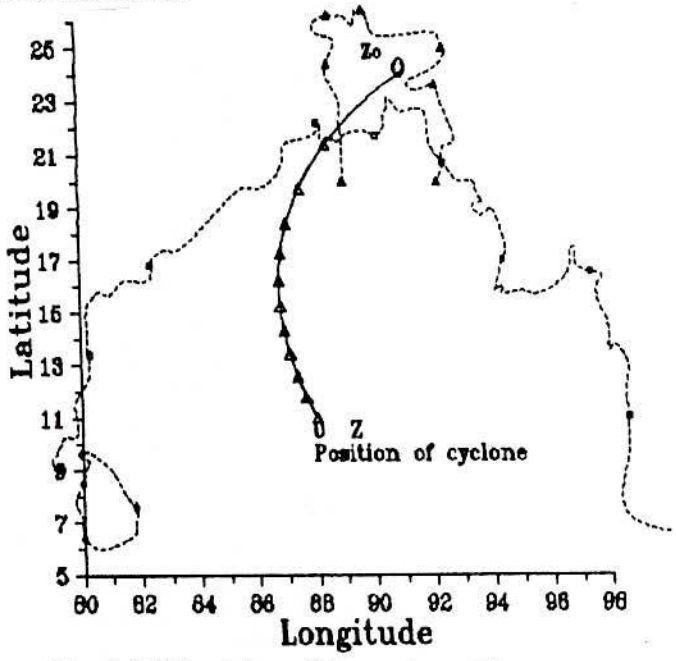

Fig.5.3.1 Position of formation of images

Therefore the total complex potential due to the vortex and the sink is

$$W(z) = w_1(z)+w_2(z)$$
$$= (m+ik)\ln(z-z_0)$$

Now

$$\frac{dW}{dz} = \frac{m+ik}{z-z_0}$$
$$= \frac{(m+ik)(\bar{z}-\bar{z}_0)}{(z-z_0)(\bar{z}-\bar{z}_0)}$$
$$= \frac{(m+ik)[(x-iy)-(x_0-iy_0)]}{|z-z_0|^2}$$

$$= \frac{(m+ik)[(x-x_0)-i(y-y_0)]}{|z-z_0|^2}$$

$$= \frac{[m(x-x_0)+k(y-y_0)]-i[m(y-y_0)-k(x-x_0)]}{|z-z_0|^2}$$

We know $$V_x = \mathrm{Re}\left(\frac{dW}{dz}\right)$$

and $$V_y = -\mathrm{Im}\left(\frac{dW}{dz}\right)$$

Therefore

$$V_x = \frac{m(x-x_0)+k(y-y_0)}{|z-z_0|^2} \qquad (5.21)$$

$$V_y = \frac{m(y-y_0)-k(x-x_0)}{|z-z_0|^2} \qquad (5.22)$$

To these values are added the constant velocity fields $\overline{V}_x$ and $\overline{V}_y$ which serve to steer. Therefore the wind velocity in the x and y components are:

$$u = V_x + Coriolis\ parameter \times V_y \times dt + \overline{V}_x \qquad (5.23)$$

$$v = V_y - Coriolis\ parameter \times V_x \times dt + \overline{V}_y \qquad (5.24)$$

where dt is the time step and the Coriolis parameter $f = 2 \times \Omega \times \sin\varphi$ and for the first case we have used the value of this parameter =0. Therefore,

$$u = V_x + \overline{V}_x \qquad (5.25)$$

$$v = V_y + \overline{V}_y \qquad (5.26)$$

5.4 Results and Discussion

We have constructed a two dimensional model neglecting the altitude variation. In a sense this reduction to two dimensions is justified because during cyclones there can not be any significant vertical wind shear (Gray 1979, Steven P.W. and Stanly Q.K., 1984), otherwise the cyclone would degenerate. It is also found from the analysis that the vertical wind shear is approximately zero near the centre of the cyclone. The different layers of the cyclone move together although the direction of azimuthal wind flow is reversed from bottom to top. In our model we have considered only one effective layer. We have tried to find the best fits and the corresponding parameters of cyclone tracks for major cyclones that formed in the Bay of Bengal and crossed the Bangladesh coast during (1970-1994).

TABLE 1

Best parameter fits for track of different cyclones in the Bay of Bengal

Status	Date of formation	Sink Strength m deg.^{2}/hr.	Steering Wind $\bar{V}_x$ Km/hr.	Steering Wind $\bar{V}_y$ Km/hr.	Vortex Strength k deg.^{2}/hr	Observed Time (hours)	Predicted Time (hours)
SCS(H)	08-11-70	-1.00	12.58	3.50	0.30	108.0	113.40
SCS(H)	24-11-74	-1.00	10.38	0.65	0.15	90.0	92.00
SCS(H)	05-12-81	-0.70	5.84	0.00	0.20	132.0	134.90
SCS(H)	22-05-85	-0.78	9.08	1.17	0.10	69.0	69.00
SCS(H)	24-11-88	-1.00	13.62	0.18	0.15	129.0	101.40
SCS(H)	25-04-91	-1.05	11.03	0.00	0.30	115.0	117.10
SCS(H)	17-11-92	-1.10	17.77	3.89	0.45	102.0	101.80
SCS(H)	29-04-94	-1.19	7.14	0.00	0.20	84.0	81.20
CS	17-05-92	-1.80	17.51	0.00	0.85	57.0	56.80

In the model we have considered a static sink and a vortex over land in Bangladesh to attract the cyclone. In addition a steady steering wind is added to account for the east

west motion. The complex velocity and the steady steering wind have been simultaneously integrated in small steps to find the track of the cyclones. The values of different parameters for different cyclones are shown in Table 1.

Reasonable fits are found for the tracks of the severe cyclonic storms with core of hurricane intensity occurred in 1970, 1985, 1991, 1992 and 1994 and the cyclonic storm of 1992 as shown in Figs.5.4.1 (a), (d), (f), (g), (h) & (i) respectively. But for the cyclones of 1974, 1981 and 1988 where the tracks recurve, only an average fit is found. These are shown in Figs.5.4.1 (b), (c) & (e) respectively.

We, therefore, next tried to generalise our simple model to obtain a better fit for the last three cyclones and also the others. It is obvious that recurving involves variable winds. This can be due to a complex interaction between the cyclonic vortex and the rest of the atmosphere during the motion of the cyclone. The complicated nature of such effects cannot be reproduced in a two-dimensional simplified model such as ours. However, we thought it might be possible to replace the constant steering wind by a variable one that may take care of the recurving of the track, even multiple changes of curvature. Though it would not increase the number of parameters in our model, it might enlighten us as to whether our simple model could in principle also account for the most complex trajectories observed. In this more general model we also included the actual Coriolis force on the cyclone centre as it moved northward, which of course varied with the latitude.

In Table 2 we give a more generalised choice of steering winds with variable durations. The fitted tracks in this generalized model are shown in Figs. 5.4.2 (a), (b), (c), (d), (e), (f), (g), (h) & (i) for the severe cycloninc storm with a core of hurricane winds of 1970, 1974, 1981, 1985, 1988, 1991, 1992 and 1994 and the cyclonic storm of 1992 respectively.

TABLE 2

Best parameter fits for track of different cyclones in the Bay of Bengal

Date of formation	Sink Strength m deg.2/hr.	Steering Wind Vx Km/hr. (figure within parentheses is duration in hours)	Steering Wind Vy Km/hr.	Vortex Strength k deg.2/hr	Observed Time (hours)	Predicted Time (hours) (without Coriolis force)	Predicted Time (hours) (with Coriolis force)
08-11-70	-0.99	15.7(23), 9.5(68), 15.7(21.9)	2.42	0.30	108.0	112.90	107.90
24-11-74	-0.92	44.84(2), 21.3(23), 5.6(21), -13.45(19), 0(16), -5.6(15.1)	0.84	0.10	90.0	96.10	95.80
05-12-81	-0.63	50.45(6),13.45(14),0(26),5.6(20), -11.2(15.5), 9(31), 1.1(12),24(6)	0.56	0.20	132.0	130.50	129.50
22-05-85	-0.78	17.94(7), 7.18(49), 2.24(11.9	0.11	0.10	69.0	67.90	67.80
24-11-88	-0.65	0(24), 8.97(20), 47.1(7),24.66(8), 3.36(21),-8.97(14) , 0(33.7)	0.11	0.10	129.0	123.70	123.50
25-04-91	-1.05	8.97(23),67.3(2), 9(70),15.7(21.)	0.00	0.30	115.0	116.10	115.40
17-11-92	-1.10	50(11),13.5(64), 19(13),28(18.5)	3.47	0.45	102.0	106.50	105.90
29-04-94	-1.00	3.7(43),21.3(4), 5.6(30), -7.85(3), 33.6(1),7.85(3.4)	0.56	0.20	84.0	84.40	84.30
17-05-92	-1.20	3.4(18),11(13),5.6(15), -6.7(12.4)	0.00	0.30	57.0	58.40	58.10

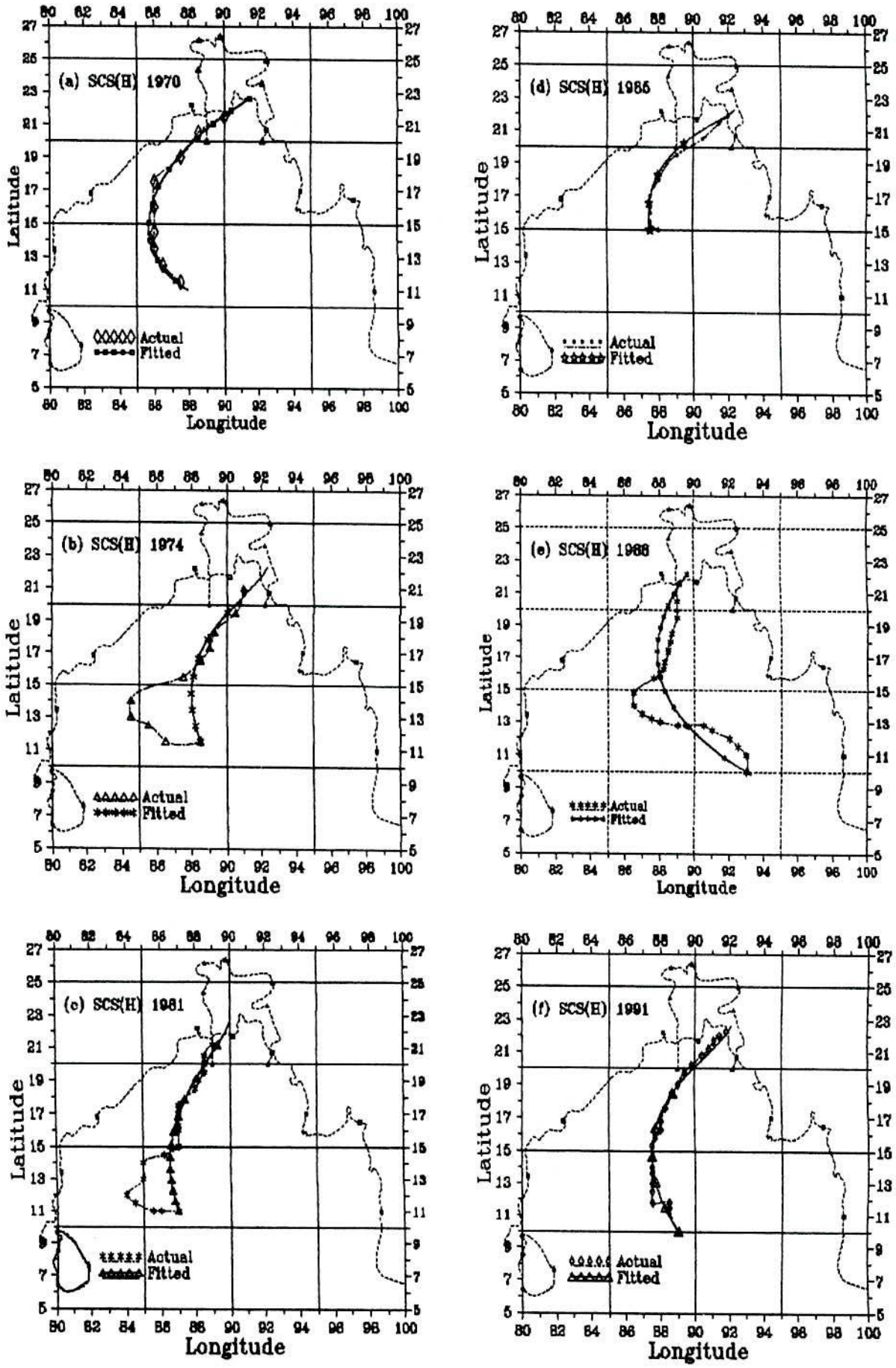

Figs. 5.4.1(a-f) Track of Severe Cyclonic Storm with a core of hurricane winds of 1970, 1974, 1981, 1985, 1988 and 1991 are predicted by using a constant steering wind..

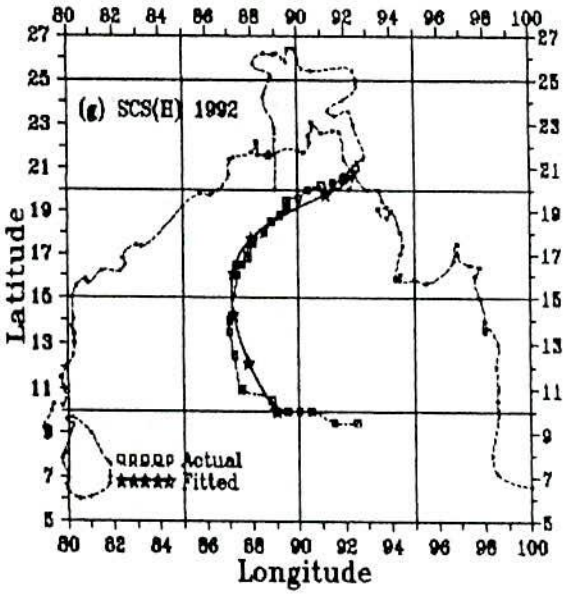

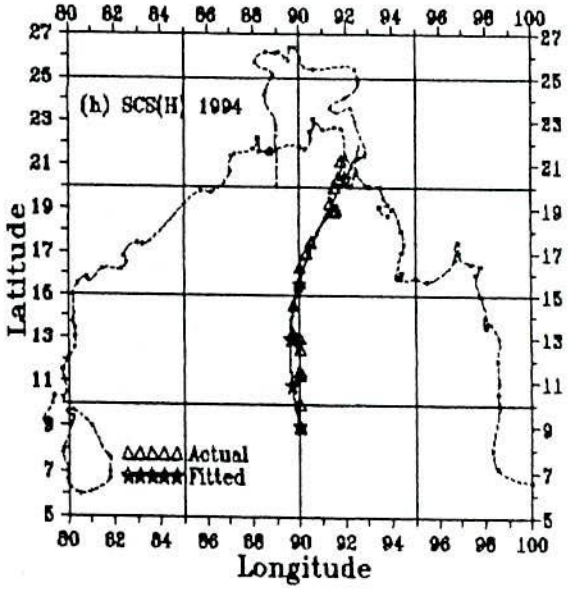

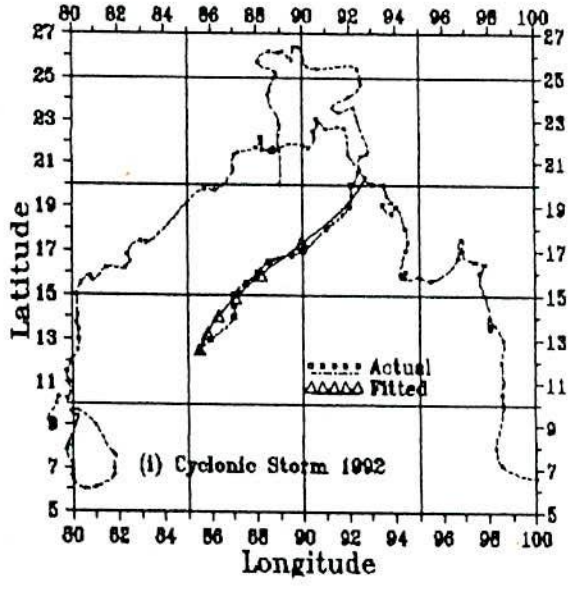

Figs. 5.4.1(g-i) Track of Severe Cyclonic Storm with a core of hurricane winds of 1992, 1994 and the cyclonic storm of 1992 are predicted by using a constant steering wind..

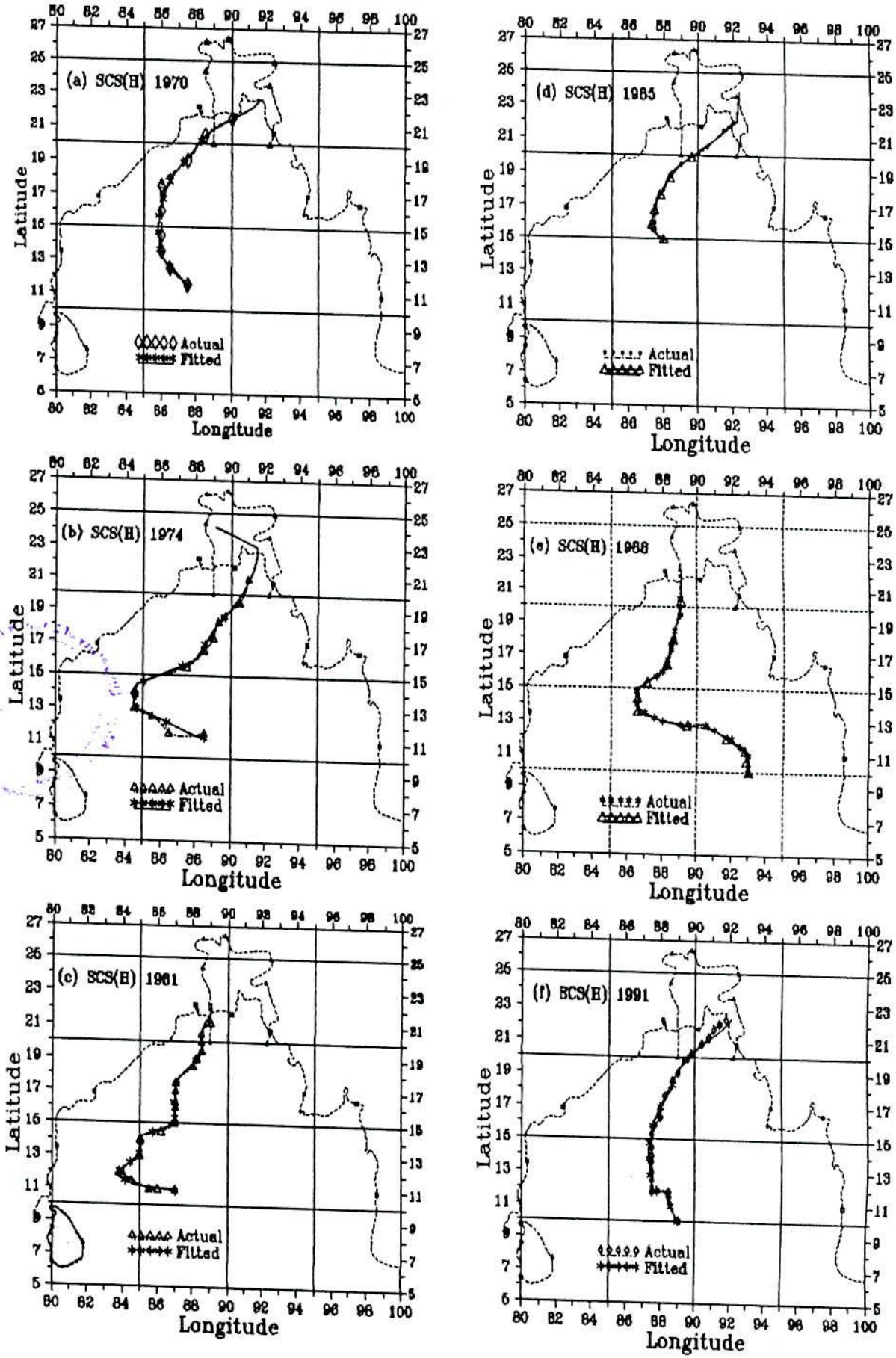

Figs. 5.4.2(a-f) Track of Severe Cyclonic Storm with a core of hurricane winds of 1970, 1974, 1981, 1985, 1988 and 1991 are predicted by using a time dependent steering wind..

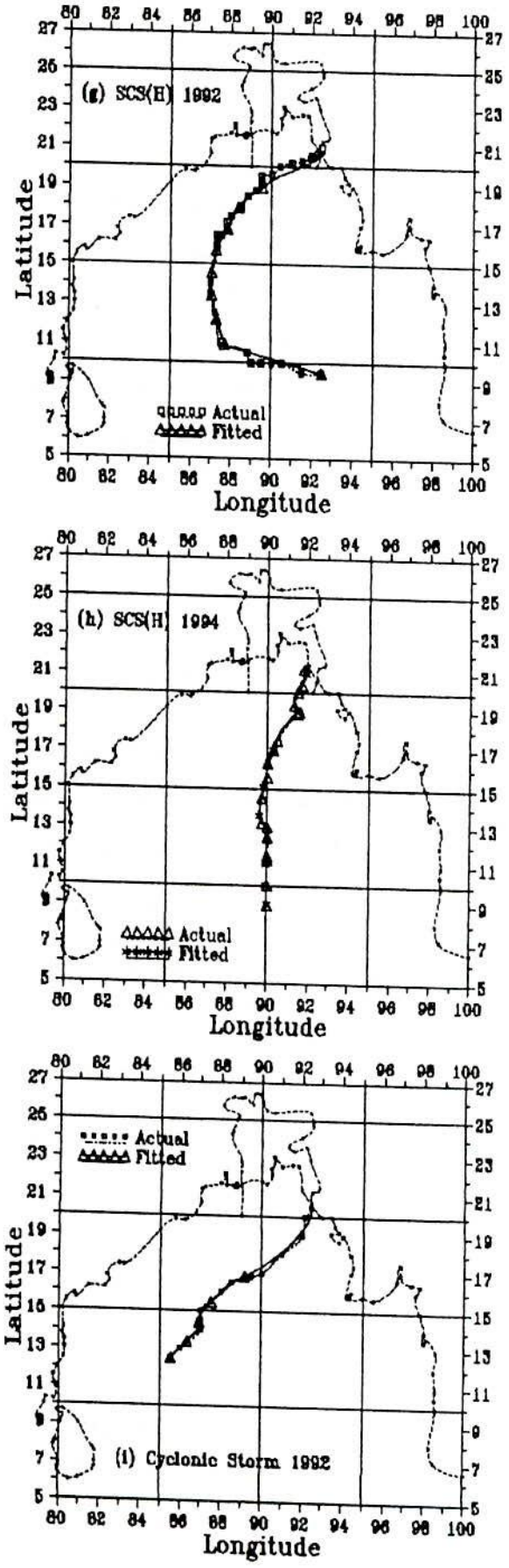

Figs. 5.4.2(g-i) Track of Severe Cyclonic Storm with a core of hurricane winds of 1992, 1994 and the cyclonic storm of 1992 are predicted by using a time dependent steering wind..

We can see that in almost all cases with very reasonable variable steering winds we can fit all the cyclone tracks very accurately. Only for the cyclones of 1991 & 1992 we have to use somewhat high steering winds but even they are within physically possible values. For the others the values are in conformity with steering wind speeds usually observed. Even multiple recurvings can be nicely fitted by the procedure. It was interesting to note that if we omitted the Coriolis force from this general model, but included only the variable steering wind, we could fit the track well, but the time taken for landfall was somewhat less precise. Coriolis force seems to speed up landfall and bring agreement with observed time.

5.5 Conclusions

On the basis of the study presented in this chapter, the following conclusions can be drawn

- It is found from the result that the travel time for the cyclones obtained by the model is approximately equal to that of the exact travel time (from the time of formation to the time of crossing the land) of the cyclone as shown in Tables 1 and 2.
- Accurate fits were not found by the simple model with constant steering wind for the severe cyclonic storms with a core of hurricane intensity of 1974, 1981 and 1988 due to the complexity of their courses.
- However, when variable steering winds are used in our model, we get very good fits for all the cyclones, showing that our model is in principle correct, though for actual predictive use we would need more information from existing atmospheric conditions to estimate the steering wind parameters.
- Coriolis force seems to be needed to forecast a precise time for landfall.

Chapter 6

A Three Dimensional Numerical Tropical Cyclone Model

6.1 Introduction

Studies of tropical cyclone formation in numerical weather prediction models have been conducted by many researchers (e.g. Davidson and Kumar, 1990; Puri and Miller, 1990: Tuleya, 1988, 1994; Krishnamurti *et al.* , 1972, 1994; Shapiro, 1992; Wang and Holland, 1995; Flatau *et al* , 1994).

Shapiro (1992), in the three layer model, includes convective heat release in response to boundary layer friction and the convective momentum transports. Wang and Holland (1995) include a frictional boundary layer with a wind speed-dependent drag coefficient, and horizontal and vertical diffusion of momentum and heat on the grid scale. Flatau *et al.* (1994) superposed analytical heating function directly over the surface pressure centre, which would tend to maintain the low centre in its present location.

In this work we have developed a 5-layer model in the pressure co-ordinate for tropical cyclone formation. We have considered the sensible heat transfer from the surface above the boundary layer. Also the latent heat of condensation, which has three components i) moisture convergence above the cloud base, ii) Ekman pumping of moisture from the boundary layer and iii) the surface evaporation.

Krishnamurti *et al.* (1972) considered a grid length of 220 km and the time step as 5 minutes. We have in this work tried with a smaller step of 80 km to see greater detail. We experimented with various numerical procedures, e.g. smoothing and filtering, variation of time steps and finally on the very critical question of discovering the right vertical distribution of energy to sustain a cyclone.

6.2 The Primitive Equations in P - co-ordinate

The equations governing the evolution of the different meteorological variables can be summarised in a system of six equations. These are in the x- and y- component momentum equation, the thermodynamic energy equation, the continuity equation, the hydrostatic approximation and the equation of state. Scale analysis indicates that to a high degree of accuracy, the pressure field is in a hydrostatic equilibrium, thus, the hydrostatic approximation is used. This set which constitutes a closed system in the dependent variables u, v, ω, Φ, α, and T is referred to the primitive equations. The basic equations (Holton, 1979) are:

1. the momentum equations

$$\frac{\partial u}{\partial t} + \vec{V}.\nabla u + \omega \frac{\partial u}{\partial p} = -\frac{\partial \Phi}{\partial x} + fv + F_x \tag{6.1}$$

$$\frac{\partial v}{\partial t} + \vec{V}.\nabla v + \omega \frac{\partial v}{\partial p} = -\frac{\partial \Phi}{\partial y} - fu + F_y \tag{6.2}$$

2. the thermodynamic energy equation

$$C_p \frac{dT}{dt} = \frac{RT}{P}\omega + Q \tag{6.3}$$

3. the continuity equation

$$\nabla_p.\vec{V} + \frac{\partial \omega}{\partial p} = 0 \tag{6.4}$$

4. the hydrostatic approximation

$$\frac{\partial \Phi}{\partial p} + \frac{RT}{P} = 0 \tag{6.5}$$

5. the equation of state

$$P\alpha = RT \tag{6.6}$$

where

$$\frac{d}{dt}() = \frac{\partial}{\partial t}() + \vec{V}.\nabla() + \omega\frac{\partial}{\partial p}() \tag{6.7}$$

$$\vec{V}.\nabla() = u\frac{\partial}{\partial x}() + v\frac{\partial}{\partial y}() \tag{6.8}$$

and

$$\omega = \frac{d\,P}{d\,t} \tag{6.9}$$

In the above equations, u and v are the zonal (x-) and meridional (y-) components of the horizontal wind vector, $\vec{V}$, respectively; Φ is the geopotential; f is the Coriolis parameter and equal to $2\,\Omega \sin\phi$ where $\Omega = 7.29 \times 10^{-5}$ sec^{-1}, the angular speed of the earth rotation and ϕ is the latitude; P is the pressure and t is time. F_x and F_y are the x- and y-components of the frictional forces; Q is the diabatic heating rate; ω is the vertical velocity in isobaric co-ordinates; α is the volume of a unit mass of air; R is the gas constant of dry air and T is the temperature. ∇ is the horizontal gradient operator.

Some of the advantages of using the pressure co-ordinate system are that meteorological observations are normally made at constant pressure surfaces and that vertically propagating sound waves are completely filtered out from the solution of the equations.

6.3 Finite Differencing

The horizontal x, y space is divided into a grid of M × N points separated by a distance increment d. Then we can write the co-ordinate distances as x = m d and y = n d, where m= 1, 2, 3, ...,M and n = 1, 2, 3, ...,N. Thus any point on the grid is uniquely identified by the indices (M, N). A portion of such grid space is shown in Fig. 6.1.

The derivative of any function A(x, y) by the use of finite differences comes from the Taylor's expansion of the variables.

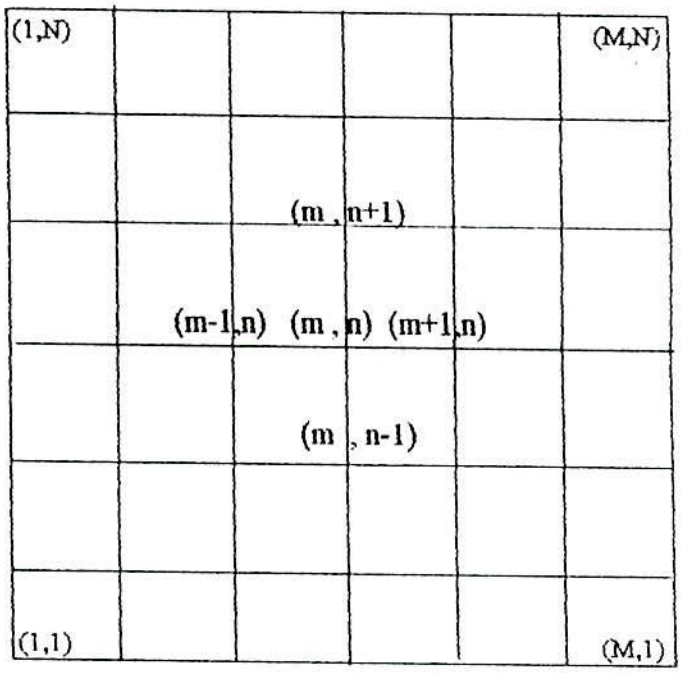

Fig. 6.1 Identification of mesh points on a finite difference grid of M × N points.

Using centred difference formulae (Holton, 1979), derivative of any function A(x, y) at the point (M,N) may be expressed in terms of the values of A at surrounding points:

$$\left(\frac{\partial A}{\partial x}\right)_{m,n} \approx \frac{A_{m+1,n} - A_{m-1,n}}{2d} \qquad (6.10)$$

Similarly

$$\left(\frac{\partial A}{\partial y}\right)_{m,n} \approx \frac{A_{m,n+1} - A_{m,n-1}}{2d} \qquad (6.11)$$

In a similar fashion second derivatives at any point can be evaluated by adding the equations (6.10) and (6.11) and are given by:

$$\left(\frac{\partial^2 A}{\partial x^2}\right)_{m,n} \approx \frac{A_{m+1,n} - 2A_{m,n} + A_{m-1,n}}{d^2}$$

and

$$\left(\frac{\partial^2 A}{\partial y^2}\right)_{m,n} \approx \frac{A_{m,n+1} - 2A_{m,n} + A_{m,n-1}}{d^2} \qquad (6.12)$$

Thus, we may write the horizontal Laplacian in terms of finite difference approximations:

$$\nabla^2 A \approx \frac{A_{m+1,n} + A_{m-1,n} + A_{m,n+1} + A_{m,n-1} - 4A_{m,n}}{d^2} \qquad (6.13)$$

The finite difference form of the Laplacian is simply proportional to the difference between the value of A at the central point and the average value at the four surrounding points.

6.4 Leapfrog Scheme

The advection equation is:

$$\frac{\partial F}{\partial t} + c\frac{\partial F}{\partial x} = 0 \qquad (6.14)$$

where, $c > 0$.

The finite difference method is applied for solving this partial differential equation. Let $x = m\ \Delta x$, m = 0, ± 1, ± 2, ± 3 ------- etc. and $t = n\Delta t$, n=0, 1, 2,----etc. which replaces the continuous (x, t) space by a mesh or grid of discrete points. The use of second - order finite difference approximation for the derivatives in equation gives

$$\frac{F_{m,n+1} - F_{m,n-1}}{2\Delta t} + c\frac{F_{m+1,n} - F_{m-1,n}}{2\Delta x} = 0$$

or

$$F_{m,n+1} = F_{m,n-1} - \frac{c\,\Delta t}{\Delta x}\left(F_{m+1,n} - F_{m-1,n}\right) \qquad (6.15)$$

which is referred to as a three-level scheme because three time levels are involved.

This equation represents a simple marching procedure, called the Leapfrog scheme, whereby the value of F at some point m Δx and time (n+1) Δt is derived from values at previous times n and n-1. Clearly (6.16) cannot be used to calculate $F_{m,1}$ (i.e. for the first time step), since the values are not known at n =-1 (i.e. prior to t=0).

6.5 Time Integration: Linear Computational Stability

To forecast the future circulation we extrapolate ahead in time using a finite difference approximation. Choosing a centred differencing scheme, we may write

$$\psi(t_0 + \delta t) = \psi(t_0 - \delta t) + 2\delta t \chi(t_0) \qquad (6.16)$$

This scheme requires knowledge of ψ at two time levels, $\psi(t_0 - \delta t)$ and $\psi(t_0)$ in order to compute $\psi(t_0 + \delta t)$. Since at the first time step of the forecast t_o=0 only $\psi(t_0)$ is known. We use a forward time step for the first step.

$$\psi(\delta t) = \psi(0) + \delta t\ \chi(0) \qquad (6.17)$$

After the calculation of the first time step, we have two sets of data. By using these two sets of data the centred difference scheme has been used.

A number of time differencing schemes exist that have different stability characteristics. The well-known CFL (Courant-Frederich-Levy) condition (Haltiner, 1979) must be satisfied for the stability of a time differencing scheme.

For a two dimensional grid with uniform grid spacing d, in the x and y directions it can be shown that δ t and d must satisfy:

$$\frac{c\delta t}{d} \leq \frac{1}{\sqrt{2}} \qquad (6.18)$$

where c is the propagation speed of the fastest moving disturbance generated by the model.

6.6 Smoothing and Filtering

In the finite difference integration schemes, explicit or implicit diffusion can be included in the difference equations to suppress the high wave numbers. In order to gain some insight about smoothing techniques, the one-dimensional three-point operator (Shapiro, 1970, 1975) has been considered:

$$\bar{f}_j = (1-S)f_j + \frac{S}{2}(f_{j+1} + f_{j-1}) \tag{6.19}$$

Now one-dimensional smoother can be extended in two dimensions. The simple smoothing technique can be applied sequentially to the two directions:

$$\bar{f}_{ij}{}^{ij} = \frac{1}{2}(\bar{f}_{ij}{}^{i} + \bar{f}_{ij}{}^{j})$$

The sequential application is a five-point operator. Expanding

$$\bar{f}_{ij}{}^{ij} = (1-S)f_{ij} + \frac{S}{4}(f_{i+1j} + f_{i-1j} + f_{ij+1} + f_{ij-1})$$

For special case with $S = \frac{1}{2}$, we have:

$$\bar{f}_{ij}{}^{ij} = \frac{f_{ij}}{2} + \frac{1}{8}(f_{i+1j} + f_{i-1j} + f_{ij+1} + f_{ij-1})$$

$$or, \quad \bar{f}_{ij}{}^{ij} = \frac{1}{8}(f_{i+1j} + f_{i-1j} + f_{ij+1} + f_{ij-1} + 4f_{ij}) \tag{6.20}$$

6.7 Teten's Formula

Vapour pressure (Krishnamurti, 1986) can be given by,

$$e_s = 6.11 e^{\frac{a(T-273.16)}{(T-b)}} \tag{6.21}$$

where the saturation over water, a = 17.26, b = 35.86 and for saturation over ice, a = 21.87, b = 7.66. The separation between the water and ice phase as 263° K. Now saturation specific humidity is:

$$q_s = 0.622 \frac{e_s}{P - 0.378\, e_s} \tag{6.22}$$

The unit of q_s is in gm/gm.

6.8 Bulk aerodynamic calculation over the Ocean and Land

The surface fluxes of sensible heat, water vapour and momentum can be expressed (Krishnamurti, 1986) by:

$$\left.\begin{aligned} F_H &= C_p \rho C_H |V_a|(T_w - T_a) \\ F_Q &= \rho L_q\, C_q |V_a|(q_w - q_a) \\ F_M &= \rho C_D |V_a| |V_a| \end{aligned}\right| \tag{6.23}$$

Here V_a and T_a denote the wind speed and the air temperature at the anemometer level, while T_w and q_w denote the water temperature and the saturation specific humidity. The accepted values of the non dimensional exchange coefficients (Krishnamurti, 1986) are:

$$C_H = 1.4 \times 10^{-3}$$
$$C_q = 1.6 \times 10^{-3} \qquad (6.24)$$
$$C_D = 1.1 \times 10^{-3}$$

The drag coefficient depend as a function of the wind speed (Krishnamurti, 1986) as given below:

$$\begin{aligned} C_D &= C_{DO} = 1.1\times10^{-3} && \text{for, } V<5.8 \text{ m/sec} \\ &= C_{DO}(0.74+0.046\,V) && \text{for, } 5.8 \le V \le 16.8 \text{ m/sec} \\ &= C_{DO}(0.94+0.034\,V) && \text{for, } V \ge 16.8 \text{ m/sec} \end{aligned} \qquad (6.25)$$

6.9 Mathematical Formulation

As with other atmospheric motions, tropical cyclones are described using Newton's second law, augmented by conservation laws of mass, thermodynamic energy and water vapour. The origin of the co-ordinates coincides with the axis of rotation. The governing equations for the motions of the atmosphere in cylindrical co-ordinates with pressure as a vertical co-ordinate are used in the following formulation. The independent variables are radial distance r, pressure p, and time t. The dependent variables are the three velocity components u, v and ω, potential temperature θ, moisture variable q and the geopotential height of the pressure surface z.

6.9.1 Momentum Equation

The horizontal momentum equation in vector form is:

$$\frac{d\vec{V}}{dt} = -f\vec{k}\times\vec{V} - \frac{1}{\rho}\nabla P + F_r + F_v \qquad (6.26)$$

where, F_r = frictional force and F_v = horizontal mixing term.

If we consider the pressure as a vertical co-ordinate then the total differential can be written as

$$\frac{d}{dt} = \frac{\partial}{\partial t} + \frac{dx}{dt}\frac{\partial}{\partial x} + \frac{dy}{dt}\frac{\partial}{\partial y} + \frac{dp}{dt}\frac{\partial}{\partial p}$$

$$= \frac{\partial}{\partial t} + u\frac{\partial}{\partial x} + v\frac{\partial}{\partial y} + \omega\frac{\partial}{\partial p}$$

$$i.e. \quad \frac{d}{dt} = \frac{\partial}{\partial t} + \vec{V}.\nabla + \omega\frac{\partial}{\partial p} \tag{6.27}$$

and when the hydrostatic approximation is valid, then

$$\frac{1}{\rho}\frac{\partial p}{\partial z} = -g$$

$$\Rightarrow \frac{1}{\rho}\frac{\partial \vec{\tau}}{\partial z} = -g\frac{\partial \vec{\tau}}{\partial p} \tag{6.28}$$

and

$$\left(\frac{\partial p}{\partial x}\right)_z = -\left(\frac{\partial p}{\partial z}\right)_x \left(\frac{\partial z}{\partial x}\right)_p$$

$$\Rightarrow -\left(\frac{\partial p}{\partial x}\right)_z = -\rho g\left(\frac{\partial z}{\partial x}\right)_p$$

$$\Rightarrow -\frac{1}{\rho}\left(\frac{\partial p}{\partial x}\right)_z = -g\left(\frac{\partial z}{\partial x}\right)_p = -\left(\frac{\partial \phi}{\partial x}\right)_p \tag{6.29}$$

Combining equation (6.26), (6.27), (6.28) and (6.29) we get

$$\frac{\partial \vec{V}}{\partial t} + (\vec{V}.\nabla)\vec{V} + \omega\frac{\partial \vec{V}}{\partial p} + f\,\hat{k} \times \vec{V} + \nabla\phi + g\frac{\partial \vec{\tau}}{\partial p} = \vec{F}_v \tag{6.30}$$

The vector identity can be written as:

$$(\vec{V}.\nabla)\vec{V} = \nabla\left(\frac{\vec{V}.\vec{V}}{2}\right) + \zeta\hat{k}\times\vec{V}$$

$$= \nabla\left(\frac{V^2}{2}\right) + \zeta\hat{k}\times\vec{V}$$

$$= \vec{\nabla}E + \zeta\hat{k}\times\vec{V} \qquad (6.31)$$

Putting the value of equation (6.31) in equation (6.30) we get the equation of motion in vector form as

$$\frac{\partial\vec{V}}{\partial t} + (\zeta + f)\hat{k}\times\vec{V} + \nabla E + \omega\frac{\partial\vec{V}}{\partial p} + \nabla\phi + g\frac{\partial\vec{\tau}}{\partial p} = \vec{F}_v$$

or

$$\frac{\partial\vec{V}}{\partial t} + (\zeta + f)\hat{k}\times\vec{V} + \nabla(\phi + E) + \omega\frac{\partial\vec{V}}{\partial p} + g\frac{\partial\vec{\tau}}{\partial p} = \alpha_d\nabla^2\vec{V} \qquad (6.32)$$

where the horizontal mixing term

$$F_v = \alpha_d\nabla^2 V$$

This is the momentum equation in vector form in the (x, y, p) co-ordinate system. In cylindrical co-ordinates x = r, y=0 and z = p,

$$\nabla^2\vec{V} = \left(\nabla^2 - \frac{1}{r^2}\right)\vec{V}$$

The component form of the momentum equation is

$$\vec{r}\left[\frac{\partial u}{\partial t}+\frac{\partial}{\partial r}(\phi+E)-(\zeta+f)v+\omega\frac{\partial u}{\partial p}+g\frac{\partial \tau_u}{\partial p}\right]+$$

$$\vec{\theta}\left[\frac{\partial v}{\partial t}+(\zeta+f)u+\omega\frac{\partial v}{\partial p}+g\frac{\partial \tau_v}{\partial p}\right]$$

$$=\vec{r}\,\alpha_d\left(\nabla^2-\frac{1}{r^2}\right)u+\vec{\theta}\alpha_d\left(\nabla^2-\frac{1}{r^2}\right)v$$

The momentum equation in cylindrical co-ordinates can be written in the form:

$$\frac{\partial u}{\partial t}-(\zeta+f)v+\frac{\partial}{\partial r}(\phi+E)+\omega\frac{\partial u}{\partial p}+g\frac{\partial \tau_u}{\partial p}=\alpha_d\left(\nabla^2-\frac{1}{r^2}\right)u$$

$$\frac{\partial v}{\partial t}+(\zeta+f)u+\omega\frac{\partial u}{\partial p}+g\frac{\partial \tau_v}{\partial p}=\alpha_d\left(\nabla^2-\frac{1}{r^2}\right)v$$

For different vertical levels we can write these equations in the form

$$\frac{\partial u_k}{\partial t}-(\zeta_k+f)v_k+\frac{\partial}{\partial r}(\phi_k+E_k)+\left(\omega\frac{\partial u}{\partial p}\right)_k+g\left(\frac{\partial \tau_u}{\partial p}\right)_k$$

$$=\alpha_d\left(\nabla^2-\frac{1}{r^2}\right)u_k \quad (6.33)$$

$$\frac{\partial v_k}{\partial t}+(\zeta_k+f)u_k+\left(\omega\frac{\partial v}{\partial p}\right)_k+g\left(\frac{\partial \tau_v}{\partial p}\right)_k=\alpha_d\left(\nabla^2-\frac{1}{r^2}\right)v_k \quad (6.34)$$

where the suffix k indicates different vertical levels.

6.9.2 The Continuity Equation

The Lagrangian control volume may be written as:

$$\delta v=\delta x\,\delta y\,\delta z$$

The hydrostatic equation can be written in the form

$$\frac{1}{\rho}\frac{\delta p}{\delta z} = -g$$

Therefore,

$$\delta z = -\frac{1}{\rho g}\delta p$$

$$\delta v = -\frac{\delta x \delta y \delta p}{\rho g}$$

$$\Rightarrow \rho \delta v = -\frac{\delta x \delta y \delta p}{g}$$

The mass of the fluid element is:

$$\delta M = \rho \delta v = -\frac{\delta x \delta y \delta p}{g}$$

where $\delta p < 0$. Since the mass of the fluid element is conserved following the motion, we have:

$$\frac{1}{\delta M}\frac{d}{dt}\delta M = 0$$

$$\Rightarrow \frac{g}{\delta x \delta y \delta p}\frac{d}{dt}\left(\frac{\delta x \delta y \delta p}{g}\right) = 0$$

$$\frac{1}{\delta x \delta y \delta p}\frac{d}{dt}(\delta x \delta y \delta p) = 0$$

$$\frac{1}{\delta x \delta y \delta p}\left[\delta y \delta p \frac{d}{dt}(\delta x) + \delta x \delta p \frac{d}{dt}(\delta y) + \delta x \delta y \frac{d}{dt}(\delta p)\right] = 0$$

Taking the limit, we get the continuity equation in the isobaric system:

$$\frac{\partial u}{\partial x}+\frac{\partial v}{\partial y}+\frac{\partial \omega}{\partial p}=0 \qquad (6.35)$$

where, $\delta u=\frac{d}{dt}(\delta x), \delta v=\frac{d}{dt}(\delta y), \delta \omega=\frac{d}{dt}(\delta p)$. This can also be written as,

$$\left(\frac{\partial u}{\partial x}+\frac{\partial v}{\partial y}\right)_p+\frac{\partial \omega}{\partial p}=0$$

$$or, \qquad \nabla_p.\vec{V}+\frac{\partial \omega}{\partial p}=0 \qquad (6.36)$$

6.9.3 Hydrostatic Equation

We know

$$P=h\rho g \qquad (h=z)$$

Now

$$dP=-\rho g dz$$

dP is -ve since pressure decreases with height. Therefore,

$$dP=-\rho d(gz)=-\rho d\phi$$

$$\frac{d\phi}{dP}=-\frac{1}{\rho}=-\alpha=-\frac{RT}{P}$$

$$=-\left(\frac{R}{P}\right)\left(\frac{P}{P_0}\right)^K\theta \qquad (6.37)$$

where θ is the potential temperature and is defined as

$$\theta=T\left(\frac{P_0}{P}\right)^K \qquad (6.38)$$

6.9.4 Thermodynamic Energy Equation

The first law of thermodynamics can be written in the form:

$$Q = C_v \frac{dT}{dt} + P\frac{d\alpha}{dt} \tag{6.39}$$

Since $C_v = C_p - R$,

$$\begin{aligned} Q &= (C_p - R)\frac{dT}{dt} + P\frac{d\alpha}{dt} \\ &= C_p \frac{dT}{dt} - R\frac{dT}{dt} + P\frac{d\alpha}{dt} \\ &= C_p \frac{dT}{dt} - \alpha\frac{dP}{dt} \end{aligned}$$

or

$$\begin{aligned} \frac{Q}{C_p T} &= \frac{1}{T}\frac{dT}{dt} - \frac{1}{C_p}\frac{\alpha}{T}\frac{dP}{dt} \\ &= \frac{d}{dt}(\ln T) - \frac{R}{C_p}\frac{d}{dt}(\ln P) \\ &= \frac{d}{dt}(\ln T) - k\frac{d}{dt}(\ln P) \\ &= \frac{d}{dt}(\ln T) - \frac{d}{dt}(\ln P^k) \\ &= \frac{d}{dt}(\ln T) + \frac{d}{dt}\ln\left(\frac{P_0}{P}\right)^k \\ &= \frac{d}{dt}\left[\ln T\left(\frac{P_0}{P}\right)^k\right] \\ &= \frac{d}{dt}[\ln\theta] \end{aligned} \tag{6.40}$$

$$\frac{d}{dt}(\ln\theta) = \frac{Q}{C_p T}$$

$$\frac{1}{\theta}\frac{d\theta}{dt} = \frac{Q}{C_p T}$$

$$\frac{d\theta}{dt} = \theta\frac{Q}{C_p T}$$

We add the small scale turbulent mixing or friction F_θ in the energy equation. Therefore, the energy equation can be written in the form

$$\frac{d\theta}{dt} = \theta\frac{Q}{C_p T} + F_\theta \tag{6.41}$$

The term F_θ can be written as

$$F_\theta = \alpha_d \nabla^2\theta \tag{6.42}$$

Using equation (6.41) and (6.42), we get,

$$\frac{d\theta}{dt} = \theta\frac{Q}{C_p T} + \alpha_d \nabla^2\theta \tag{6.43}$$

In cylindrical co-ordinates, neglecting the variation of θ co-ordinate

$$\frac{d}{dt} = \frac{\partial}{\partial t} + u\frac{\partial}{\partial r} + \omega\frac{\partial}{\partial P} \tag{6.44}$$

Therefore equation (6.43) can be written as:

$$\frac{\partial\theta}{\partial t} + u\frac{\partial\theta}{\partial r} + \omega\frac{\partial\theta}{\partial P} = \theta\frac{Q}{C_p T} + \alpha_d \nabla^2\theta \tag{6.45}$$

The hydrostatic equation is

$$\frac{\partial \phi}{\partial P} = -\alpha = -\frac{RT}{P} = -\frac{R}{P}\left(\frac{P}{P_0}\right)^k \theta$$

Therefore,

$$\theta = -\left(\frac{P}{R}\right)\left(\frac{P_0}{P}\right)^k \frac{\partial \phi}{\partial P} \tag{6.46}$$

Now the equation (6.45) becomes

$$-\left(\frac{P}{R}\right)\left(\frac{P_0}{P}\right)^k\left[\frac{\partial}{\partial t}\left(\frac{\partial \phi}{\partial P}\right)+u\frac{\partial}{\partial r}\left(\frac{\partial \phi}{\partial P}\right)\right]+\omega\frac{\partial \theta}{\partial P}=\theta\frac{Q}{C_pT}$$
$$+\alpha_d\left(-\frac{P}{R}\right)\left(\frac{P_0}{P}\right)^k\nabla^2\left(\frac{\partial \phi}{\partial P}\right)$$

In case of isobaric co-ordinate pressure is constant but $\frac{\partial \phi}{\partial P}$ is not constant.

$$-\rho\theta\left[\frac{\partial}{\partial t}\left(\frac{\partial \phi}{\partial P}\right)+u\frac{\partial}{\partial r}\left(\frac{\partial \phi}{\partial P}\right)\right]+\omega\frac{\partial \theta}{\partial P}=\theta\frac{Q}{C_pT}-\alpha_d\rho\theta\nabla^2\left(\frac{\partial \phi}{\partial P}\right)$$

$$\left[\frac{\partial}{\partial t}\left(\frac{\partial \phi}{\partial P}\right)+u\frac{\partial}{\partial r}\left(\frac{\partial \phi}{\partial P}\right)\right]-\frac{1}{\rho}\left(\frac{1}{\theta}\frac{\partial \theta}{\partial P}\right)\omega=-\frac{Q}{C_p\rho T}+\alpha_d\nabla^2\left(\frac{\partial \phi}{\partial P}\right)$$

$$\Rightarrow\left[\frac{\partial}{\partial t}\left(\frac{\partial \phi}{\partial P}\right)+u\frac{\partial}{\partial r}\left(\frac{\partial \phi}{\partial P}\right)\right]-\frac{1}{\rho}\left(\frac{\partial \ln\theta}{\partial P}\right)\omega=-\frac{Q}{C_p\left(\frac{P}{R}\right)}+\alpha_d\nabla^2\left(\frac{\partial \phi}{\partial P}\right)$$

$$\Rightarrow\left[\frac{\partial}{\partial t}\left(\frac{\partial \phi}{\partial P}\right)+u\frac{\partial}{\partial r}\left(\frac{\partial \phi}{\partial P}\right)\right]+\sigma\omega=-\left(\frac{R}{C_p}\right)\left(\frac{Q}{P}\right)+\alpha_d\nabla^2\left(\frac{\partial \phi}{\partial P}\right) \tag{6.47}$$

where $\sigma = -\frac{1}{\rho}\frac{\partial \ln\theta}{\partial P}$ is the static stability parameter.

From equation (6.47), we have:

$$\frac{\partial}{\partial t}\left(\frac{\partial \phi}{\partial P}\right) = -u\frac{\partial}{\partial r}\left(\frac{\partial \phi}{\partial P}\right) - \sigma\omega - \left(\frac{R}{C_p}\right)\left(\frac{Q}{P}\right) + \alpha_d \nabla^2\left(\frac{\partial \phi}{\partial P}\right) \quad (6.48)$$

Since ϕ increases as the pressure P decreases. So if ϕ is +ve, the pressure P is -ve.

Now the thermodynamic energy equation can be written in the form:

$$\frac{\partial}{\partial t}\left[\frac{\phi_k - \phi_{k+1}}{-\Delta P_k}\right] = -u_k \frac{\partial}{\partial r}\left[\frac{\phi_k - \phi_{k+1}}{-\Delta P_k}\right] - \sigma_k \omega_k$$

$$-\frac{R}{C_p}\frac{Q_k}{P_k} + \alpha_d \nabla^2\left[\frac{\phi_k - \phi_{k+1}}{-\Delta P_k}\right]$$

$$\Rightarrow \frac{\partial}{\partial t}(\phi_k - \phi_{k+1}) = -u_k \frac{\partial}{\partial r}(\phi_k - \phi_{k+1}) + \sigma_k \omega_k \Delta P_k$$

$$+\frac{R}{C_p}\frac{Q_k \Delta P_k}{P_k} + \alpha_d \nabla^2(\phi_k - \phi_{k+1}) \quad (6.49)$$

where the suffix k indicates vertical level.

6.9.5 Diabatic Heating

The diabatic heating is given by

$$Q = \frac{L}{P_B}\left[-\int_0^{P_B} \nabla.(\vec{V}\, q)dP - \omega_B q_B + E_1 + \frac{E_s}{L}\right] \quad (6.50)$$

where the first term on the right represents the large scale moisture convergence over the column above the boundary layer, the second term represents Ekman pumping effect which arises from the modification of the large scale flow in the Planetary boundary layer resulting from eddy momentum transfer, the last two terms represent the latent heat

and sensible heat available from the moisture flux from the surface and sensible heat arising due to the temperature difference between the surface and the boundary layer.

The surface contribution of moisture flux E_l due to turbulence and contribution of sensible heat E_s is parameterized as

$$E_l = \rho_s g C_q \left|\vec{V}_a\right| (q_w - q_B)$$

$$\text{and} \quad E_s = C_p \rho_s g C_H \left|\vec{V}_a\right| (T_w - T_B) \tag{6.51}$$

where,

q_B = Specific humidity at the boundary layer

q_w = Specific humidity over water or Sea surface

C_q = surface exchange coefficient of water vapour

C_p = specific heat at constant pressure

C_H = coefficient of sensible heat flux

6.9.6 Surface Pressure Tendency Equation

The continuity equation in pressure co-ordinate system (Haltiner, 1979) may be written in the form

$$\vec{\nabla}_p . \vec{V} + \frac{\partial \omega}{\partial p} = 0 \tag{6.52}$$

This equation may be integrated from $p = 0$, where $\omega = 0$, to an arbitrary level p to yield an equation for ω, that is,

$$\omega = -\int_0^p \vec{\nabla}_p . \vec{V} dp \tag{6.53}$$

At the surface the kinematic boundary condition assumes no normal flux, hence

$$\omega_s = \frac{dp_s}{dt} = \frac{\partial p_s}{\partial t} + \vec{V}_s . \vec{\nabla} p_s \tag{6.54}$$

Thus, if the integration is taken to $p_s(x,y,t)$ and equation for the surface pressure tendency is,

$$\frac{\partial p_s}{\partial t} + \vec{V}_s.\vec{\nabla} p_s = -\int_0^{p_s} \vec{\nabla}_p.\vec{V} dp \qquad (6.55)$$

6.9.7 The Moisture Equation

In many of the axially symmetric hurricane models no moisture variable has been used. A steady source of moisture in the boundary layer is assumed and its effect in the thermal equation is introduced via the heating terms. In our model we have used the explicit moisture variable equation (Elsberry, 1995).

$$\frac{\partial q}{\partial t} + u\frac{\partial q}{\partial r} + \omega\frac{\partial q}{\partial p} = E - C + \alpha_d\left(\nabla^2 - \frac{1}{r^2}\right)q \qquad (6.56)$$

where E is the evaporation and C is the condensation. The condensation is possible only when the specific humidity is greater than that of its saturation value, i.e. $q - q_s > 0$

6.9.8 Frictional Force

The surface stress (Haltiner, 1979) is parallel to the surface wind V_s and proportional to "drag" coefficient C_D as follows.

$$\vec{\tau}_s = \rho_s C_D \left|\vec{V}_s\right| \vec{V}_s \qquad (6.57)$$

We have considered the friction at the surface and above the surface level. The frictional terms of the momentum equations are expressed as

$$g\left(\frac{\Delta \tau}{\Delta p}\right)_k = g\frac{\tau_k - \tau_{k-1}}{P_k - P_{k-1}} \qquad (6.58)$$

where P_k-P_{k-1} is the pressure difference between the levels, In our model above 850 hPa level the frictional force term is zero. Above the surface layers we use the density term as $\rho = -\frac{\partial \phi}{\partial p}$, where $\partial \phi$ is the difference of geopotential between two levels. The drag coefficient C_D is dependent on the wind speed.

$$\tau_k = \rho_k C_D \left({u_k}^2 + {v_k}^2 \right)^{\frac{1}{2}} \left(\vec{i}\ u_k + \vec{j}\ v_k \right)$$

The radial and tangential components of stress can be written as

$$\left(\tau_k \right)_u = \rho_k C_D \left({u_k}^2 + {v_k}^2 \right)^{\frac{1}{2}} u_k \qquad (6.59)$$

$$\left(\tau_k \right)_v = \rho_k C_D \left({u_k}^2 + {v_k}^2 \right)^{\frac{1}{2}} v_k \qquad (6.60)$$

6.9.9 Static Stability

The static stability parameter σ can be written in the form

$$\sigma = -\frac{1}{\rho}\frac{\partial \ln \theta}{\partial p} = -\frac{1}{\rho \theta}\frac{\partial \theta}{\partial p}$$

The potential temperature is

$$\theta = T\left(\frac{P_0}{P}\right)^k$$

The static stability parameter in the finite difference form is

$$\sigma_{i,jk} = -\frac{1}{\rho}\frac{\theta_{i,jk+1} - \theta_{i,jk}}{\frac{1}{2}\left(\theta_{i,j,k+1} + \theta_{i,j,k}\right)\left(P_{k+1} - P_k\right)}$$

$$= -\frac{2}{\rho\left(P_{k+1} - P_k\right)}\left[\frac{\theta_{i,jk+1} - \theta_{i,jk}}{\theta_{i,jk+1} + \theta_{i,jk}}\right] \qquad (6.61)$$

6.10 Model Description

The model has been constructed in 5 layers with variable vertical resolution. The vertical structure of the model is shown in Fig. 6.2.

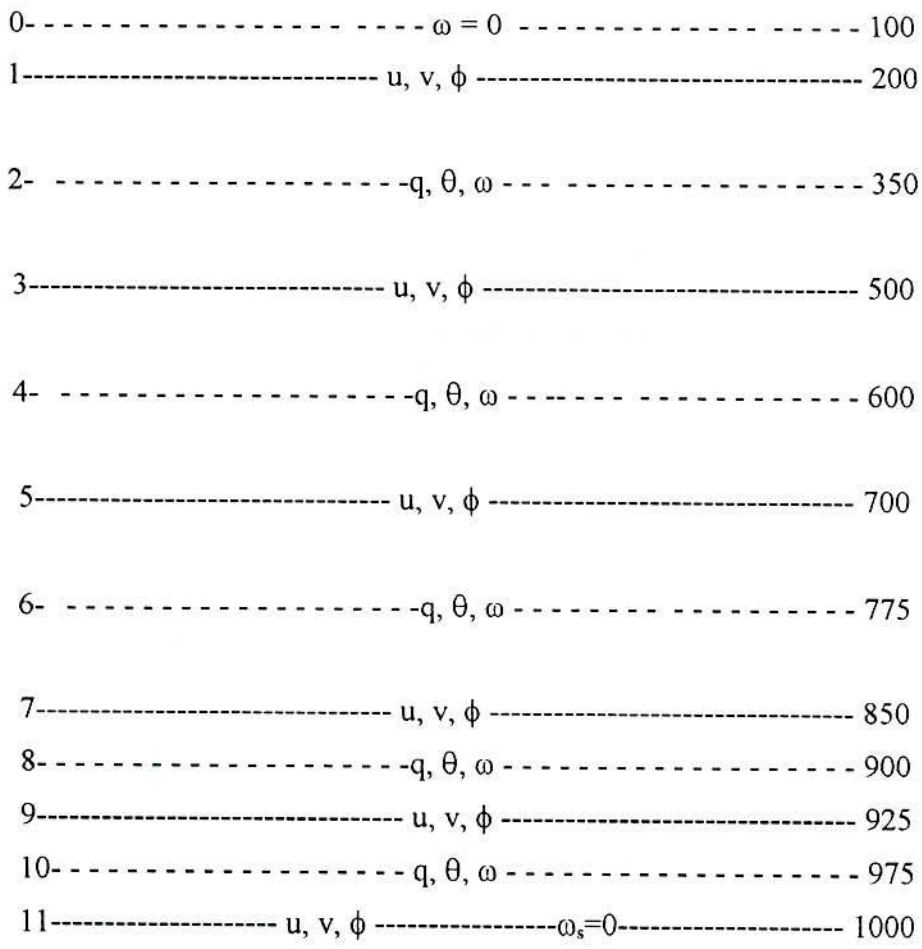

Fig. 6.2 Vertical structure of the five layer Model

The model is extended over a horizontal domain of 1200 km with horizontal grid size of 80 km. The time step of 60 seconds has been used for the integration of the model equations.

6.11 Numerical Model

The model uses the horizontal grid resolution of 80 km in latitude and longitude. The model domain is assumed to be entirely over the ocean to avoid complication with sea-land contrasts. There are five layers in the vertical. A variable Coriolis parameter is used. The parameterized physics included in the model are Kuo's cumulus scheme and boundary layer. The model uses bulk aerodynamic formulation to compute the momentum and the surface sensible and latent heat fluxes. To simulate a tropical cyclone, an initial idealised vortex embedded in a tropical environment with no wind is spun up to create a steady state tropical cyclone.

Centred time differences are used throughout the study with the exception of the first time step which is forward.

An integration was performed with the multilevel primitive equation model for the tropics described by Krishnamurti *et al* (1972). A description of the formulation of the model will not be reported here; instead, a comparison between the present model and that of Krishnamurti *et al* will be made.

The 5-level tropical cyclone prediction model initially proposed by Krishnamurti (1969) has undergone various improvements in recent years (Krishnamurti *et al* , 1972). The simultaneous integration of the primitive equations has been accomplished by using the quasi-Lagrangian advection scheme that has been improved by Mathur (1970). Besides the quasi-Lagrangian scheme used in the time integration of the equations, the following are the important features incorporated in the model:

1. terrain effects
2. horizontal and vertical diffusion
3. boundary layer exchanges of momentum, moisture and sensible heat
4. long wave radiation
5. dry convective adjustment
6. parameterization of cumulus convection

TABLE

Comparison between the two tropical cyclone predictions models.

(The present and Krishnamurti *et al.* 1972)

No.	Properties	Present Model	Krishnamurti *et al*
1.	Domain size (in grids)	16 ×16	15 ×33
2.	Grid distance	80 km	220 km
3.	Number of levels	5	5
4.	Vertical co-ordinate	Pressure	Pressure
5.	Predicted variables	Winds, Pressure, Geopotential, Vorticity, Static stability, Vertical velocity	Winds, Pressure, Temperature, Humidity, Precipitation
6.	Levels where winds are predicted	P = 200, 500 , 700, 850, 925 hPa , Surface	P= 200, 400, 600, 800, 1000 hPa
7.	Physical effects like friction, convection, etc	Included	Included
8.	Time integration	Leap frog	Quasi- Lagrangian
9.	Time step	60 seconds	5 Minutes

Periodic boundary conditions have been used on the eastern and the western boundaries.

The model presented in this study include the following features:

1. horizontal and vertical diffusion
2. boundary layer exchanges of momentum, moisture and sensible heat

3. parameterization of cumulus convection

Furthermore, the formulation of the lateral boundary conditions and time integration schemes are different in the two models. In summary, a table is presented to show the contrast between the two models.

6.12 Basic model assumptions

The Coriolis force is considered as a variable (starting from 10° N to 21° N).

1. Local time changes of air density are neglected in the continuity equation. This approximation has been shown to filter out acoustic waves (Ogura and Charney, 1962; Ogura and Philips, 1962).
2. As an approximation the θ derivatives of the fields is neglected.
3. Friction is considered at surface, 925 and 850 hPa level.
4. Diffusion of heat and moisture is included.
5. No periodic boundary conditions are imposed.
6. An interpolation method is used at the boundaries for unknown variables.

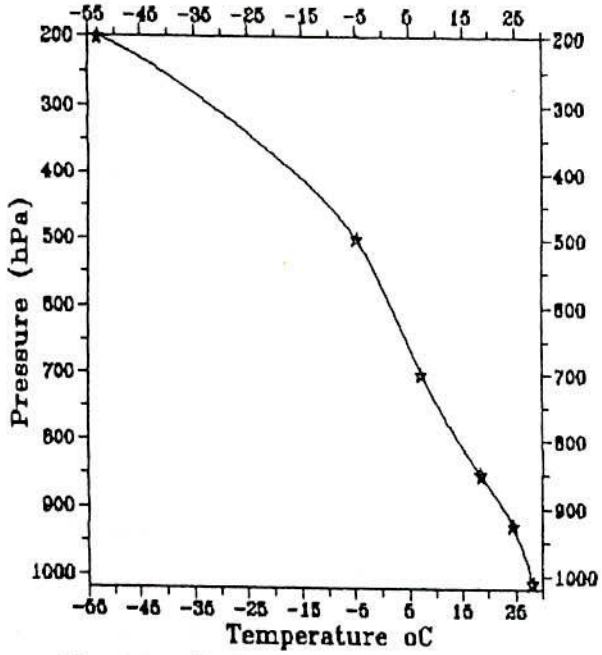

Fig. 6.3 Initialization of temperature

6.13 Model Initialization

The initial basic tangential wind and radial wind are assumed to be zero at all levels. The temperature decreases from 28 ° C at the sea surface to -54 ° C at the top (200 hPa) of the model simulation as shown in Fig. 6.3. The surface pressure is 1010 hPa, while the basic pressure and density at higher levels are assumed to be in hydrostatic equilibrium.

6.14 Boundary conditions

6.14.1 Lower boundary

The lower boundary is assumed rigid. The vertical velocity at the surface is assumed zero. The surface pressure P_s at the rest condition of the atmosphere is taken as 1010 hPa and the sea surface temperature has been taken 28°C during the model simulation. The density of air near the surface is considered as 1.2 kg/m^3, which is consistent with the initial surface temperature and pressure.

6.14.2 Upper boundary

Like the lower boundary, the upper boundary is assumed free-slip with no vertical motion.

6.14.3 Horizontal boundary

The horizontal structure of the model is shown in Fig. 6.4. The values of all parameters at the inner grid are calculated by using the centred difference approximations. The values at the outer boundary are calculated by using interpolation method.

6.14.4 Partitioning of Heating

The heat generated by the model due to the consideration of latent heat release from the atmosphere and sensible heat transfer from the surface to above the boundary layer. If this heat were used at different grid points from where the heat generated the cyclone would not generate. The heat generated by the model is integrated vertically at different grid points. The total amount of heat is collected at different grid points and then this heat is

would not generate. The heat generated by the model is integrated vertically at different grid points. The total amount of heat is collected at different grid points and then this heat is used at different level. Most of the heat is used between 500 hPa level to 200 hPa level. The intensity of the cyclone depends on which level how much heat is used. The partition of heating at pressure level is shown in Fig. 6.5.

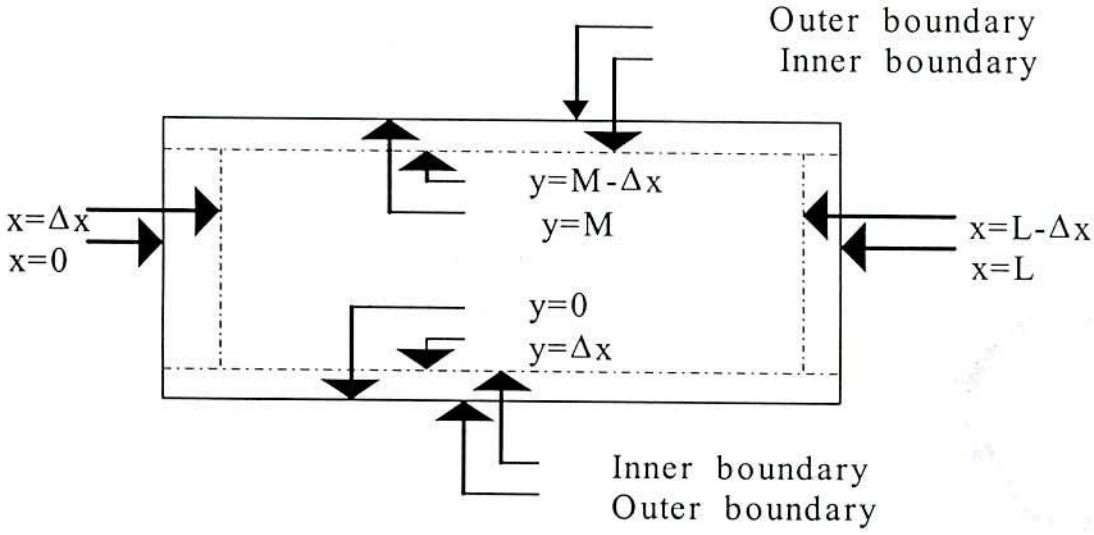

Fig. 6.4 The horizontal domain used in the model.

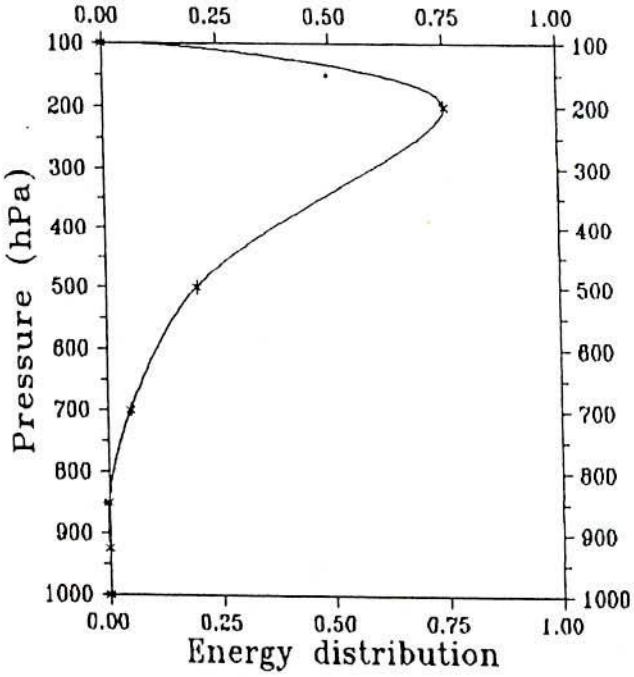

Fig. 6.5 The vertical distribution of heat used in the model

6.15 Results and Discussion

We have constructed three dimensional tropical cyclone prediction model in cylindrical co-ordinate. On the basis of the model different variables have been predicted at different time. The variables are radial wind, tangential wind, surface pressure, temperature tendency, geopotential tendency, diabatic heating, vorticity, static stability parameter, and horizontal structure of vertical velocity and vertical structure of vertical velocity around the cyclone centre. The model has been run up to 72 hours and has forecasted the above parameters for different time such as 36, 42, 48, 54 and 60 hours. After 60 hours, the changing pattern of the variables is almost identical. We have predicted all the variables at different pressure levels (prescribed in the model) but the diagrams have been presented for the surface and at 200 hPa level except with a bit variation.

The model has been run for 3 days with a time step of 60 seconds. At this stage of the run, the cumulus convective process becomes active and the resultant latent heat releases due to condensation helps the vortex to intensify. The results of the modelling experiment are discussed below.

6.15.1 Prediction of different parameters for cyclone formation

The Fig. 6.15.1(a) shows that the temporal evolution of the maximum tangential wind speed at the surface near the centre, the Fig. 6.15.1(b) shows the central surface pressure at the centre and Fig. 6.15.1(c) shows the maximum heating rate (Q_{max}) at 200 hPa. It is clearly seen from Figs. 6.15.1(a) and 6.15.1(b) that the storm intensifies slowly during the first day (developing stage), intensify rapidly during day 2 and then approximately constant at day 3 (mature stage). Thus the model produces a vortex with a minimum surface pressure and maximum tangential wind similar to the observed storms.

The intensification and the shrinking of the vortex take place for two days when the tangential wind reaches its peak value of 42 m/s near the cyclone centre and the central pressure drops by 30 hPa indicating a pressure drop of 15 hPa/day. After two days of

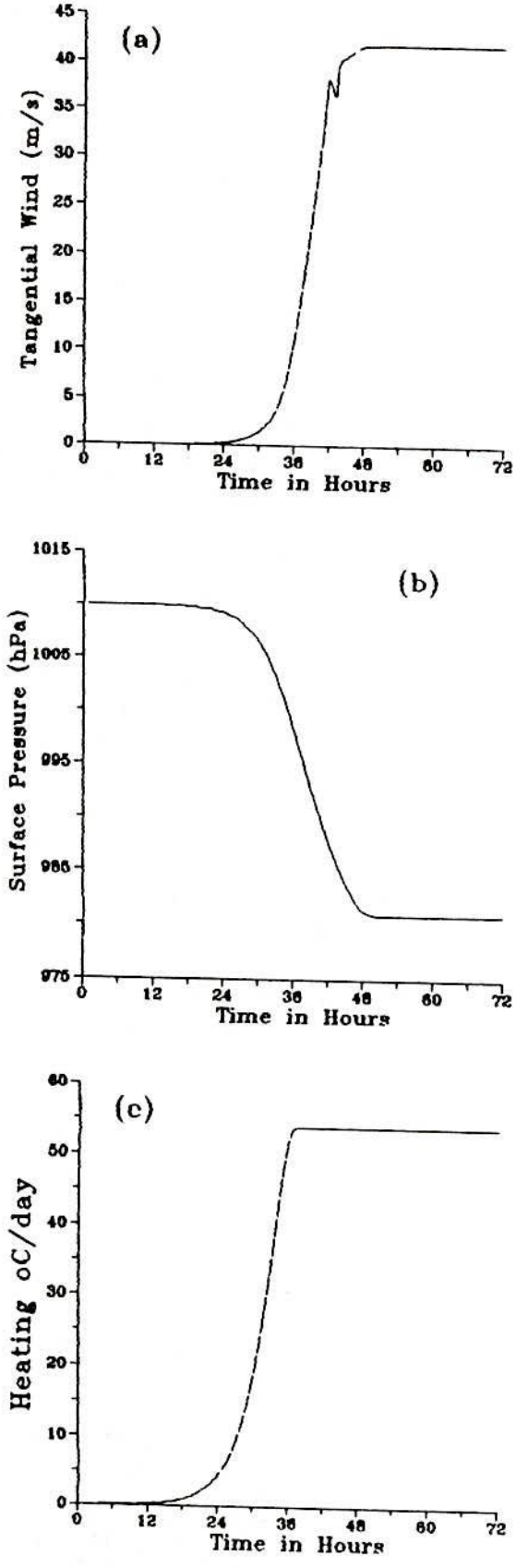

Fig. 6.15.1(a-c) Temporal evolution of (a) maximum tangential wind at the surface (b) central surface pressure (hPa) and (c) maximum diabatic heating (^{o}C/day).

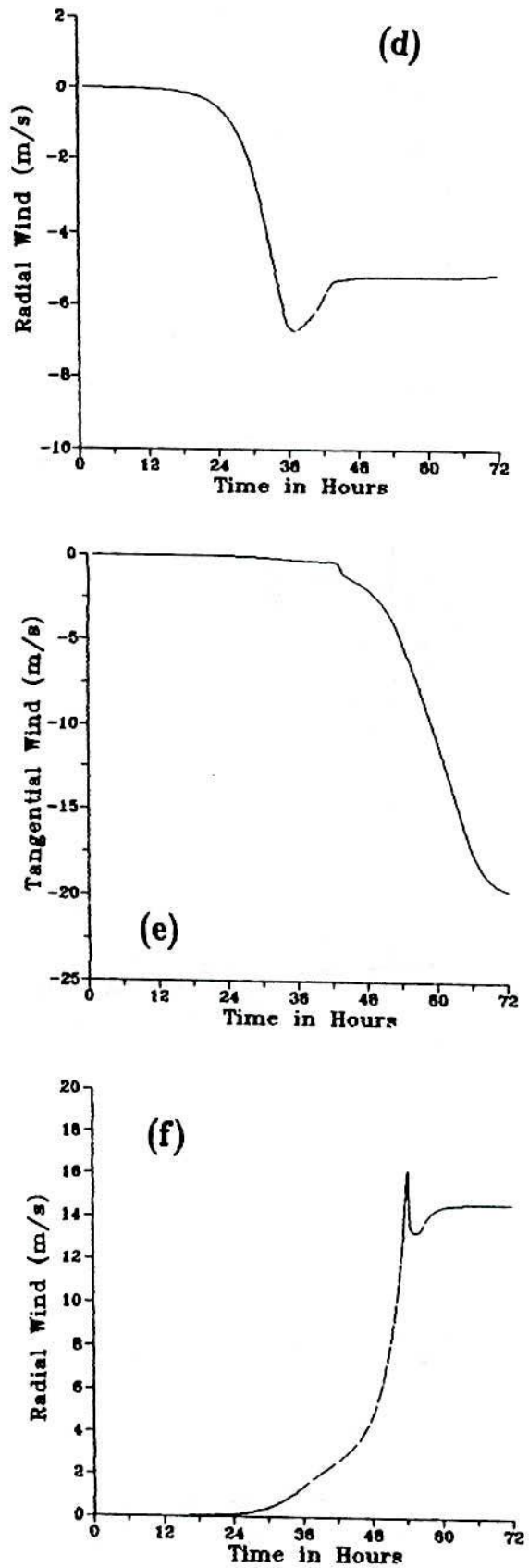

Fig. 6.15.1(d-f) Temporal evolution of (d) maximum radial wind at the surface (e) tangential wind at 200 hPa level and (f) radial wind at 200 hPa level.

intensification, the vortex attains maturity and thereafter it maintains a quasi-steady condition in all the above parameters.

The behaviour of the maximum heating (Fig. 6.15.1(c)) near the cyclone centre is similar to that of the maximum tangential wind at the surface.

Fig. 6.15.1.(d) shows that the temporal evolution of radial wind at the surface near the centre of the cyclone. From this figure it is observed that the inflow is not significant during first 24 hours, it increases significantly during 24 to 39 hours, it decreases from 39 to 48 hours and almost constant during 48 to 72 hours. The maximum evolution of radial wind at 39 hour is -7 m/s.

Fig. 6.15.1.(e) shows that the temporal evolution of tangential wind at 200 hPa near the centre of the cyclone. The wind is almost constant up to 42 hours and then it increases significantly during 48 to 72 hours. The maximum evolution of tangential wind at 200 hPa is -20 m/s at 72 hour.

In Fig. 6.15.1(f), it is observed that the evolution of radial wind at 200 hPa is almost zero up to 24 hours then it increases and reaches the maximum value of 16 m/s at 54 hours, again it decreases and shows the constant value from 60 to 72 hours.

6.15.2 Tangential Wind

The Figs. 6.15.2(a-e) show that the horizontal structure of the surface tangential wind for different time at 36, 42, 48, 60 and 72 hours respectively. The gradual intensification of the tangential wind is quite clear in these figures. The tangential wind is cyclonic at all radii in the surface and anticyclonic in layer 1. At 36 hour, 10 m/s tangential wind is observed near the centre of the cyclone. The tangential wind decreases gradually towards the surroundings. At 42 hour, 35 m/s tangential wind is observed near the centre of the cyclone. The pattern of tangential wind is irregular. After 42 hours, the tangential wind speed is smoothed in every time loop so that the pattern became regular. The tangential

wind reaches its maximum value at 48 hours and the pattern is almost constant up to 72 hours as shown in Figs. 6.15.2(c-e).

The tangential wind at 200 hPa in different time 36, 42, 48, 60 and 72 hours are anticyclonic as shown in Figs. 6.15.2(f-j) respectively. The maximum tangential wind is observed towards the north of the cyclone centre. The maximum tangential wind at 36, 42, 48, 60 and 72 hours are -0.45, -1.2, -2.3, -11.0 and -19.0 m/s respectively.

6.15.3 Radial Wind

The horizontal structure of radial wind at the surface as shown in Figs. 6.15.3(a-e). From these figures it is found that the wind flowing in the inward direction at the surface. At 36 hours maximum inflow is observed towards the south of the cyclone centre as shown in Fig. 6.15.3(a). The maximum value of radial wind is -7 m/s. At 42 hour -9.5 m/s maximum radial wind is observed towards the south of the cyclone centre. From Figs. 6.15.3(c-e) at 48, 60 and 72 hours, it is observed that the maximum inflow occurred towards the south of the cyclone centre and the pattern is almost constant throughout.

The horizontal structure of radial wind at 200 hPa are shown in Figs. 6.15.3(f-j) for 36, 42, 48, 60 and 72 hours respectively. At 36 hour, in Fig. 6.15.3(f) the maximum outflow at 200 hPa is 1.35 m/s. At 42 hour, in Fig. 6.15.3(g) the maximum outflow observed in this level is 2.7 m/s. The maximum outflow observed towards the north of the cyclone centre. Fig. 6.15.3(h) shows that the maximum 4.8 m/s radial wind is observed towards the north of the cyclone centre. The pattern of radial wind (Figs. 6.15.3(i-j)) is almost identical at 60 and 72 hour. A maximum outflow 14.5 m/s is observed during the time. From Figs. 6.15.3(a-j) it is found that the maximum inflow occurred towards the south of the cyclone centre at the surface and the maximum outflow occurred towards the north of the cyclone centre at 200 hPa . The outflow in the upper troposphere is caused due to the fact that the vertical motion associated with the convection cannot penetrate through the highly stable stratosphere and thus the air outflows along the horizontal.

6.15.4 Surface Pressure

Figs. 6.15.4(a-e) represent the evolution of horizontal structure of surface pressure at 24, 30, 36, 42 and 48 hours respectively. In Fig. 6.15.4(a) the central surface pressure dropped by 1 hPa at 24 hours. At 30 hours the central surface pressure dropped by about 3 hPa is shown in Fig. 6.15.4(b). In Fig. 6.15.4(c), at 36 hours, the central surface pressure dropped by about 11 hPa. The central surface pressure attains a minimum value of about 999 hPa at this time. At 42 hour, in Fig. 6.15.4(d), the central surface pressure attains a minimum value of about 988 hPa. In all these cases the pattern is symmetric. The central surface pressure reaches its minimum value 981 hPa at 48 hours in Fig. 6.15.4(e). From the horizontal distribution of surface pressure it is observed that the rapid intensification takes place during 30 to 48 hours. At 48 hour, the evolution of the central surface pressure reaches its minimum value and after that the central surface pressure remains constant up to 72 hours, up to which the model run.

6.15.5 Heating Generation

The horizontal structure of heating predicted at 24, 30, 36, 48, 60 and 72 hours are represents as in Figs. 6.15.5(a-f) respectively. In Fig. 6.15.5(a), at 24 hours, the heating generated at 3.5°C/day. The maximum heating generated at 30 hours is 18°C/day as shown in Fig. 6.15.5(b). At 24 and 30 hours the maximum heating is concentrated around 200 km from the centre. In Fig. 6.15.5(c), at 36 hours, the maximum evolution of heating is 52°C/day. The heating is concentrated within 100 km from the cyclone centre and after that it decreases significantly. In Figs. 6.15.5(d-f), at 48, 60 and 72 hours, the pattern of heating distribution is the same and the maximum heating (52 °C/day) remains constant during 48 - 72 hours.

6.15.6 Temperature Change

The horizontal structure of temperature change at 200 hPa level at 36, 42, 48, 54, and 60 hours are represents as in Figs. 6.15.6(a-e) respectively. The maximum temperature increase 3.5°C, at 36 hours, is shown in Fig. 6.15.6(a). The temperature increase 7.0°C, at 42hour, and 11°C, at 48 hour, are shown in Figs. 6.15.6 (b-c) respectively. The maximum

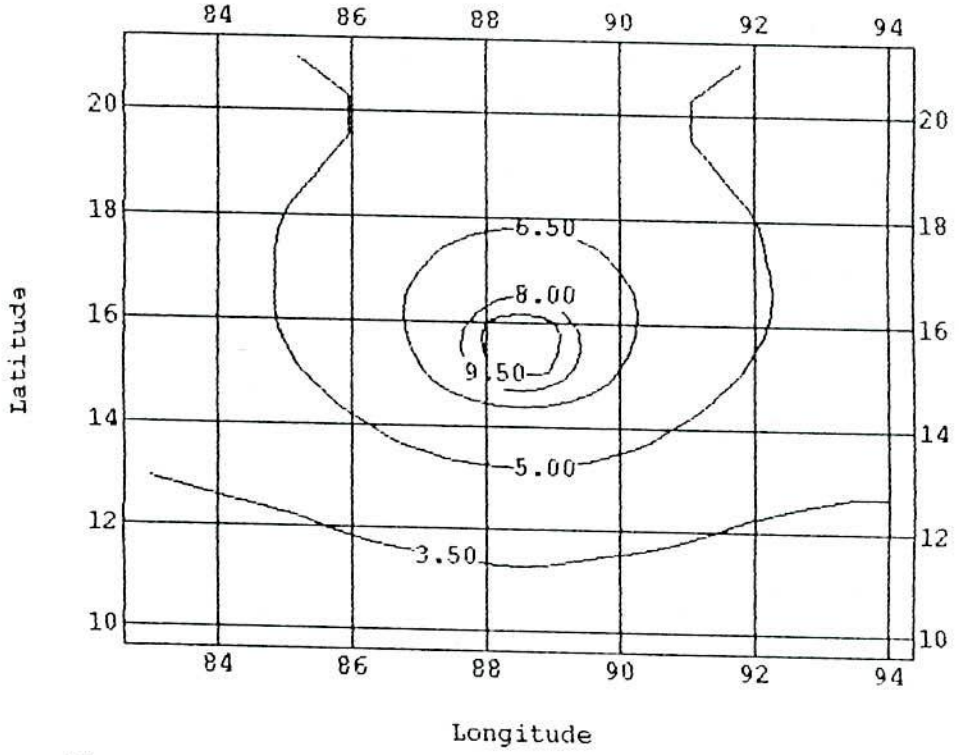

Fig. 6.15.2(a) 36-hr forecast of tangential wind (m/ sec) at the surface

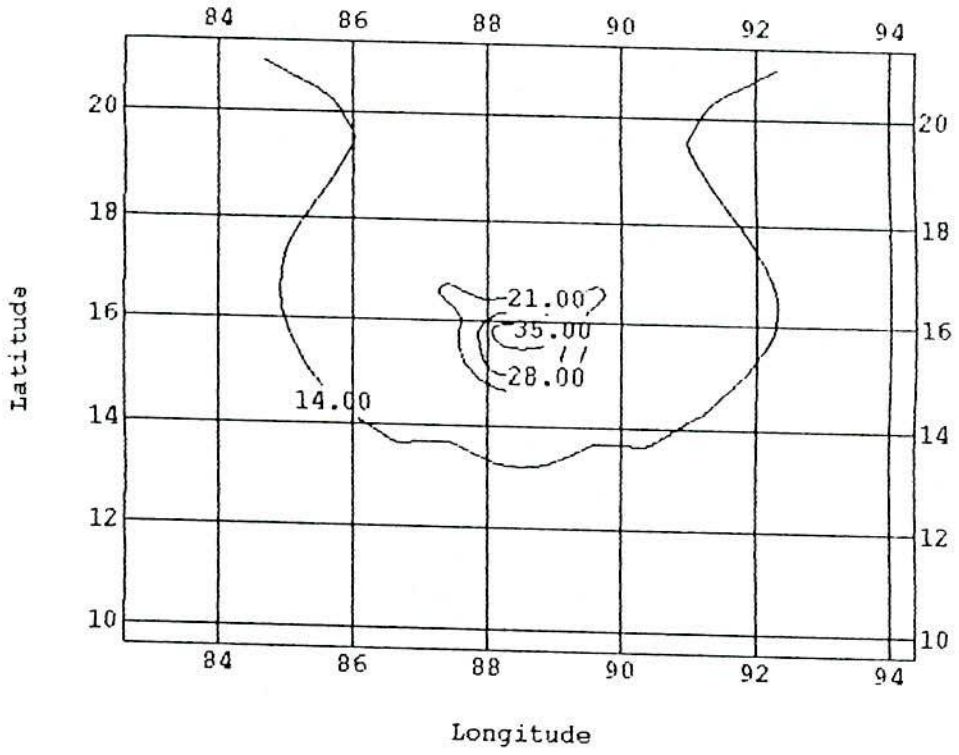

Fig. 6.15.2(b) 42-hr forecast of tangential wind (m/ sec) at the surface

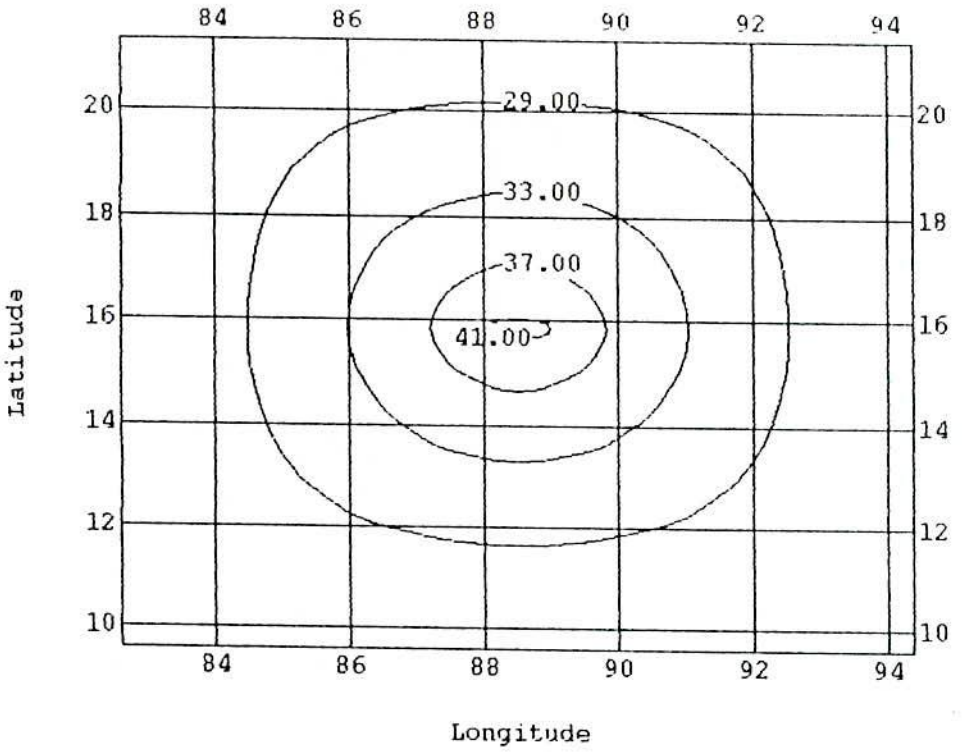

Fig. 6.15.2(c) 48-hr forecast of tangential wind (m /sec) at the surface

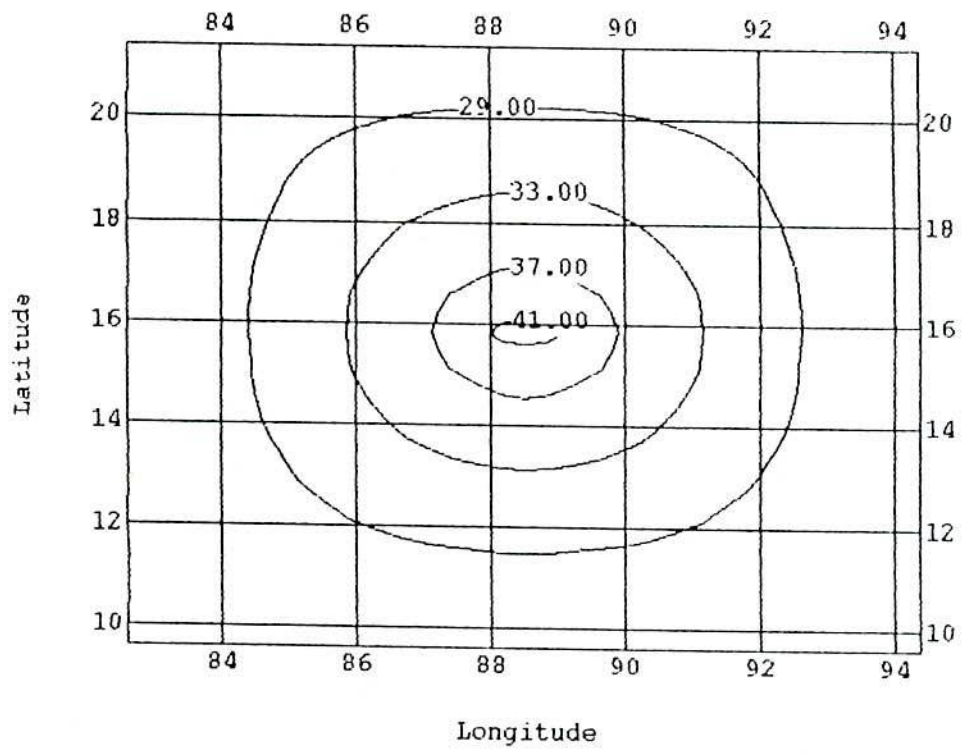

Fig. 6.15.2(d) 60-hr forecast of tangential wind (m /sec) at the surface

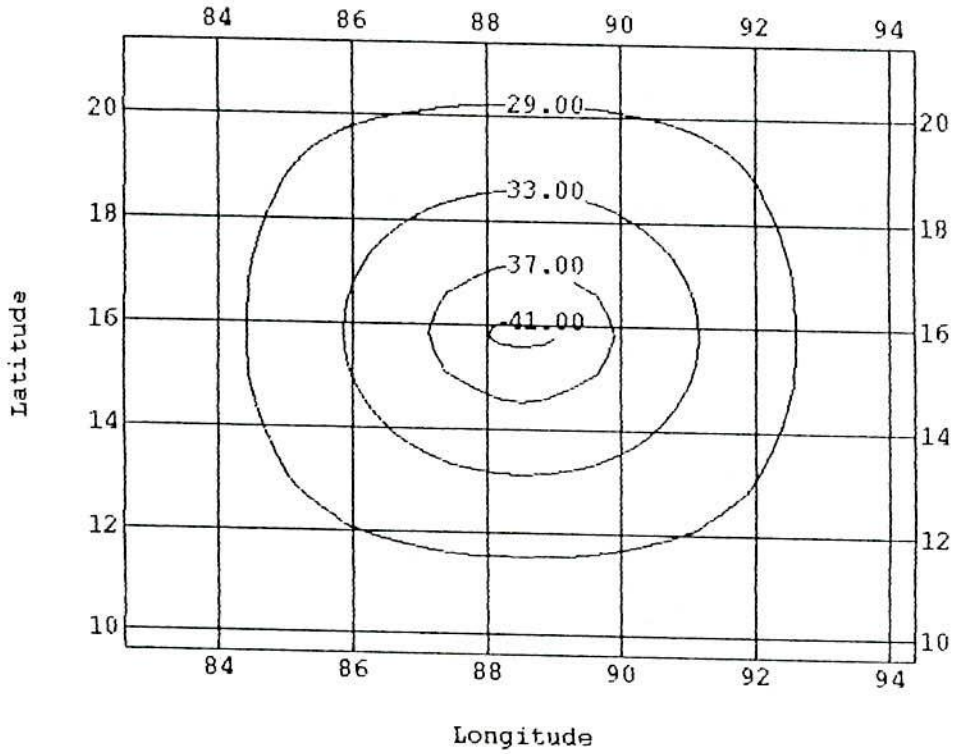

Fig. 6.15.2(e) 72-hr forecast of tangential wind (m/ sec) at the surface

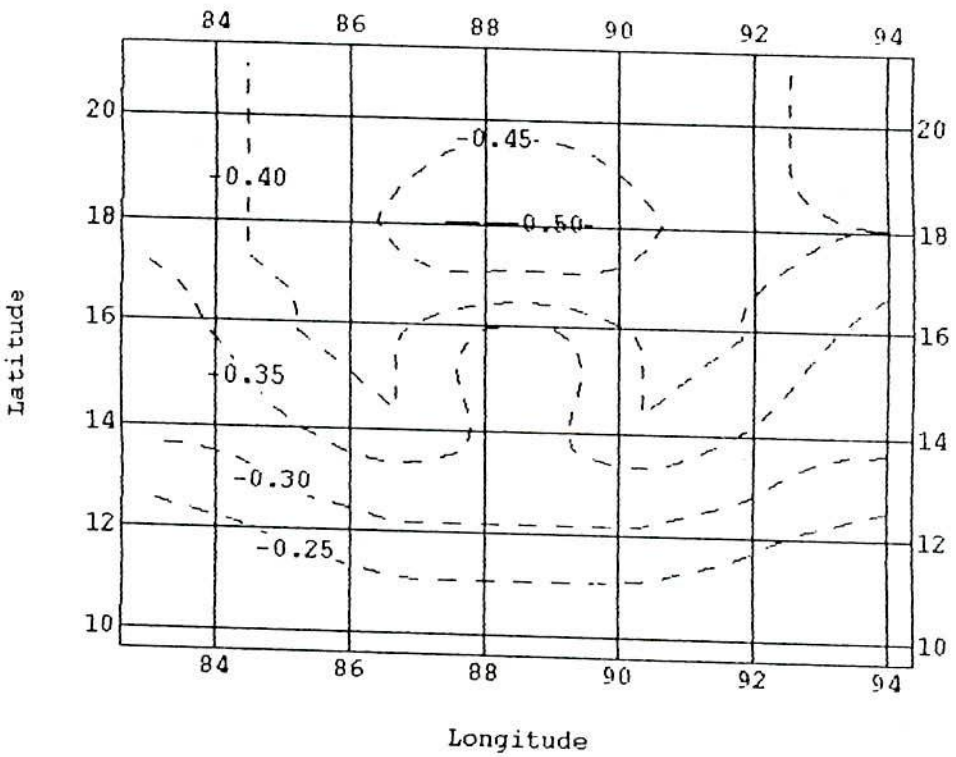

Fig. 6.15.2(f) 36-hr forecast of tangential wind (m /sec) at 200 hPa

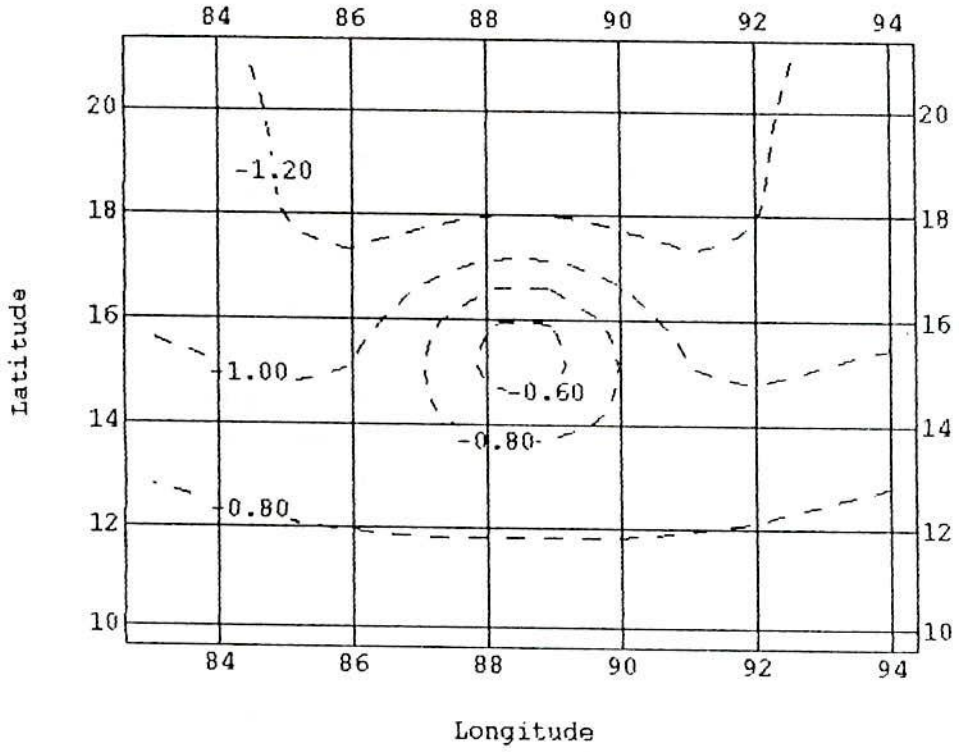

Fig. 6.15.2(g) 42-hr forecast of tangential wind (m /sec) at 200 hPa

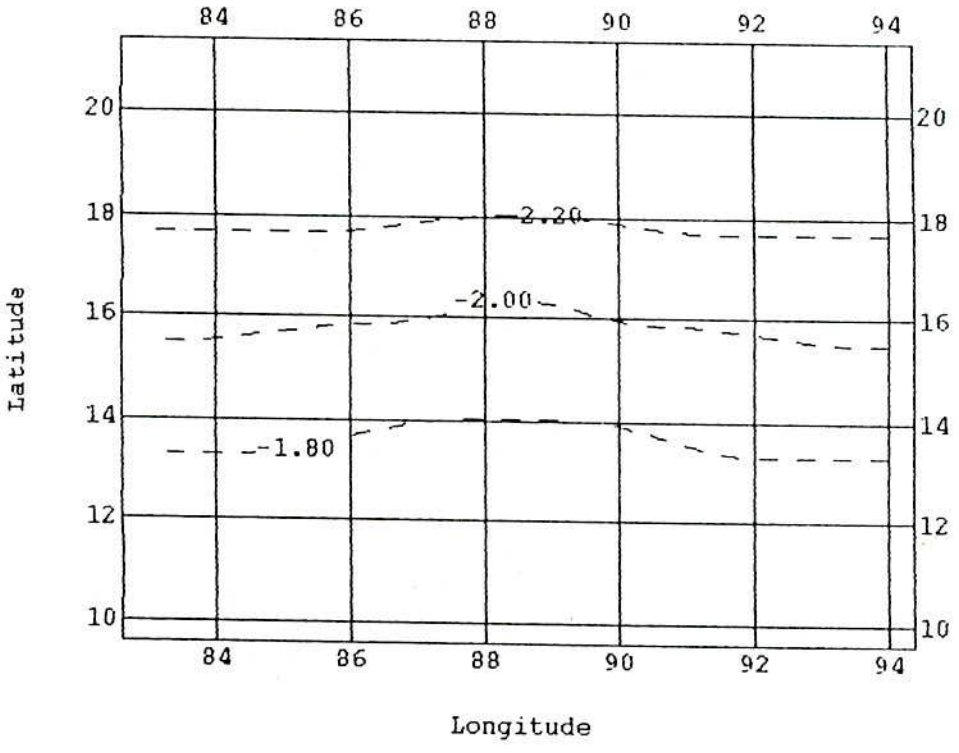

Fig. 6.15.2(h) 48-hr forecast of tangential wind (m/sec) at 200 hPa

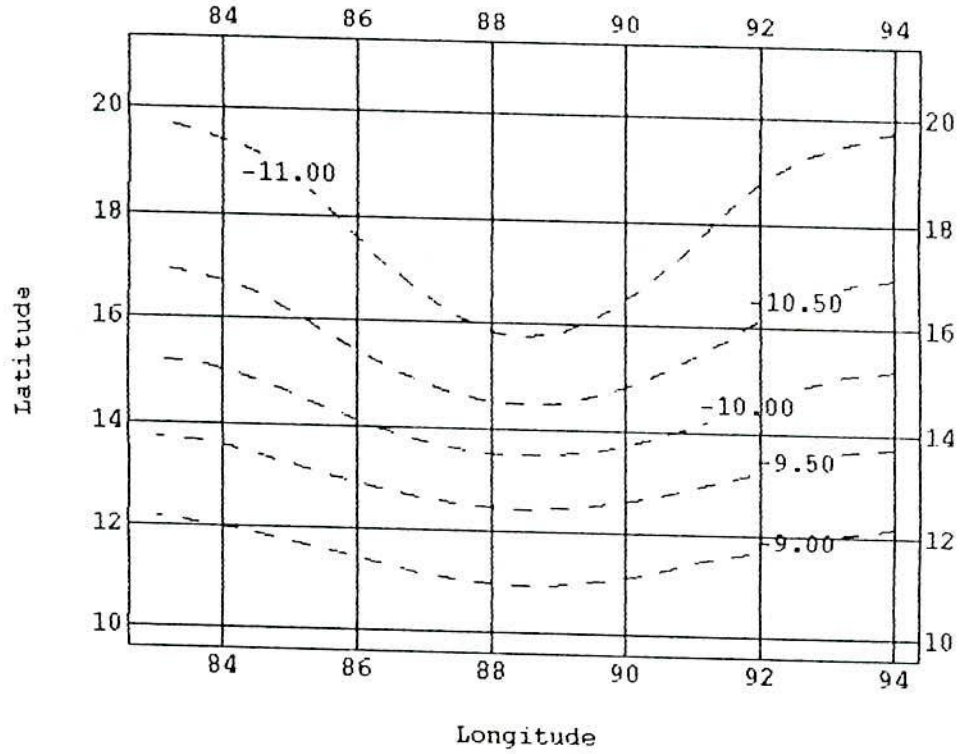

Fig. 6.15.2(i) 60-hr forecast of tangential wind (m/sec) at 200 hPa

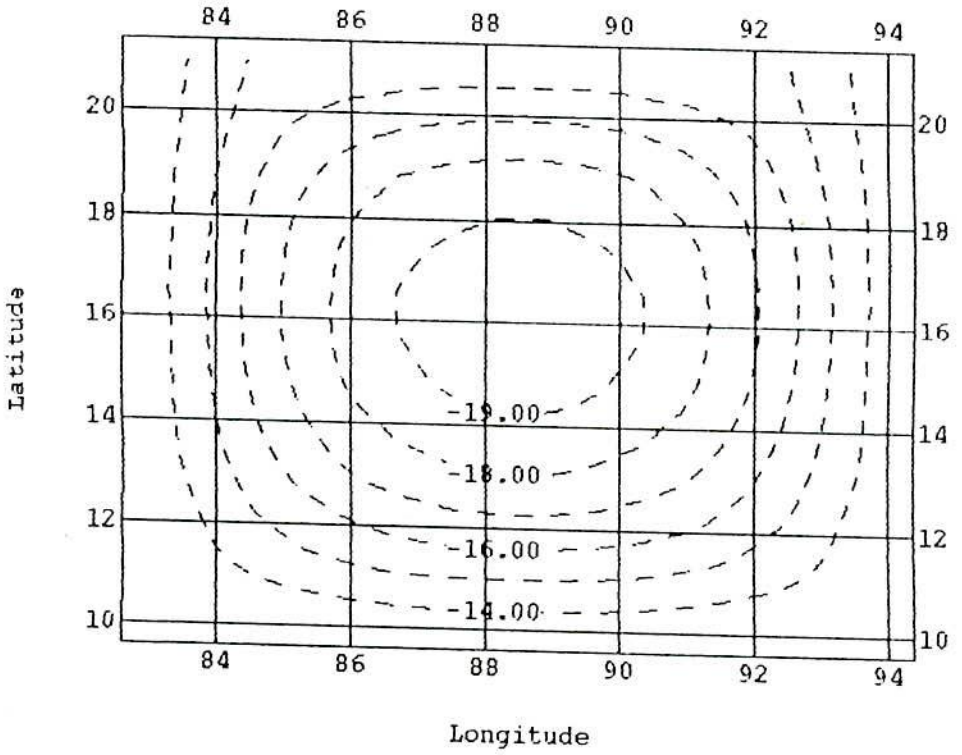

Fig. 6.15.2(j) 72-hr forecast of tangential wind (m/ sec) at 200 hPa

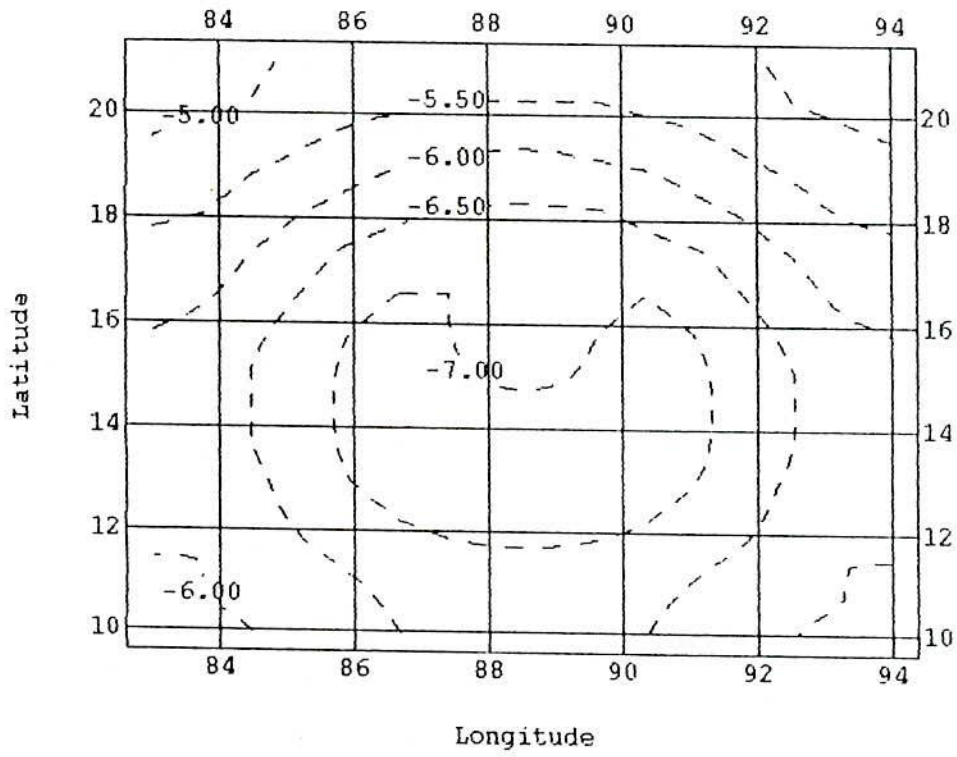

Fig. 6.15.3(a) 36-hr forecast of radial wind (m/sec) at the surface

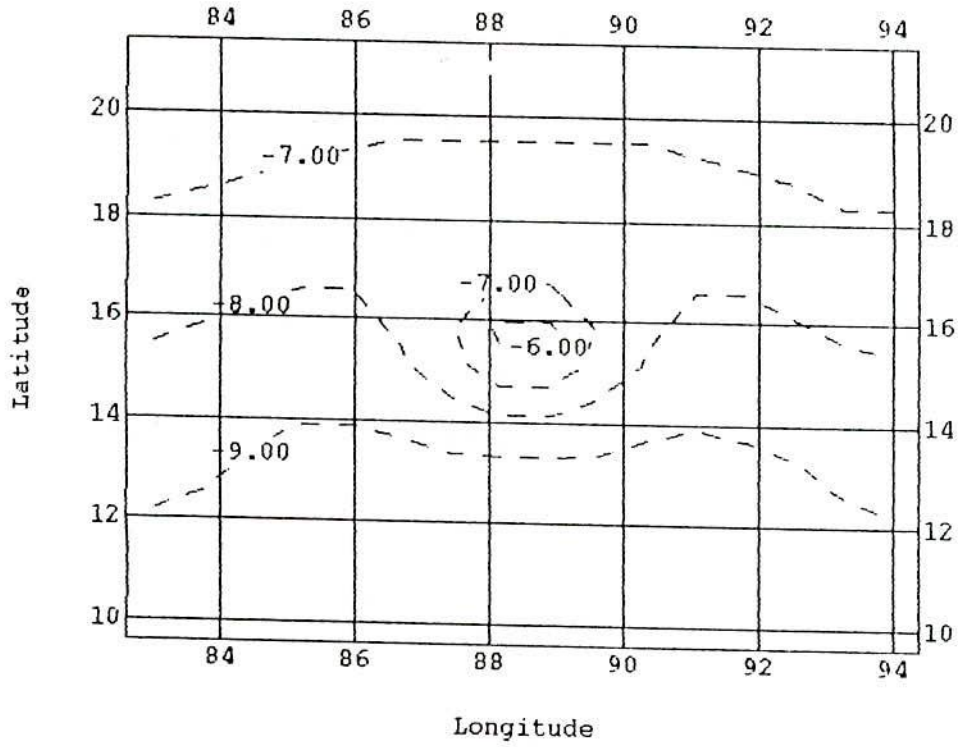

Fig. 6.15.3(b) 42-hr forecast of radial wind (m/sec) at the surface

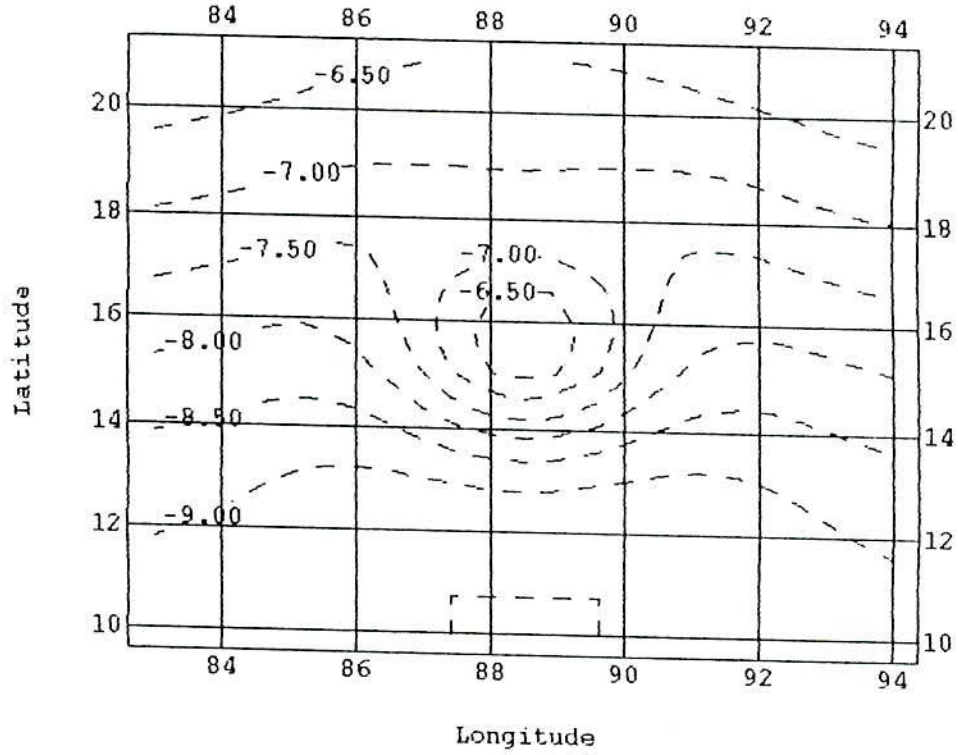

Fig. 6.15.3(c) 48-hr forecast of radial wind (m /sec) at the surface

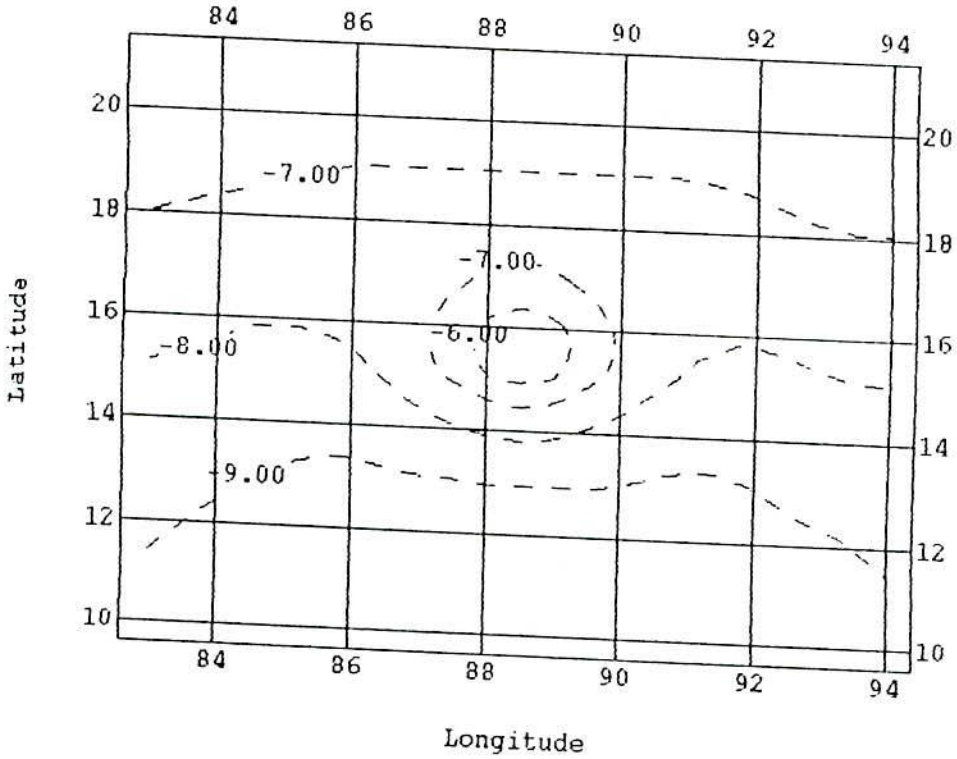

Fig. 6.15.3(d) 60-hr forecast of radial wind (m /sec) at the surface

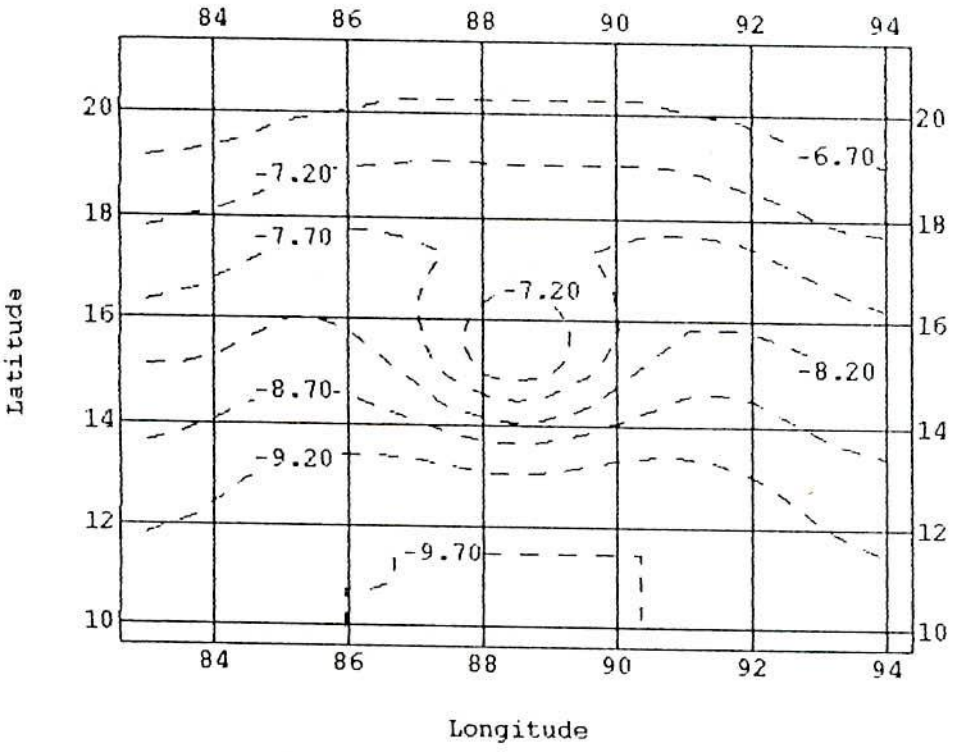

Fig. 6.15.3(e) 72-hr forecast of radial wind (m /sec) at the surface

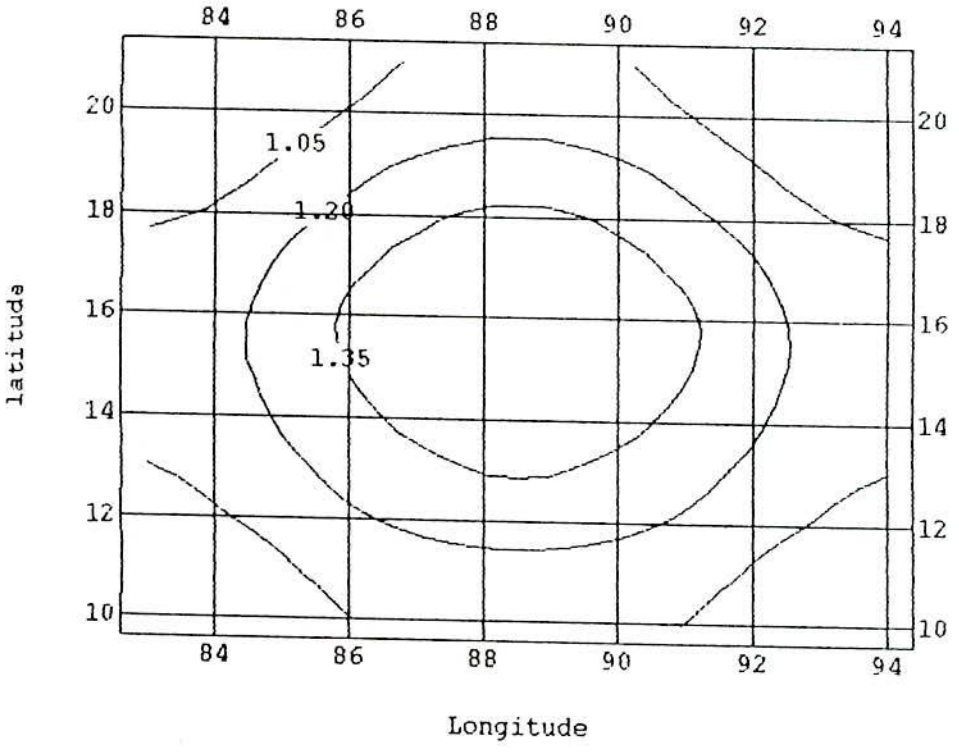

Fig. 6.15.3(f) 36-hr forecast of radial wind (m/ sec) at 200 hPa

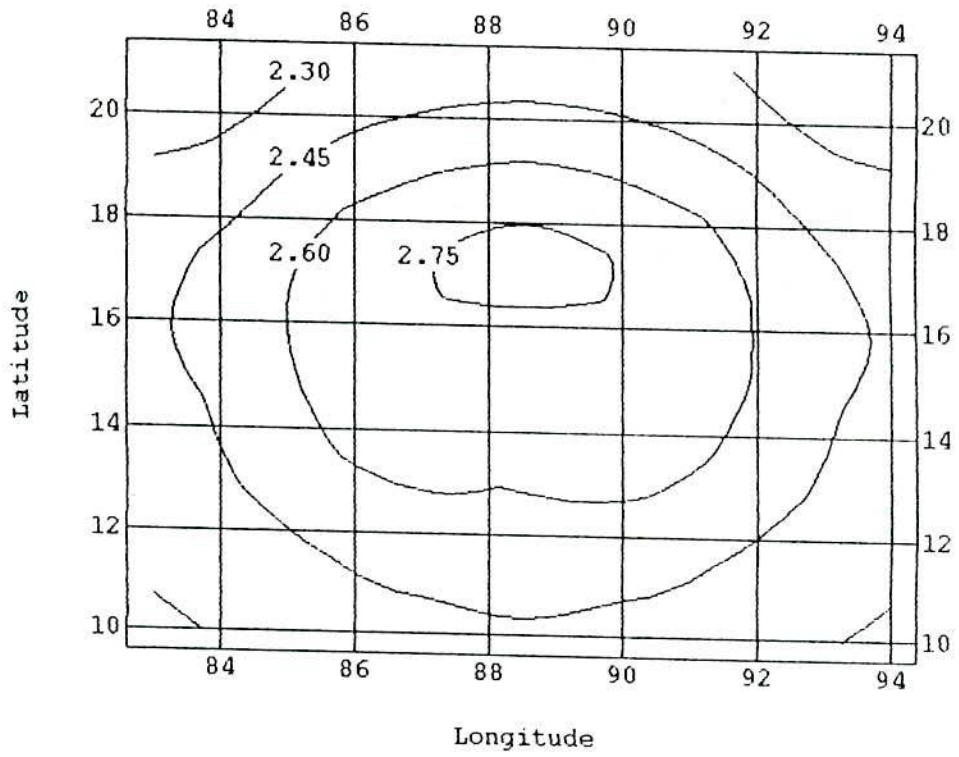

Fig. 6.15.3(g) 42-hr forecast of radial wind (m /sec) at 200 hPa

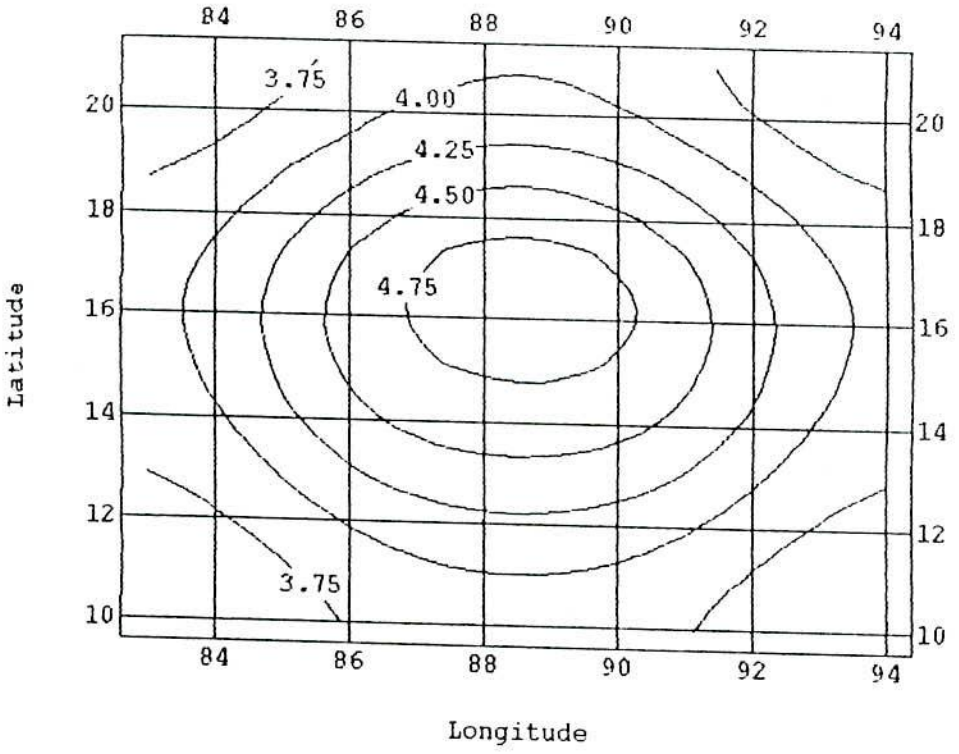

Fig. 6.15.3(h) 48-hr forecast of radial wind (m/ sec) at 200 hPa

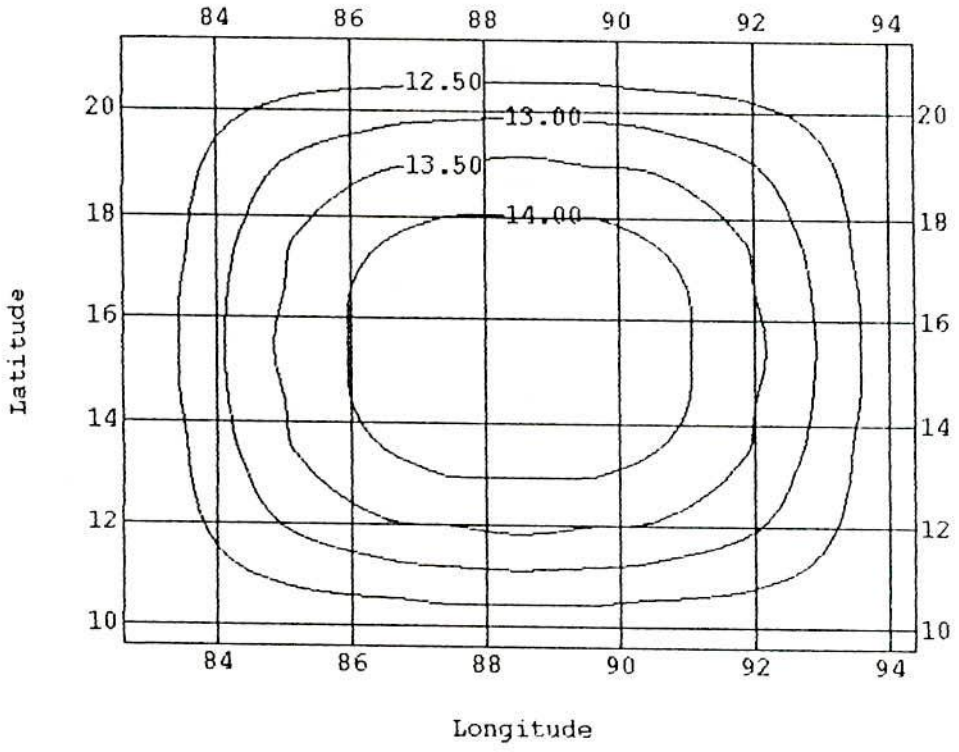

Fig. 6.15.3(i) 60-hr forecast of radial wind (m/ sec) at 200 hPa

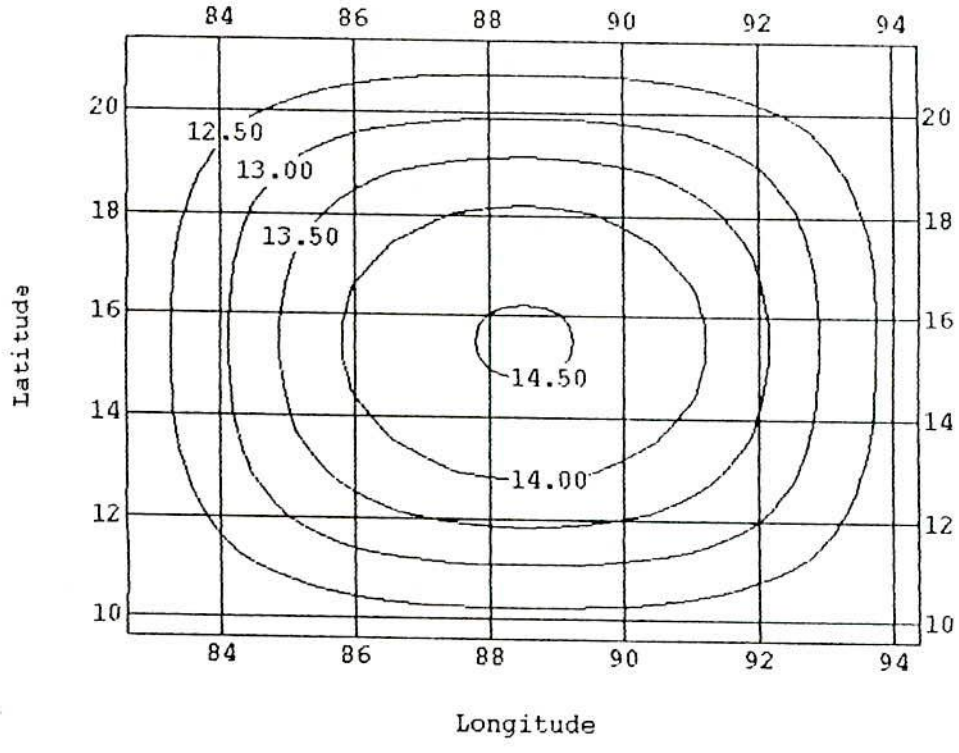

Fig. 6.15.3(j) 72-hr forecast of radial wind (m/ sec) at 200 hPa

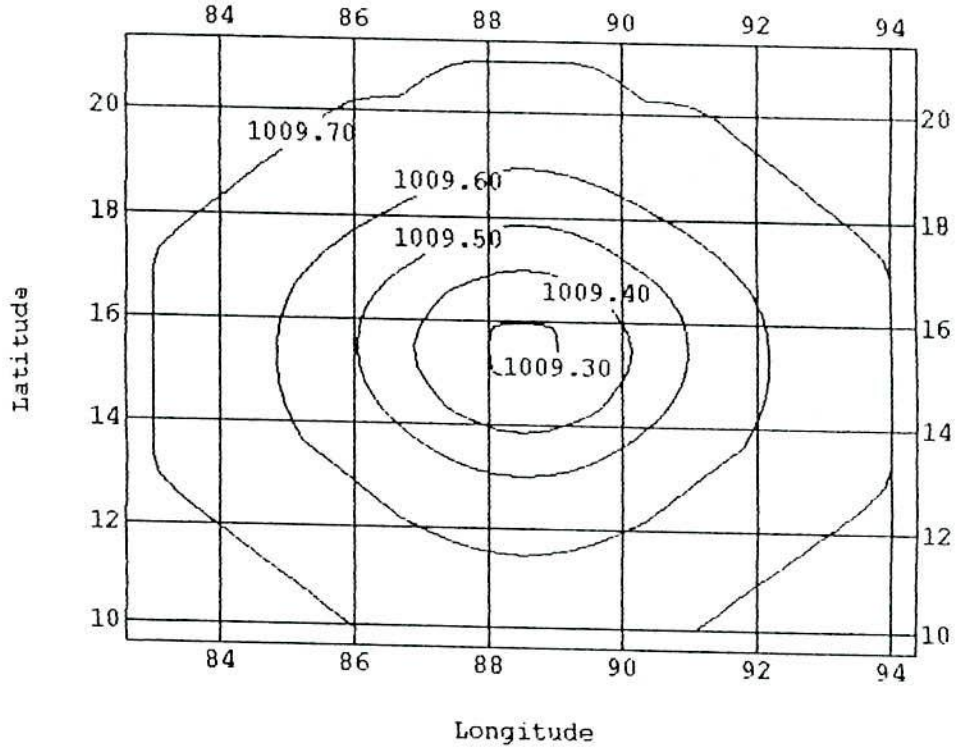

Fig. 6.15.4(a) 24-hr surface pressure (hPa) forecast

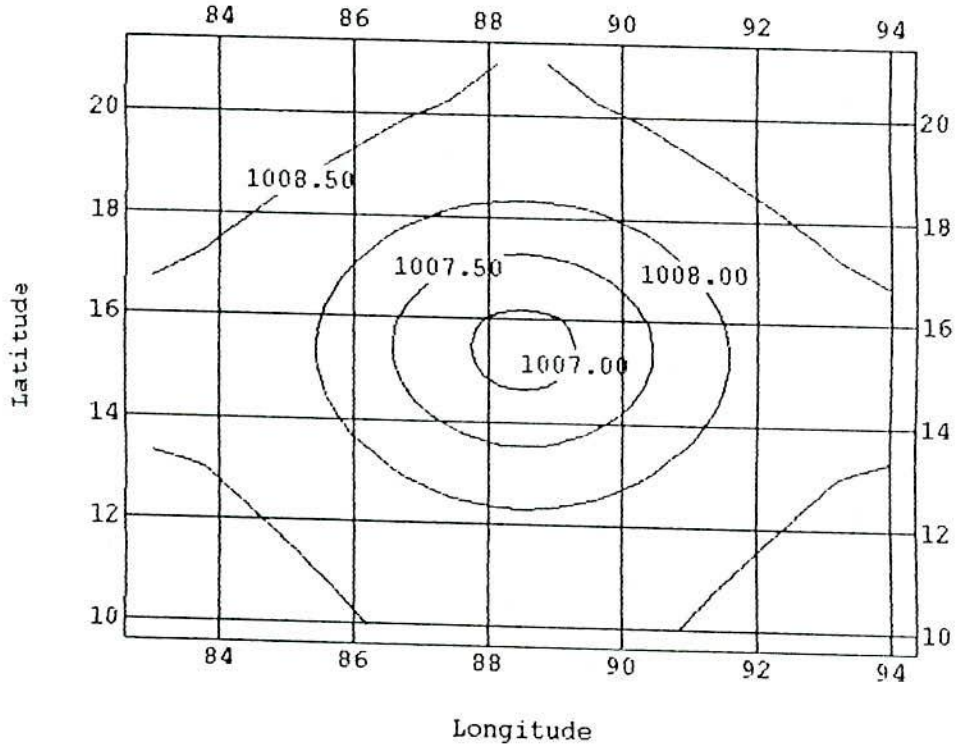

Fig. 6.15.4(b) 30-hr surface pressure (hPa) forecast

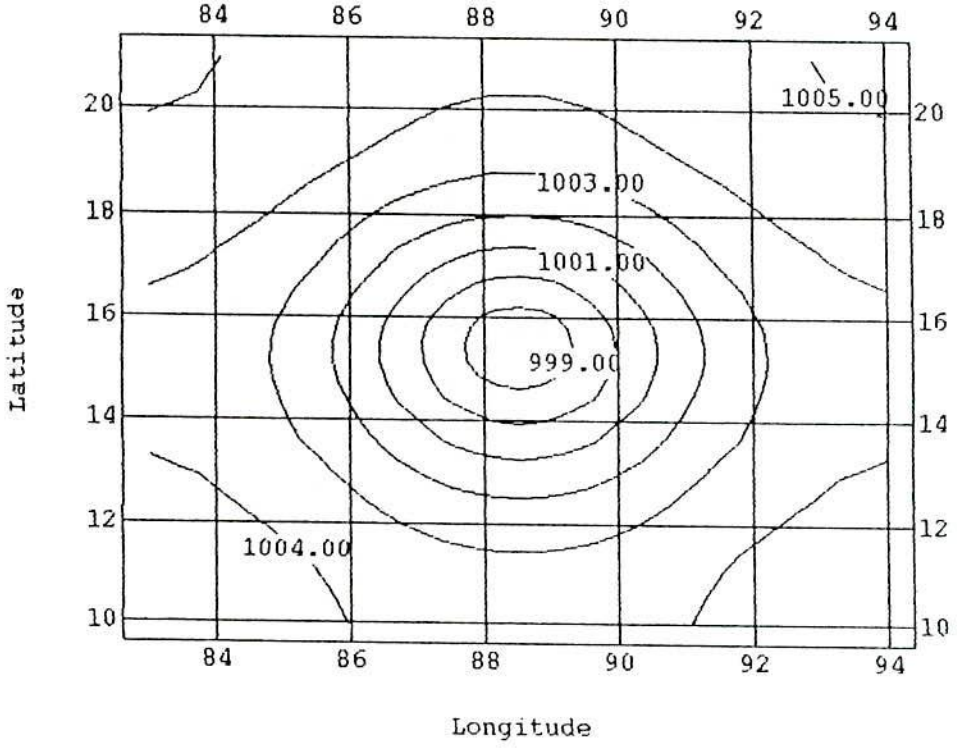

Fig. 6.15.4(c) 36-hr surface pressure (hPa) forecast

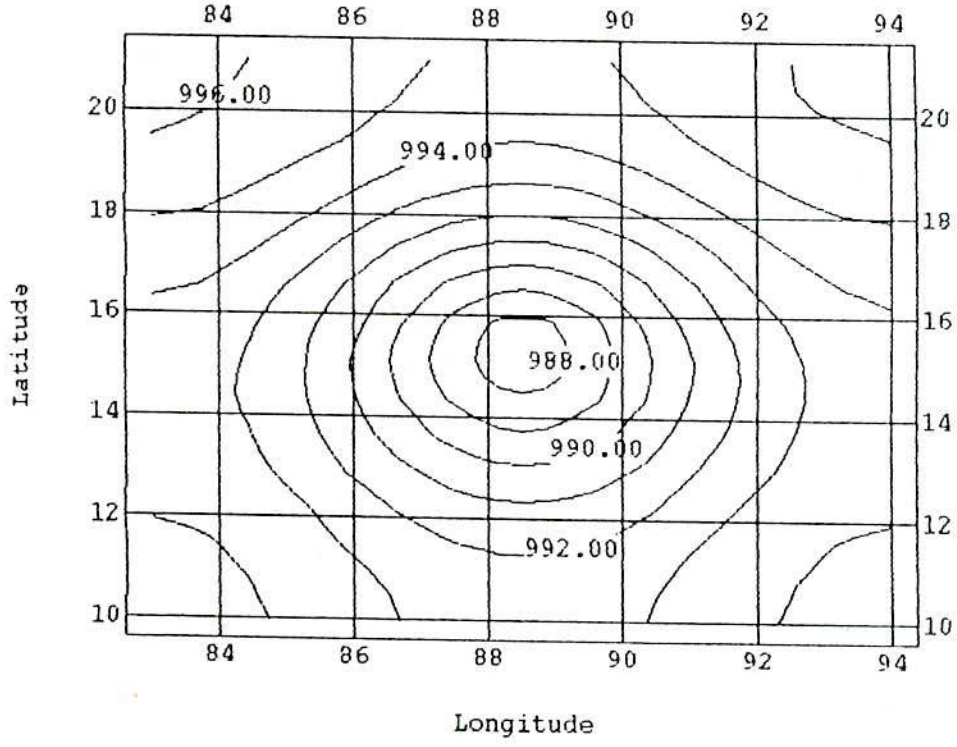

Fig. 6.15.4(d) 42-hr surface pressure (hPa) forecast

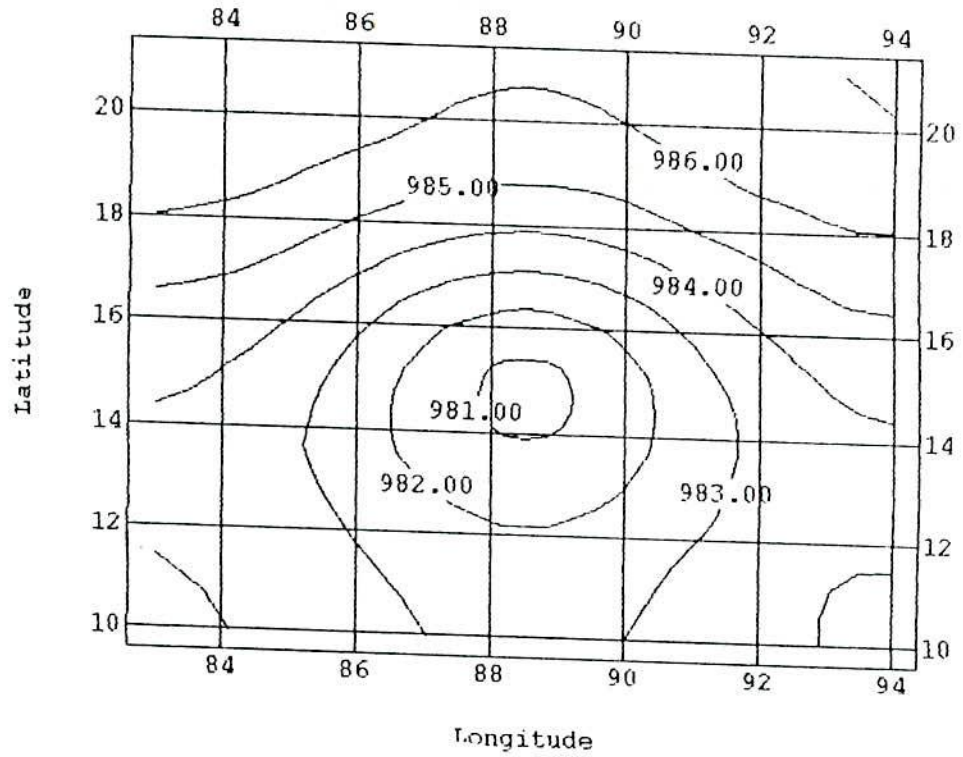

Fig. 6.15.4(e) 48-hr surface pressure (hPa) forecast

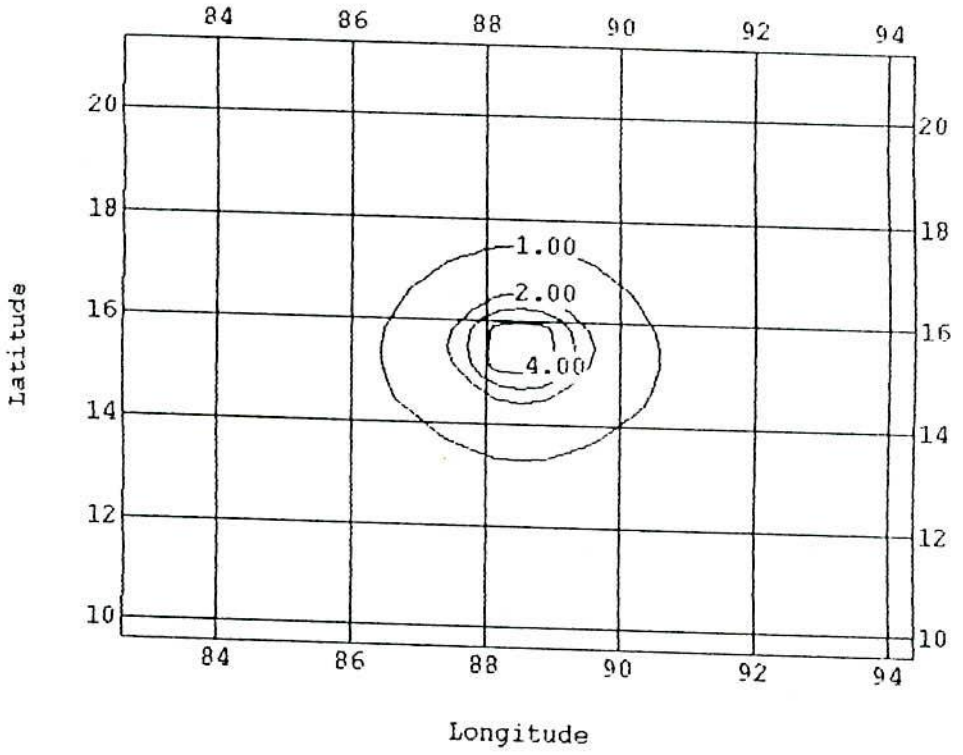

Fig. 6.15.5(a) 24-hr evolution of diabetic heating rate (° K/Day)

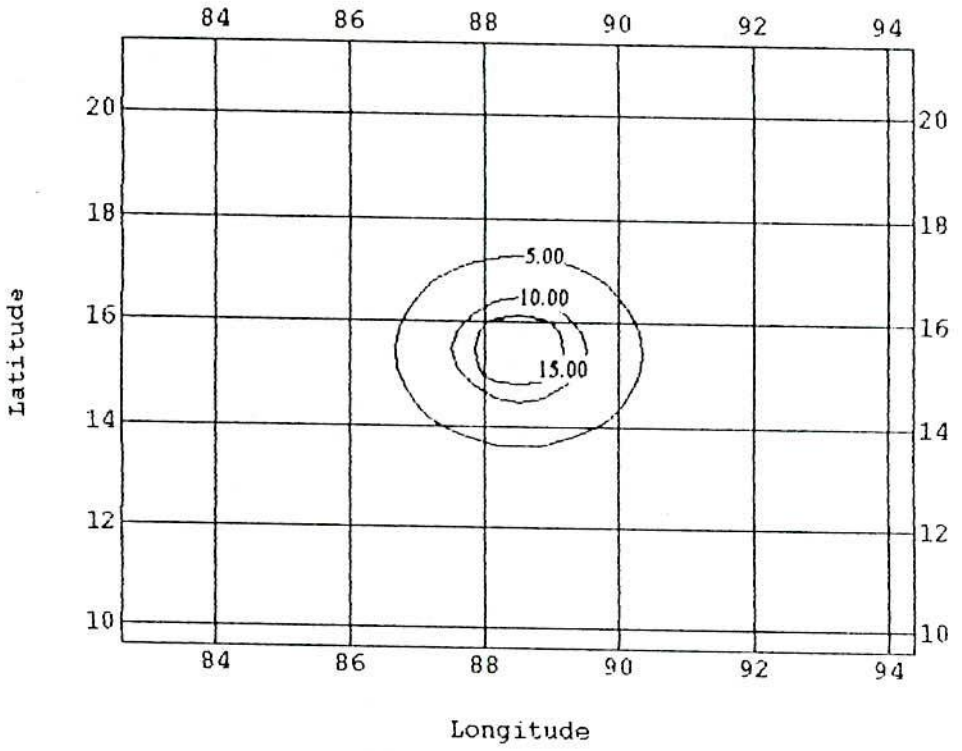

Fig. 6.15.5(b) 30-hr evolution of diabetic heating rate (° K/Day)

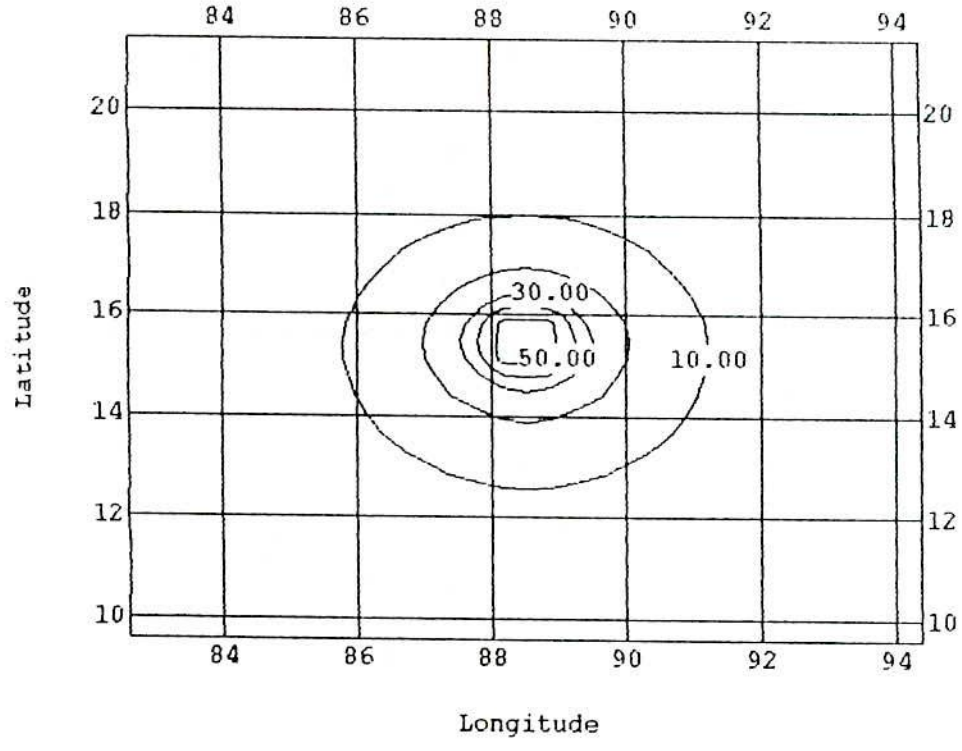

Fig. 6.15.5(c) 36-hr evolution of diabetic heating rate (° K/Day)

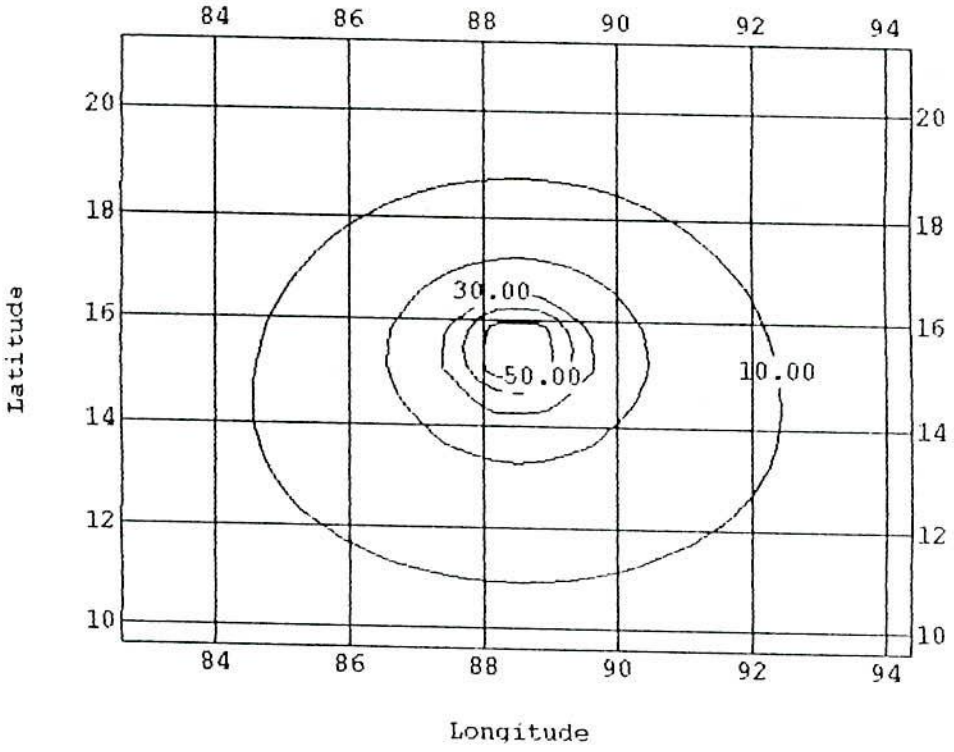

Fig. 6.15.5(d) 48-hr evolution of diabetic heating rate (°K/Day)

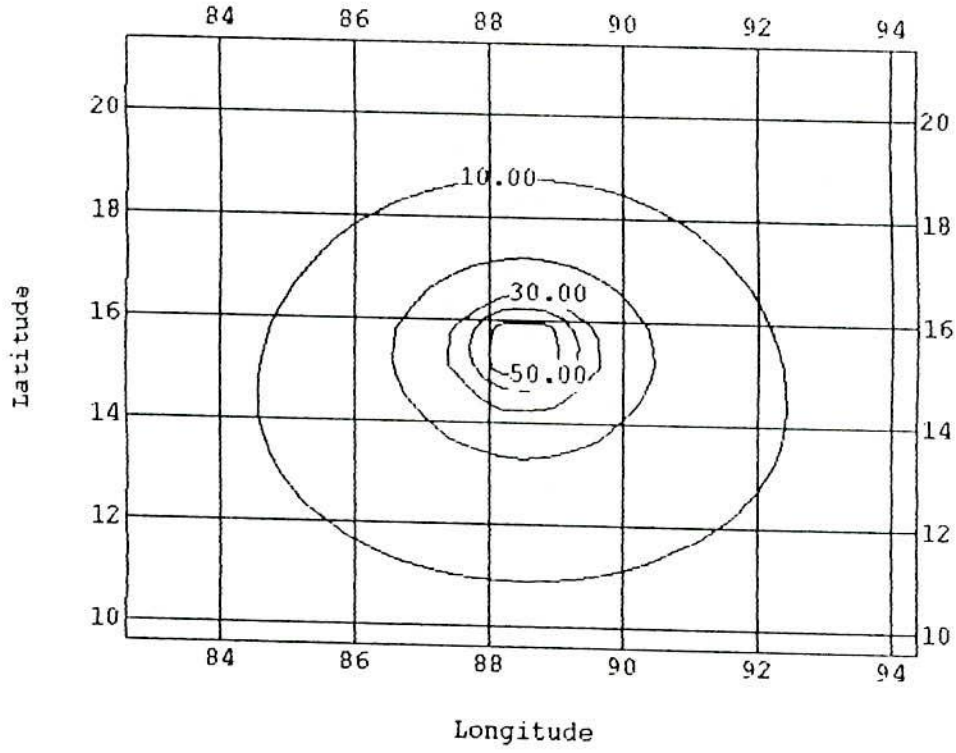

Fig. 6.15.5(e) 60-hr evolution of diabetic heating rate (°K/Day)

temperature increase 20°C at 54 hours is shown in Fig. 6.15.6(d). At 60 hours the maximum temperature increase is the same but the pattern is different at 54 and 60 hours. The horizontal structure of temperature change at 500 hPa are shown in Figs. 6.15.6(f-i). The temperature increases by 0.42°C, 0.95°C, 3.5°C and 4.2°C at 42, 48, 54 and 60 hours respectively.

From the above figures a warm core of the cyclone has been observed over the large horizontal domain with the maximum warming at 200 hPa near the centre of the vortex. This warm core is a well-established feature of the tropical cyclone, which has also been simulated by the model.

6.15.7 Geopotential Change or D - Value

The horizontal structure of geopotential change has been predicted at 200 hPa level at different time such as 36, 42, 48, 54, and 60 hours and are presented in Figs. 6.15.7(a-e) respectively. The geopotential change predicted at 36 hour is 300 m^2/s^2, at 42 hour 600 m^2/s^2, at 48 hour 1150 m^2/s^2 and at 54 hours 2600 m^2/s^2 . These are shown in Figs. (a-d) respectively. The observed changing patterns in all these cases are symmetric. The geopotential change predicted at 60 hours of 2800 m^2/s^2 is represented as in Fig. 6.15.7(e).

The horizontal structure of geopotential change has been predicted at 500 hPa at different time such as 36, 42, 48, 54, and 60 hours and are presented in Figs. 6.15.7(f-j) respectively. The geopotential changes predicted at this levels are -180 m^2/s^2 at 36 hour, -300 m^2/s^2 at 42 hour, -360m^2/s^2 at 48 hour, -300 m^2/s^2 at 54 hour and -100 m^2/s^2 at 60 hour these are shown in Figs. 6.15.7(f-j) respectively. In this level the observed change in the pattern is systematic and symmetric.

6.15.8 Vertical Velocity

The Fig. 6.15.8(a) shows the radial-vertical structure of the ω-field after 36 hours of evolution, when the core of ω-field is concentrated within 200 km from the vortex centre. The maximum ω is -4.5×10^{-3} hPa/s at 500 hPa and is observed around the centre. At 42

hour, in Fig. 6.15.8(b) the maximum ω of -8×10^{-3} hPa/s is observed around centre. The pattern of ω at 36 and 42 hours are almost identical. At 48 hour the maximum ω is concentrated within 160 km from the vortex centre and the maximum value of ω of -5×10^{-3} hPa/s is observed at 500 hPa.

Figs. 6.15.8(c-g) show the horizontal structure of vertical velocity at 850 hPa after 36, 42, 48, 60 and 72 hours respectively. From Figs. 6.15.8(c-f) it is observed that the maximum ω is -3.5×10^{-3} hPa around the centre. The ω-field is concentrated within 250 km from the centre. At 72 hour as shown in Fig. 6.15.8(g), the ω is -8.0×10^{-3} hPa around the centre. The ω-field is concentrated within 200 km from the centre at 72 hour.

6.15.9 Vorticity

The horizontal structure of the vortex at the surface after 36 hours of evolution is shown in Fig. 6.15.9(a). The vortex core is concentrated within 120 km from the centre. The maximum 16×10^{-5}/s vorticity is observed around the centre. In Figs. 6.15.9(b-d), the horizontal structure of vorticity at the surface after 48, 60 and 72 hours of evolution are presented. At these times the vortex core is concentrated within 150 km from the centre and the pattern of the structure is similar. The maximum 70×10^{-5} /s vorticity observed at these times around the centre. The vorticity is positive in the lower troposphere and negative in the upper troposphere. The profile is also very similar to those obtained by Williams (1970) and Reed and Recker (1971) for active cloud clusters.

6.15.10 Static Stability

The horizontal structure of the static stability of the atmosphere are presented as in Figs. 6.15.10(a-b) at the time 36 and 48 hours. At 36 hour, in Fig. 6.15.10(a), the static stability of the atmosphere is zero at the centre. In Fig. 6.15.10(b) the stability of the atmosphere is negative at the surface at 48 hour and the maximum value of the stability is -1.1×10^{-5}. After 36 hour, the stability of the surface is negative and it continues up to 72 hours up to which the model run. The negative stability arises due to the instability of the atmosphere. Figs. 6.15.10(c-d) show the static stability at 850 hPa after 36 and 48 hour of evolution of

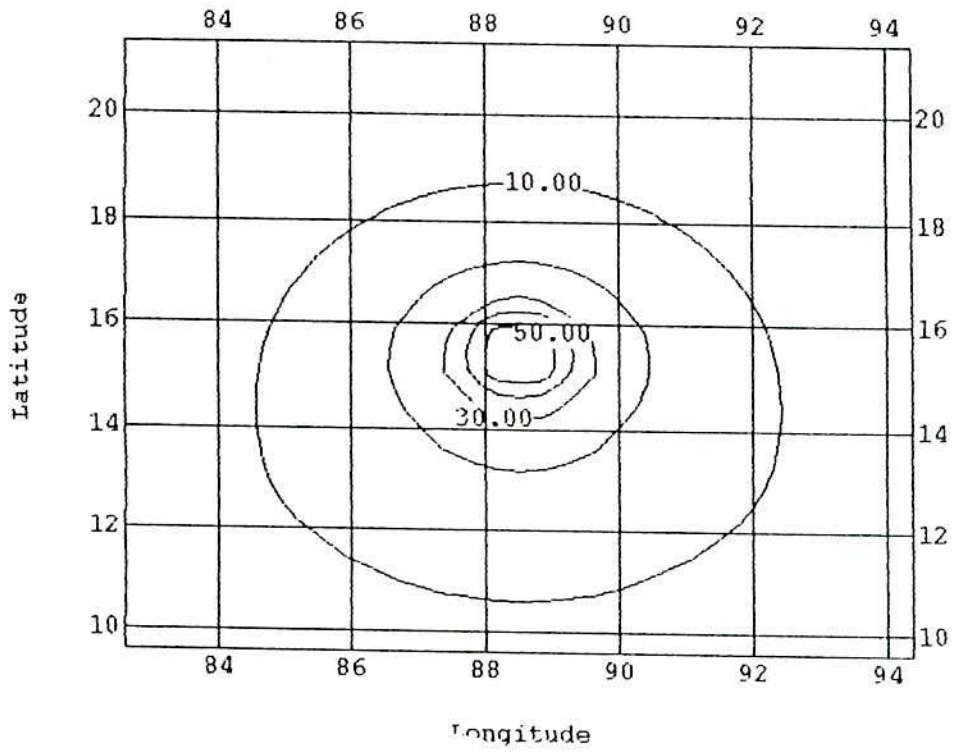

Fig. 6.15.5(f) 72-hr evolution of diabetic heating rate (°K/Day)

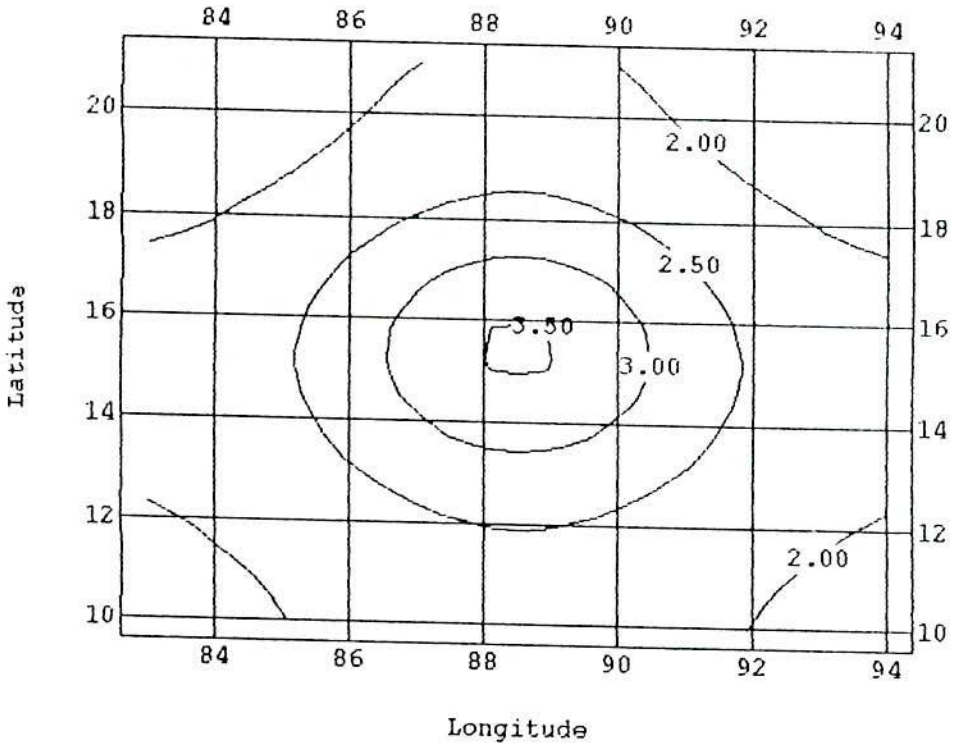

Fig. 6.15.6(a) 36-hr forecast of temperature change (°K) at 200 hPa

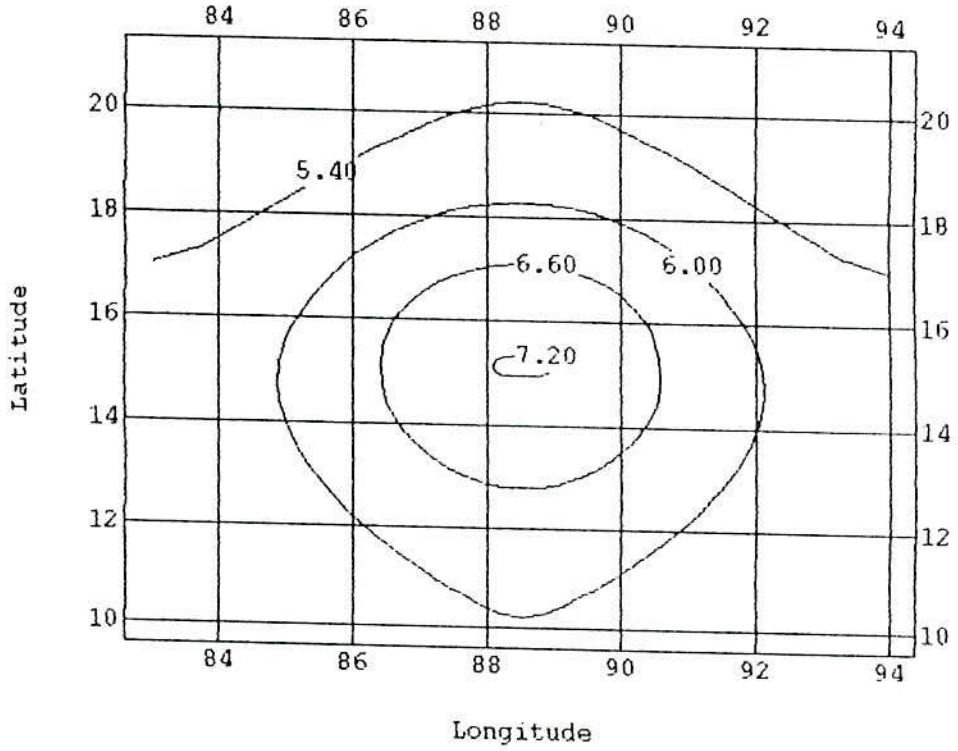

Fig. 6.15.6(b) 42-hr forecast of temperature change (°K) at 200 hPa

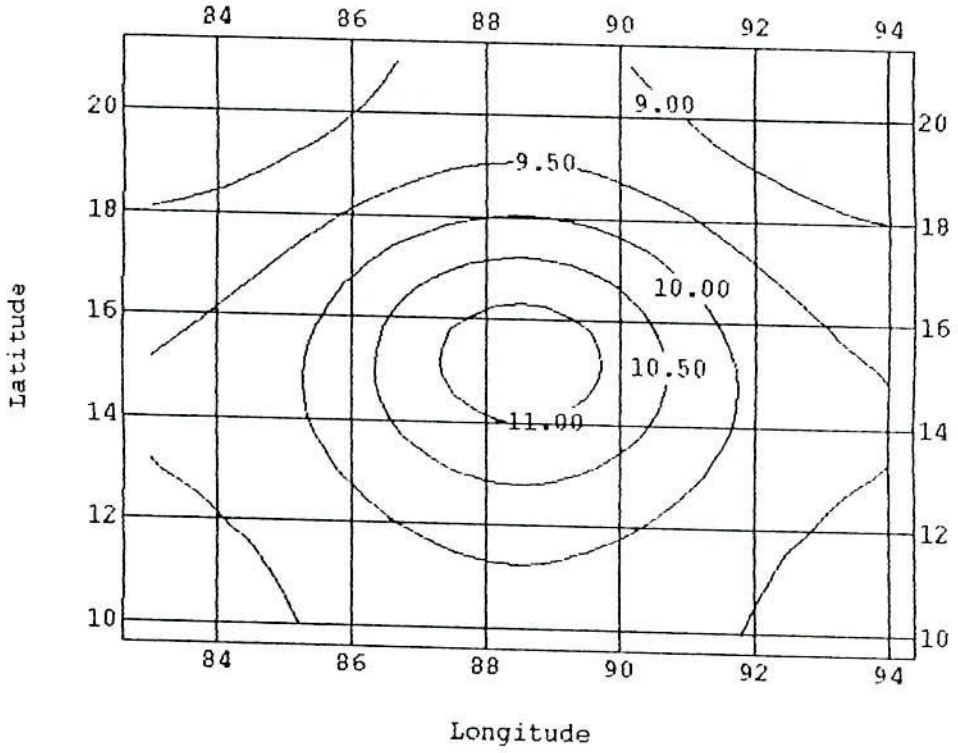

Fig. 6.15.6(c) 48-hr forecast of temperature change (°K) at 200 hPa

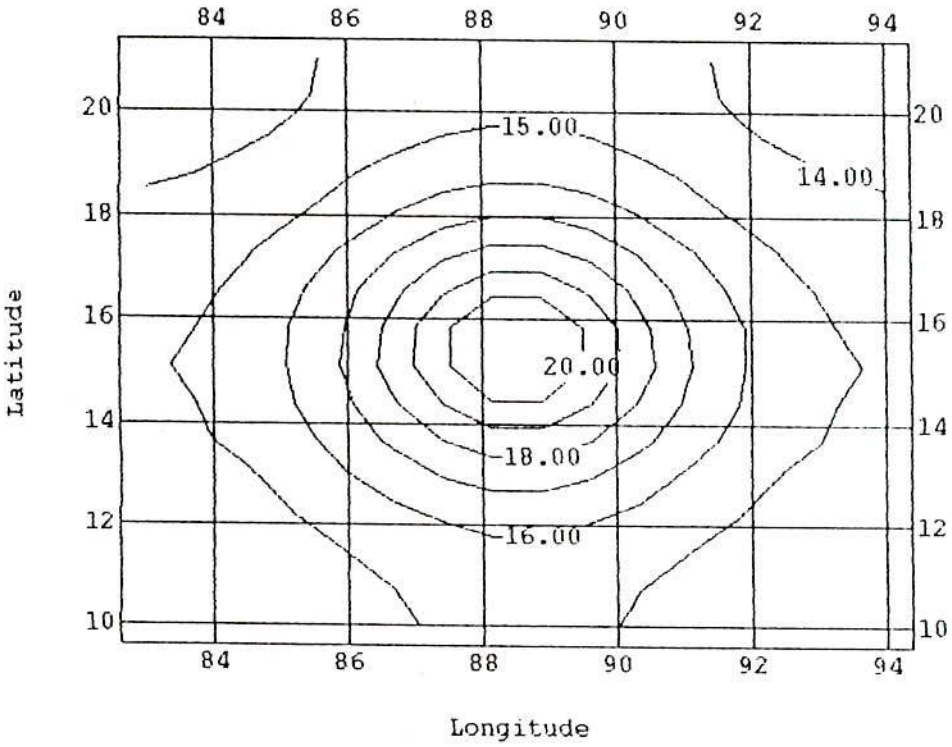

Fig. 6.15.6(d) 54-hr forecast of temperature change (°K) at 200 hPa

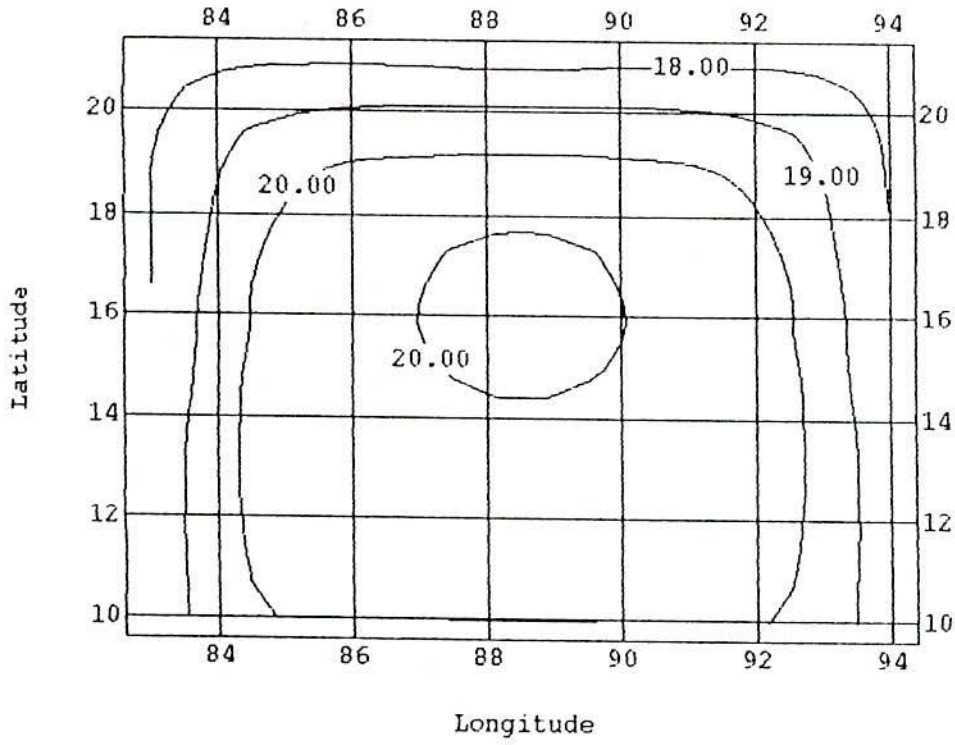

Fig. 6.15.6(e) 60-hr forecast of temperature change (°K) at 200 hPa

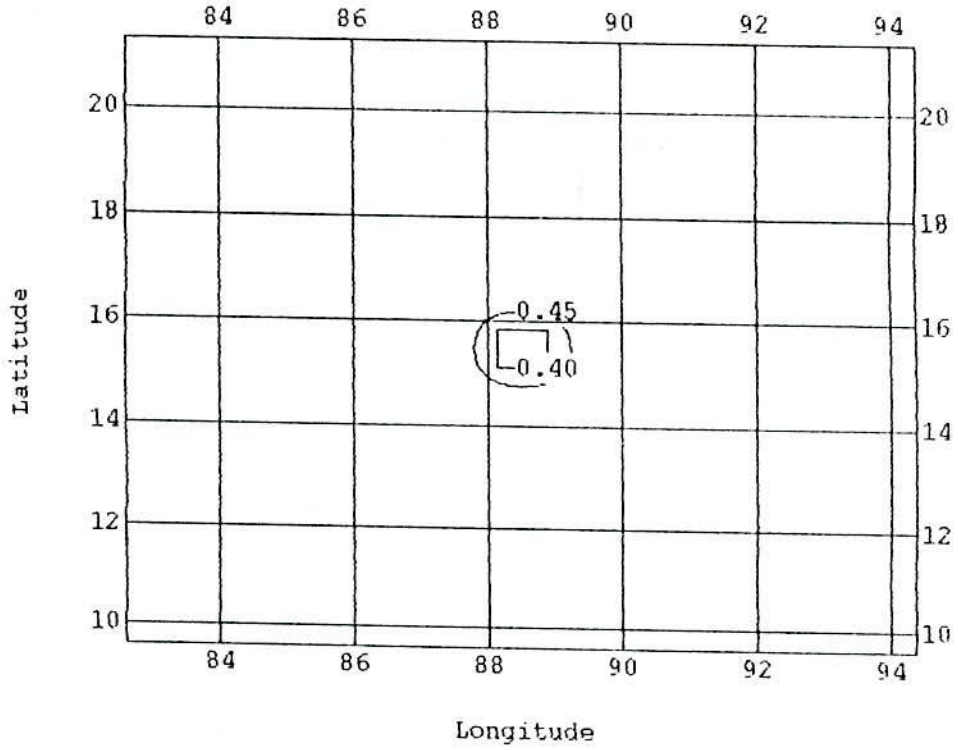

Fig. 6.15.6(f) 42-hr forecast of temperature change (°K) at 500 hPa

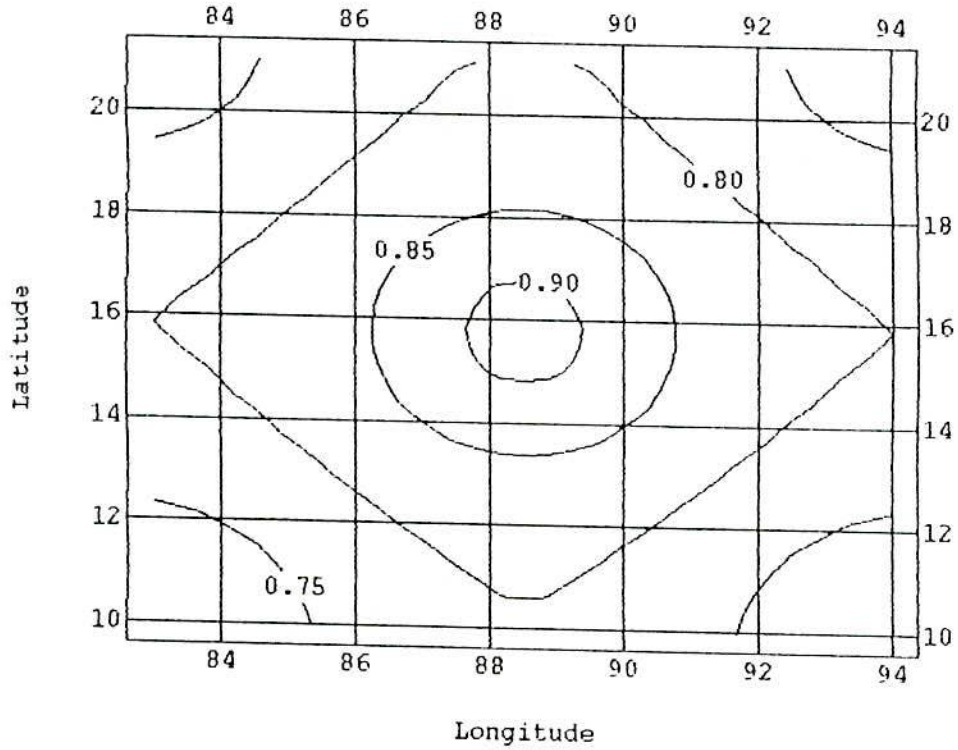

Fig. 6.15.6(g) 48-hr forecast of temperature change (°K) at 500 hPa

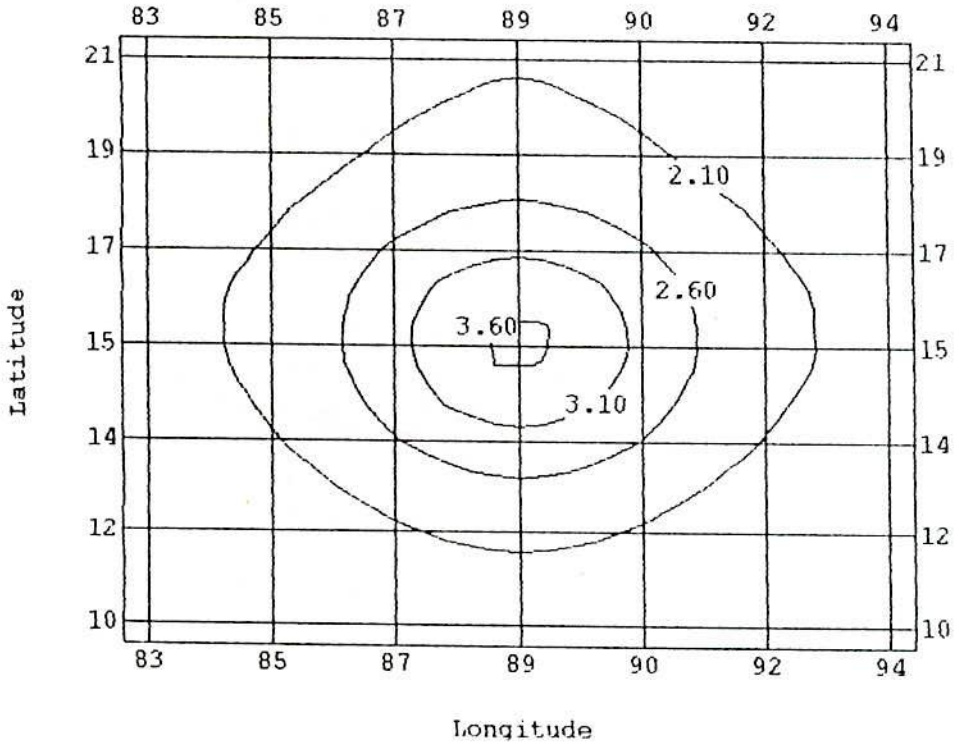

Fig. 6.15.6(h) 54-hr forecast of temperature change (°K) at 500 hPa

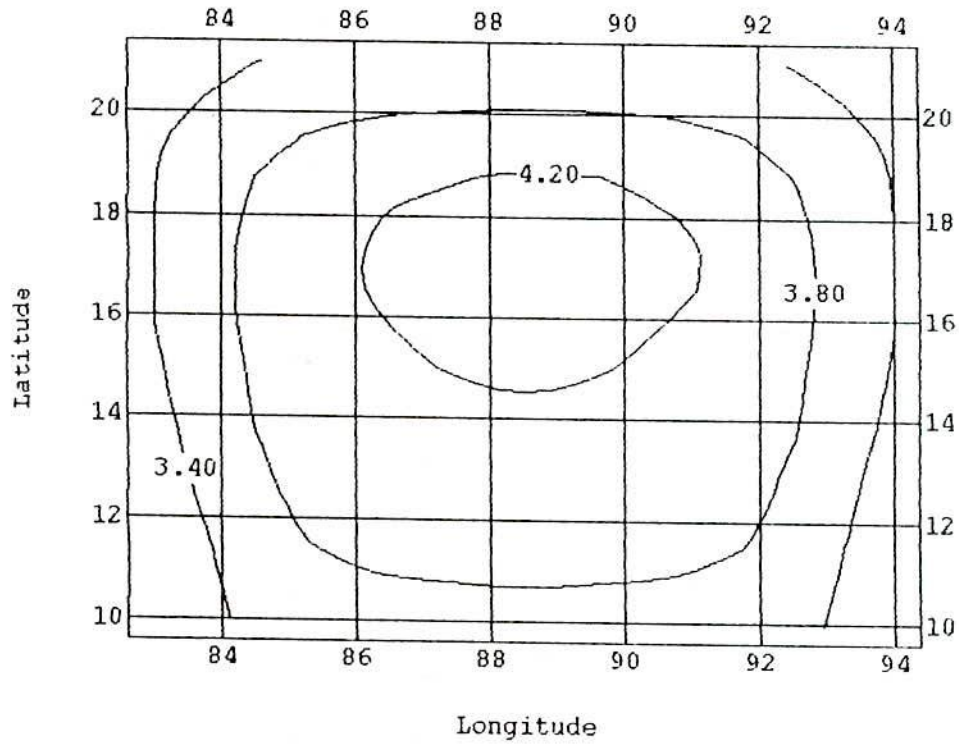

Fig. 6.15.6(i) 60-hr forecast of temperature change (°K) at 500 hPa

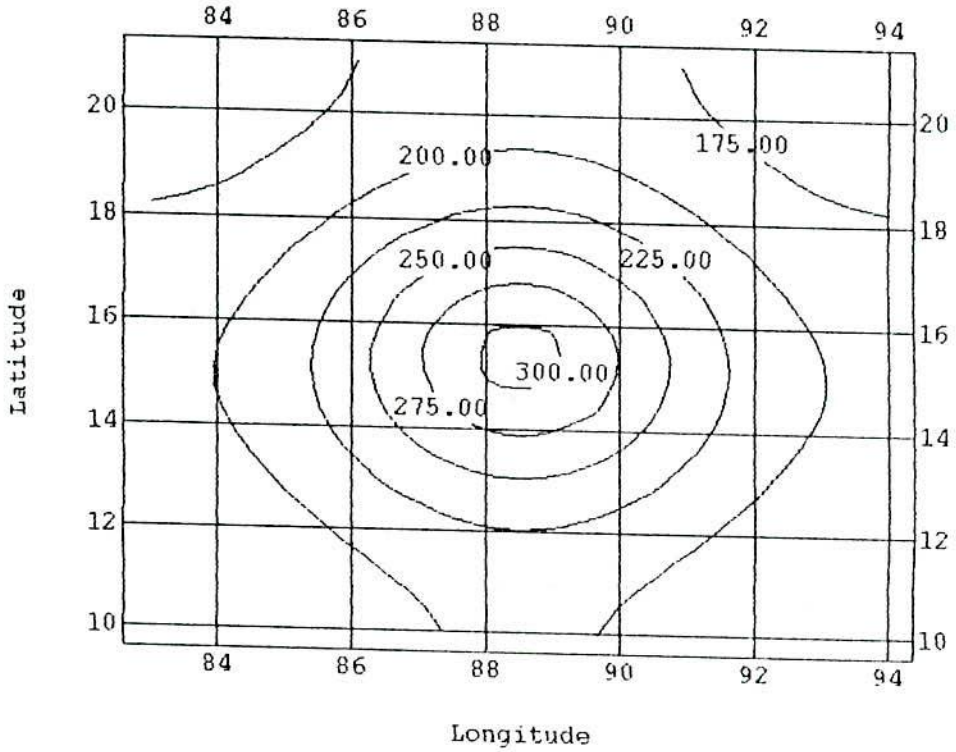

Fig. 6.15.7(a) 36-hr forecast of geopotential change (m^2/ $sec.^2$) at 200 hPa

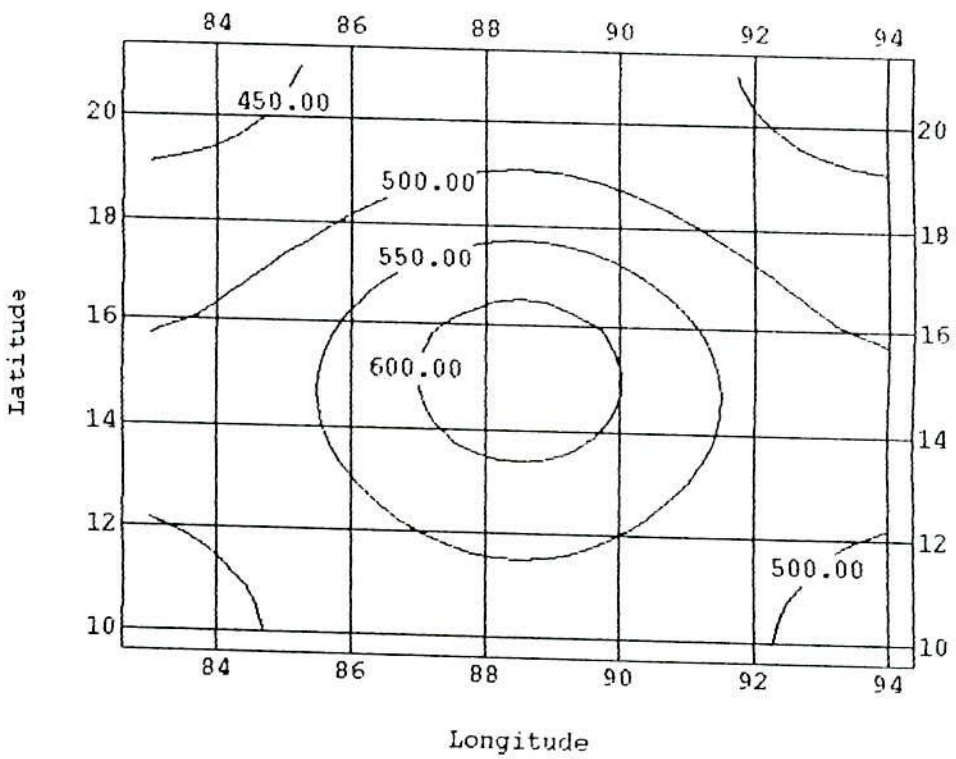

Fig. 6.15.7(b) 42-hr forecast of geopotential change(m^2/ $sec.^2$) at 200 hPa

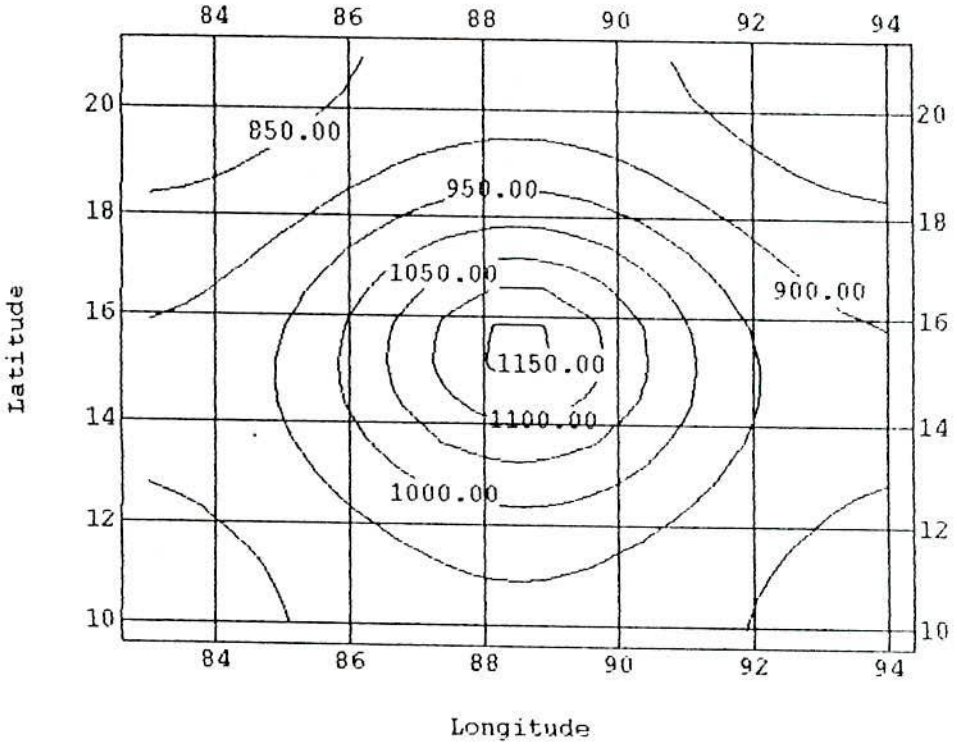

Fig. 6.15.7(c) 48-hr forecast of geopotential change (m^2/ $sec.^2$) at 200 hPa

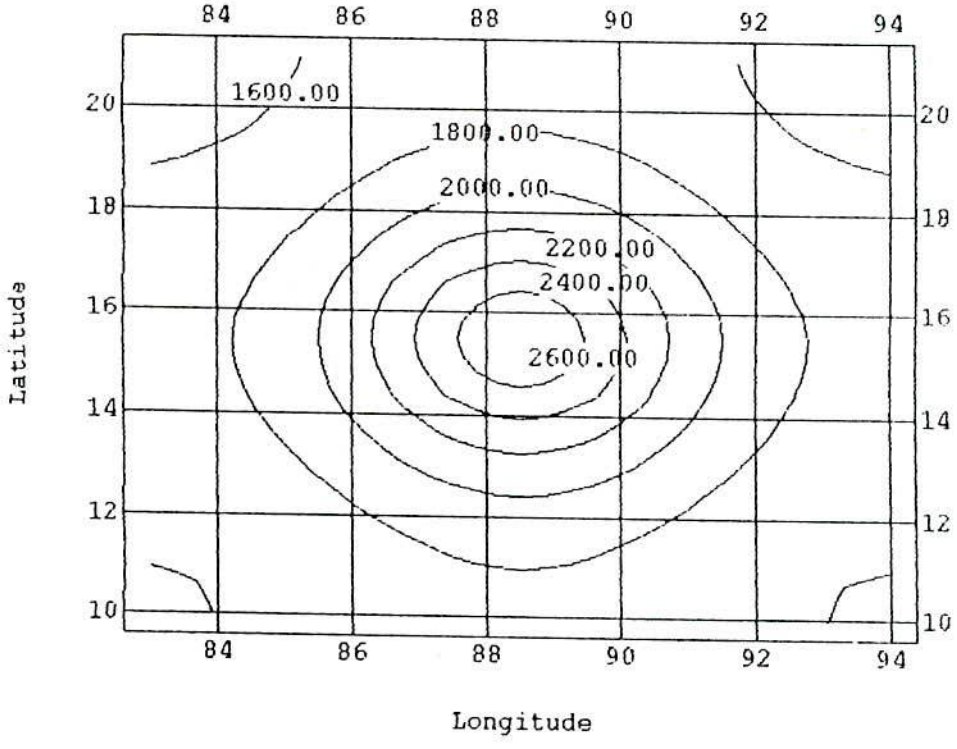

Fig. 6.15.7(d) 54-hr forecast of geopotential change (m^2/ $sec.^2$) at 200 hPa

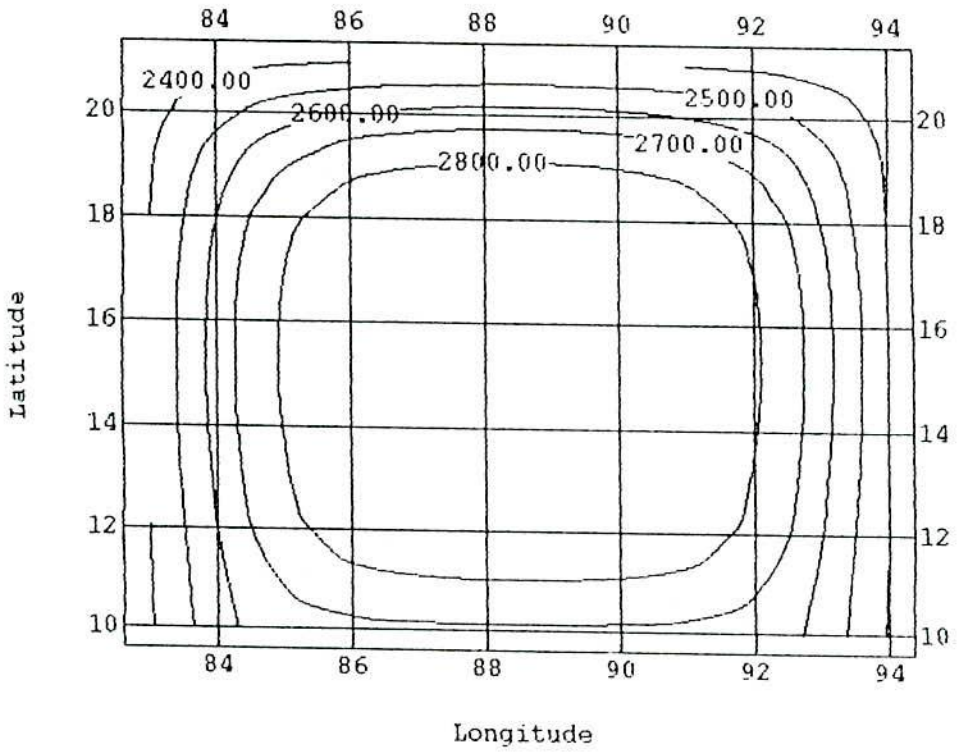

Fig. 6.15.7(e) 60-hr forecast of geopotential change (m^2/ $sec.^2$) at 200 hPa

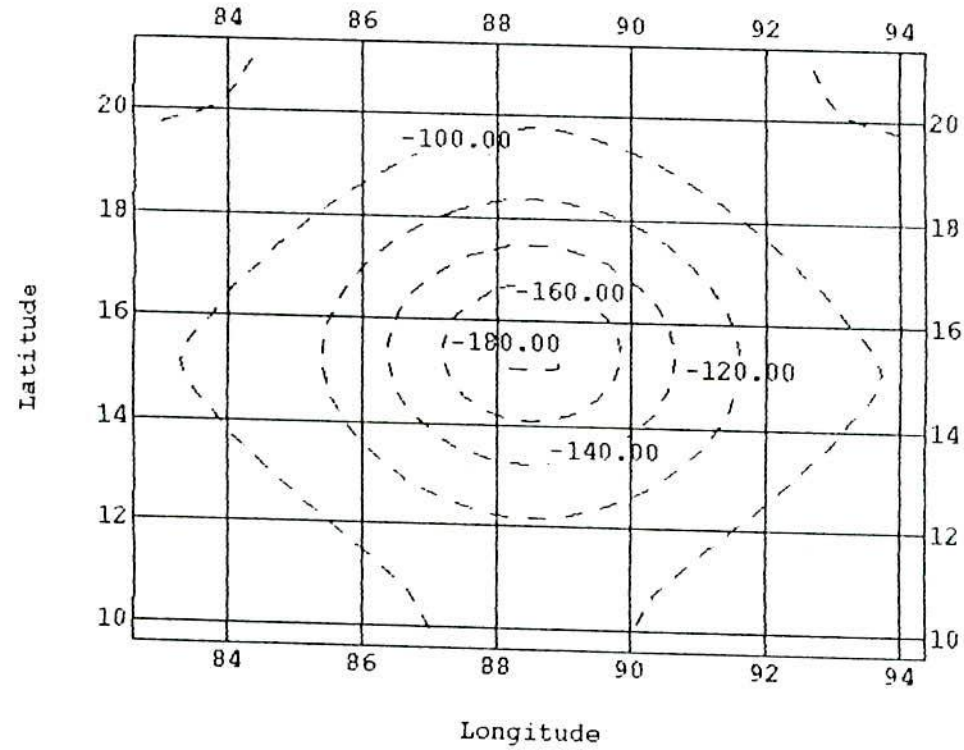

Fig. 6.15.7(f) 36-hr forecast of geopotential change (m^2/ $sec.^2$) at 500 hPa

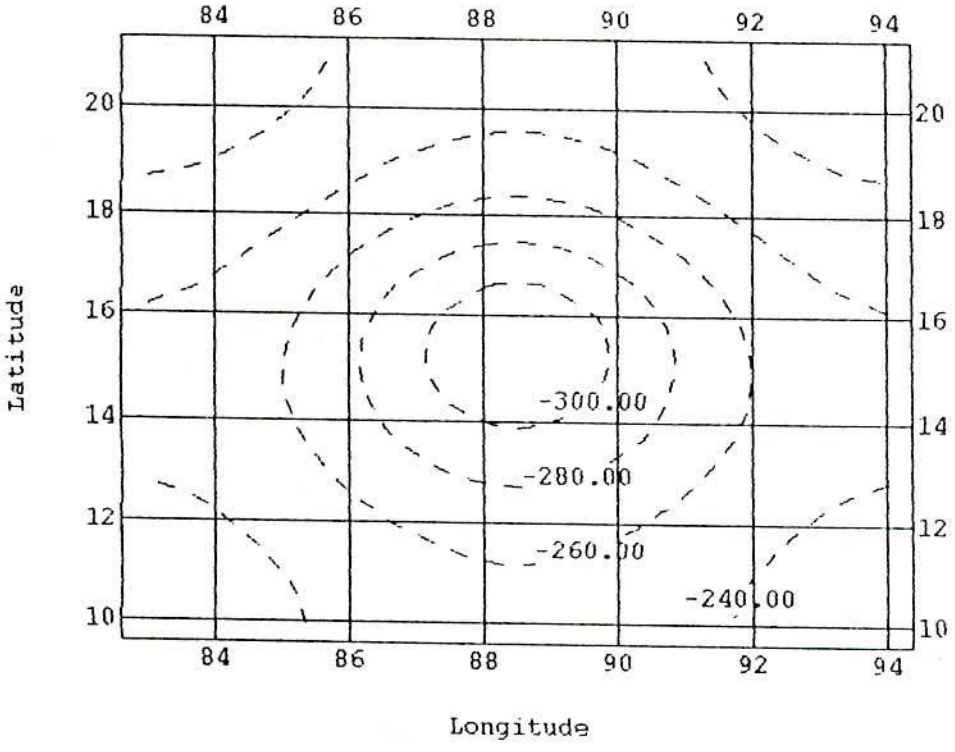

Fig. 6.15.7(g) 42-hr forecast of geopotential change (m^2/ $sec.^2$) at 500 hPa

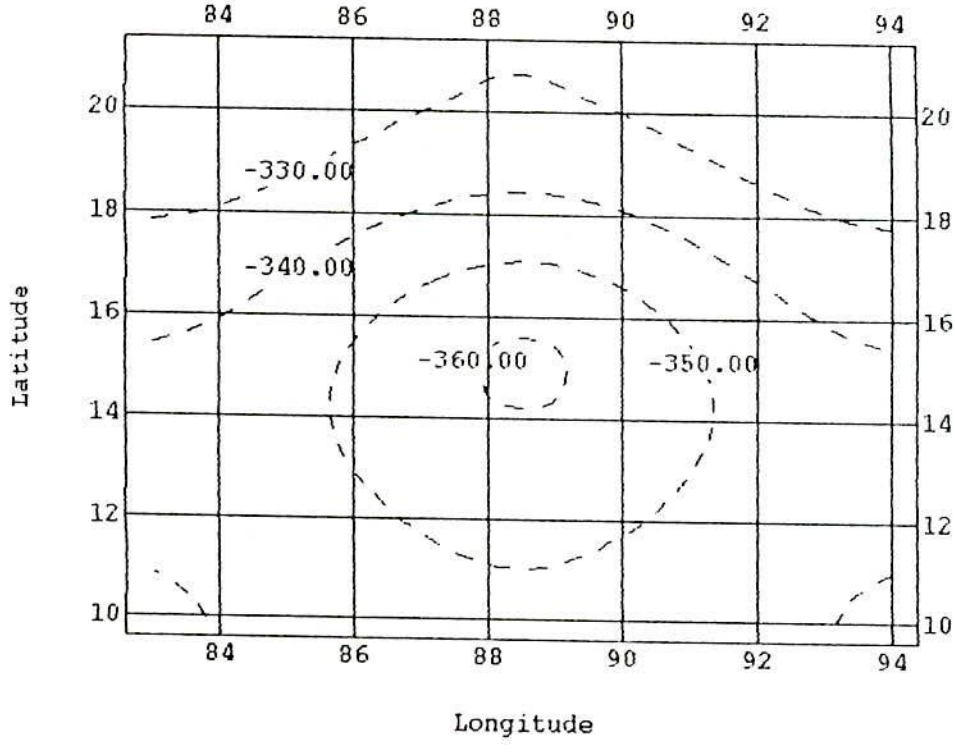

Fig. 6.15.7(h) 48-hr forecast of geopotential change (m^2/ $sec.^2$) at 500 hPa

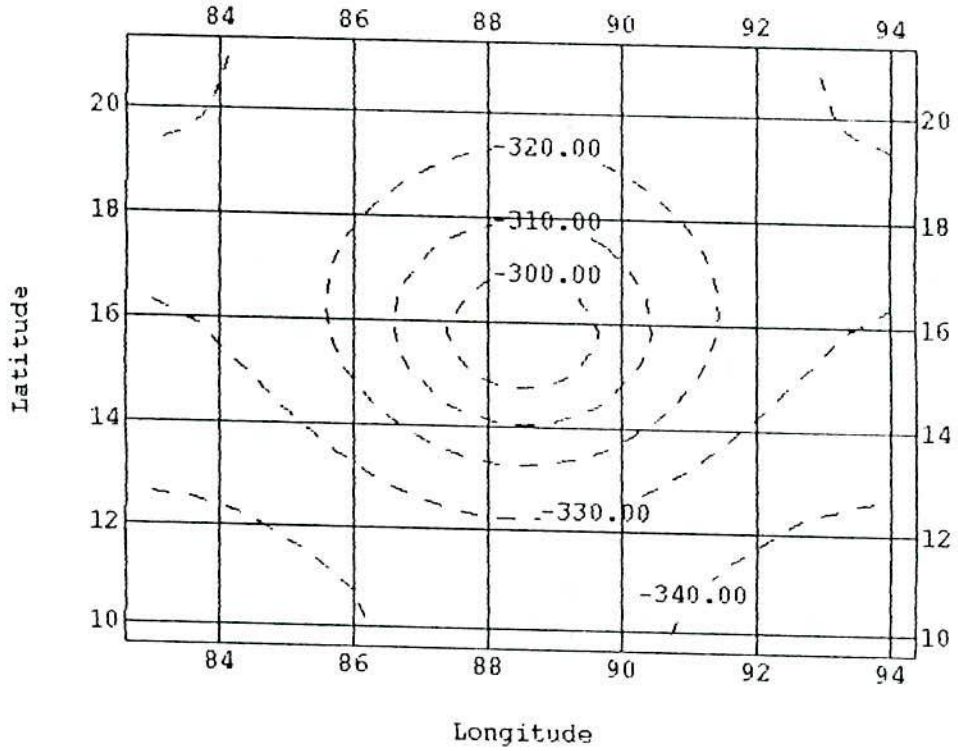

Fig. 6.15.7(i) 54-hr forecast of geopotential change (m^2/ $sec.^2$) at 500 hPa

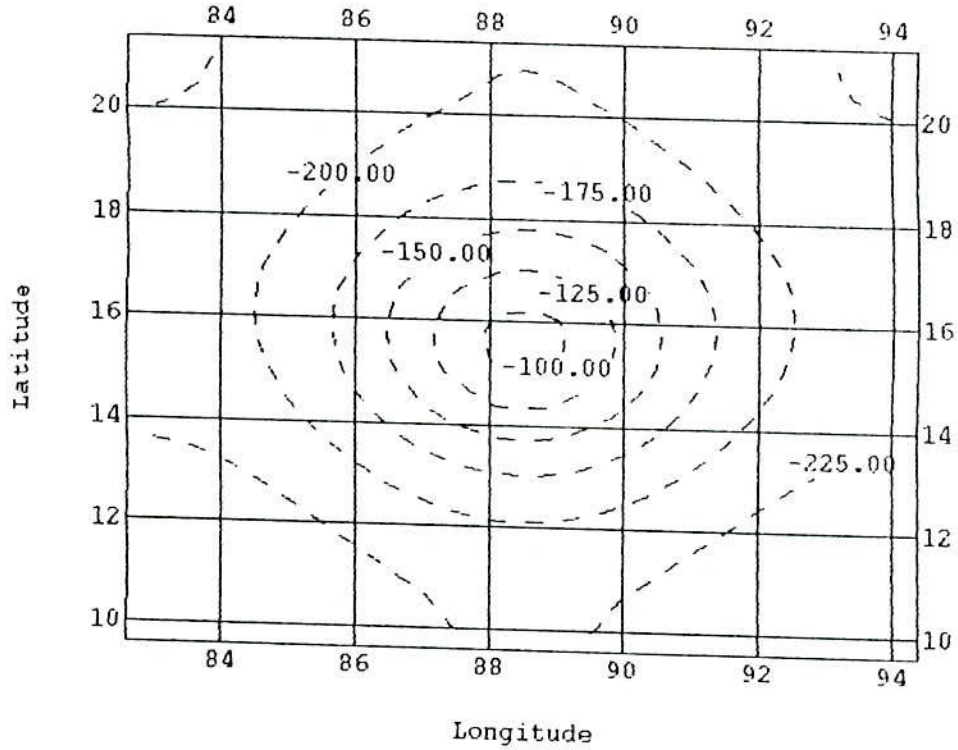

Fig. 6.15.7(j) 60-hr forecast of geopotential change (m^2/ $sec.^2$) at 500 hPa

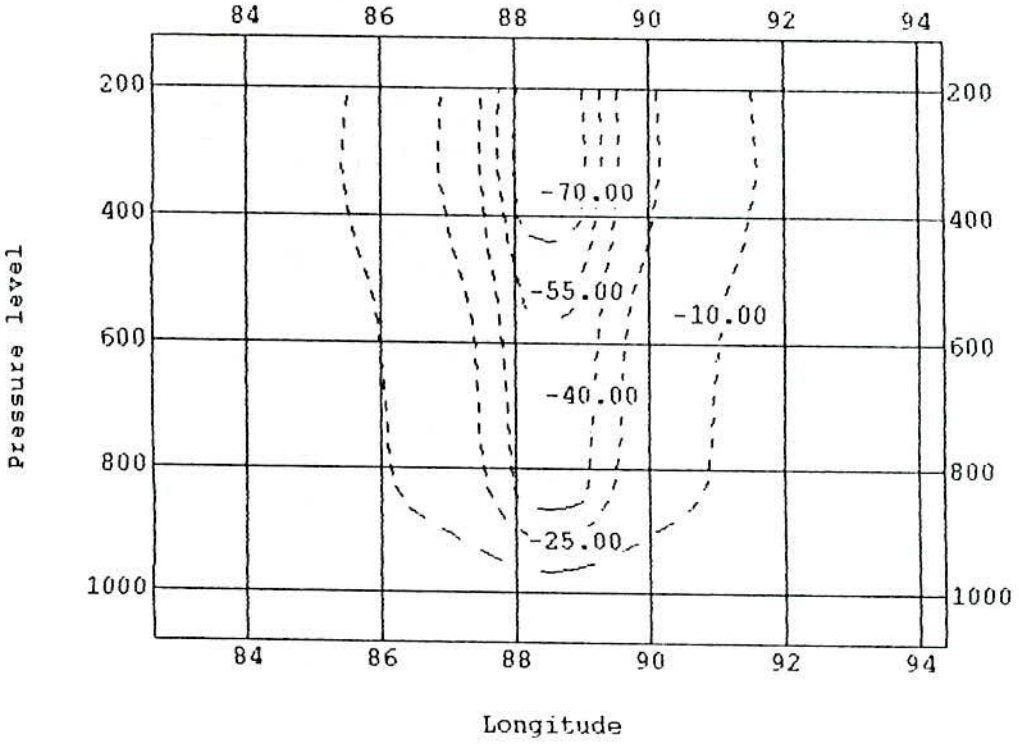

Fig. 6.15.8(a) 36-hr forecast of radial vertical distribution of p-velocity ($\times 10^{-4}$ hPa)

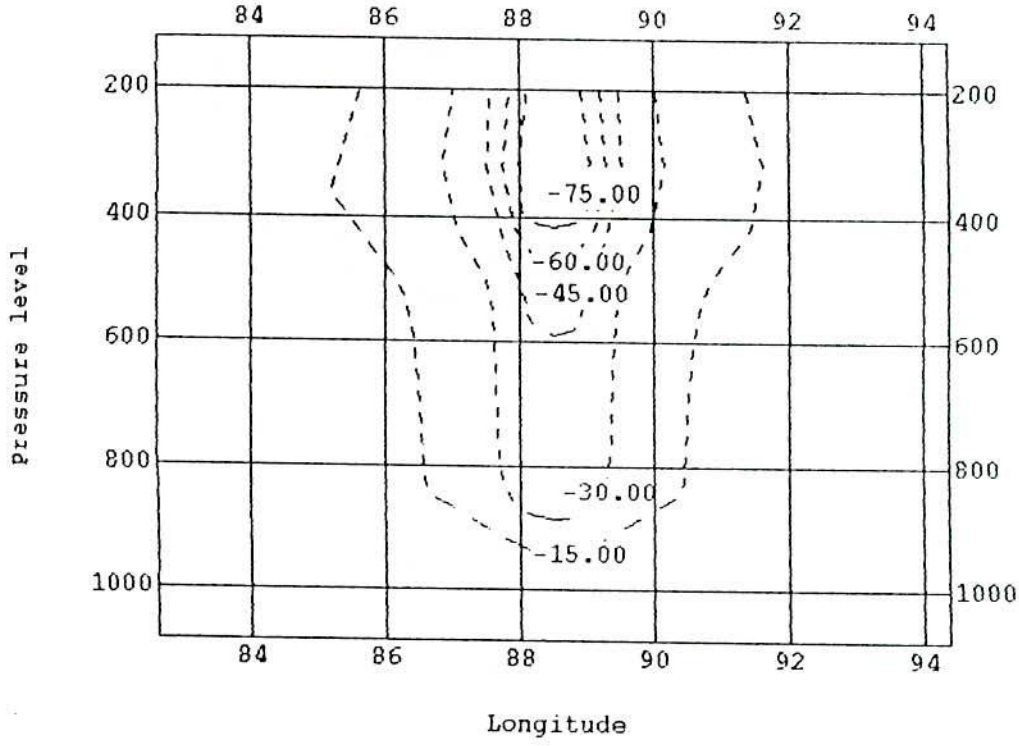

Fig. 6.15.8(b) 42-hr forecast of radial vertical distribution of p-velocity ($\times 10^{-4}$ hPa)

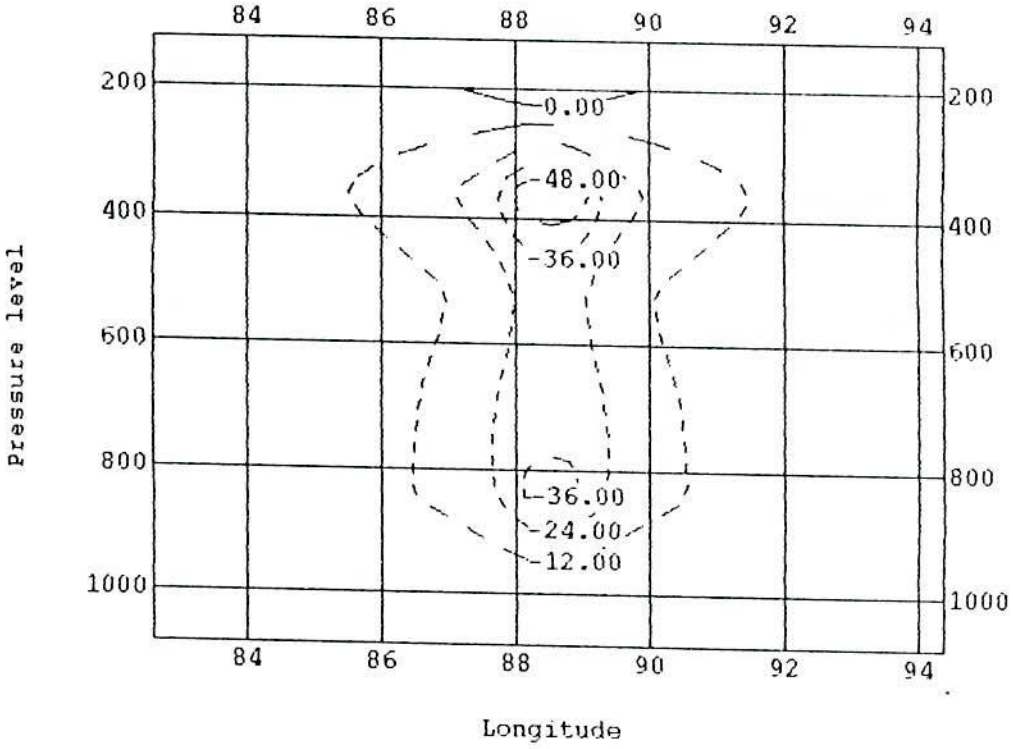

Fig. 6.15.8(c) 48-hr forecast of radial vertical distribution of p-velocity ($\times 10^{-4}$ hPa)

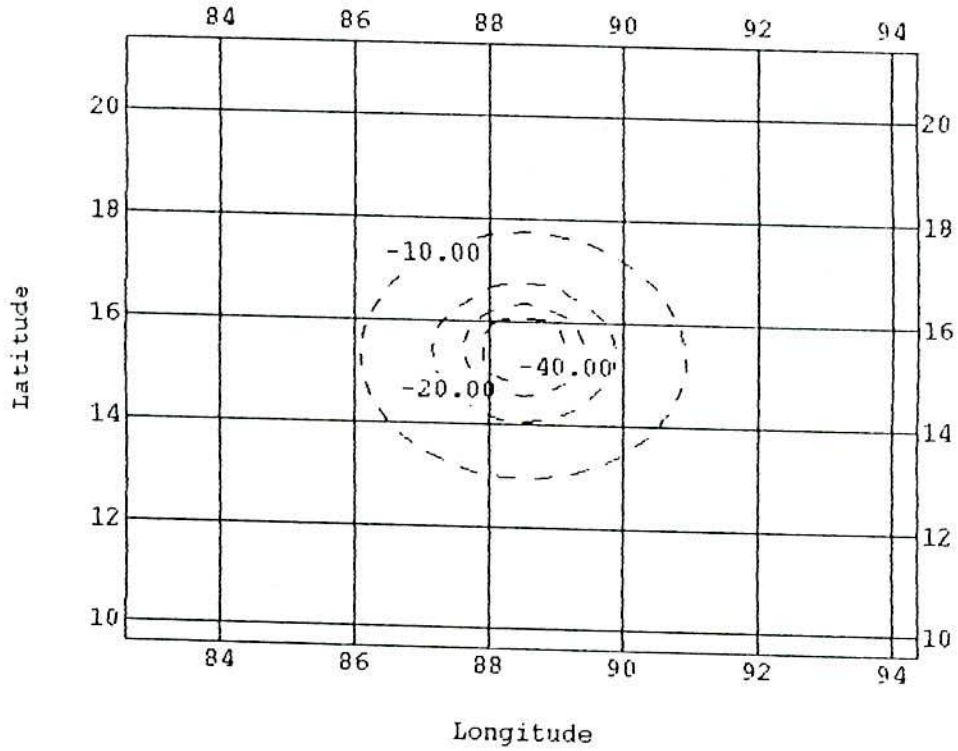

Fig. 6.15.8(d) 36-hr forecast of vertical p-velocity ($\times 10^{-4}$ hPa) at 850 hPa

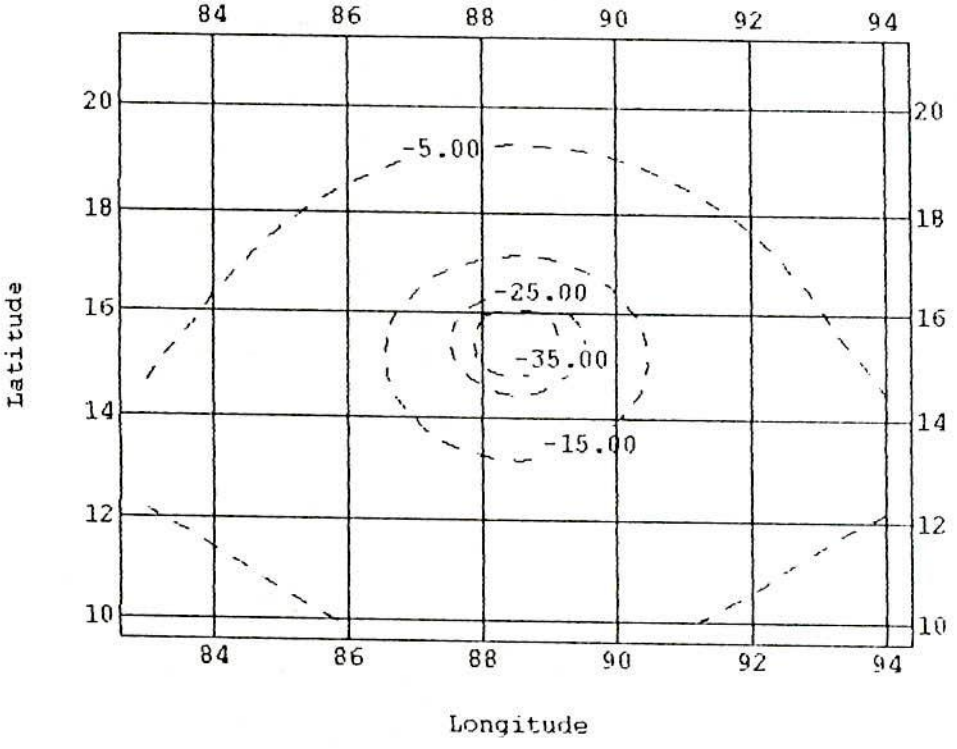

Fig. 6.15.8(e) 42-hr forecast of vertical p-velocity ($\times 10^{-4}$ hPa) at 850 hPa

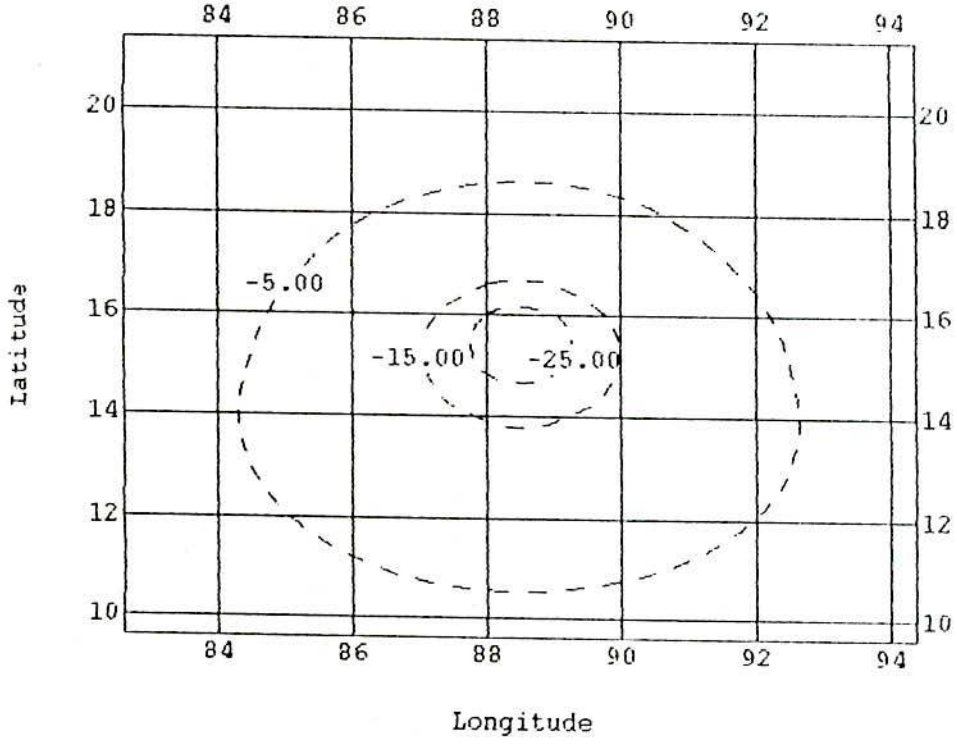

Fig. 6.15.8(f) 48-hr forecast of vertical p-velocity ($\times 10^{-4}$ hPa) at 850 hPa

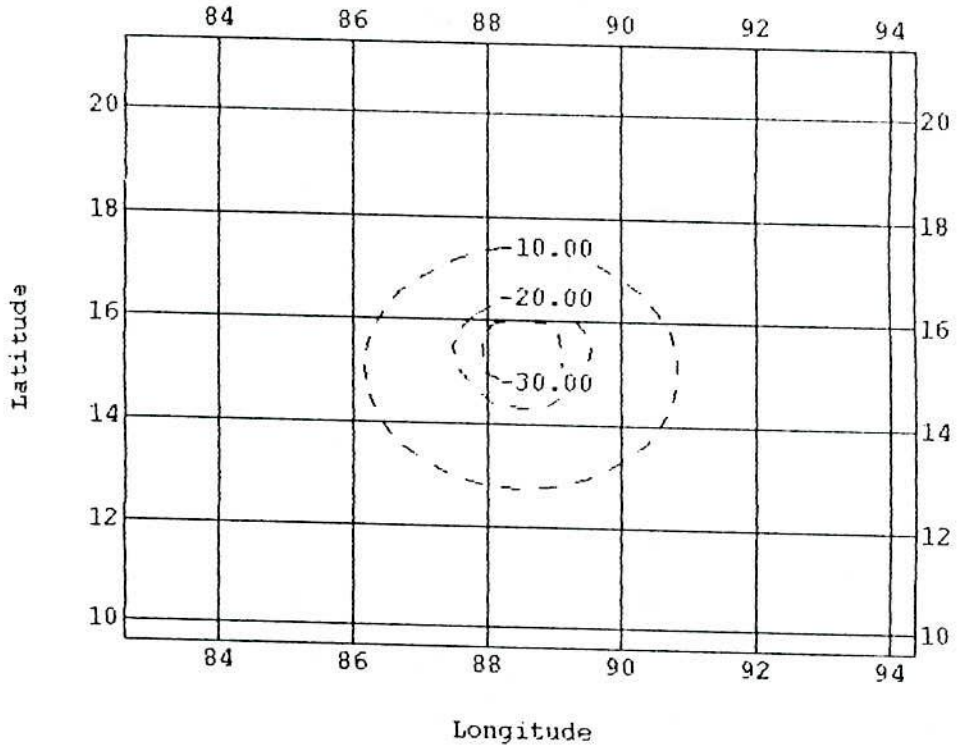

Fig. 6.15.8(g) 60-hr forecast of vertical p-velocity ($\times 10^{-4}$ hPa) at 850 hPa

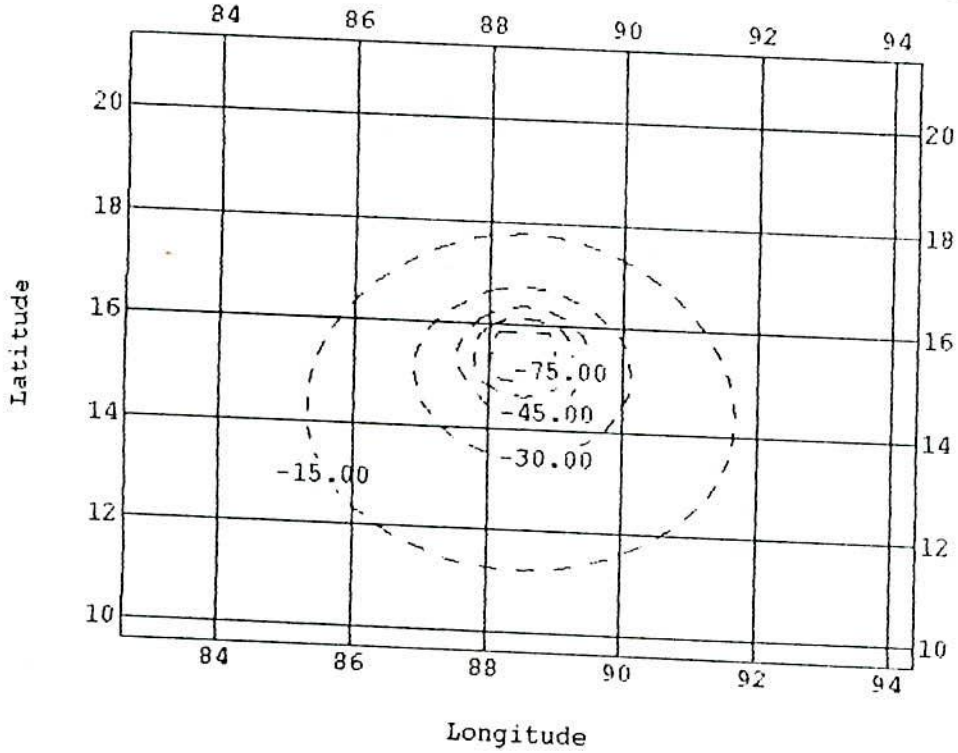

Fig. 6.15.8(h) 72-hr forecast of vertical p-velocity ($\times 10^{-4}$ hPa) at 850 hPa

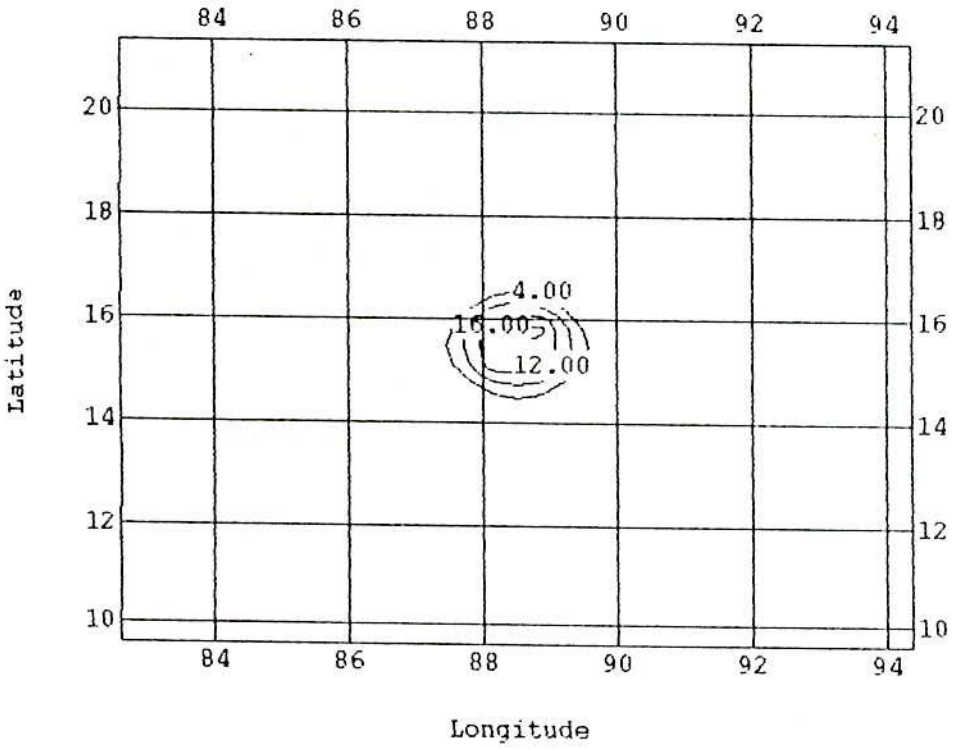

Fig. 6.15.9(a) 36-hr forecast of vorticity ($\times 10^{-5}$/s) at the surface

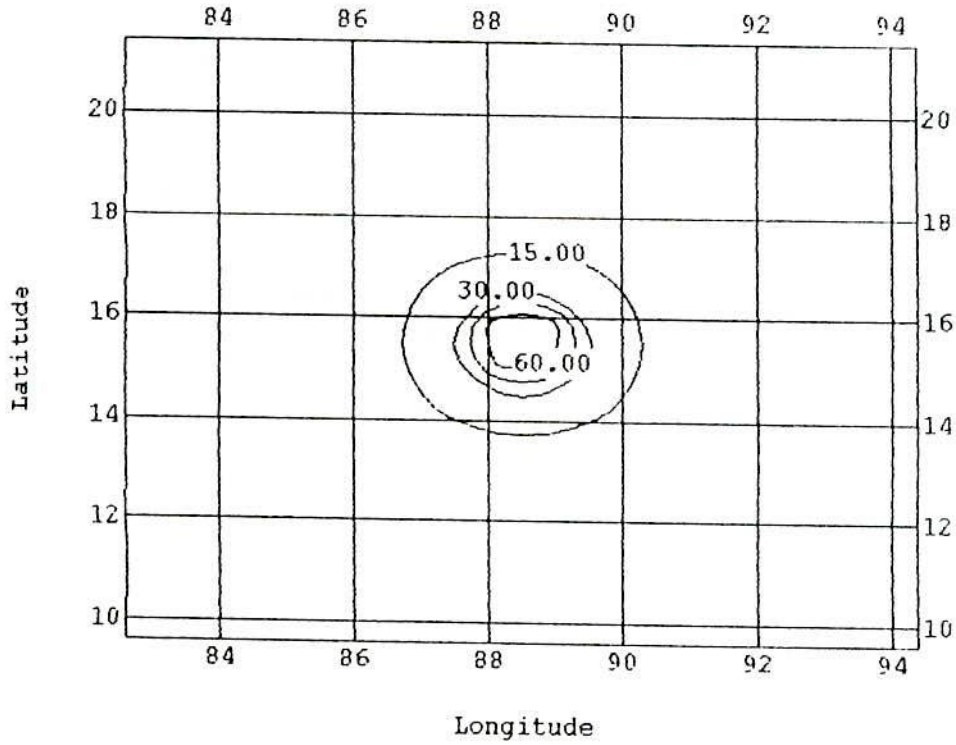

Fig. 6.15.9(b) 48-hr forecast of vorticity ($\times 10^{-5}$/s) at the surface

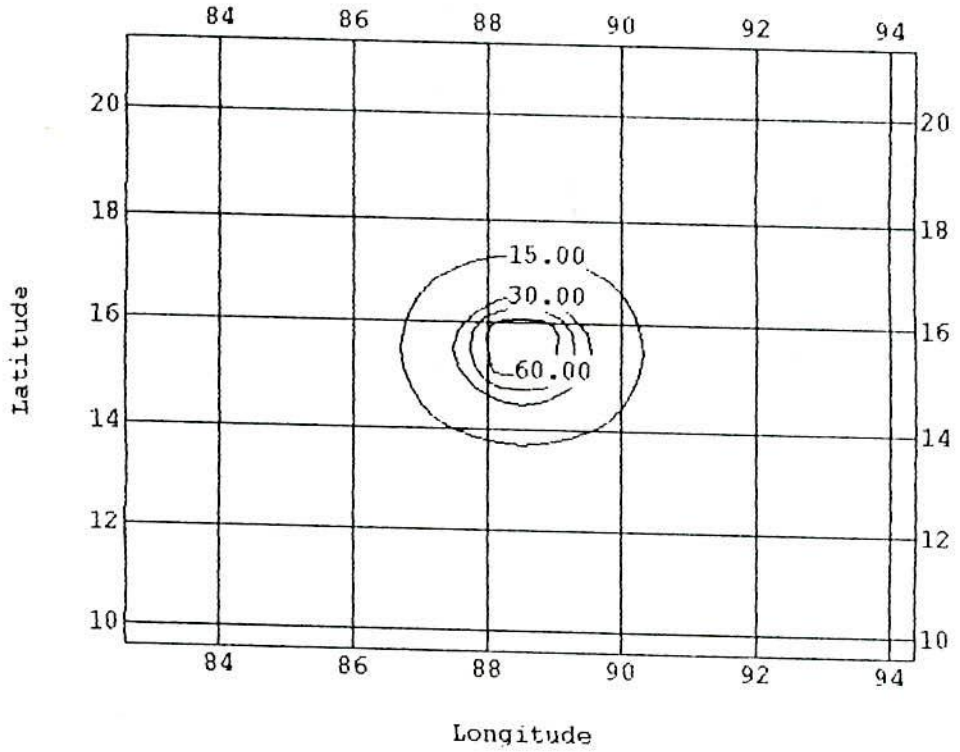

Fig. 6.15.9(c) 60-hr forecast of vorticity ($\times 10^{-5}$/s) at the surface

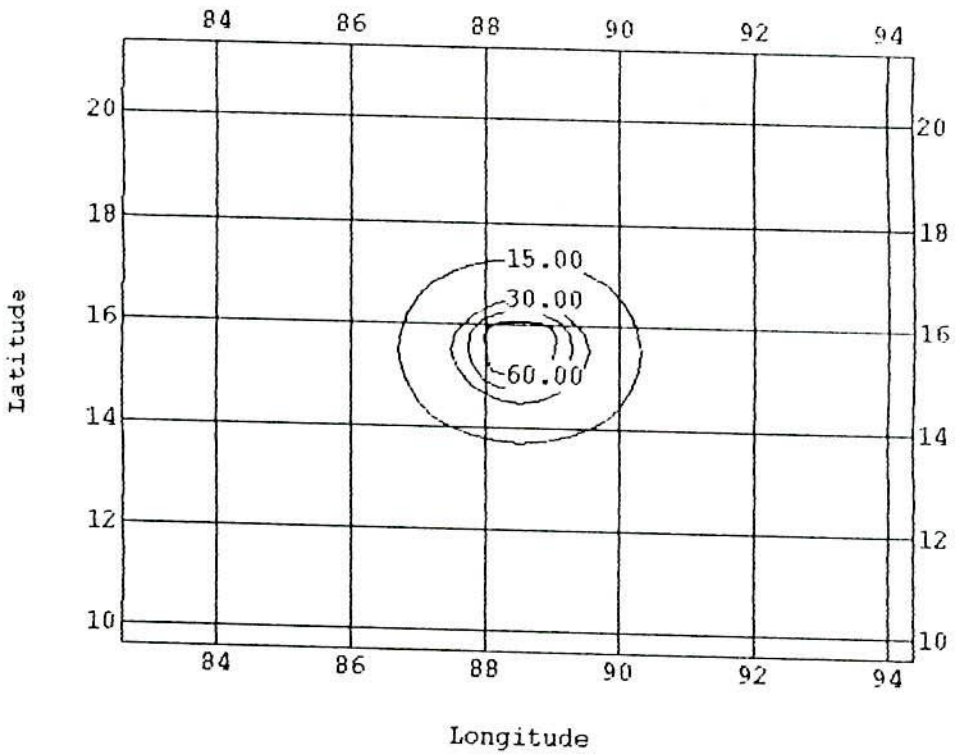

Fig. 6.15.9(d) 72-hr forecast of vorticity ($\times 10^{-5}$/s) at the surface

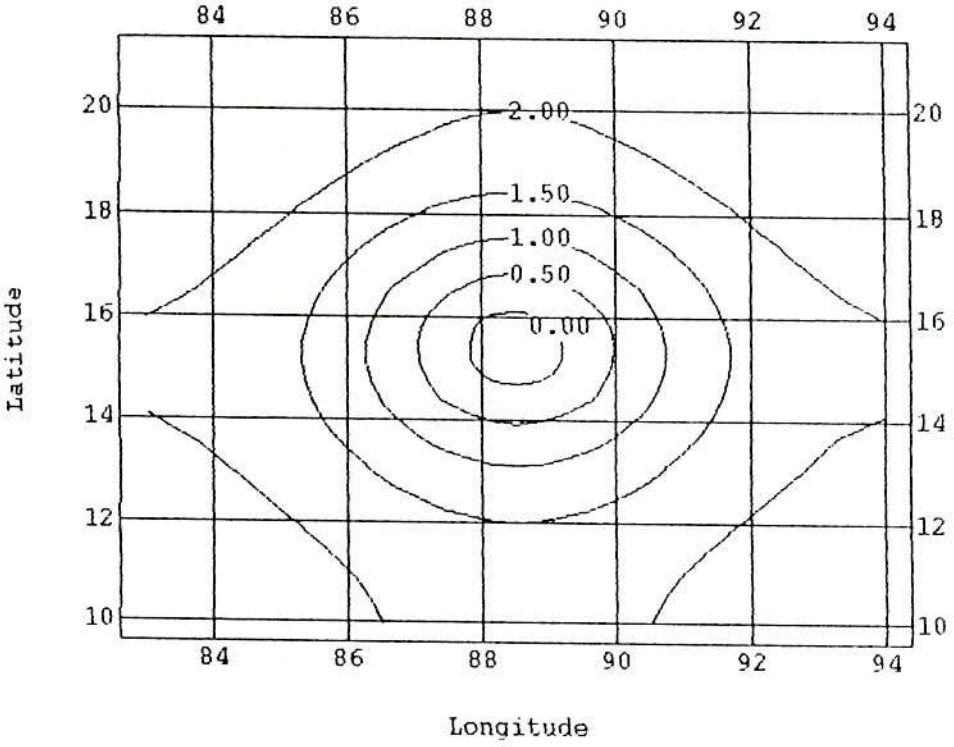

Fig. 6.15.10(a) 36-hr forecast of static stability ($\times 10^{-6}$/s) at the surface

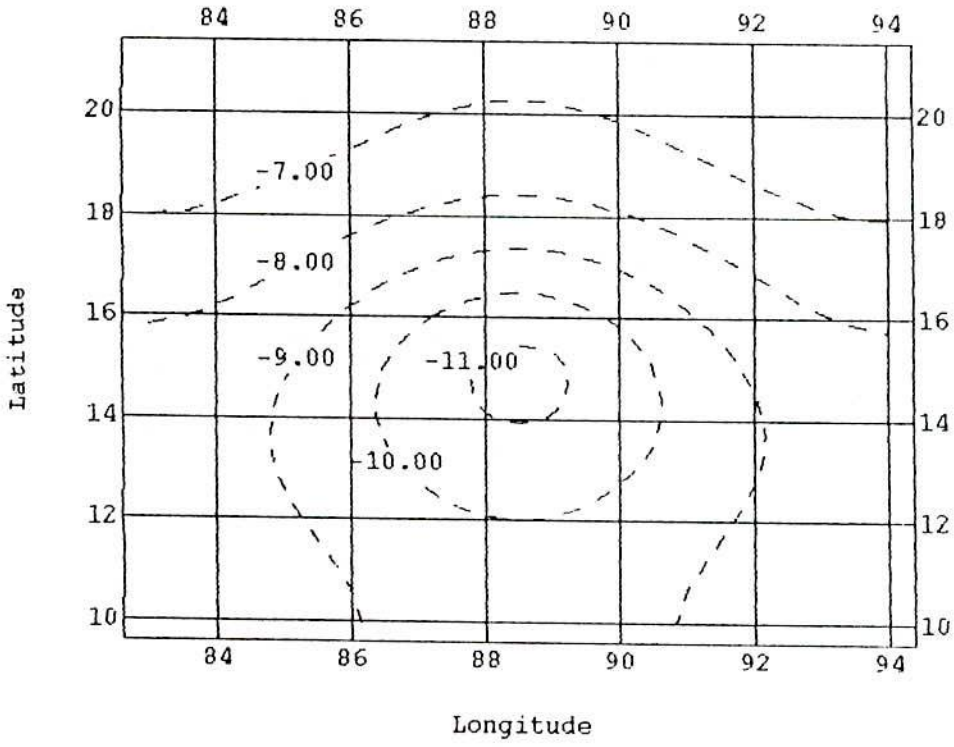

Fig. 6.15.10(b) 48-hr forecast of static stability ($\times 10^{-6}$/s) at the surface

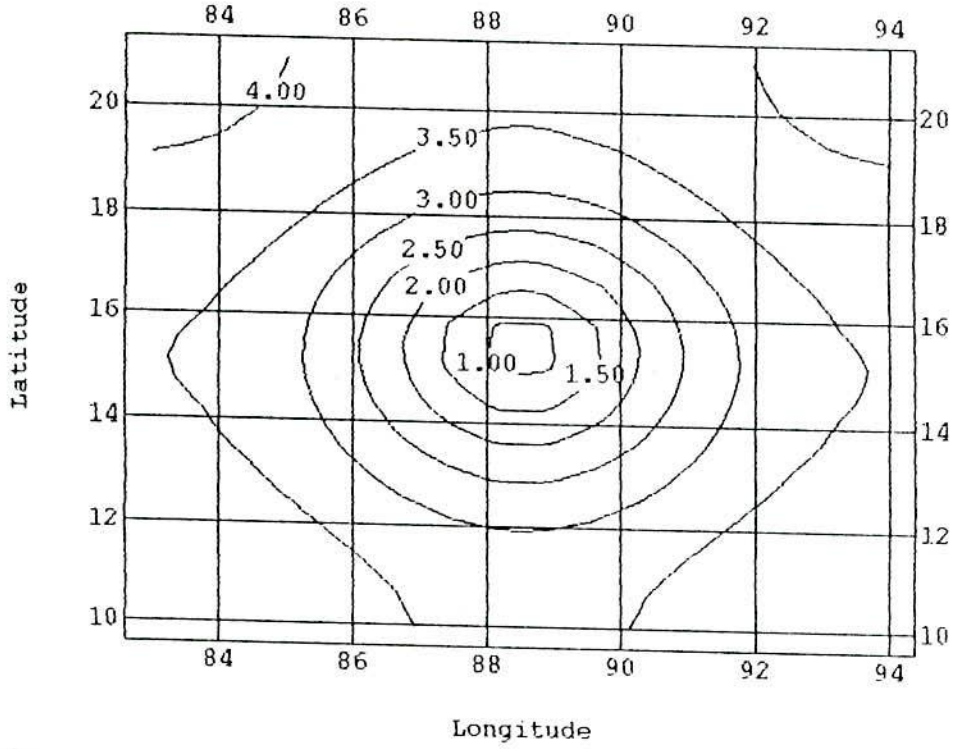

Fig. 6.15.10(c) 36-hr forecast of static stability ($\times 10^{-6}$/s) at 850 hPa

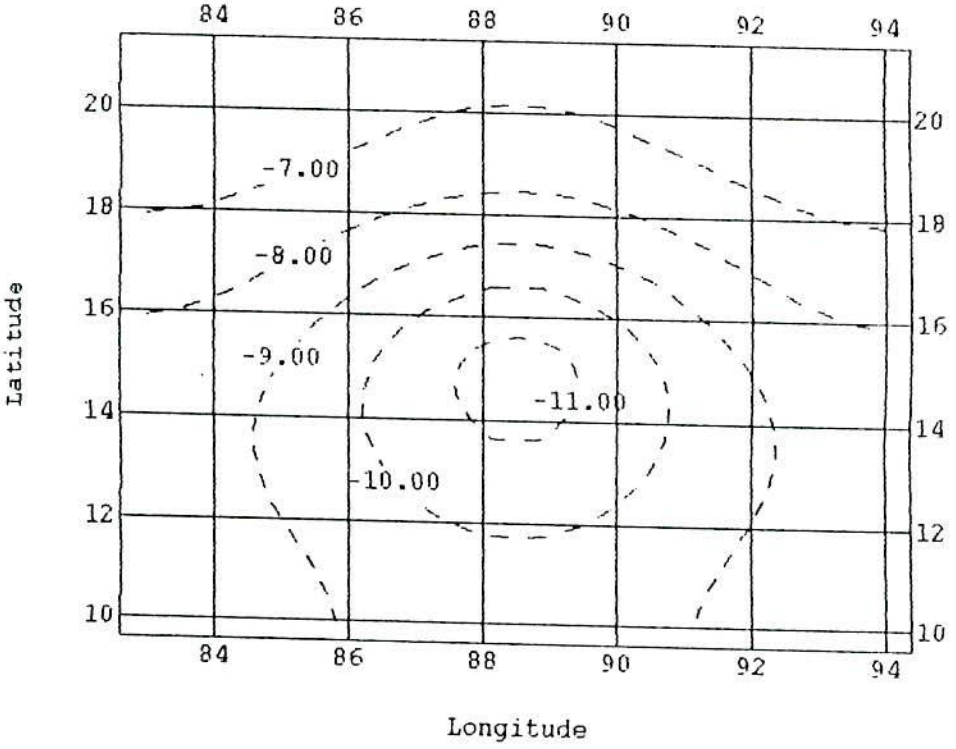

Fig. 6.15.10(d) 48-hr forecast of static stability ($\times 10^{-6}$/s) at 850 hPa

the model cyclone. The stability at 850 hPa at 36 and 48 hour is nearly the same as that of the surface.

6.16 Conclusions

The three-dimensional tropical cyclone model has been constructed in 5 layers with horizontal grid size 80 km. The model produces many features of the tropical cyclone.

Inertia-gravitational oscillations have been effectively controlled by using the implicit and explicit smoothing of the variables. A 1-minute time step has been found sufficient to keep the computations stable even without the use of a time filter in the time integration.

The latent heat release due to condensation has been parameterized in the model, which is the primary source of energy for the tropical cyclone. In this model we have used the sensible heat and latent heat as the source of energy. The characteristics of the horizontal and vertical structures of the various features of the modelled cyclone obtained in this experiment are consistent with those of usual observations.

A simplified but comprehensive system of equations, which can simulate the life cycle of tropical cyclones, has been used. The model equations are solved using the finite difference method. Numerical solutions show that the model can simulate the developing, rapidly intensifying and mature stages of tropical cyclones.

The primary purpose of this work is to develop a system of equations for tropical cyclone simulation with some simplification. Although the model can simulate some aspects of tropical cyclone development, it also has limitations. The limitation is that θ derivatives of the fields is neglected, although this could probably be relaxed. Another limitation is related to the lack of vertical resolution. The pressure thickness of the upper layer is 300 hPa, which is considerably larger than the outflow layer of observed storms.

We have found that numerical stability depends critically on numerical procedure adopted. Without smoothing it is not possible to obtain convergent development. Even

the choice of the time step is also highly critical and we found the best value at $\Delta t \approx 1$ minute or less.

Another interesting discovery is the distribution of vertical energy. As cumulus cloud convection has to be parameterized, somewhat arbitrarily, we tried to obtain the best vertical distribution of energy that can sustain a developing cyclone and obtained a good result.

Lastly we have discovered that even with the optimal vertical distribution of energy adopted, we could not simulate a developing cyclone for SST < 25°C or when there is a substantial vertical wind shear. Also if we changed our co-ordinates towards the equator where the Coriolis acceleration is quite small the cyclone simply died down. All these results are in agreement with observational data.

Chapter 7

Summary

Tropical cyclone is one of the most important weather activities in the tropics and sub-tropics. However, only limited work has been done previously for the prediction of formation and track of cyclone in the Bay of Bengal especially using the principle of dynamics as a basis. This motivated us to carry out this work.

It is known that the track and intensity of tropical the cyclone largely depend on the steering wind at the anticyclonic level and on sea surface temperature. The intensity of the cyclone may be sensitive to even a small change in temperature in the ocean or land. The changes of tropospheric energy and fluxes are important in the surrounding of the Bay of Bengal during the development and movement of tropical cyclone. The role of energy fluxes is to govern the atmospheric circulation as well as the physical processes responsible for the formation and movement of tropical cyclones. Here it is essential to study the role of tropospheric energy and fluxes and their vertical distribution in prediction of formation and movement of tropical cyclones in respect of their intensity, track and landfall.

In view of the great importance of atmospheric variables, we have studied different meteorological parameters such as wind speed and temperature in the surroundings of the Bay of Bengal during different cyclonic periods. The study also includes different tropospheric energy (such as dry static energy, latent heat energy, moist static energy and total energy) and fluxes (such as meridional flux of moist static energy and zonal flux of moist static energy) and their vertical distribution in the surroundings of the Bay of Bengal during different cyclonic periods. We have selected several severe cyclonic storms with a core of hurricane wind and one cyclonic storm formed in the Bay of Bengal and crossed the Bangladesh coast in the last decade. The severe cyclonic storm with a core of hurricane wind of 1985, 1988, 1991, 1992 and 1994 and the cyclonic storm of 1992 are considered for analysis. We have also studied the vertical wind shear for all the mentioned

cyclones. On the basis of the analysis of all the variables we have drawn the following conclusions:

The upper-air data were not available for some cases during the analysis period for all stations in the region. If we got upper-air data at 6 hourly interval in the surrounding, then the prediction of track and landfall is more accurate.

- The westerly wind decreases significantly at all levels over the area towards which the cyclones move for ultimate landfall.
- The southerly wind has a tendency to increase significantly at all levels over the area towards which the cyclones move and this increase depends on the tracks of the cyclones.
- There is a tendency for the temperature to decrease in the lower troposphere and increase in the upper troposphere over the areas towards which the cyclones move. The temperature of the troposphere remains almost constant in other areas surrounding the Bay of Bengal.
- The vertical wind shear is approximately zero near the centre of the cyclone.
- The dry static energy decreases or almost remains constant in the lower troposphere and increases in the upper troposphere on the day of landfall with respect to that of the previous day in the nearby stations. The dry static energy increases in case of the weakened cyclone and in case of the cyclonic storm on the day of landfall with respect to that of the previous day.
- The latent heat energy decreases with little anomalies in case of all the severe cyclonic storms with a core of hurricane winds from surface to 750 hPa level or 700 hPa level in the nearby stations and increases in the far away stations on the day of landfall with respect to that of the previous day. The latent heat energy increases in the nearby stations and decreases in the far away stations in case of the weakened cyclone and in case of the cyclonic storm on the day of landfall with respect to that of the previous day.
- The moist static energy decreases with little anomalies in case of all the severe cyclonic storms with a core of hurricane winds from surface to 800 hPa level or 700 hPa level and increases from these levels to 200 hPa level in the nearby stations and increases

significantly in the far away stations on the day of landfall with respect to that of the previous day. The moist static energy increases at all levels in the nearby stations and decreases in the far away stations in case of the weakened cyclone and in case of the cyclonic storm on the day of landfall with respect to that of the previous day.

- The dry static energy, the latent heat energy and the moist static energy decreases towards the region where the cyclone moves.
- The south-easterly flux was flowing at all levels with effect of southerly component is greater over Chittagong on 2nd May 1994. The significant amount of southerly flux was flowing over Chittagong on 2nd May, which is related to the movement of cyclone towards the Cox's Bazaar-Teknaf coast.
- A large amount of south-easterly flux was flowing at all levels over Chittagong and Calcutta on 29th November 1988. The significant amount of south-easterly flux was flowing over the above mentioned stations on 29th November which is related to the movement of the cyclone to the Khulna coast of Bangladesh and West Bengal coast of India.
- The south-westerly flux was flowing in the upper troposphere over Chittagong on 19th and 20th May 1992. The significant north-westerly flux exists around 500 hPa and north-easterly around 400 hPa on 21st November over the station. Due to the north-westerly at 500 hPa level and north-easterly at 400 hPa level on 21st November the cyclone moves away from Chittagong coast and finally crossed the Mayanmar coast as land depression.
- The tremendous amount of south-easterly was flowing from 900 to 500 hPa and south-westerly exists from 500 to 200 hPa level on 29th April 1991 over Chittagong. Due to this south-easterly in the lower troposphere and south-westerly in the upper troposphere the cyclone crossed Chittagong coast.
- The increase of north-westerly flux during the period over Dhaka and south-westerly over Chittagong on 18th and 19th May 1992 the cyclonic storm hit the Cox's Bazaar coast.

In our attempts to build models related to cyclones, we have first tried to formulate the simplest physical model for a Bay of Bengal cyclone track, which was inspired by an earlier work by Choudhury (1978). However, unlike the previous work, we intended to

make it a model for simulating the track over time, instead of simply predicting the shape of the track. We have developed a model for the track prediction of cyclone by using the complex potential function. We have adjusted different parameters for different major cyclones that formed in the Bay of Bengal and crossed the Bangladesh coast during (1970 - 1994) to fit the model track with the actual track.

- The observed time for the model is approximately equal to that of the exact travel time (from the time of formation to the time of crossing the land) of the cyclone. Reasonable fits are obtained with a constant steering wind for the severe cyclonic storms with core of hurricane winds of 1970, 1985, 1991, 1992 and 1994 and the cyclonic storm of 1992. In the case of the severe cyclonic storm with a core of hurricane winds of 1974, 1981 and 1988 only average fits could be obtained with a constant steering wind, because the tracks of the cyclones were complicated by recurvings. Our generalized model with variable steering wind and Coriolis force, however, was able to fit even the complex tracks of these cyclones and also gives correct times for landfall, indicating that despite the obvious simplifications of this model, it has the potential of accurately predicting even unusually complicated tracks, if sufficient data can be made available to parameterize the effective steering winds.

Next we have tried to construct a three dimensional model for the formation of a cyclone over the sea, taking into consideration all dynamical equations related to momentum and energy conservation, equation of continuity, equation for moisture conservation etc. This three-dimensional tropical cyclone model has been constructed in 5 - layers with horizontal grid size 80 km. A simplified system of equations that can simulate the development of tropical cyclones has been obtained.

- The model equations are solved using the finite difference method.
- Numerical solutions show that the model can simulate the developing and rapidly intensifying and mature stages of tropical cyclones.
- Inertia-gravitational oscillations have been effectively controlled by using the implicit and explicit smoothing of the variables.

- A 1 - minute time step has been found sufficient to keep the computations stable even without the use of a time filter in the time integration.
- The latent heat release due to condensation has been parameterized in the model.
- The sensible heat is also considered as the source of energy.
- The model produces axisymmetric features of the tropical cyclone.
- The model produces the cyclonic flow in the lower troposphere and anticyclonic flow in the upper troposphere.
- The model produces the inflow in the lower troposphere and outflow in the upper troposphere.

The characteristics of the horizontal and vertical structures of the various features of the modelled cyclone obtained in this experiment are consistent with expectations based on usual observations.

Although the model can simulate most of the aspects of tropical cyclone development it also has a few limitations.

- Axisymmetric assumption, although this could be relaxed.
- Horizontal grid size which is uniformly 80 km is probably too large near the eye. It is probably necessary to take the grid size as small as possible near the eye to reproduce its structure.
- Lack of vertical resolution. The pressure thickness of the upper layer is 300 hPa, which is considerably larger than the outflow layer of observed storms.
- To produce a realistic model that can be used for prediction sufficient data is necessary at or near all grid points. This cannot be done by extrapolation or interpolation of presently available data.

Nevertheless, we find it satisfying that our model based only on the laws of physics, does predict that cyclone formation is critically dependent on a number of variables, e.g. sea-surface temperature, vertical wind shear, presence of Coriolis acceleration etc. It may, therefore, be possible to build upon this initial effort for a more complete numerical model for Bay of Bengal cyclones.

References

1) Anjaneyulu, T.S.S., Sikka, D. R., and Gurunadham, G., 1965, Some aspects of Bay of Bengal Cyclone of October 1963, *Indian Journal of Meteorology and Geophysics*, Vol. 16, No. 4, 539-556.

2) Annette, P., 1978, Cyclogue-Analogic prediction of the course of tropical cyclones by National Meteorological Analysis Center, Melbourne, Tech. Rep. 28, Bur. Met., Australia, 22pp.

3) Batchelor, G. K., 1980, An Introduction to Fluid Dynamics, *Cambridge University Press*, 106-108.

4) Bolton, D., 1980, Application of the Miles theorem to forced linear perturbations, *J. Atmos. Sci.*, 37, 1639-1642.

5) Byers, H.R., 1974, General Meteorology, Fourth edition.

6) Chan, J. C. L., 1984, An observational study of the physical processes responsible for tropical cyclone motion, *J. Atmos. Sci.*, 41, 1036-1048.

7) Chen, D. R., Yeh, T. C., Huang, K. N., Peng, M. S., and Chang, S.W., 1995, A new operational typhoon track prediction system at the Central Weather Bureau in Taiwan, *Preprints, 21st Conf. Hurr. Trop. Meteor.*, Amer. Meteor. Soc., Boston, MA 02108, 50-51.

8) Charney, J. G., 1963, A note on the large-scale motions in the tropics, *J. Atmos. Sci.*, 20, 607-609.

9) Charney, J. G. and Eliasen, E., 1964, On the growth of the hurricane depression, *J. Atmos. Sci.*, 21, 901-924.

10) Choudhury, A. M., 1978, Rose petal for tropical cyclones. *Nuc. Sci. and App.*, Vol. 11(B).

11) Chowdhury, M.H.K. and Karmakar, S., 1995, ``A study on some characteristics of the April Cyclone 1991" *The Atmosphere*, 1, 1, pp. 1-7.

12) Davidson, N. E., 1995, Vorticity budget for AMEX. Part I. Diagnostics, *Mon. Wea. Rev.*, 123, 1620-1635.

13) Davidson, N. E., and Kumar, A., 1990, Numerical simulation of the development of AMEX tropical cyclone Irma, *Mon. Wea. Rev.*, 118, 2001-2019.

14) Dvorak, V. F., 1975, Tropical cyclone intensity analysis and forecasting from satellite imagery, *Mon. Wea. Rev.*, 103, 420-430.

15) Dvorak, V. F., 1984, Tropical cyclone intensity analysis using satellite data, NOAA Tech. Rep. NESDIS 11, U. S. Dept. of Commerce, Washington, DC, 47p.

16) Elsberry, R. L., 1987, Tropical cyclone motion, Chap. 4, *A Global View of Tropical Cyclones*, Office of Naval Research, Arlington, VA 22217, 91-171.

17) Elsberry, R. L., 1995, Global Perspectives on Tropical Cyclones, World Meteorological Organization Technical Document, WMO/TD - No. 693.

18) Emanuel, K.A., 1989, The finite-amplitude nature of tropical cyclogenesis, *J. Atmos. Sci.*, 46, 3431-3456.

19) Emanuel, K.A., 1993, The physics of tropical cyclogenesis over the Eastern Pacific, *Tropical Cyclone Disasters*, J. Lighthill, Z. Zhemin, G. J. Holland, K. Emanuel(Eds.), Peking University Press, Beijing, 136-142.

20) Emanuel, K.A., Neelin, J. D., and Bretherton, C. S., 1994, On large-scale circulations in convecting atmospheres, *Quaart. J. Roy. Meteor. Soc.*, 120, 1111-1143.

21) Essenwanger, O. M., 1985, World Survey of Climatology, 1B, 337p.

22) Fiorino, M. and Elsberry, R. L., 1989a, Some aspects of vortex structure in tropical cyclone motion, *J. Atmos. Sci.* , 46, 979-990.

23) Fiorino, M. J., Goerss, S., Jensen, J. J., and Harrison, E. J., 1993, An evolution of the real-time tropical cyclone forecast skill of the Navy operational global atmospheric prediction system in the western North Pacific, *Wea. and Forecasting*, 8, 3-24.

24) Flatau, M., Schubert, W. H., and Stevens, D. E., 1994, The role of baroclinic processes in tropical cyclone motion: The influence of vertical tilt, *J. Atmos. Sci.* , 51, 2589-2601.

25) Fleagle, R.G. and Businger, J.A., 1980, An Introduction to Atmospheric Physics, Academic Press, Vol. 25, Second Edition.

26) Flatau, M., Schubert, W. H., and Stevens, D. E., 1994, The frole of baroclinic processes in tropical cyclone motion. The influence of vertical tilt, *J. Atmos. Sci.* , 51, 2589-2601.

27) Fraedrich, K., and McBride, J. L., 1995, Large scale convective instability revisited, *J. Atmos. Sci.* , 52, 1914-1923.

28) Frank, W. M., 1987, Tropical cyclone formation. Chap. 3, A Global View of Tropical Cyclones, Office of Naval Research, Arlington, VA 22217, 53-90.

29) Gray, W.M., 1968, Global view of the origin of tropical disturbances and storms, *Mon. Wea. Rev.* , 96, 669-700.

30) Gray, W.M., 1975, Tropical cyclone genesis. *Dept. of Atmos. Sci.* Paper No. 323, Colorado State University, Ft. Collins, CO 80523, 121p.

31) Gray, W.M., 1979, Hurricanes: Their formation, structure and likely role in the tropical circulation. Meteorology Over the Tropical Oceans. D. B. Shaw (Ed.), *Roy. Meteor. Soc.* , James Glaiser House, Grenville Place, Bracknell, Berkshire, RG12 1BX, 155-218.

32) Haltiner G. J. and Williams, R. T., 1979, Numerical Prediction and Dynamic Meteorology, *John Wiley & Sons* , Second Edition.

33) Haurwitz, B., 1935, The height of the tropical cyclones and the eye of the storm, *Mon. Wea. Rev.* , 63, 45-49.

34) Hayashi, Y., 1970, A theory of large-scale equatorial waves generated by condensation heat and accelerating the zonal wind, *J. Meteor. Soc. Japan* , 48, 140-160.

35) Holton, J. R., 1979, An Introduction to Dynamic Meteorology, *Academic Press* , Vol. 23.

36) Hope, J. R., and Neumann, C. J., 1970, An operational technique for relating the movement of existing tropical cyclones to past tracks. *Mon. Wea. Rev.* , 98, 925-933.

37) Hubert, L. F., 1955, A case study of hurricane formation, *J. Meteor.* , 12, 486-492.

38) Iwasiki, T., Nkano, H., and Sugi, M., 1987, The performance of a typhoon track prediction model with cumulus parameterization, *J. Meteor. Soc. Japan* , 65, 555-570.

39) Jarrel, J. D., and Somervell, W. L., 1970, A computer technique for using typhoon analogs as a forecast aid, Naval Weather Research Facility Technical Paper No. 6-70, 47pp.

40) Jarrel, J. D., Mauck, C. M. and Renard, R. J., 1975, The Navy's analog scheme for forecasting tropical cyclone motion over the Northeastern Pacific Ocean, Technical

Paper No. 6-75, Naval Environmental Prediction Research Facility, Monterey, CA, 27pp.

41) Khanam, F., 1989, The prediction of tropical cyclones formed in the Bay of Bengal using numerical method, *M. Phil. Dissertation* .

42) Krishnamurti, T.N., 1969, An experiment in Numerical Prediction in Equatorial Latitudes, *Quart. J. Roy. Meteor. Soc.* , 95, 594-620.

43) Krishnamurti, T.N. and Kanamitsu, M., 1972, A study of a Coasting Easterly Wave, Numerical Weather Prediction over the Tropics, Report No. 72-1, April 1972, Dept. of Meteor., Florida State University.

44) Krishnamurti, T.N., Kanamitsu, M., Ceselski, B. and Mathur, M. B., 1972, F. S. U. Tropical Prediction Model, Numerical Weather Prediction over the Tropics, Report No. 72-1, April 1972, Dept. of Meteor., Florida State University.

45) Krishnamurti, T.N., 1979, Compendium of Meteorology, WMO No. 364, Vol. 2, Part 4, 186p.

46) Krishnamurti, T.N., 1986, Workbook on Numerical Weather Prediction for the Tropics for the training of class I and class II meteorological personnel, WMO - No. 669.

47) Krishnamurti, T. N., Bedi, H. S., Oosterhof, D., and Hardiker, V., 1994, The formation of hurricane Fredric of 1979, *Mon. Wea. Rev.* , 122, 1050-1074.

48) Kuo, H. L., 1965, On formation and intensification of tropical cyclones through latent heat release by cumulus convection, *J. Atmos. Sci.* , 22, 40-63.

49) Kuo, H. L., 1974, Further studies of the parameterization of the influence of cumulus convection on large-scale flow. *J. Atmos. Sci.* , 31, 1232-1240.

50) Kurihara, Y., and Kawase, M., 1985, On the transformation of a tropical easterly wave into a tropical depression: A simple numerical study, *J. Atmos. Sci.* , 42, 68-77.

51) Kurihara, Y. and Kawase, M., 1986, Reply. *J. Atmos. Sci.* , 43, 3284-3286.

52) Kurihara, Y., Tuleya, R.E., Bender, M.A., and Rebecca J.R., 1992, Advanced Modelling of Tropical Cyclones, Tropical Cyclone Disasters, Proceedings of ICSU/WMO, *International Symposium, October 12-16* , Beijing, China, 190-201.

53) Leftwich, P, and Neumann, C. J., 1977, Statistical guidance on the prediction of eastern North Pacific tropical cyclone motion, Part 2, NOAA Tech. Memo. NWS WR-125, 12pp.

54) Lindzen, R. S., 1974, Wave-CISK in the tropics, *J. Atmos. Sci.*, 31, 156-179.

55) Lorenz, E. N., 1963, Deterministic non periodic flow, , *J. Atmos. Sci.*, 20, 130-140.

56) Mandal, G.S., Rao, A.V.R.K. and Gupta, S.C., 1981, Characteristics of an Arabian Sea cyclone, *Mausam*, 32, 2, 139-144.

57) Mathur, M. B., 1972, Simulation of an Asymmetric Hurricane with a Fine-Mesh Multiple Grid Primitive Equation Model. Numerical Weather Prediction over the Tropics, Report No. 72-1, April 1972, Dept. of Meteor., Florida State University.

58) Mathur, M. B., 1991, The National Meteorological Center,s Quasi-Lagrangian model for hurricane prediction. *Mon. Wea. Rev.*, 115, 1419-1447.

59) McBride, J. L., 1981a, Observational analysis of tropical cyclone formation, Part I. Basic definition of data sets, *J. Atmos. Sci.*, 38, 1117-1131.

60) McBride, J. L., 1981a, Observational analysis of tropical cyclone formation, Part III. Budget analysis, *J. Atmos. Sci.*, 38, 1152-1156.

61) McBride, J. L., Davidson, N. E., and Puri, K., 1993, An evolution of the skill of a real-time large-scale NWP model at predicting tropical cyclone development, Presented at *20th Conf. Hurr. and Trop Meteor.*, San Antonio, TX, Amer. Meteor. Soc., Boston, MA 02108.

62) McBride, J. L., and Willoughby, H. E., 1986, Comment-An interpretation of Kurihara and Kwase's two dimensional tropical cyclone development model, *J. Atmos. Sci.*, 43, 3279-3283.

63) Miller, B. I., 1958, On the maximum intensity of hurricanes, *J. Meteor.*, 15, 184-195.

64) Milne-Thompson, L. M., 1972, Theoretical Hydrodynamics, *Macmillan Press Ltd.*, London, 152-156.

65) Montgomery, M. T., and Farrell, B. F., 1993, Tropical cyclone formation, *J. Atmos. Sci.*, 50, 285-310.

66) Neumann, C. J., 1972, An alternate to the HURRAN tropical cyclone forecast system, *Mon. Wea. Rev.*, 100, 245-255.

67) Ogura, Y. and charny, J. G., 1962, A numreical model of thermal convection in the atmosphere, Proc. Int. Symp. Numerical W. P., Tokyo, *J. Meteor. Soc. Japan*, 431-451.

68) Ogura, Y., and Philips, N. A., 1962, Scale analysis of deep and shallow convection in the atmosphere, *J. Atmos. Sci.* , 19, 173-174.

69) Ogura, Y., 1964, Frictionally controlled, thermally driven circulation in a circular vortex with application to tropical cyclones, *J. Atmos. Sci.* , 21, 610-621.

70) Ooyama, K. V., 1964, A dynamical model for the tropical cyclone development, *Geofis. Int.* , 4, 187-198.

71) Ooyama, K. V., 1982, Conceptual evolution of the theory and modeling of the tropical cyclone, *J. Meteor. Soc. Japan* , 60, 369-380.

72) Palmen, E., and Newton, C.W., 1969, Atmospheric Circulation System, Academic Press, *International Geophysics Series* , Vol. 13, 497.

73) Puri, K., and Miller, M. J., 1990, Sensitivity of ECMWF analyses-forecasts of tropical cyclones to cumulus parameterization, *Mon. Wea. Rev.* , 118, 1709-1741.

74) Reed, R. J. and Recker, E. E., 1971, Structure and properties of synopic-scale wave disturbances in the equatorial western Pacific, *J. Almos. Sci.* , 28, 1117-1133.

75) Riehl, H., 1948, On the formation of typhoons, *J. Meteor.* , 5, 247-264.

76) Riehl, H., and Malkus, J. S., 1961, Some aspects of hurricane Daisy, 1958, *Tellus* , 13, 181-213.

77) Roger, G.B., and Richard, J.C., 1982, Atmosphere, Weather and Climate, 4th edition, 62-63.

78) Srinivasan, V., and Ramanamurty, K., 1973, Forecasting Manual, III-4, *India Meteorological Department* , New Delhi, India.

79) Shapiro, R., 1970, Smoothing, filtering, and boundary effects, *Rev. Geophys. and Space Phys.* , 8, 359-387.

80) Shapiro, R., 1975, Linear filtering, *Math. Comp.* , 29, 1094-1097.

81) Shapiro, L. J., 1992, Hurricane vortex motion and evolution in a three-layer model, } *J. Atmos. Sci.*, 49, 140-153.

82) Steven, P.W., and Stanly, Q. K., 1984, On the use of wind shear and vorticity difference in forecasting eastern Pacific tropical cyclone formation, *American Meteorological Society* , 15th Conference on hurricane and tropical meteorology, 276-280.

83) Syono, S., and Yamasaki, M., 1966, Stability of symmetrical motions driven by latent heat release by cumulus convection under the existence of surface friction, *J. Meteor. Soc. Japan* , 44, 353-375.

84) Tarakanov, G. G., 1980, Tropical Meteorology, *Mir Publishers* , Moscow, pp. 157-158.

85) Tuleya, R. E., 1988, A numerical study of the genesis of tropical storms observed during the FGGE year, *Mon. Wea. Rev.* , 116, 1188-1208.

86) Tuleya, R. E., 1994, Tropical storm development and decay: Sensitivity to surface boundary conditions, *Mon. Wea. Rev.* , 122, 291-304.

87) Yanai, M., 1961, A detailed analysis of typhoon formation, *J. Meteor. Soc. Japan* , 39, 187-214.

88) Wang, B. and Li, X. F., 1992, The beta drift of three dimensional vortices, A numerical study, *Mon. Wea. Rev.* , 120, 579-593.

89) Wang, Y., and Holland, G.J., 1995, On the baroclinic dynamics of tropical cyclone motion: The influence of vertical structure, submitted to *J. Atmos. Sci.* , 52.

90) Webster, P. J., 1983, The large-scale structure of the tropical atmosphere, Large-Scale Dynamical Processes in the Atmosphere, B. J. Hoskins and R. P. Pearce (Eds.), Academic Press.

91) Wexler, H., 1947, Structure of hurricanes as determined by radar, *Ann. N. Y. Acad. Sci.* , 48, 821-844.

92) Williams, K. T., 1970, A statistical analysis of satellite observed trade wind cloud clusters in the Western North Pacific. Atmos. Sci. Paper No. 161, Colorado state University, Fort Collins, 80p.

93) Wu, C. C., and Emanuel, K., 1993, Interection of a baroclinic vortex with background shear: Application to hurricane movement, *J. Atmos. Sci.* , 50, 62-76.

94) Xu, Y. and Neumann, C. J., 1985, A statistical model for the prediction of western North Pacific tropical cyclone motion (WPCLPR), *NOAA Tech. Memo* . NWS-NHC 28, National Hurricane Center, Miami, FL, 30pp.

95) Yamasaki, M., 1969, Large-scale disturbances in a conditionally unstable atmosphere in low latitudes, Papers in Meteor, *Geophys.* , 20, 289-336.

96) Yamasaki, M., 1988, Towards an understanding of the interaction between convection and the large-scale in the tropics, *Aust. Meteor., Mag.* , 36, 171-182.

97) Yano, J. I., and Emanuel, K., 1991, An improved model of the equatorial tropopuse and its coupling with the stratosphere, *J. Atmos. Sci.*, 48, 377-389.